The influence of two phosphotransferases involved in caprazamycin biosynthesis and resistance
&
Mycothiol peroxidase activity as a part of the self-resistance mechanisms against the antitumoral cosmomycin D

Dissertation

der Mathematisch-Naturwissenschaftlichen Fakultät

der Eberhard Karls Universität Tübingen

zur Erlangung des Grades eines

Doktors der Naturwissenschaften

(Dr. rer. nat.)

vorgelegt von

Roger David Castillo Arteaga

aus Ipiales (Kolumbien)

Tübingen

2022

Gedruckt mit Genehmigung der Mathematisch-Naturwissenschaftlichen Fakultät der Eberhard Karls Universität Tübingen.

Tag der mündlichen Qualifikation:	29.03.2022
Dekan:	Prof. Dr. Thilo Stehle
1. Berichterstatter:	Prof. Dr. Harald Groß
2. Berichterstatter:	Prof. Dr. Leonard Kaysser

Table of Content

Table of Content ..... *II*

Publications and posters ..... *VI*

Publications ..... **VI**

Poster presentations ..... **VI**

Abbreviations ..... *VII*

Chapter I ..... *X*

Summary ..... *XI*

Zusammenfassung ..... *XII*

1. Introduction *13*

1.1 Secondary metabolites **13**

1.2 Self-resistance mechanisms **13**

1.3 Multidrug resistance transporters (MDRs) **14**

1.4 Transporters in natural product gene clusters **14**

1.4.1 ABC transporters 15

1.4.2 ATP binding and hydrolysis 16

1.4.3 ABC Transporters in Actinobacteria 18

1.5 Nucleoside antibiotics **20**

1.5.1 Caprazamycin biosynthesis 24

1.6 Self-resistance mechanisms against liponucleoside antibiotics 26

Aims of this study *28*

2. Materials and methods *30*

2.1 Columns, reagents, enzymes and kits **30**

2.2 Vectors and strains **35**

2.2.1 Plasmids and cosmids 35

2.2.2 Strains 38

2.3 Media, buffers and solutions **41**

2.3.1 Media for bacterial cultivation 41

2.4 Antibiotics **44**

2.5 Buffers and solutions **45**

2.5.1 Buffers and solutions for plasmid isolation 45

2.5.2 Buffers and solutions for DNA gel electrophoresis 45

2.5.3 Buffers for protein purification by nickel affinity chromatography 46

2.6 Culture conditions **48**

2.6.1 Cultivation of *Escherichia coli* 48

2.6.2 Cultivation of *Streptomyces* 48

2.7 Methods of molecular biology **48**

2.7.1 Isolation of cosmid/plasmid-DNA from *Escherichia coli* 48

2.7.2 Preparation of electro-competent cells 49

2.7.3 Transformation of *E. coli* ... 49
2.7.4 Intergeneric conjugation of *Streptomyces* ... 49
2.7.5 Polymerase chain reaction (PCR) ... 50
2.7.6 PCR for Red/ET-mediated recombination: ... 53
2.7.7 Agarose gel electrophoresis of DNA ... 54
2.7.8 Restriction analysis of DNA ... 54
2.7.9 Ligation reaction calculation ... 54
2.7.10 Red/ET-mediated recombination in *E. coli* ... 55
2.7.11 Cre-lox recombination ... 56
2.7.12 DNA sequencing ... 56
2.7.13 Cloning and overexpression in pUWL vector ... 56
2.7.14 Cloning and protein overexpression in pHIS8 vector ... 57
2.7.15 Site-directed mutagenesis of mycothiol peroxidase (MPx) ... 58
2.7.16 Cloning and overexpression in pGM1190 and pGM1192 vectors ... 59
2.7.17 Generation of single gene knock outs of *cpz12, cpz22, cpz23*, and *cpz27* in cpzLK09 cosmid ... 60
2.7.18 Generation of double gene knock outs ... 60
2.7.19 Total RNA isolation and cDNA synthesis ... 61
2.7.20 qPCR analysis ... 62
2.7.21 Denaturing polyacrylamid gel electrophoresis (SDS-PAGE) ... 62
2.7.22 Heterologous production of recombinant protein in *E. coli* ... 62
2.7.23 Heterologous production of recombinant protein in *S. lividans* TK24 ... 63
2.7.24 Purification of recombinant proteins Cpz12, Cpz27, MPx and Mutant MPx ... 63

2.8 Methods of biochemistry ... 64

2.8.1 In vitro studies on Cpz12 and Cpz27 ... 64

2.8.2 Enzymatic fatty acid activation with CoA ... 64

2.8.3 Enzyme assay of Cpz23 ... 64

2.8.4 In vitro studies with micothiol peroxidase enzyme (MPx) ... 65
2.8.4.1 Peroxide and protein quantification ... 65
2.8.4.2 Ferrous oxidation of xylenol orange (FOX) assay ... 65

2.9 Determination of Minimal Inhibitory Concentrations (MICs) ... 66

2.10 Analytical methods ... 66
2.10.1 High performance liquid chromatography (HPLC) ... 66
2.10.2 Purification of caprazamycin and intermediates ... 67
2.10.3 Purification of cosmomycin ... 68
2.10.4 Liquid chromatography-electrospray ionization mass spectrometry (LC-ESI/MS) and MS^2 ... 68
2.10.5 High resolution LC-ESI/MS and MS^2 analysis ... 69
2.10.6 NMR methods and structural characterization ... 69

2.11 Bioinformatic methods ... 69
2.11.1 Construction of Sequence similarity Networks (SSN) and Genome Neighborhood Network (GNN) for MPx enzyme ... 70

3. Results ... 71

3.1 Identification of plausible caprazamycin resistance determinants ... 71

3.2 Generation of knock-out mutants ... 82
3.2.1 Effect of *cpz12* and *cpz27* deletions ... 83
3.2.2 Effect of *cpz23* deletion ... 86
3.2.3 NMR elucidation of phosphorylated caprazol ... 91
3.2.4 In-vitro assays with Cpz23 ... 91
3.2.5 In-vitro studies of Cpz12 and Cpz27 ... 93
3.2.6 Effect of *cpz22* deletion ... 96

3.3 Effects of overexpression of Cpz12, Cpz22 and Cpz27 on caprazamycin resistance 99

4. Discussion 106

5. Conclusion 108

Chapter II 110

Mycothiol peroxidase activity as a part of the self-resistance mechanisms against the antitumoral cosmomycin D 110

Summary 111

Zusammenfassung 112

6. Introduction 113

6.1 Anthracyclines 113

6.1.1 Activity 114
6.1.2 Toxicity 114
6.1.3 Cosmomycins 115
6.2 Self-resistance of anthracyclines 115
6.2.3 Self-resistance mechanism of *Streptomyces olindensis* against cosmomycin D 118

Aims of this study 122

7. Materials and methods 122

8. Results 123

8.1 Self-resistance genes allocated within the cosmomycin D cluster 123

***8.2* Self-resistance mechanisms are essential for *S. olindensis*, when challenged with DOX and COSD 136**

***8.3* Self-resistance genes are mostly expressed during the production of COSD 140**

8.4 Mycothiol peroxidase (MPx) response against ROS stress 141

..... 144

8.5 *S. olindensis* peroxidase detoxification is important for survival under cosmomycin D production 144

9. Discussion 145

10. Conclusion 148

11. References 150

List of figures 160

List of tables 162

Appendix 163

Acknowledgements 164

Curriculum Vitae ..... Error! Bookmark not defined.

Appendix 166

Publications and posters

Publications

- Castillo Arteaga R., Funck C., Saad H., Bhattarai K., Majer T., Ishikawa S., Kulik A., Hoffer J., Gross H., Gust B. “Investigations of two phosphotransferases involved in caprazamycin biosynthesis and resistance”. (2022), “in preparation”
- Castillo Arteaga R., Maza L., Pedré B., Helmle I., Gross H., Gust B., Padilla, G. Mycothiol peroxidase activity as a part of the self-resistance mechanisms against the antitumor antibiotic cosmomycin D (2022), “accepted” Microbiology Spectrum, ASM

Poster presentations

- Peroxidase activity as a part of self-resistance mechanisms in cosmomycin D producing strain *Streptomyces olindensis* DAUFPE 5622. Castillo R., Garrido L., Ortiz R., Ferreira A., Dourado M., Araújo W., Long P., Gust B., Padilla G. *VAAM-Workshop,* Frankfurt, 2018

Abbreviations

°C	degree Celsius
×g	ground acceleration
aac(3)IV	apramycin resistance gene
ABC	ATP-Binding-Cassette
Amp	ampicillin
Apra	apramycin
ATP	adenosine triphosphate
bla	ampicillin/carbenicillin resistance gene
bp	base pair
cfu	colony forming unit
Cm	chloramphenicol
CoA	coenzyme A
CPZ	caprazamycin
COS	cosmomycin
Da	dalton
DMSO	dimethyl sulfoxide
DOX	doxorubicin
DNR	daunorubicin
DNA	deoxyribonucleic acid
dNTP	deoxyribonucleoside 5´-triphosphate
DTT	1,4-dithiothreitol
E. coli	*Escherichia coli*
ED50	50% effective dose
EDTA	ethylendiamine tetra-acetic acid
ESI	electrospray ionization
FLP	flippase
FRT	FLP recognition target
GPx	glutathione peroxidase
h	hour
HAC	hydroxyacylcaprazol
HCl	hydrochloric acid
HCOOH	formic acid

His8	octahistidine
HPLC	high performance liquid chromatography
IPTG	isopropyl-*β*-thiogalactoside
k	kilo
KAc	potassium acetate
Kan	kanamycin
kb	kilo base pairs
L	liter
LB	Luria Bertani
lacZ	gene portion for α-complementation of β-galactosidase
LC	liquid chromatography
loxP	Cre-recombinase recognition site
LPM	liposidomycin
m	milli
µ	Micro
M	molar
m/z	mass-to-charge ratio
MATE	multidrug and toxic compound extrusion
MDRs	multidrug resistance transporters
MDA	malonaldehyde
MFS	major facilitator superfamily
MIC	minimal inhibitory concentration
MPx	micothiol peroxidase
min	minute
MS	mass spectrometry
MW	molecular weight
n	nano
Ndx	nalidixic acid
NBD	nucleotide binding domain
NMR	nuclear magnetic resonance
nt	nucleotide
OD 600	optical density at 600 nm
ORF	open reading frame
oriT	origin of transfer

PACE	proteobacterial antimicrobial compound efflux
PAGE	polyacrylamide gel electrophoresis
PAPS	3’-phosphoadenosine 5’-phosphosulfate
PCR	polymerase chain reaction
PEG	polyethylene glycol
PKS	polyketide synthase
PMSF	phenylmethylsulfonyl fluoride
R	resistant
RNA	ribonucleic acid
RNase	ribonuclease
RND	resistance-nodulation-division
RP	reverse phase
rpm	rounds per minute
ROS	reactive oxygen species
RT	room temperature
s	second
S.	*Streptomyces*
SDS	sodium dodecyl sulphate
SMR	small Multidrug Resistance
TEMED	N´-tetramethylethylenediamine
Tet	tetracycline
TES	N-Tris(hydroxymethyl)-methyl-2 aminoethanesulfonicacid
Thio	thiostrepton
TMD	transmembrane domain
Tris	2-amino-2-(hydroxymethyl)-1,3-propanediol
UV	ultraviolet
WT	Wild type

Chapter I
The influence of two phosphotransferases involved in caprazamycin biosynthesis and resistance

Summary

Streptomyces sp. MK730-62F2 naturally produces the anti-mycobacterial compounds caprazamycins, potent MraY translocase inhibitors interfering with peptidoglycan biosynthesis. Structure activity relationship studies of caprazamycins and derivatives thereof gained deep insights into structural moieties required for efficient MraY inhibition. Although biosynthesis of caprazamycins and related liponucleoside antibiotics has been studied to some detail, only limited knowledge is available on plausible resistance mechanisms for this class of antibiotics. The caprazamycin biosynthetic gene cluster encodes for two phosphotransferases, Cpz12 and Cpz27 with high sequence similarities to the wide family of tunicamycin-resistance proteins. In this study, we investigated the function of both phosphotransferases as well as the cluster-encoded ATP-dependent efflux pump Cpz22. Deletion of *cpz12* resulted in the accumulation of (+)-caprazol, lacking the ß-hydroxy fatty-acyl side chain. The same chemotype was observed by deleting *cpz23* encoding for the lipase responsible for fatty-acid attachment but this time, formation of phosphorylated (+)-caprazol was observed in addition. Since deletion of *cpz27* resulted in no-exconjugants to be obtained, this phosphotransferase may provide the major resistance determinant against caprazamycins. Biochemical analysis of Cpz27 indicated its involvement during early biosynthesis, likely to inactivate a biological active intermediate of caprazamycin biosynthesis. Mutants, overexpressing *cpz12*, *cpz22* or *cpz27* were analyzed for their ability to strengthen resistance towards caprazamycins by determining their minimal inhibitory concentration (MIC). Our findings now emphasize a more complex resistance mechanism for caprazamycins in which both phosphotransferases interfere with caprazamycin biosynthesis.

Zusammenfassung

Streptomyces sp. MK730-62F2 produziert auf natürliche Weise die antimykobakteriellen Verbindungen Caprazamycine, starke MraY-Translokase-Inhibitoren, die die Peptidoglycan-Biosynthese stören. Struktur-Aktivitäts-Beziehungsstudien von Caprazamycinen und Derivaten davon lieferten tiefe Einblicke in Struktureinheiten, die für eine effiziente MraY-Hemmung erforderlich sind. Obwohl die Biosynthese von Caprazamycinen und verwandten Liponucleosid-Antibiotika zum Teil detailliert untersucht wurden, ist nur wenig über plausible Resistenzmechanismen für diese Klasse von Antibiotika bekannt. Das Caprazamycin-Biosynthese-Gencluster kodiert für zwei Phosphotransferasen, Cpz12 und Cpz27, mit hohen Sequenzähnlichkeiten zu der großen Familie von Tunicamycin-Resistenzproteinen. In dieser Studie untersuchten wir die Funktion beider Phosphotransferasen sowie der clusterkodierten ATP-abhängigen Efflux-Pumpe Cpz22. Die Deletion von *cpz12* führte zur Akkumulation von (+)-Caprazol, dem die ß-Hydroxy-Fettsäure-Seitenkette fehlte. Derselbe Chemotyp wurde durch Deletion von *cpz23* beobachtet, das für eine Lipase kodiert, die für den Transfer der Fettsäure verantwortlich ist. Die Cpz23-Deletionsmutante zeigte dieses Mal aber zusätzlich die Bildung von phosphoryliertem (+)-Caprazol. Da die Deletion von *cpz27* dazu führte, dass keine Exkonjuganten erhalten werden konnten, könnte diese Phosphotransferase die wichtigste Resistenzdeterminante gegen Caprazamycine darstellen. Die biochemische Analyse von Cpz27 zeigte eine Beteiligung während der frühen Biosyntheseschritte von Caprazamycinen, die wahrscheinlich ein biologisch aktives Zwischenprodukt inaktiviert. Mutanten, die *cpz12, cpz22* oder *cpz27* überexprimieren, wurden auf ihre Fähigkeit hin analysiert, die Resistenz gegen Caprazamycine zu stärken, indem ihre minimale Hemmkonzentration (MIC) bestimmt wurde. Unsere Ergebnisse deuten auf einen komplexeren Resistenzmechanismus für Caprazamycine hin, bei dem beide Phosphotransferasen in die Biosynthese von Caprazamycinen eingreifen.

1. Introduction

1.1 Secondary metabolites

Cell growth is determined by primary metabolic activity, resulting in the production of enzymes, organic acids, ethanol, among others. Secondary metabolites, on the other hand, are not essential and only accompany synthesis in some phases of cell growth (Kleinkauf and Von Döhren 1996). Microbial secondary metabolites are low molecular mass products of secondary metabolism, usually produced during the late growth phase (idiophase) of a relatively small sort of microorganisms. Secondary metabolites are not essential for the growth of the producing cultures but serve diverse survival functions in nature (Cundliffe and Demain 2010; Ruiz et al. 2010). Secondary metabolism is interesting due to the production of a variety of compounds that are of great use, such as: antibiotics, antifungals, immunosuppressive agents, antitumor, enzyme inhibitors, toxins and pigments. Most are complex organic molecules produced by a chain of enzymatic reactions (Cundliffe and Demain 2010; Kleinkauf and Von Döhren 1996).

Secondary metabolites include polyketides (PKS) non ribosomal peptides (NRPS) and hybrids PKS-NRPS, which are a structurally broad family of compounds with a diverse spectrum of activity. Approximately one third of the bioproducts approved as drugs are based on structures of secondary metabolites (Hopwood 2004; Solecka et al. 2012; Wang et al. 2006).

1.2 Self-resistance mechanisms

Antibiotics are secondary metabolites, that are not essential for growth, but that can inhibit growth or kill different microorganisms to protect the producer organism. For antimicrobial agents, resistance is normally quantified as the minimum concentration necessary for inhibiting growth in a cell population (Hopwood 2007; Kümmerer 2004).

Antibiotic resistance is innate in producing microorganisms, but it can develop in other organisms through three main mechanisms: the acquisition of resistance genes or gene complexes through plasmids and other transposable elements, the recombination of DNA from other bacteria into the chromosome or by transformation or through spontaneous mutations in the genome (Lewis 2008; Pope et al. 2008).

The main mechanisms that can provide antibiotic resistance are:

A) Transport mechanisms linked to the cytoplasmic membrane. B) Enzymatic mechanisms through the alteration of the antimicrobial agent or modification of the target of action. C) DNA repair mechanisms (Arteaga 2016).

1.3 Multidrug resistance transporters (MDRs)

Multidrug resistance transporters (MDRs) are ubiquitous and key players in microbial and cancer drug resistance. Furthermore, MDRs are commonly found in the biosynthetic gene clusters of natural products, playing a key role in export and/or self-resistance. Families of transporter proteins including MDRs are the ATP-Binding-Cassette (ABC) superfamily, the Major Facilitator Superfamily (MFS), the Resistance-Nodulation-Division (RND) superfamily, the Multidrug and Toxic Compound Extrusion (MATE) family and the Small Multidrug Resistance (SMR) family. Recently, a sixth MDR family was identified, the Proteobacterial Antimicrobial Compound Efflux (PACE). To understand multidrug resistance, obtaining structural information is important, since high-resolution structures provide mechanistic insights into chemical transport, aiding in inhibitor design (Mousa and Bruner 2016).

1.4 Transporters in natural product gene clusters

Although limited structural information has been published regarding the mechanism of these specific transporters, multiple studies provide insight into the function of biosynthetic gene cluster embedded transporters. Natural product gene clusters commonly harbor MFS and ABC transporters and rarely MATE, as it is the case for colibactin (Mousa and Bruner 2016).

Most of the MFS contain 12-transmembrane helixes. Although individual proteins can be highly specific, the MFS can transport a highly diverse substrate class including ions, sugars, amino acids, nucleosides, peptides, and drugs, among others. Furthermore, a subclass within the MFS has been classified as multidrug transporters, capable of transporting structurally diverse drug molecules (Mousa and Bruner 2016). For example the protein EmrD, a homolog of MdfA, has been shown to transport ethidium, tetraphenylphosphonium, benzalkonium, ciprofloxacin, chloramphenicol, thiamphenicol and erythromycin.(Adler and Bibi 2004; Edgar and Bibi 1997; Mousa and Bruner 2016).
These transporters have been well studied functionally, capable of transporting cationic molecules as well as antibiotics such as erythromycin and many fluoroquinolones (Ahmed et

al. 1995; Mousa and Bruner 2016; Poelarends, Mazurkiewicz, and Konings 2002; Tennent et al. 1989).

The protein superfamily of the ABC group is one of the largest protein groups and it is found in the 3 domains (Archeas, Bacteria, Eukaryotes). These systems importing and exporting various substances in cellular processes, as well as in regulatory processes of sugars, amino acids, antibiotics, toxins, lipids, sterols, bile salts, peptides, nucleotides, endogenous metabolites and ions. (Bouige et al. 2002).

1.4.1 ABC transporters

The ABC superfamily consists of at least two nucleotide-binding domains (NBDs), and two transmembrane domains (TMDs) (Figure. 1). The highly conserved NBDs bind and hydrolyze ATP, providing energy for drug translocation across the cell membrane by the TMD. TMDs are highly diverse, indicative of the large substrate diversity of this transporter superfamily. The (ABC)-type multidrug transporters use the free energy of ATP hydrolysis to pump drugs out of the cell (Putman, van Veen, and Konings 2000; Wilkens 2015).

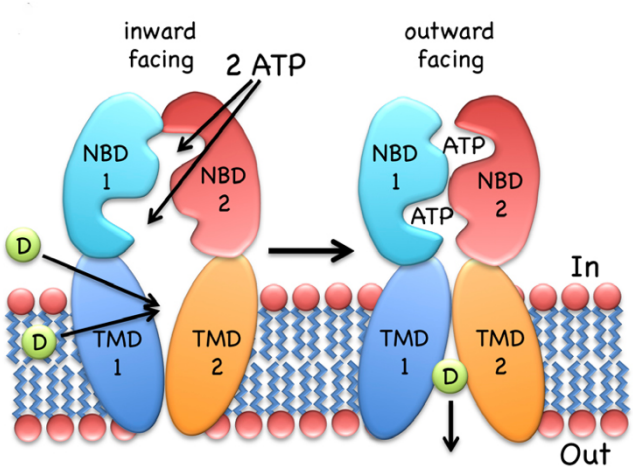

Figure 1. Schematic of the structural organization of the components forming an ABC-type transport in bacteria.

The inward-facing exporter binds substrate “D” (drug) from the cytoplasm or the inner leaflet of the bilayer. After binding two molecules of Mg-ATP, the nucleotide binding domains (NBDs) dimerize and switch the transmembrane domain (TMDs) from the inward to the outward-facing conformation, followed by the release of the drug to the extracellular milieu. ATP hydrolysis, ADP/Pi release and NBD dissociation resets the transporter to the inward-facing conformation (Wilkens 2015)

One of the components associated with the membrane is responsible for the formation of the chanel through which the substance will be transported. This component is, in general, formed by two hydrophobic proteins that cross the cytoplasmic membrane, forming the integral membrane domain (TM or permease). TMs are formed by proteins that have four to eight alpha helix structures (usually six) that are organized as homodimers. The protein is composed of an aqueous chanel, formed by TMD, with a large opening in the extracellular surface of the membrane. The NBD is found in the cytoplasmic face of the membrane in close juxtaposition with the TMD. (Arteaga 2016; Holland 2011) (Figure 2).

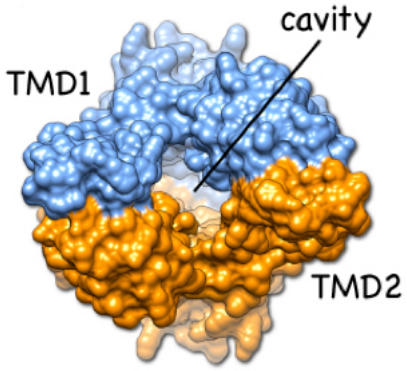

Figure 2. Structure of TMD pore.

The cavity formed by the TMDs of outward-facing Sav1866. Note that the cavity does not provide access to the outer leaflet of the lipid bilayer (Wilkens 2015).

1.4.2 ATP binding and hydrolysis

The basic catalytic cycle of ABC transporters starting from the ground state consists of a series of steps. These include the binding of substrate-binding proteins (for importers) or the direct binding of a substrate (for exporters) to the TMDs, binding of two Mg-ATP molecules to the NBDs, dimerization of the NBDs, switching of the TMDs between the in- and outward or out and inward-facing conformations (depending on transporter type), ATP hydrolysis, phosphate, ADP and transport substrate release concomitant with NBD dissociation to reset the transporter to the ground state for the next cycle (Wilkens 2015).

ABC protein NBDs have three highly conserved motifs that play a critical role in ATP binding, the Walker A and Walker B motifs, found in many proteins that bind to ATP or GTP, and a unique LSGGQC signature for the ABC superfamily. Targeted mutagenesis approaches have revealed the importance of these three regions in the catalytic function (Frelet and Klein

2006). Structural studies of NBD subunits isolated from many ABC proteins have produced useful information on the catalytic cycle. Each ATP binding site is formed from the Walker A and B motifs of an NBD subunit and the CLSGGQ signature motif of the NBD subunit (Figure 3). Two ATP molecules are linked at these locations at the dimer interface. This sandwich structure was observed for the NBD subunit of the bacterial ABC proteins MJ0796 and HlyB (Hanekop et al. 2006; Sharom 2008).

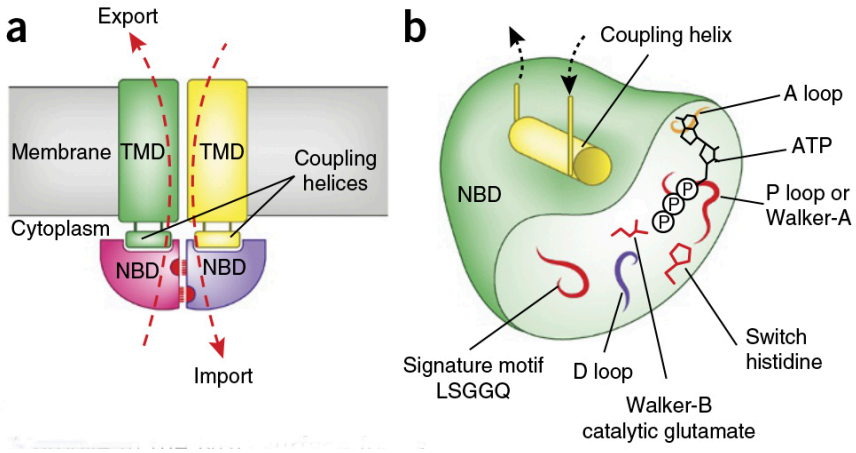

Figure 3. Architecture of ABC transporters

a) Domain arrangement of ABC transporters: at the NBD interface, red half-circles and dashed lines indicate the P loops and ABC signature motifs, respectively. Any given ABC transporter is either an importer or an exporter. Coupling helices transmit conformational changes between the NBDs and the TMDs.
(b) Schematic of a single NBD. The locations of the conserved and functionally critical motifs are indicated and labeled. They include the P loop (or Walker-A motif), which binds the α- and β-phosphates of ATP; the A loop, which provides an aromatic side chain that packs against the purine ring of adenine; a Walker-B motif, which provides the catalytic glutamate; a signature LSGGQ motif, which pins and orients ATP during hydrolysis; a 'switch histidine', which stabilizes the transition-state geometry; a Q loop, which provides contacts to the TMD (not shown); and a dimerization or D loop, which has a role in coupling hydrolysis to transport. A groove in the NBD surface forms the contact interface with the coupling helix of the TMD. Although the coupling helix is not the only contact between TMDs and NBDs, it is the only architecturally conserved contact among distinct TMD folds and provides the majority of contacts between domains.
(Locher 2016)

The hydrolysis of ATP and the release of inorganic phosphate drives the NBDs apart and, by transmitting this motion to the TMDs via the coupling helices, converts the outward-facing conformation into an inward-facing conformation (Figure 4). This step is irreversible given the large amount of energy gained from the hydrolysis of ATP (approaching 50 kJ mol−1 per ATP molecule). It is unclear whether the hydrolysis of two ATP molecules is simultaneous or consecutive, nor is it certain that both ATP molecules are hydrolyzed during every transport cycle (Locher 2016).

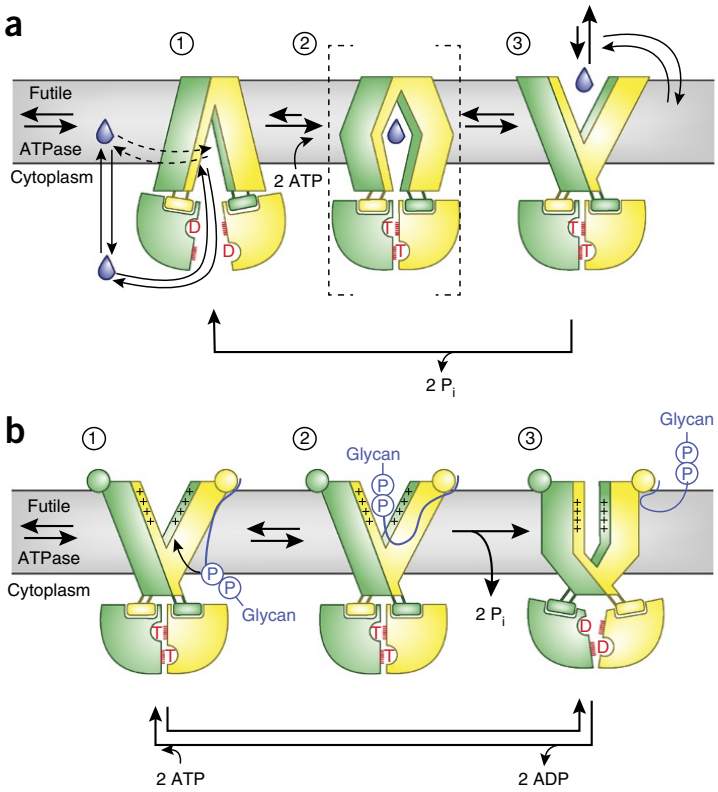

Figure 4. Distinct mechanisms of B-family ABC exporters

Green and yellow, half-transporters; T, ATP; D, ADP. Dotted red lines in the NBDs depict the ABC signature motifs. Circled numbers denote states. In outward-open conformations, the TMDs of the transporters form two wings toward the external side of the membrane. Each wing contains two TM helices from one TMD and four TM helices from the other. Details are described in the main text. (a) Alternating access proposed for multidrug or peptide transporters. (b) Outward-only mechanism with substrate loading directly into the outward-facing cavity, as proposed for the LLO flippase PglK. Pi, inorganic phosphate (Locher 2016).

1.4.3 ABC Transporters in Actinobacteria

Actinomycetes are producers of about three quarters of all known antibiotics. This group of Gram-positive bacteria has developed, through evolution, specific resistance mechanisms to facilitate their survival during the production of potentially toxic compounds (Arteaga 2016; Cundliffe and Demain 2010; Méndez and Salas 1998). Interestingly, many of the resistance mechanisms found in producing organisms have homologues in clinically isolated bacteria and this raised a question about the origin of resistance to antibiotics found in bacteria. It has been described that organisms that produce antibiotics may represent the source of at least some of the resistance determinants found in clinical isolates (Benveniste and Davies 1973; Jiang et al. 2017).

Most of the transport systems encoded by gene- clusters are involved in secretion and resistance. The first ABC transporters identified were a consequence of the cloning of

determinants of antibiotic resistance. The different ABC carriers, so far described, are of three types, designated as type I, II and III (Figure 5) (Méndez and Salas 2001).

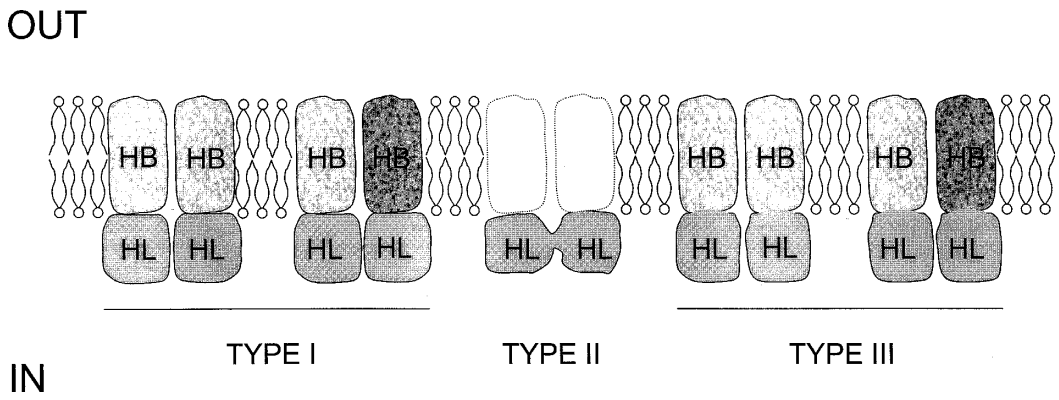

Figure 5. Structure and organization of the different types of ABC transporters in antibiotic-producing actinomycetes:

HB (Hydrophobic) HL (Hydrophilic). In the case of type II transporters, there are no identified HB domains (Méndez and Salas 2001).

This classification is based on the number and organization of nucleotide binding domains (NBDs), and the composition of the transport system (Table 1). In type I, the transport system consists of two proteins encoded by independent genes: an ATP-binding protein, with a single nucleotide-binding domain (a Walker A and B motif) and one (or two) of proteins from hydrophobic membrane containing six transmembrane domains. Type II transporters are formed by two hydrophilic domains of the protein containing binding nucleotides (each containing Walker A and B motifs) and encoded by a single gene (Méndez and Salas 2001).

Table 1. Features of antibiotic ABC transporters from producing actinomycetes

ABC transporter	Number of genes involved	Gene encoding ATP binding domain	Gene encoding membrane domain	Nucleotide binding domains	Both domains fused in a gene
Type I	two/three	present	present	one	no
Type II	one	present	not identified	two	no
Type III	one/two	present	present	two	yes

(Méndez and Salas 2001).

Type I and type III transporters form a more related cluster, while type II transporters appear to form a clearly separate class. This analysis suggests that type II transporters may have evolved from a single ancestor of two domains, rather than having evolved individually as a result of duplicating independent genes. Another conclusion of this analysis is that the macrolide transporters present some degree of grouping within the type II group (Méndez and Salas 2001).

All antibiotic transporters contain typical ATP-binding domains with the characteristic Walker A and B motifs separated by a different number of amino acids, depending on the type of transporter. In type I, the amino acid residues among the conserved lysine are about 115, while in type III it is 120, on average. However, in type II (transporters containing two ATP-binding domains), they consist of approximately 137 amino acids (Méndez and Salas 2001).

1.5 Nucleoside antibiotics

One class of nucleoside antibiotics is represented by the uridylpeptide antibiotics. Member of this class comprises the pacidamycins, mureidomycins, napsamycins and the sansanmycins (Figure 6). These compounds share a 3'-deoxyuridine and a non-ribosomal derived peptide backbone, which are linked by a enamide bond (Gust, Eitel, and Tang 2013; Rackham et al. 2010; Zhang, Ostash, and Walsh 2010). Recently, the biosynthetic gene clusters for pacidamycins (Rackham et al. 2010; Zhang et al. 2010), napsamycins (Kaysser et al. 2011) and sansanmycins (Li et al. 2013; Shi et al. 2016) were identified and characterized, indicating that the assembly of the pseudo-tetrapeptide chain is catalyzed by a nonribosomal peptide synthetases (NRPSs) with a highly dissociated modules organization (Zhang et al. 2011).

Napsamycins differ from the pacidamycins in some structural features (Figure 6). While the pacidamycins contain an L-alanine and differ in the C-terminal amino acid, the napsamycins and mureidomycins incorporate an L-methionine and a C-terminal meta-tyrosine. An N-terminal bicyclic amino acid, 6-hydroxytetrahydroisoquinolone carboxylic acid, is present in all four known napsamycins but not in mureidomycins (Gust et al. 2013).

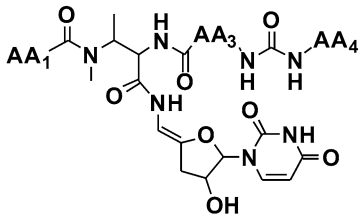

Name	AA_1	AA_3	AA_4
sansanmycin A	*m*-Tyr	Met	Trp
sansanmycin B	*m*-Tyr	Leu	Trp
sansanmycin C	*m*-Tyr	Met^{SO}	Trp
sansanmycin H	*m*-Tyr	Met	Tyr
sansanmycin I	*m*-Tyr	Phe	Trp
sansanmycin J	bicyclic b	Met	Tyr
sansanmycin M	bicyclic a	Phe	Trp
pacidamycin 4	*m*-Tyr	Ala	Trp
pacidamycin 4N	bicyclic a	Ala	Trp
pacidamycin D	Ala	Ala	Trp
pacidamycin S	Ala	Ala	Phe
napsamycin A	bicyclic b	Met	*m*-Tyr
mureidomycin A	*m*-Tyr	Met	*m*-Tyr
mureidomycin E	bicyclic a	Met	*m*-Tyr

Met^{SO}: methionine sulfoxide

bicyclic a bicyclic b

Figure 6. Structures of known uridylpeptide antibiotics

(Shi et al. 2016)

The second class of nucleoside antibiotics are the liponucleoside antibiotics. These can further be subdivided into the tunicamycin-type and the liposidomycin-type. The tunicamycin-type comprises the tunicamycins, the streptoviridins and the corynetoxins (Figure 7) as they contain an additional N-acetyl- glucosamine moiety and a unique 11-carbon dialdose sugar, which is called tunicamine (Gust et al. 2013). The liponucleoside antibiotics of the liposidomycin-type include the caprazamycins, the liposidomycins and A-90289 (Figure 8). They all share structural features such as uridyl, aminoribosyl, fatty acyl-moieties and the (+)-caprazol core skeleton (Gust et al. 2013).

a

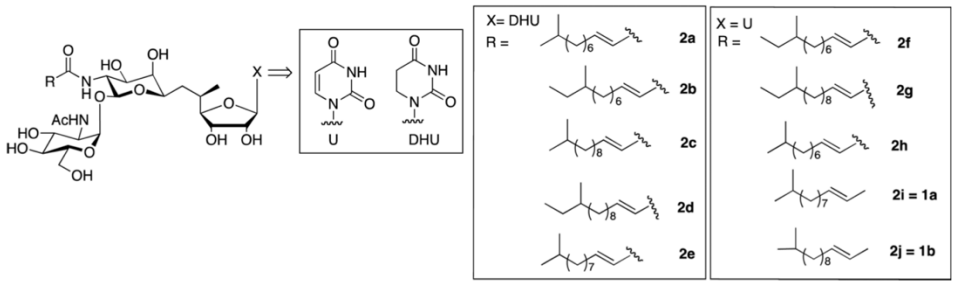

b

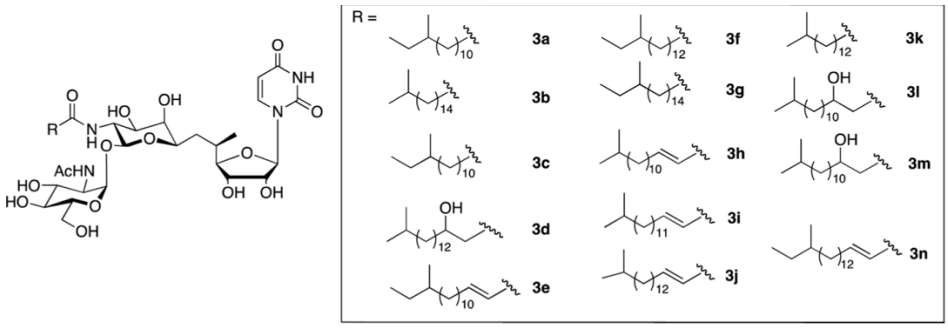

Figure 7. a) Structures of streptovirudins 2a−j. b) Structures of corynetoxins 3a−n

(Serpi, Ferrari, and Pertusati 2016)

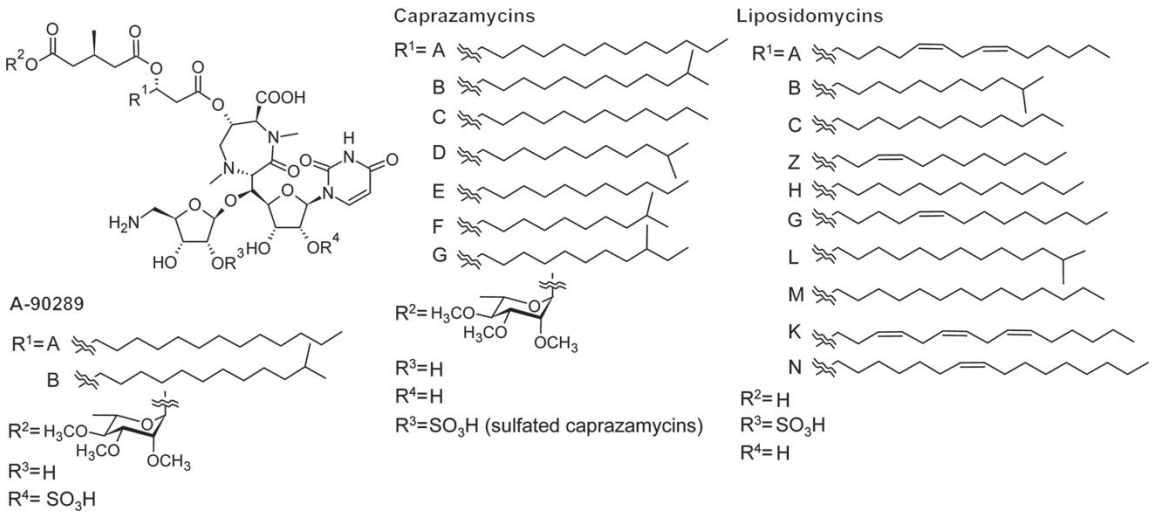

Figure 8. Structures of liponucleoside antibiotics

(Gust, Eitel and Tang 2013)

The third class represent the capuramycin-type of compounds (Figure 9) as capuramycin. A-500359s, A-503083 and the muraymycins cannot be classified into these groups (Gust et al. 2013).

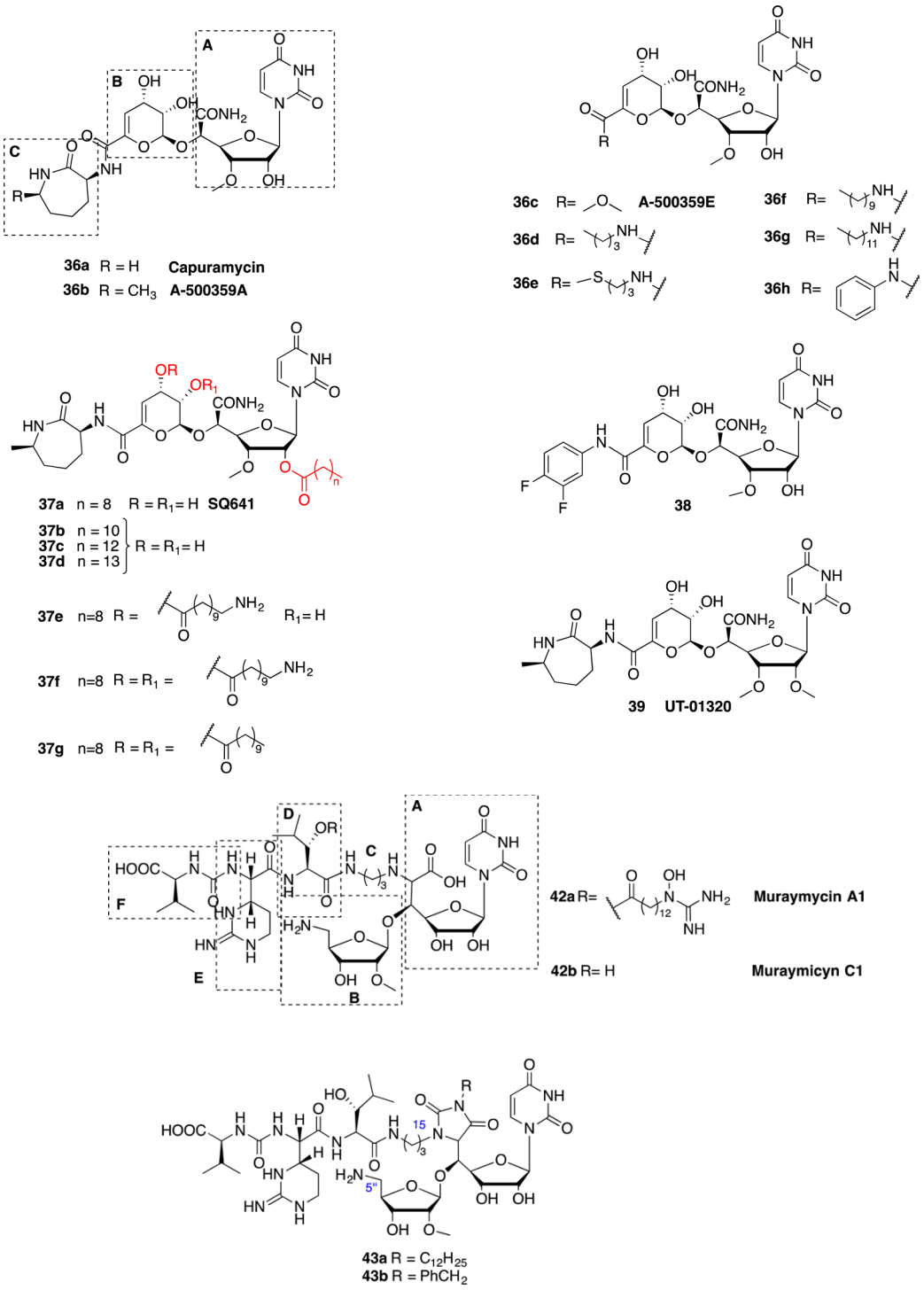

Figure 9. Structured of capuramycin analogues 36a−h, 37a−g, and 39. Muraymycins 42a-43b.

(Serpi et al. 2016)

1.5.1 Caprazamycin biosynthesis

Heterologous expression of the caprazamycin gene cluster from *Streptomyces* sp. MK730-62F2 in *Streptomyces coelicolor* M512 resulted in the production of caprazamycin aglycones lacking the permethylated L-rhamnose. The genes required for biosynthesis of the L-rhamose were identified elsewhere on the genome of the wildtype producer *S.* sp. MK730-62F2 and were assembled to the cloned CPZ gene cluster. Heterologous expression of the completed gene cluster now readily led to the accumulation of intact caprazamycins (Figure 10) (Kaysser et al. 2009; Kaysser, Wemakor, et al. 2010).

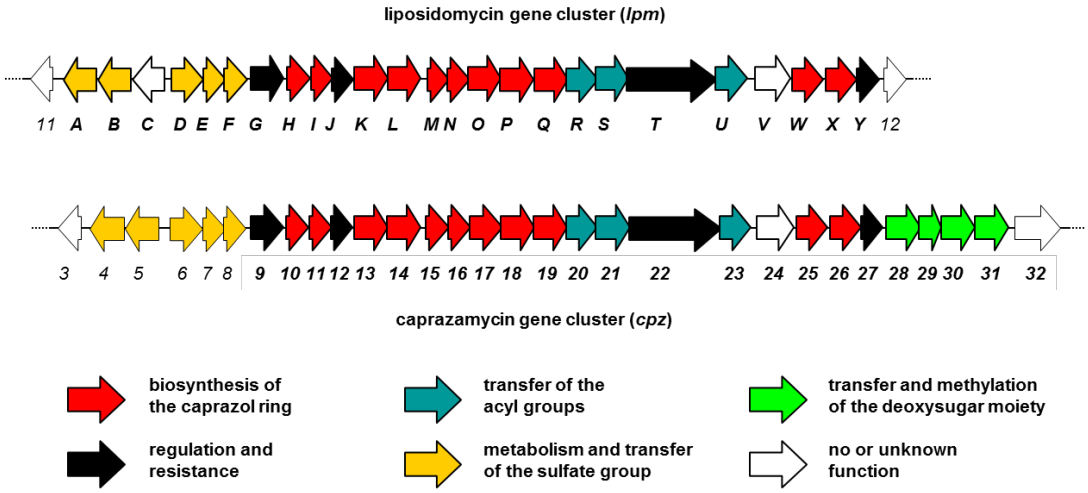

Figure 10. Organization of the liposidomycin and the caprazamycin gene cluster

Assignment of genes to different steps of their biosynthesis is indicated by different colors.

A cosmid-clone harboring the entire caprazamycin gene cluster was obtained by generation and screening of a cosmid library. In-frame deletions were generated for most genes by the use of Red/ET recombination (Gust et al. 2003). The mutagenized cosmids were then introduced into the heterologous producer strain, *Streptomyces coelicolor* M512, to elucidate the currently proposed biosynthesis of caprazamycins (Figure 11) (McErlean et al. 2021).

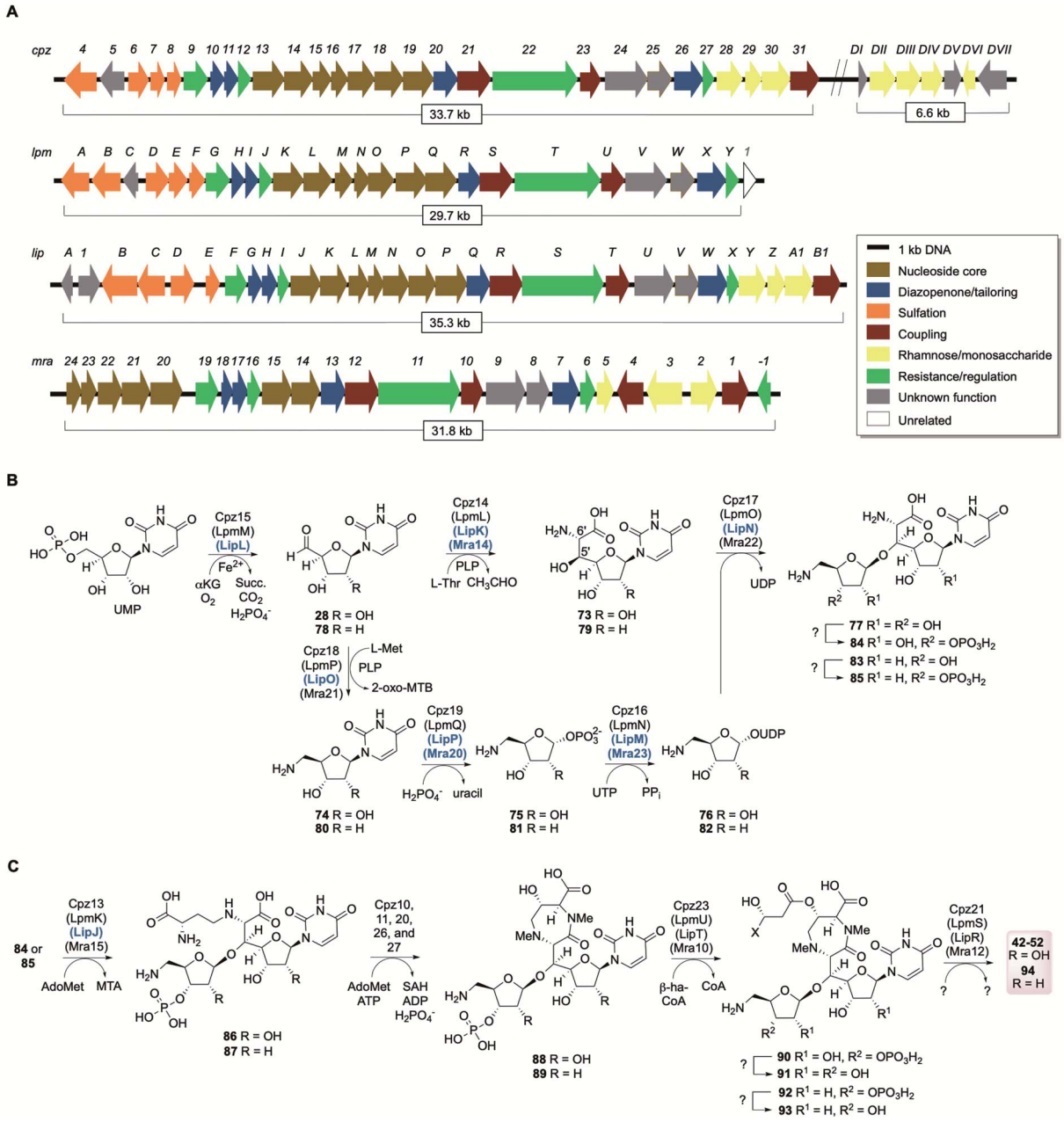

Figure 11. Biosynthetic gene clusters and proposed biosynthesis of liponucleoside antibiotics
(McErlean et al. 2021).

(A) Genetic organization of liponucleoside biosynthetic gene clusters. NCBI accession numbers are caprazamycin (*cpz*) from *Streptomyces* sp. MK730F-62F2, FJ490409 and HM051054; liposidomycin (lpm) from *Streptomyces griseoporeus*, GU219978; A-90289 (lip) from *Streptomyces* sp. SANK 60405, AB530986; muraminomicin (mra) from *Streptosporangium amethystogenes* SANK 60709, AB746937. (B) Pathway for the biosynthesis of the disaccharide core structure. (C) Pathway for the biosynthesis of the diazapenone ring and subsequent acylation steps. Proteins labelled in bold blue have been functionally assigned in vitro using recombinant enzymes. Orthologs of the respective caprazamycin proteins are indicated in parenthesis. X (90–93) indicated the different saturated or unsaturated aliphatic chains. aKG, a-ketoglutarate; PPi, inorganic pyrophosphate; Succ., succinate; 2-oxo-MTB, 2-oxo-4- methylthio-butanoate; MTA,

methylthioadenosine; AdoMet, S-adenosyl-L-methionine; SAH, S-adenosyl-L-homocysteine; PLP, pyridoxal-50- phosphate; CoA, coenzyme A; b-ha-CoA b-hydroxyacyl-CoA. *Respective homologs are LpmH, I, R, X, and Y; LipG, H, Q, W, and X; Mra18, 17, 13, 7, and 6.

1.6 Self-resistance mechanisms against liponucleoside antibiotics

Tunicamycin is an antibiotic that was first discovered in the early 1970s (Takatsuki, Arima, and Tamura 1971). The compound is composed of an uracil base, the sugar tunicamine, N-acetylglucosamine and a fatty acid (Figure 12).

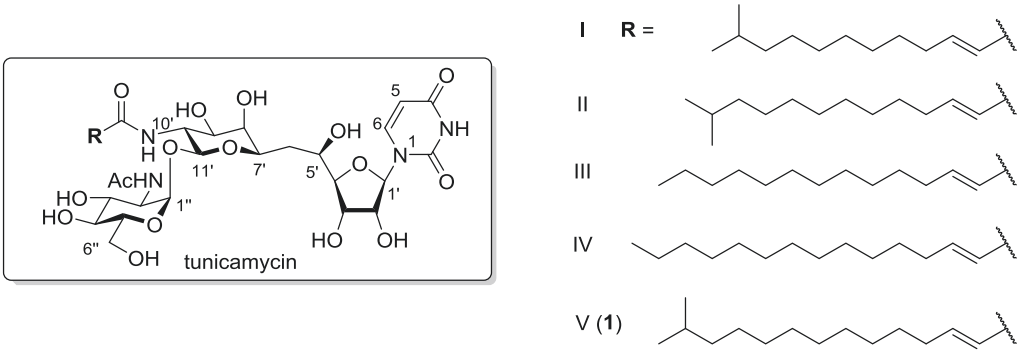

Figure 12. Structures of tunicamycins

(Yamamoto and Ichikawa 2019)

Tunicamycin-resistant strains of *Bacillus subtilis* have been identified (Nomura et al. 1978) and the gene, tmrB, that confers resistance to tunicamycin has been sequenced. It encodes for a protein of approximately 22 kDa. Later, tmrB-like sequences were also identified in a number of other bacterial genomes; however, the exact function of TmrB remained unknown. Some studies have shown the *B. subtilis* protein to be an ATP-binding membrane protein (Noda et al. 1992) and to directly bind tunicamycin (Noda et al. 1995). Another TmrB-like protein, DR_1419 from *Deinococcus radiodurans* was crystallized and its X-ray crystal structure was determined to 1.95 Å resolution (Kapp et al. 2008). The structure reveals strong structural similarity to the family of nucleoside monophosphate kinases and to the chloramphenicol phosphotransferase of *Streptomyces venezuelae*, suggesting that the mode of action is possibly a phosphorylation.

Recently, a comparison of nucleoside BGCs was reported and suggests the conservation of kinases in ~60% of all reported nucleoside natural product biosynthetic pathways. Since most of these kinases are uncharacterized, this cryptic phosphorylation may be relevant to the biosynthesis of many nucleoside natural products (Draelos et al., 2021). The

phosphotransferase CapB was shown to confer selective self-resistance to the nucleoside antibiotics capuramycin (Yang et al., 2010a) by selectively transferring the γ-phosphate to the 3´´-hydroxyl of the unsaturated hexuronic acid moiety. However, no TmrB-like protein was discovered within three tunicamycin BGCs from different producer organisms, instead an ABC-transporter and a putative S-adenosylmethionine (SAM)-dependent methyltransferase are proposed to be involved in the main self-resistance mechanism (Wyszynski et al., 2012). For another MraY translocase inhibitor, the muraymycins, Mur29 and Mur28 catalyze two types of covalent modifications that are commonplace for aminoglycoside resistance, namely, nucleotidylation and phosphorylation. Interestingly, both reactions covalently modify the same site, the 3´´-OH of the 5-amino-5-deoxyribose (ADR) component of muraymycins (Cui et al., 2018b). First, the Mg·ATP-dependent phosphotransferase Mur28 modifies the biosynthetic intermediate ADR-GlyU disaccharide. Then, the aminopropyl-linked peptide is attached to ADR-GlyU resulting in a compound with increased bioactivity (muraymycin D series). Finally, the Mg·ATP-dependent nucleotidyl-transferase Mur29 catalyzes the adenylation at the same site thereby reducing MraY inhibition 170-fold. Therefore, both enzymes are serving as complementary self-resistance mechanisms with a distinct temporal order.

The biosynthetic gene clusters of caprazamycins and liposidomycins each contain two TmrB-like homologues (*cpz12* & *cpz27*; *lpmJ* & *lpmY*), which functions are unknown to date.

A

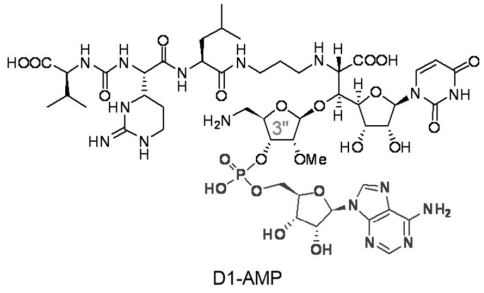

B

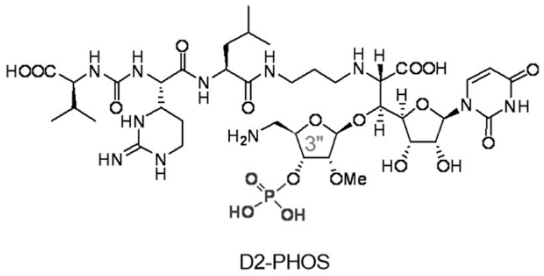

Figure 13. (A) Structure of 3-phospho-muraymycin D2 catalyzed by *mur*28. (B) Structure of 3-monoadenylated muramycin D1 catalyzed by *mur*29.

(Cui, Wang, et al. 2018).

Aims of this study

The general objective of this study was the investigation of two phosphotransferases, Cpz12 and Cpz27 together with the ABC-transporter Cpz22 regarding their function as self-resistance determinant and/or their function in caprazamycin biosynthesis. First, bioinformatic analysis tools such as phylogenetics, AntiSMASH or Multigeneblast were used to gain further information's for the aforementioned proteins or corresponding genes. A protein modeling approach, including TMD and NBD analysis should allowed the assignment of Cpz22 to a certain class of ABC-transporters. For investigation of their biological roles, knock-out mutants were generated by Red/ET recombination, including *cpz12*, *cpz22*, *cpz23, cpz27*, *cpz12*/*cpz27* and *cpz23*/*cpz4* to generate mutants containing in-frame deletion(s) of the corresponding genes. A comparison of the received extracts from WT vs. mutant was undertaken by HPLC and LC-ESI/MS. If new metabolites were identified, purification was followed by HPLC, LC-ESI/MS and NMR analysis. Deletion of *cpz27* on cosmid cpzLK09 containing the entire caprazamycin gene cluster was possible in *E. coli*, however did not resulted in obtaining exconjugants of *S. coelicolor* M512 after conjugation. Therefore, a *cpz27*/*cpz12* double-mutant was generated in order to study the possibility that a biological inactive biosynthetic intermediate might be generated by the *cpz12*-deletion and consequently would allow *cpz27* to be deleted in this background. The double mutants *cpz23*/*cpz4* was expected to produce phosphorylated and non-phosphorylated (+)-caprazol due to the deletion of the lipase Cpz23. *cpz4* was deleted in addition to facilitate analysis of phosphorylates compounds by eliminating the possibility of sulfated compounds to be produced in addition.

To complement the function of the deletion-mutants, plasmids containing intact copies of *cpz12*, *cpz27* or *cpz22* were generated with vector pUWL-apra-oriT and introduced into the corresponding *S. coelicolor* M512 mutants. The generated plasmids were also used to be introduced into the heterologous host containing the un-modified caprazamycin gene cluster to determine the effect of over-expression. The over-expression mutants were used for minimal inhibitory concentration (MIC) determinations using different concentration of caprazamycin-aglycones and hydroxyacylcaprazols.

Finally, biochemical evidence should be provided for Cpz12 and Cpz27 to act as phosphotransferases. First, both genes were cloned into vector pHIS8 for *E. coli* Rosetta™(DE3) expression or the shuttle-vector pGM1192 for heterologous expression in *Streptomyces lividans* TK24. The latter experiment was done as part of the master thesis of Ms. Julia Höfer Purified proteins were used for TmrB-like enzyme assays with ATP and

purified hydroxyacylcaprazols, caprazamycin-aglycones or other biosynthetic intermediates as substrates. The same biochemical studies were performed for the lipase Cpz23 by Mr. Cedric Funck as part of his mater thesis.

2. Materials and methods

2.1 Columns, reagents, enzymes and kits

Table 2. Columns for analytical chromatography

Name	Supplier
HPLC column Reprosil Pur Basic-C18 (250mm x 2 mm, 5µm)	Maisch, Ammerbuch
Nucleodur PolarTec (250mm x 4,6 mm, 5µm)	Macherey-Nagel
Nucleodur PolarTec (250mm x 10 mm, 5µm)	Macherey-Nagel
Luna Omega Polar C18 (250mm x 4,6 mm, 3µm)	Phenomenex
HisTrap $^{I\,M}$ HP (5 mL) column	GE Healthcare
Atlantis HILIC Silica Column 4.6 x 250 mm 5µm	Waters Corporation

Table 3. Primers designed in this study

Name	Sequence (5'-3')
∆ *cpz* 12 F	GGACAGGGACGTCCACGTGCTGTTCCGGGTGAGCCG GTGAATTCCGGGGATCCGTCGACC
∆ *cpz* 12 R	CGGCCGGGACGGGCGGGTACGGAGGTCCGGCCCAG GTCCTGTAGGCTGGAGCTGCTTC
∆ *cpz* 22 F	GGCAGCGGGCCGGTGGAGAGGCGAGGACCACCGGT GGTGAATTCCGGGGATCCGTCGACC
∆ *cpz* 22 R	CGTTGAACCTGAACTCCTCGCCGTGCGTCAACGACTT CACTGTAGGCTGGAGCTGCTTC
∆ *cpz* 27 F	GGTGCTGCGCCGCACACCGCCCCCGGCCGACCACGT GACCGCTAGCATTCCGGGGATCCGTCGACC
∆ *cpz* 27 R	CACGCGTGCGGCGCCGGCGCGGAGCGCCTGACGGAT GTCAACTAGTTGTAGGCTGGAGCTGCTTC
∆ *cpz* 23 F	GAGCAACGAGCAACCCAGGACAAGGAGACGAAGCGT GAAGGCTAGCATTCCGGGGATCCGTCGACC
∆ *cpz* 23 R	TCGTCATGTGTGGCTGTTCGTCACGGGGCCGAGCGGT TCAACTAGTTGTAGGCTGGAGCTGCTTC
pUWL *cpz* 12 F	AAAAA AAGCTT GTGATCATCGTCGTCACGGGCCC
pUWL cpz 12 R	AAAAA GAATTC TCATGTGGCTGCCTCCGCCG
pUWL *cpz* 22 F	AAAAA AAGCTT GTGAGCACGGAAGTGCGGGT
pUWL *cpz* 22 R	AAAAA GAATTCTCACGCTTCGTCTCCTTGTCCTGG
pUWL *cpz* 27 F	AAAAA AAGCTT GTGACCAGGACGGAGAAGCCCTTG
pUWL *cpz* 27 R	AAAAA GAATTC TCAGGCCTTTCCGGTGCGCC
pUWL *cos*IJ F	AAAAA AAGCTTATGGGCGGCGCCGACCTGG
pUWL *cos*IJ R	AAAAA GAATTCTTACCTGCTCAGGGCCCGGT

pUWL *cos*P F	AAAAA AAGCTTATGACCGTCTTCGACATCGC
pUWL *cos*P R	AAAAA GAATTCTCACTGCACCTGCGCGC
pUWL *cos*U F	AAAAA AAGCTTGTGAACCAGACGCCGGTCAC
pUWL *cos*U R	AAAAA GAATTCGCCTCTACCTGGCCCAGTAG
pHIS8 *cpz* 12 F	AAAAA GAATTC GTGATCATCGTCGTCACGGGCCC
pHIS8 *cpz* 12 R	AAAAA AAGCTTTCATGTGGCTGCCTCCGCCG
pHIS8 *cpz* 22 F	AAAAA GAATTC GTGAGCACGGAAGTGCGGGT
pHIS8 *cpz* 22 R	AAAAA AAGCTTTCACGCTTCGTCTCCTTGTCCTGG
pHIS8 *cpz* 23 F	AAAAAGAATTCGTGAAGTCGTTGACGCACGGCGA
pHIS8 *cpz* 23 R	AAAAAAAGCTTTCATCCGAGGCACTTCCGGATGC
pHIS8 *cpz* 27 F	AAAAA GAATTC GTGACCAGGACGGAGAAGCCCTTG
pHIS8 *cpz* 27 R	AAAAA AAGCTTTCAGGCCTTTCCGGTGCGCC
pHIS8 *cos*P F	AAAAAGAATTCATGACCGTCTTCGACATCGC
pHIS8 *cos*P R	AAAAAAAGCTTTCACTGCACCTGCGCGC
Site mutagenesis cosP F	AACGTCGCCTCCCGCTCCGCCCTGG
Site mutagenesis cosP R	CTGGCCGGCCAGGGCGGAGC
pGM *cpz* 12 F	AAAAAACATATGCACCACCACCACCACCACCACCACCT GGTTC CGCGTGGTTCCATGATCATCGTCGTCACGGGCCC
pGM *cpz* 12 R	AAAAAAAAGCTTTCATGTGGCTGCCTCCGCCG
pGM *cpz* 27 F	AAAAAACATATGCACCACCACCACCACCACCACCACCT GGTTC CGCGTGGTTCCATGACCAGGACGGAGAAGCCCTT
pGM cpz 27 R	AAAAAAAAGCTTTCAGGCCTTTCCGGTGCGCC
pUWL test F	ACGCCTGGTCGATGTCGGAC
pUWL test R	GCTCTTCCGCTTCCTCGCTC
T7 test F	GGTTATGCTAGTTATTGCTCAGC
T7 test R	ATCTCGATCCCGCGAAATTAATAC
pGM1190 test F	GATCGGGGATCTGGGCTGAG
pGM1190 test R	GGGAATTCGAGCTCGGTACC
pGM1192 test F	GAAACAGCTATGACCATGATTACGA
pGM1192 test F	TTCTCACTCCGCTGAAACTGT
Δ *cpz* 12 test F	AAAGGACCTGCCAGGATTCG
Δ *cpz* 12 test R	CTCGAAGGCGTAGTAGCACG
Δ *cpz* 22 test F1	GTTCTTCCTCTCTCCGGTGC
Δ *cpz* 22 test R1	TGGCGAACACGATGAACGTA

Δ *cpz* 22 test F2	AGCGTCGGTACGTTCATCG
Δ *cpz* 22 test R2	GAGCACTGACTTGCCGGAC
Δ *cpz* 22 test F3	GAGGTCAGGCGAGGAGAATG
Δ *cpz* 22 test R3	CGACGACTTCGACCCCTATG
Δ *cpz* 22 test F4	TGTGCATAGGGGTCGAAGTC
Δ *cpz* 22 test R4	GCACCTTCTCGTACAGGTCG
Δ *cpz* 22 test F5	GTACCAGAAGGTGCACGGAG
Δ *cpz* 22 test R5	ACACGTACAGGATGAGTGCG
Δ *cpz* 22 test F6	ATGACCATCGACATGGCACT
Δ *cpz* 22 test R6	ATCATTTCCGACGCACCGAA
Δ *cpz* 23 test F	CAAGACCGTCGTGGTCGCC
Δ *cpz* 23 test R	CGTTCTCCTCGGGTACGTCC
Δ *cpz* 27 test F	CGAAGTGGCCGGGAGAAG
Δ *cpz* 27 test R	ACCAGGACCGAGGTGAGTT
Δ *cpz* 4 test F	CCGGCGAGAAGGTGAACAC
Δ *cpz* 4 test R	CGGCCACAAACGTGTCTAC
q *cosI* F	GATCCAGACCGAAGCTCTGA
q *cosI* R	TTCCCTCGTCGTACTTCAGC
q *cosJ* F	ATCCTGATGGTGCTGCTGTT
q *cosJ* R	AGCATGTTGACGATGCTCTG
q *cosP* F	CCTGCTCATCGTCAACGTC
q *cosP* R	GTGAGGGGGAACGTGATCT
q *cosU* F	CCAGACCTGGCTCTACTCCTT
q *cosU R*	TAGTCCGCGAGCTTCTTCTC
q HrdB F	TGCACATGGTCGAGGTCATC
q HrdB R	TCATGTCGAGTTCCTTGGCC

All primers were dissolved in water (MilliQ) at a concentration of 100 pmol/µL and stored at 20°C.

Table 4. Reagents

Name	Supplier
Agar	Bacto-Difco
Acetic Acid	Sigma-Aldrich
Acetonitrile (ACN)	VWR
Agarose	Amersham Biosciences
Ammoniumpersulfate (APS)	Sigma-Aldrich
Apramycin	Fluca
Bromphenol Blue	Roth
Butan-1ol	VWR
Calcium chloride	Sigma-Aldrich
Casaminoacids	Bacto-Difco
Carbenicillin	Roth
Chloramphenicol	Merck
Comassie Brilliant Blue G250	Merck
Comassie Brilliant Blue R250	Merck
Diemethyl sulfoxide (DMSO)	Sigma-Aldrich
Dipotassium phosphate (KH_2PO_4)	Merck
Disodium phosphate	Merck
Doxorubicin	Sigma-Aldrich
dNTP mix	Bioline
Ethanol	Roth
Ethylene-diamine tetraacetic acid (EDTA)	Roth
Ethylacetate HPLC grade	Sigma-Aldrich
Formic acid	Sigma-Aldrich
Glycerol	Roth
Glycine	Roth
Imidazole	Sigma-Aldrich
Kanamycin	Sigma-Aldrich
Iron (III) chloride ($FeCl_3$)	Sigma-Aldrich
L-proline	Calbiochem
L-alanine	Merck
L-arabinose	Sigma-Aldrich
Lysozyme	Fluka
β-mercaptoethanol	VWR

Magnesium chloride ($MgCl_2$)	Sigma-Aldrich
Mannitol	Roth
Malt extract	Bacto-Difco
Maltose	Merck
Methanol LC-MS grade	Merck
Monopotassium phosphate (KH_2PO_4)	Roth
Nalidixic acid	Sigma-Aldrich
Nickel (III) chloride ($NiCl_3$)	Roth
Peptone	Bacto-Difco
Phenol/Chlorophorm/Isoamylalcohol	Roth
Phenylmethanesulfonyl fluoride (PMSF)	Sigma-Aldrich
Potassium acetate (KAc)	Roth
Potassium sulphate (K_2SO_4)	Fluka
2- Propanol	Sigma-Aldrich
Rotiphorese® Gel 30	Roth
Sodium chloride (NaCl)	Sigma-Aldrich
Sodium dodecyl sulphate (SDS) 20%	Roth
Sodium hydroxide (NaOH)	Sigma-Aldrich
Sorbitol	Roth
Soy flour	SOBO naturkost
Tetramethyl ethylendiamine (TEMED)	Fluka
Tryptone soy broth	Bacto-Difco
Trizma-base	Sigma-Aldrich
Tryptone	Bacto-Difco
Yeast extract	Bacto-Difco
Zinc chloride ($ZnCl_2$)	Sigma-Aldrich

Table 5. Enzymes and kits

Name	**Supplier**
Restriction endonucleases	New England Biolabs
T4-DNA-Ligase	New England Biolabs
Lysozyme	Fluka
Phusion® High-Fidelity DNA Polymerase	New England Biolabs
Q5® High-Fidelity DNA Polymerase	New England Biolabs

Taq DNA-Polymerase	New England Biolabs
RNase A 100 mg/mL	Macherey-Nagel
Cre Recombinase	New England Biolabs
1 Kb DNA ladder	Invitrogen
Ni-NTA Agarose	Qiagen
T4 DNA Ligase	New England Biolabs
Zeba Spin Desalting Columns	Thermo Fisher Scientific
Acyl-Coenzyme A Synthetase	Merck
QIAquick Purification Kit	Qiagen
Color Prestained Protein Standard, Broad Range (10-250 kDa)	New England Biolabs
QuikChange II Site-Directed Mutagenesis Kit	Agilent Technologies
[PM2510] ExcelBand™ Enhanced 3-color Regular Range Protein Marker (9-180 kDa)	SMOBIO Technology, Inc

2.2 Vectors and strains

2.2.1 Plasmids and cosmids

Table 6. Plasmids used in this study

Name	Description	Source or reference
pIJ773	pBS SK (+)-derivative, P1-FRT-oriT-*aac(3)IV*-FRT-P2	(Gust et al. 2003)
pIJ774	pBS SK (+)-derivative, P1-loxP-oriT-*aac(3)IV*-loxP-P2	(Gust et al. 2003)
pGEM®-T	Linearized cloning vector with T-overhangs for direct cloning of PCR- products with A-overhangs, *lacZ'*, ori, f1-origin, $Carb^R$	Promega
pHis8	Expression vector; pET-28a (+) (Merck) derivative, N-terminal His_8-tag and C-terminal His_6-tag, T7 promotor, Kan^R	(Jez, Bowman, and Noel 2001)
pUWL-apra-oriT	*E. coli - Streptomyces* shuttle vector, pUWL201 derivative, *ermE** promotor, colE1, rep; Amp^R, $Apra^R$	Andreas Günther, Universität Frankfurt
pGM1190	OriT shuttle vector for induced gene expression in *Streptomyces*	Günther Muth Universität Tübingen

pGM1192	Shuttle vector, expression vector for *Streptomyces*, SF14* promoter, Strep-tag II-mCherry, *aac(3)IV*, Tsr^R, $Apra^R$	Günther Muth Universität Tübingen
pRCWL01	PCR product from gDNA of cpzLK09 cosmid comprising *cpz12* flanked by *Hind*III/*EcoRI* restriction sites in pUWL-apra-oriT, $Apra^R$	This study
pRCWL02	PCR product from gDNA of cpzLK09 cosmid comprising *cpz22* flanked by *Hind*III/*EcoRI* restriction sites in pUWL-apra-oriT, $Apra^R$	This study
pRCWL03	PCR product from gDNA of cpzLK09 cosmid comprising *cpz27* flanked by *Hind*III/*EcoRI* restriction sites in pUWL-apra-oriT, $Apra^R$	This study
pRCWL04	PCR product from gDNA of *Streptomyces olindensis* comprising *cos*lJ flanked by *Hind*III/*EcoRI* restriction sites in pUWL-apra-oriT, $Apra^R$	This study
pRCWL05	PCR product from gDNA of *Streptomyces olindensis* comprising *cos*P flanked by *Hind*III/*EcoRI* restriction sites in pUWL-apra-oriT, $Apra^R$	This study
pRCWL06	PCR product from gDNA of *Streptomyces olindensis* comprising *cos*U flanked by *Hind*III/*EcoRI* restriction sites in pUWL-apra-oriT, $Apra^R$	This study
pCFIS01	PCR product from gDNA of *Streptomyces olindensis* comprising *cpz23* flanked by *Hind*III/*EcoRI* restriction sites in pUWL-apra-oriT, $Apra^R$	Cedric Funck
pRCHIS01	PCR product from gDNA of *Streptomyces sp. MK730-62F2* comprising *cpz12* flanked by *EcoRI* / *Hind*III restriction sites in pHis8, Kan^R	This study
pRCIS02	PCR product from gDNA of *Streptomyces sp. MK730-62F2* comprising *cpz22* flanked by *EcoRI* / *Hind*III restriction sites in pHis8, Kan^R	This study
pRCIS03	PCR product from gDNA of *Streptomyces* sp. MK730-62F2 comprising *cpz*27 flanked by *EcoR*I / *Hind*III restriction sites in pHis8, Kan^R	This study
pRCIS04	PCR product from gDNA of *Streptomyces olindensis* comprising *cosP* flanked by *EcoR*I / *Hind*III restriction sites in pHis8, Kan^R	This study

pRCIS04M	Site mutagenesis from pRCIS04 comprising *cosP* C38S flanked by *EcoR*I / *Hind*III restriction sites in pHis8, Kan^R	This study
pJH01	PCR product from gDNA of *Streptomyces* sp. MK730-62F2 comprising *cpz*12 flanked by *Nde*I / *Hind*III restriction sites in pGM1190, Tsr^R, $Apra^R$	Julia Höfer
pJH02	PCR product from gDNA of *Streptomyces* sp. MK730-62F2 comprising *cpz*27 flanked by *Nde*I / *Hind*III restriction sites in pGM1190, Tsr^R, $Apra^R$	Julia Höfer
pJH03	PCR product from gDNA of *Streptomyces* sp. MK730-62F2 comprising *cpz*12 flanked by *Nde*I / *Hind*III restriction sites in pGM1192, Tsr^R, $Apra^R$	Julia Höfer
pJH04	PCR product from gDNA of *Streptomyces* sp. MK730-62F2 comprising *cpz*27 flanked by *Nde*I / *Hind*III restriction sites in pGM1192, Tsr^R, $Apra^R$	Julia Höfer

Table 7. Cosmids used in this study

Name	Description	Source or reference
cpzLK09	from 31C2; *bla* gene replaced by cassette from pIJ787 (oriT, tet, attP, int RR φC31); Tet, Kan^R	(Kaysser, Siebenberg, et al. 2010)
pCRD1	cpzLK09 derivative, Δ*cpz12* (scar); Kan^R	This study
pCRD2	cpzLK09 derivative, Δ*cpz22* (scar); Kan^R	This study
pCRD3	cpzLK09 derivative, Δ*cpz27* (scar); Kan^R	This study
pCRD4	cpzLK09 derivative, Δ*cpz23* (scar); Kan^R	This study
pCRD5	cpzLK09 derivative, *cpz27/cpz*12 (scar); Kan^R	Cedric Funck
pCRD6	cpzLK09 derivative, Δ*cpz23/cpz4* (scar); Kan^R	Cedric Funck

2.2.2 Strains

Escherichia coli strains

Table 8. *E. coli* strains used in this study

Name	Description	Source or reference
E. coli XL1 blue MRF^{-}	*rec*A1 *end*A1 gyrA96 *hsd* R17 *sup*E44 *thi-* 1 *rel*A1 lac [F'proAB lacI^{q}Z ΔM15, Tn10, (Tet^{R})]	Stratagene
E. coli ET 12567	*dam, dcm hsdM, hsdS, hsdR,* Tet^{R}, Cm^{R}	(MacNeil et al. 1992)
E. coli BW25113/pIJ790	K-12 Derivat: *ΔaraBAD, ΔrhaBAD* Kan^{R} recombination plasmid: λ/RED (*gam, bet, exo*), *araC, rep101^{ts}* Cm^{R}	(Datsenko and Wanner 2000; Gust et al. 2003)
E. coli ET 12567/pUZ8002	*dam, dcm hsdM, hsdS, hsdR,* Tet^{R}, Cm^{R}; conjugation plasmid: *tra*, RP4 Kan^{R}	(Paget et al. 1999)
E. coli ET 12567/pUB307	*dam, dcm hsdM, hsdS, hsdR,* Tet^{R}, Cm^{R}; conjugation plasmid: *tra*, RP4, *oriT* Kan^{R}	(Flett, Mersinias, and Smith 1997)
E. coli BT340	DH5α/pCP20	(Cherepanov and Wackernagel 1995)
E. coli Rosetta (DE3) pLysS	Host for the heterologous expression of His8 tagged proteins (F- *omp*T *hsd*SB (rB- mB-) *gal dcm* λ (DE3 [*lacI lacUV5-T7* gene 1 *ind1 sam7 nin5*]) pLysSRARE); Cm^{R}	Invitrogen
E. coli Rosetta (DE3) pLysS (pRCHIS01)	*E. coli* Rosetta (DE3) with pRCHIS01 protein expression plasmid	This study
E. coli Rosetta (DE3) pLysS (pRCHIS02)	*E. coli* Rosetta (DE3) with pRCHIS02 protein expression plasmid	This study
E. coli Rosetta (DE3) pLysS (pRCHIS03)	*E. coli* Rosetta (DE3) with pRCHIS03 protein expression plasmid	This study
E. coli Rosetta (DE3) pLysS (pRCHIS04)	*E. coli* Rosetta (DE3) with pRCHIS04 protein expression plasmid	This study

E. coli Rosetta (DE3) pLysS (pCFIS01)	*E. coli* Rosetta (DE3) with pCFIS01protein expression plasmid	Cedric Funck

Table 9. *Streptomyces* strains used in this study

Name	Description	Source or reference
S. coelicolor M512	*S. coelicolor* A3(2) derivate, SCP1, SCP2, *ΔredD, ΔactII-ORF4*	(Floriano and Bibb 1996)
S. coelicolor M512(LK09)	*S. coelicolor* M512 with cpzLK09 cosmid, Kan^R	(Kaysser, Siebenberg, et al. 2010)
S. coelicolor M512 Δ*cpz12* (pCRD1)	*S. coelicolor* M512 with pCRD1 cosmid, Kan^R	This study
S. coelicolor M512 Δ*cpz22* (pCRD2)	*S. coelicolor* M512 with pCRD2 cosmid, Kan^R	This study
S. coelicolor M512 Δ*cpz23* (pCRD4)	*S. coelicolor* M512 with pCRD4 cosmid, Kan^R	This study
S. coelicolor M512 Δ*cpz27/cpz*12 (pCRD5)	*S. coelicolor* M512 with pCRD5 cosmid, Kan^R	Cedric Funck Master thesis
S. coelicolor M512 Δ*cpz23/cpz4* (pCRD6)	*S. coelicolor* M512 with pCRD6 cosmid, Kan^R	Cedric Funck Master thesis
S. coelicolor M512(pRCWL01)	*S. coelicolor* M512 with pRCWL01 plasmid, $Apra^R$	This study
S. coelicolor M512(pRCWL02)	*S. coelicolor* M512 with pRCWL02 plasmid, $Apra^R$	This study
S. coelicolor M512(pRCWL03)	*S. coelicolor* M512 with pRCWL03 plasmid, $Apra^R$	This study
S. lividans TK24	*Str-6, tipAp induced, SLP2-, SLP3-*	(Eustáquio et al. 2005)

S. lividans TK24/ pJH03	*S. lividans* with pJH03 plasmid Tsr^R, $Apra^R$	Julia Höfer, Master thesis
S. lividans TK24/ pJH04	*S. lividans* with pJH04 plasmid Tsr^R, $Apra^R$	Julia Höfer, Master thesis
S. albus J1074	*S. albus* G derivative, defective in SalGI mediated restriction, valine and isoleucine auxothroph	(Chater and Wilde 1980; Zaburannyi et al. 2014)
S. albus J1074/ pJH03	*S. albus* with pJH03 plasmid Tsr^R, $Apra^R$	Julia Höfer, Master thesis
S. olindensis DAUFPE 5622	Wild type	Gabriel Padilla University of São Paulo
Streptomyces peucetius D SM No: 40754	-	German Collection of Microorganisms and Cell Cultures GmbH (DSMZ)
S. albus J1074/ pRCWL04	*S. albus* with pRCWL04 plasmid, $Apra^R$	This study
S. albus J1074/ pRCWL05	*S. albus* with pRCWL05 plasmid, $Apra^R$	This study
S. albus J1074/ pRCWL06	*S. albus* with pRCWL06 plasmid	This study
S. coelicolor M512/Δ*cpz12*/ pRCWL01	*S. coelicolor* M512/Δ*cpz12* with pRCWL01expression plasmid	This study

2.3 Media, buffers and solutions

2.3.1 Media for bacterial cultivation

Cultivation of Escherichia coli

LB (Luria-Bertani) Medium (Sambrook & Russel, 2001)

NaCl	10.0 g
Tryptone	10.0 g
Yeast extract	5.0 g
Agar (solid media)	15.0 g
Water	up to 1000 mL

Adjusted to pH 7, sterilized by autoclaving.

SOB (Super Optimal-Broth) Medium (Sambrook & Russel, 2001)

NaCl	0.5 g
Tryptone	20.0 g
Yeast extract	5.0 g
Agar (solid media)	15.0 g
Water	up to 1000 mL

Adjusted to pH 7, sterilized by autoclaving. Prior use, add 0.5 mL of sterile $MgCl_2$ solution (2 M)

SOC Medium (Sambrook & Russel, 2001)

NaCl	0.5 g
Tryptone	20.0 g
Yeast extract	5.0 g
Agar (solid media)	15.0 g
Water	up to 1000 mL

Adjusted to pH 7, sterilized by autoclaving. Prior to use, add 0.5 mL of sterile $MgCl_2$ solution

(2 M) and 1.0 mL glucose solution (2 M) per 100 mL.

2.3.2 Cultivation of Streptomyces

MS (Mannitol Soya flour) Agar (Kieser et al. 2004)

Mannitol	20.0 g
Soy flour	20.0 g
Agar	20.0 g

The total volume was adjusted to 1 L with tap water and pour 100 mL into 300 mL Erlenmeyer flasks, each containing 2 g agar. Sterilized by autoclaving twice at 115°C for 15 min.

TSB (Tryptone Soy Broth) Medium (Kieser et al. 2004)

Tryptone Soy Broth	30.0 g

Ingredients were dissolved in 1 L water and sterilized by autoclaving.

Caprazamycin and derivates production medium (P-medium) (Fronko et al. 2000)

Soytone	10.0 g
Soluble starch	10.0 g
D-maltose	20.0 g
Trace elements solution	5 mL

Ingredients were dissolved in 1 L water. Adjusted to pH 6.7, sterilized by autoclaving.

R2YE Medium (Kieser et al. 2004)

Sucrose	103.0 g
K2SO4	0.25 g
$MgCl_2$ x 6 H2O	10.12 g
Glucose	10.0 g
Difco Casaminoacids	0.1 g

Ingredients were dissolved in 1 L water and 100 mL of the solution was poured into 300 mL Erlenmeyer flasks. After autoclaving, following sterile solutions were added to each flask:

Difco Yeast extract (10%)	5mL
KH_2PO_4 (0,5%)	1.0 mL
$CaCl_2$ x 2 H_2O	8 mL
L-proline (20%)	1.5 mL
NaOH (1N)	0.5 mL
TES buffer (5,73%, adjusted to pH 7,2)	5.73 g
Trace element solution	0,2 mL

Trace elements solution

$ZnCl_2$	40 mg
$FeCl_3$ x 6 H2O	200 mg
$CuCl_2$ x 2 H2O	10 mg
$MnCl_2$ x 4 H2O	10 mg
$Na_2B_4O_6$ x 10 H_2O	10 mg
$(NH_4)6Mo_7O_{24}$ x 4 H_2O	10 mg

Ingredients were dissolved in 1 L distilled water and sterilized by autoclaving.

Cosmomycin production medium R5M (Furlan et al. 2004)

Glucose	10 g
Yeast extract	5 g
Casamino acids	0,1 g
$MgCl_2$•6H2O.	10,1 g
Adjust pH 7,2 with KOH	

After sterilize add:	
0,5% KH_2PO_4	2,5 mL/L
$CaCl_2$ 5M	1 mL/L
Trace elements	2mL/L

2 X YT medium (Kieser et al., 2000)

Difco Bacto Tryptone	16 g
Difco Bacto yeast extract	10 g

NaCl	5 g
Water	ad 1000 mL

YEME (Yeast Extract – Malt Extract) (Kieser et al., 2000)

Yeast Extract	3.0 g
Peptone	5.0 g
Malt extract	3.0 g
Glucose	10.0 g
Sucrose	340.0 g

Bennet's Agar DSMZ

Beef extract	1.0 g
Glucose	10.0 g
N-Z amine A	
(Enzymatic digest of casein)	2.0 g
Yeast extract	1.0 g
Agar	15.0 g

Ingredients were dissolved in 1 L water. Sterilized by autoclaving. Before use, 5 mL of a sterile 1 M $MgCl_2$ solution

2.4 Antibiotics

Table 10. Antibiotics stocks solutions

Antibiotic	(Stock solution) mg/mL	(medium) µg/mL	Solvent
Apramycin	50	50	water
Carbenicillin	50	50	water
Chloramphenicol	25	25	ethanol
Kanamycin	50	50	water
Tetracycline	25	25	ethanol
Nalidixic acid	25	25	0.3M NaOH

All antibiotics were stored at -20°C.

2.5 Buffers and solutions

2.5.1 Buffers and solutions for plasmid isolation

Table 11. Buffers and solutions for plasmid isolation

*For plasmid isolation from *Streptomyces* strains, Lysozyme 10mg/mL in Sol I was added

Solution	Components	Final concentration	Comments
Sol I	Glucose EDTA Tris (pH 8) RNase A	50 mM 10 mM 5 mM 100 µg/mL	Adjust to pH 8.0. Add RNase directly bevor use
Sol II	NaOH SDS	0,2 N 1% (w/v)	Store at room temperature
Sol III	KAc	3 M	Adjust to pH 4,8 with glacial acetic acid

2.5.2 Buffers and solutions for DNA gel electrophoresis

Table 12. Buffers and solutions for DNA gel electrophoresis

Solution	Components	Final concentration	Comments
50x TAE	Tris Base EDTA	2 M 50 mM	Adjust to pH 8.0 with glacial acetic acid
Loading buffer	Bromophenol blue Xylanol FF Glycerin 98% EDTA Tris-HCl (pH=7,6)	0,03% 0,03% 60% 60 mM 10 mM	Store at 4°C

2.5.3 Buffers for protein purification by nickel affinity chromatography

Table 13. Buffers for protein purification by nickel affinity chromatography

Solution	Components	Final concentration
Lysis buffer	Tris-HCl pH 8 NaCl Glycerin Tween® 20 Imidazol ß-mercaptoethanol Lysozyme PMSF	50 mM 500 mM 10 % (v/v) 1 % (v/v) 20 mM 10 mM 0.5 mg/mL 0.5 mM
Washing buffer	Tris-HCl pH 8 NaCl Glycerin ß-mercaptoethanol	50 mM 500 mM 10 % (v/v) 10 mM
Elution buffer	Tris-HCl pH 8 NaCl Glycerin Imidazol ß-mercaptoethanol	50 mM 500 mM 10 % (v/v) 250 mM 10 mM

Lysozyme, PMSF, imidazole and ß-mercaptoethanol were added directly before use. All buffers were filtrated (4 µm) before use.

Table 14. Buffers and solutions for protein gel electrophoresis (SDS-page)

Solution	Components	Final concentration
10 x electrophoresis buffer	Tris-HCl pH 8.3 Glycin SDS	250 mM 1.5 M 1 %
Stacking gel (4 % (w/v))	Tris-HCl pH 6.8 Rotiphorese® Gel 30 SDS TEMED Ammoniumpersulfate	125 mM 4 % (w/v) 0.1 % (w/v) 1 mL/L 0.1 % (w/v)

Table 15. Solutions for protein gel electrophoresis

Solution	Components	Final concentration
Resolving gel (12 % (w/v))	Tris-HCl pH 6.8 Rotiphorese® Gel 30 SDS TEMED Ammoniumpersulfate	375 mM 12 % (w/v) 0.1 % (w/v) 1 ml/L 0.1 % (w/v)
4 x SDS sample buffer	Tris-HCl pH 6.8 Glycerin SDS Bromphenolblue ß-mercaptoethanol	250 mM 40 % (v/v) 8 % (w/v) 0.04 % (w/v) 0.2 mL/mL
Staining and fixing solution	Acetic acid Ethanol 98 % H_2O Coomassie brilliant blue R/G 250 [1%]	50 mL 100 mL add 1 L 150 µg per 50 mL volume before use

APS and TEMED were added immediately before the polymerization of the gels.

Table 16. Fatty acid activation solutions

Solution	Components	Final concentration
2 x fatty acylation reaction buffer	Tris-HCL $MgCl_2$ DTT	20 mM 10 mM 2 mM
ATP solution	ATP	25 mM
LiCoA solution	LiCoA	20 mM
Fatty acid solution	β-hydroxy-fatty acid	10 mM
Acyl-CoA synthetase solution	Acyl-CoA synthetase	(1 unit/mL) In 50 mM HEPES pH 7.3

Table 17. Cpz23 enzymatic assay buffers

Solution	Components	Final concentration
5x Reaction buffer	K_2HPO_4	500 mM
Activated fatty acyl solution	β-hydroxy-fatty acyl thioesters	30 mM

2.6 Culture conditions

2.6.1 *Cultivation of Escherichia coli*

E. coli was grown at 37°C, *E. coli* BW12567/pIJ790 at 30ºC and *E. coli* BL21 Rossetta at 18ºC in oven or shaker for 18 hours at 220 rpm in LB medium, adding antibiotics or IPTG when necessary.

2.6.2 *Cultivation of Streptomyces*

Streptomyces strains were cultivated at 30°C in an oven or orbital shaker at 200 rpm.

For production of antibiotics or derivates, liquid precultures were performed in 80 mL TSB-medium for 3 days. Following, culture flasks with a stainless-steel spring were incubated containing 70mL of P medium or R5M, during 7 days. Appropriate antibiotics were added when necessary.

Cultivation of *Streptomyces* strains for sporulation was carried out in MS solid medium. The plates were incubated at 30ºC during 14 days. 5 mL of sterile H_2O (MilliQ) were added to each plate and the spores were scraped of the surface using a sterile cotton bud. The spores were separated from the mycelium by passing the suspension through sterile cotton plugged in a disposable syringe. Spores were collected by centrifugation (4000 rpm, 10 min, 4°C) and resuspended in 250 µL – 1000 µL of 25% glycerol. The spore suspensions were stored at -80°C.

2.7 Methods of molecular biology

2.7.1 *Isolation of cosmid/plasmid-DNA from Escherichia coli*

Based on (Sambrook, Fritsch, and Maniatis 1989)

The alkaline method of DNA isolation was carried out at mini or large scale (*), with 3 mL or 100 mL overnight culture respectively.

3 mL or (100mL*) overnight culture were harvested by centrifugation for 5 min at 13200 rpm and the pellet resuspended in 100 µL (5mL*) Sol I. 200 µL (10mL*) of Sol II were mixed with the suspension by gently inverting the tube. Subsequently 150 µL (7.5mL*) of Sol III were added and mixed by inversion. The suspension was centrifuged (15 min, 13200 rpm, 4°C) and the supernatant transferred into a new tube. The supernatant was vortex mixed with the same amount of phenol/chloroform/Isoamylalcohol and centrifuged (13200 rpm, 4°C, 20 min). The DNA was precipitated by addition of 0,8 volume of isopropanol and centrifuged (13.200

rpm, 4°C, 30 min). The pellet was washed with ice-cold 70% ethanol by centrifugation for 10 min at 13200 rpm and 4°C and afterwards in a speed vac dried, and resuspended in 50 µL of (MilliQ) water. Resuspended DNA was verified with the Spectrometer™NanoDrop1000 (Peglab Biotechnology) at 260/280 nm rate and additionally by comparison of the fluorescent intensity with DNA ladders on Electrophoresis agarose gel and subsequently stored at -20 ºC.

2.7.2 Preparation of electro-competent cells

100 mL LB-medium was inoculated with 2 mL of an overnight culture of *E. coli* and cultivated at 37°C or 30°C in the case of *E. coli* BW25113 and 220 rpm until an OD_{600} of 0.6. The cells were harvested by centrifugation at 4000 rpm, 4°C for 5 min and washed twice with 25 mL ice-cold 10 % glycerol solution (v/v). The supernatant was discharged and the pellet was resuspended in the remaining drops. The cells were dispensed in 50 µL aliquots and stored at -70°C.

2.7.3 *Transformation of E. coli*

~100 ng of DNA in a volume up to 8 µL (MilliQ) water were added to 50 µL of electro competent *E. coli* cells and mixed gently on ice. The mixture was transferred to a pre-cold 0.2 cm electroporation cuvette. The electroporation was performed on a BioRad equipment configured at 2.5 kV. After the shock, 1 mL of cold LB-medium was added and transferred into a microtube. The cells were incubated for 60 min at 37°C or 30ºC in the case of *E. coli* BW25113 (REDIRECT© technology kit for PCR targeting), subsequently 50-200 µL were spread onto LB-agar plates containing appropriate antibiotic(s). The agar plates were incubated overnight at 37°C or 30 ºC.

2.7.4 *Intergeneric conjugation of Streptomyces*

Intergenic conjugation is an efficient method for the transfer of recombinant DNA vectors into *Streptomyces* strains. The vector DNA must contain an *ori*T first by the transformation into the non-methylating strain *E. coli* ET12567/pUZ8002 harbouring the *tra*-genes required for mobilization and transfer of circular DNA.

For biparental conjugation, a culture of *E. coli* ET12567/pUZ8002 containing the vector was grown in 10 mL LB supplemented with the appropriate antibiotics at 37°C until an OD600 of 0.6. Afterwards the cells were harvested by centrifugation (4000 rpm, 4°C, 5 min), and

washed twice with 10 mL ice-cold LB medium without antibiotics (4000 rpm, 4°C, 5 min). The cell pellet was suspended in 1 mL LB medium. In parallel 10-20µL of 10^8 spores of the selected *Streptomyces* strain were incubated in 500 µL 2XYT medium for 10min at 50°C, with a following temperature stabilization at room temperature during 15min. Subsequently, 500 µL of the *E. coli* ET12567/pUZ8002 suspension was added to the spores and the mixture was spin (13200 rpm, 1 min). The supernatant was discarded and the pellet resuspended in the remaining medium. Dilutions were performed in sterile water (10^{-2}, 10^{-4}) were spread on MS agar plates supplemented with 10 mM $MgCl_2$. After 16-20 h incubation at 30°C, the plates were overlaid with 1 mL of H_2Odd including the required antibiotics for selection of mutants and nalidixic acid for selectively kill *E. coli* strains. Incubation was continued for further 3-7 days.

For triparental conjugation, vector DNA was introduced into *E. coli* ET12567. Two parallel cultures, one with *E. coli* ET12567 containing the vector and one with *E. coli* ET12567/pUB307 were set up as described above. After washing and resuspension of the cells, 250 µL of each *E. coli* culture was added to 500 µL 2XYT medium containing the *Streptomyces* spores. Triparental conjugation was necessary for Vector DNA referring to the same antibiotic resistance as pUZ8002.

Three single sporulated colonies were transfer to MS fresh agar plates containing the required antibiotics and incubated at 30°C for 2 weeks until sporulation for further analysis.

2.7.5 Polymerase chain reaction (PCR)

General conditions

PCR amplifications were carried out with the iCycler Thermocycler (Bio-Rad, USA) or the peqSTAR Thermocycler (VWR, USA).

Table 18. Standard PCR reaction and amplification conditions using the *Taq* or *Pfu*-polymerase system.

Reagent	Final concentration	Volume [µL]
Polymerase	3U	1
10x reaction buffer	1x	5
Primer_R 10 µM	0,2 µM	1
Primer_F 10 µM	0,2 µM	1
dNTPs 2,5 mM	200 µM	4
DMSO	10 %	5
Template-DNA	100 ng	-
H_2O miliq.		Up to 50

Table 19. Standard PCR reaction and amplification conditions using the Phusion® High-Fidelity system.

Reagent	Final concentration	Volume [µL]
Polymerase	1U	0,5
5X Phusion HF buffer	1x	10
Primer_R 10 µM	0,5 µM	2,5
Primer_F 10 µM	0,5 µM	2,5
dNTPs 2,5 mM	200 µM	4
DMSO	10 %	5
Template-DNA	100 ng	-
H_2O miliq.		Up to 50

Cycle	Temperature	Time	Cycles
Hot start	94°C	2 min	1
Denaturing	94°C	30 s	30
Annealing	50°C-70°C	30 s	
Elongation	72°C	70s/Kb	
Final elongation	72°C	5-8 min	1
Storage	4°C	∞	-

Table 20. Standard colony PCR reaction and amplification conditions using the *Taq* or *Pfu*-polymerase system.

Cycle	Temperature	Time	Cycles
Hot start	98°C	30s	1
Denaturing	98°C	10 s	30
Annealing	60°C-70°C	30 s	
Elongation	72°C	20s/Kb	
Final elongation	72°C	8 min	1
Storage	4°C	∞	-

Single colonies were picked using a toothpick and transferred into 30 µL of DMSO 100%. 6 µL of the bacterial suspension were used as a template for the PCR reaction.

Cycle	Temperature	Time	Cycles
Hot start	94°C	2 min	1
Denaturing	94°C	30 s	30
Annealing	50°C-70°C	30 s	
Elongation	72°C	70s/Kb	
Final elongation	72°C	5-8 min	1
Storage	4°C	∞	-

Reagent	Final concentration	Volume [µL]
Phusion polymerase	3U	2
10x reaction buffer	1x	5
Primer_R 10 µM	0,5 µM	2,5
Primer_F 10 µM	0,5 µM	2,5
dNTPs 2,5 mM	200 µM	4
Bacterial suspension	-	6
H_2O miliq.		28

5-10 µL of the PCR reaction were analyzed by gel electrophoresis.

2.7.6 PCR for Red/ET-mediated recombination:

The conditions were carried out following the method proposed by (Gust et al. 2003). Elongation of the resistance cassettes was obtained by PCR with overhanging primers designed for the plasmids pIJ773 and pIJ774.

Table 21. PCR conditions for amplification of resistance cassettes for targeting recombineering

Reagent	Final concentration	Volume [µL]
Phusion polymerase	1U	0,5
5X Phusion HF buffer	1x	10
Primer_R 10 µM	0,5 µM	2,5
Primer_F 10 µM	0,5 µM	2,5
dNTPs 2,5 mM	200 µM	4
DMSO	10 %	5
Template-DNA	100 ng	-
H_2O miliq.		Up to 50

Cycle	Temperature	Time	Cycles
Hot start	98°C	30 s	1
Denaturing	98°C	10 s	10
Annealing	50°C	30 s	
Elongation	72°C	60 s	
Denaturing	98°C	10 s	15
Annealing	55°C	30 s	
Elongation	72°C	60 s	
Final elongation	72°C	2 min	-
Storage	4°C	∞	

2.7.7 Agarose gel electrophoresis of DNA

DNA length determination was carried out via gel electrophoresis with 0.8 – 1% (w/v) agarose gels in 1x TAE buffer. 5-25 µL of the DNA samples were mixed with 1 µL amount of 6x loading buffer for each 5 µL sample. The gels were run at max 5V/cm^2 up to 90 min. Gels were stained with fluorescent dye peqGREEN 20 (VWR, USA) and evaluated under UV light at 312 nm using the Eagle Eye II System (Stratagene, Heidelberg, Germany). When necessary, DNA fragments were isolated from agarose gels using a QIAquick Purification Kit (Qiagen, Germany) according to the manufacturer's protocol.

2.7.8 Restriction analysis of DNA

Restriction of DNA was carried out following the instructions of the manufacturer NEB Biolabs. 0.5- 3µg of DNA was digested in a volume reaction up to100µL.

2.7.9 Ligation reaction calculation

Ligation was carried out using this calculation:

$$\underline{(\boldsymbol{ng\ of\ vector\ X\ Kb\ size\ of\ insert})/(\boldsymbol{Kb\ size\ of\ vector})} \\ \underline{\times\ \boldsymbol{molar\ ratio\ of\ \ insert/vector}}$$

The reaction mixture contained insert and vector DNA, usually in a molar ratio of 3:1. Ligation of DNA fragments was achieved by using T4-DNA ligase NEB Biolabs. The ligation preparation contained 1U ligase, 1X ligation buffer and up to 250 ng of DNA mixture of linearized vector and insert in a final volume of 10 µL. The mixture was incubated overnight at 16°C.

2.7.10 Red/ET-mediated recombination in E. coli

Gene knock-outs were achieved by PCR-targeted gene replacement (Gust et al. 2003). Red/ET-mediated recombination was applied to introduce linear DNA fragments into the respective cosmids. The required fragments were amplified by PCR using primers with 39-nt extensions homologous to the respective regions up- and downstream of the gene of interest. The cassette from pIJ773 and pIJ774 was used as template to generate the knock-out cassettes.

For Red/ET-mediated recombination, *E. coli* BW25113/pIJ790 cells were transformed with the cosmid cpzLK09 or its derivatives. 5 % of a pre-culture of these *E. coli* BW25113 strains were then inoculated in 10 mL SOB medium containing the required antibiotics. To induce the λ-Red genes, 100 µL of a 1 M arabinose solution was added and the culture was incubated at 30°C and 200 rpm until an OD_{600} of 0.5 was reached. Cells were harvested via centrifugation (5 min, 3000 rpm, 4°C), washed twice with 10 mL of ice cold 10% glycerol and resuspended in 100 µL ice cold 10 % glycerol. Afterwards 100 ng of the appropriate DNA fragment was introduced into *E. coli* BW25113/pIJ790 containing the respective vector via transformation. Positive clones were selected by adding the required antibiotics at 37°C to the transformation plates. For separation of wild type and mutated vector DNA, isolated cosmid DNA was retransformed into *E. coli* XL1 blue and reisolated. Successful recombination was verified by restriction digest or colony PCR and sequencing.

Excision of the resistance marker located between the two FRT sites, flanking the resistance cassette from pIJ773 or pIJ774, was achieved via use of a FLP-recombinase. To this end, *E. coli* BT340 was transformed with the respective cpzLK09 derivative and incubated for two days at 30°C on solid LB medium containing the appropriate antibiotics. Single colonies were picked, streaked again on LB medium without antibiotics and incubated at 42°C, overnight (temperature sensitive expression of the flippase). Apramycin sensitive clones were screened via colony PCR and successful excision of the resistance cassette was verified via restriction analysis and sequencing.

If a resistance cassette based on pIJ774 was used, the resistance marker was excised via an in vitro reaction with a Cre-recombinase, taking advantage of the two lox P-sites, flanking the cassette. The reaction mixture contained 1U Cre-recombinase, 1x reaction buffer and about 100 ng DNA in a final volume of 10 µL. The mixture was incubated for 30 min at 37°C and used to transform *E. coli* XL1 cells. Apramycin sensitive clones were screened via colony PCR and successful excision of the resistance cassette was verified via restriction analysis and sequencing.

Alternatively, appropriate restriction sites were introduced on both ends of the cassette during PCR with elongated PCR primers. Excision of the resistance marker was subsequently achieved by restriction digest, taking advantage of the restriction sites, and religation.

2.7.11 Cre-lox recombination

Cre-lox recombination was carried according to the manufacturers description leaving only one functional loxP site at the site of recombination. Afterwards, the reaction was precipitated for further transformation.

2.7.12 DNA sequencing

DNA sequencing was performed by Eurofins Genomics (Ebersberg, Germany) using an ABI 3730XL- sequencing device. Evaluation of the chromatogram data was carried out with the software Lasergene 7.1 (DNASTAR, Inc) and Geneious Prime ® 2021 (Biomatters Ltd).

2.7.13 Cloning and overexpression in pUWL vector

cpz12, *cpz*22, and *cpz*27 were amplified by PCR from cpzLK09 DNA. *cosI, cosJ, cosP, cosU* genes were amplified from *S. olindensis* DAUFPE 5622 genomic DNA using the Phusion® High-Fidelity DNA Polymerase from New England Biolabs Inc, according to the manufacturer's instructions, and primers listed in Table 3. The resulting PCR products were cloned into the pUWL_Apra-oriT vector containing an apramycin resistance gene cassette under the control of the constitutively active promoter *ermE** to ensure a high level of expression. These constructs (Figure 14) were transferred into *E. coli* XL1 blue and further into *E. coli* ET12567/pUZ8002 to obtain non-methylated DNA. The constructs the pRCWL01 (*cpz12*), pRCWL02 (*cpz22*), pRCWL03 (*cpz27*), were finally transferred into *S. coelicolor* M512 and pRCWL04 (*cosI, cosJ*), pRCWL05 (*cosP*) and pRCWL06 (*cosU*) were transferred into *S. lividans* TK24 by biparental conjugation. Three independent clones were selected for

sporulation and subsequent MIC analysis.

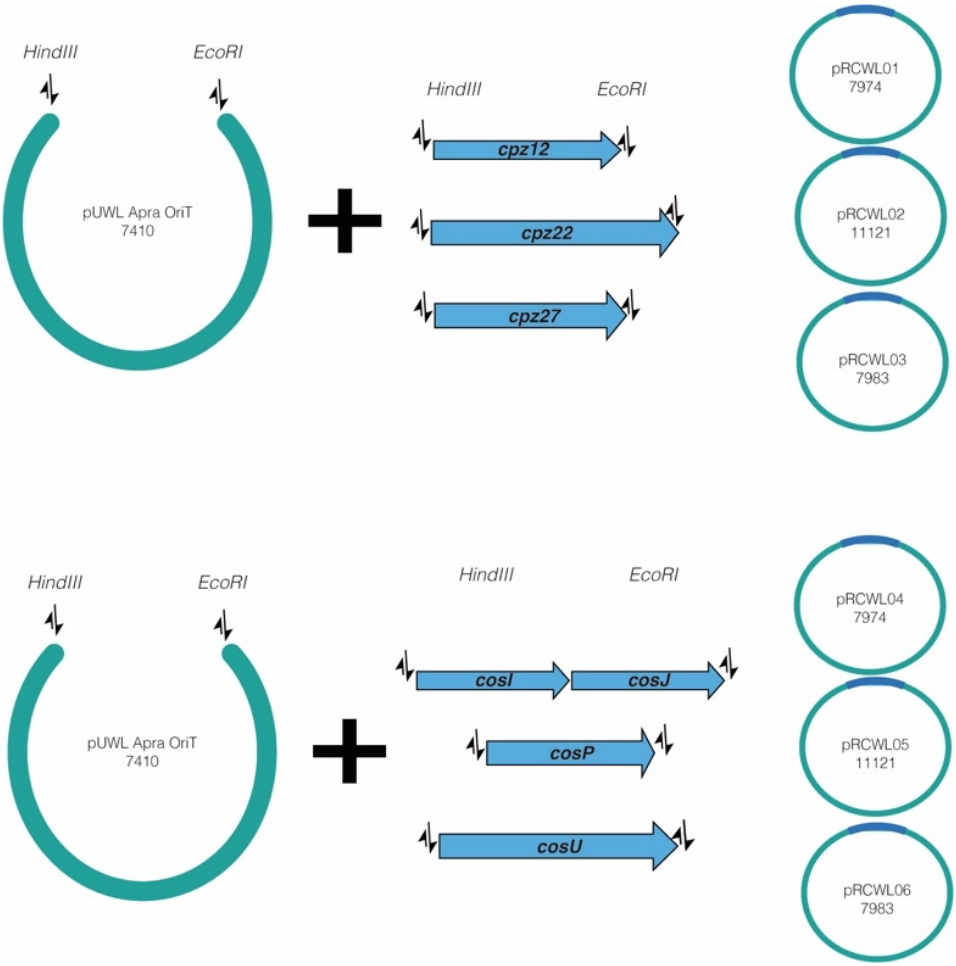

Figure 14. Working steps to prepare the constructs on pUWL expression vector.

Preparation of pUWL through restriction and gene insertion taking advantage of *HindIII* and *EcoRI* sites following a classic ligation

2.7.14 Cloning and protein overexpression in pHIS8 vector

The cloning and expression of the enzymes were carried out in the pHIS8 vector, to generate an N-terminal His8-taged-Cpz12, Cpz27 or Cpz23. The corresponding genes were amplified by PCR from cpzLK09 DNA and *cos*P was amplified by PCR from gDNA of *S. olindensis* WT. Additionally, the primers contained restriction sites for *Eco*RI and *Hind*III. The PCR products were cloned into the expression vector pHIS8 through ligation taking advantage of the *Eco*RI/*Hind*III restriction sites, generating the constructs pRCHIS01, pRCWL02, pRCWL03 and pRCWL04 (Figure 15). The integrity of the resulting plasmids was verified via sequencing.

Heterologous expression and purification of His8-tagged proteins were carried out using *E. coli* Rosetta2 (DE3) pLys (Novagen, Darmstadt, Germany) as the recombinant host strain. Strains containing the corresponding plasmid were cultivated in 1 L LB broth supplemented with 25 µg/mL chloramphenicol and 50 µg/mL kanamycin at 37°C and 220 rpm. At OD_{600} 0.6, the temperature was adjusted to 18°C and isopropylgalactoside (IPTG) was added to a final concentration of 0.5 mM.

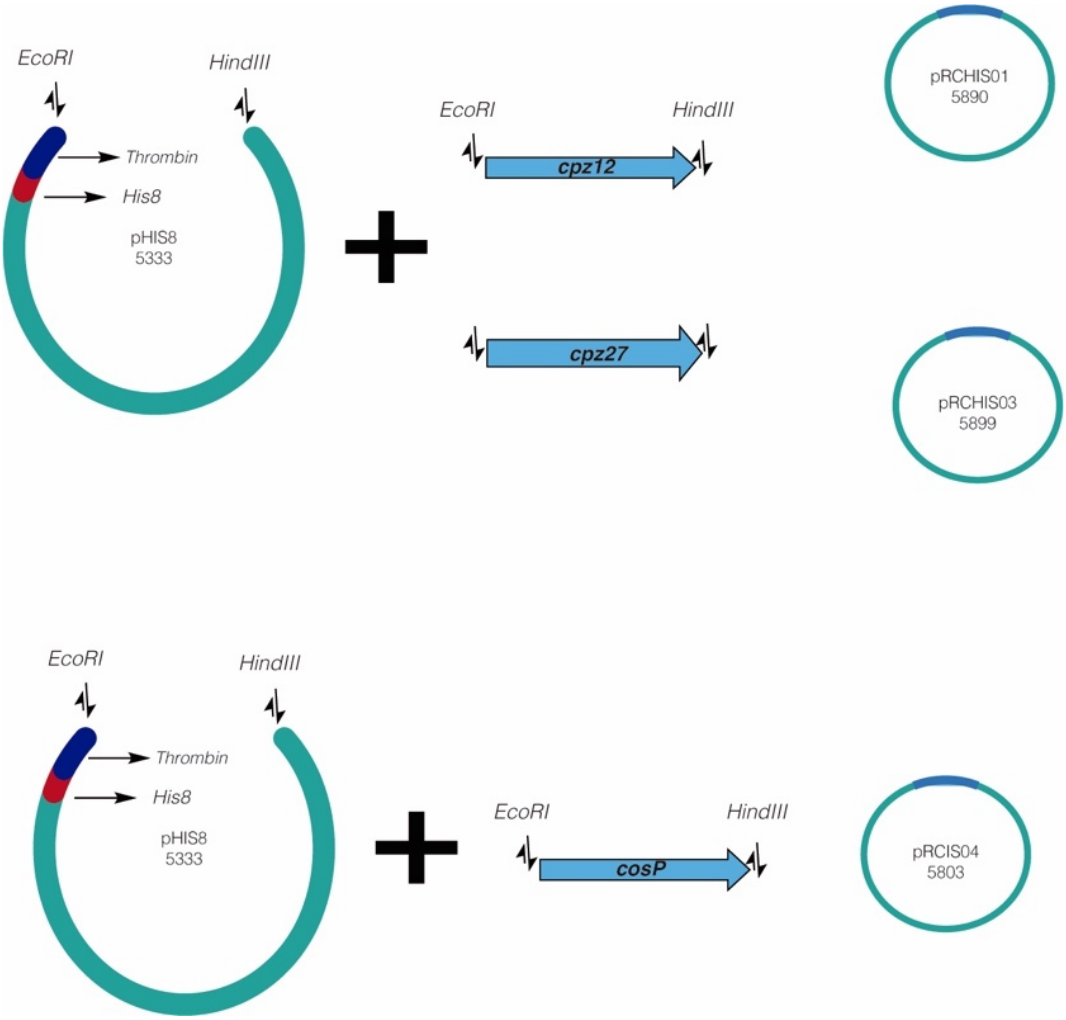

Figure 15. Working steps to prepare the constructs on pHIS8 protein expression vector.

Preparation of pHIS8 through restriction and gene insertion taking advantage of *HindIII* and *EcoRI* sites following a classic ligation

2.7.15 Site-directed mutagenesis of mycothiol peroxidase (MPx)

Plasmid pRCWL04 was further modified in the coding “CALA” region of the enzyme (MPx), exchanging cysteine (C) for serine (S) at position 38, using the QuikChange II Site-Directed Mutagenesis Kit (Agilent Technologies), resulting in plasmid pRCWL04M (Figure 16).

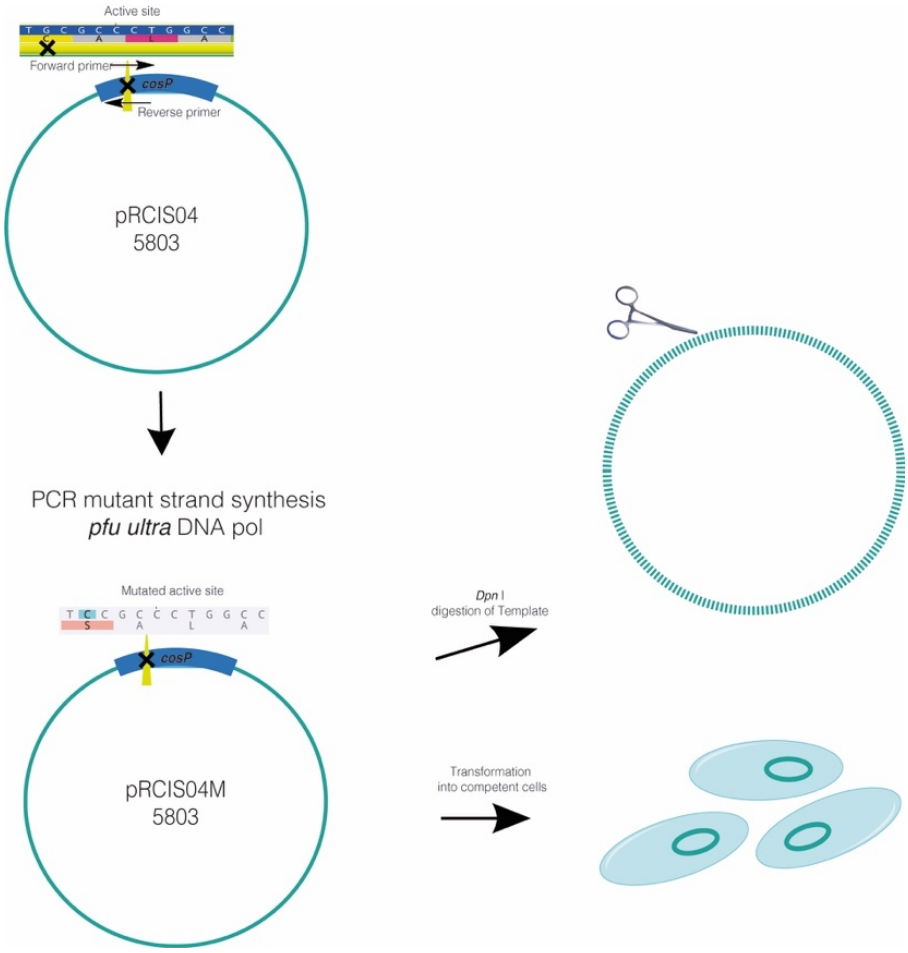

Figure 16. Overview of the site-directed mutagenesis method

2.7.16 Cloning and overexpression in pGM1190 and pGM1192 vectors

This process was carried out in collaboration with the master student Julia Höfer. Phosphotransferases genes (*cpz*12 and *cpz*27) were amplified by PCR from cpzLK09 cosmid DNA. The primers contain enzyme flanked regions for *Nde*I and *Hind*III. The PCR products were ligated into pGM1190 and pGM1192 vectors, generating the constructs, pJH01, pJH02, pJH03 and pJH04. The resulting constructs were transferred by transformation to *E. coli* XL1 blue and verified via sequencing.

The confirmed constructs were isolated and transferred into *E. coli* ET12456/pUZ8002. The clones containing the constructs were transferred into *S. lividans* TK24 and *S. albus* J1074 via biparental conjugation and selected by flooding with apramycin. Three independent clones were selected for sporulation and subsequent protein production analysis.

2.7.17 Generation of single gene knock outs of cpz12, cpz22, cpz23, and cpz27 in cpzLK09 cosmid

For single gene inactivation of *cpz*12, *cpz*22, *cpz*23, and *cpz*27 on cpzLK09 cosmid, an apramycin resistance cassette was amplified from plasmid pIJ773 via PCR, with designed primers (Table 3). The genes were replaced in *E. coli* BW25113/pIJ790/cpzLK09 using the PCR targeting system. The resulting cosmids pCRD1 (Δ*cpz12*), pCRD2 (Δ*cpz22*), pCRD3 (Δ*cpz27*) and pCRD4 (Δ*cpz23*), were confirmed by restriction analysis. Excision of the resistance marker was achieved via a FLP-recombinase taking advantage of the FRT sites flanking the cassette (Figure 17). Constructed cosmids were verified by sequencing analysis, transferred into *E. coli* ET12567 and introduced into *S. coelicolor* M512 by triparental intergeneric conjugation with the help of *E. coli* ET12567/pUB307. Kanamycin resistant clones were selected, designated as *S. coelicolor* M512 Δ*cpz12-22-27-23* and verified by PCR and sequencing.

2.7.18 Generation of double gene knock outs

For inactivation of *cpz12* on pCRD3 cosmid and *cpz4* on pCRD4, an apramycin resistance cassette was amplified from plasmid pIJ774 and pRS03 via PCR. The resulting cosmids pCRD5, pCRD6 were confirmed by restriction analysis. Excision of the resistance markers was achieved via a Cre-recombinase taking advantage of the loxP sites flanking the cassette. Regarding pRS03, the excision of the resistance markers was achieved via restriction with *Xba*I and *Pst*I and religation of the cosmid. The constructed cosmid was verified via restriction analysis and sequencing, transferred into *E. coli* ET12567 and finall into *S. coelicolor* M512 by triparental intergeneric conjugation. Kanamycin resistant clones were selected, designated as *S. coelicolor* M512 Δ*cpz12/*Δ*cpz27* and Δ*cpz23/*Δ*cpz4* following a verification by PCR and sequencing. (Figure 17)

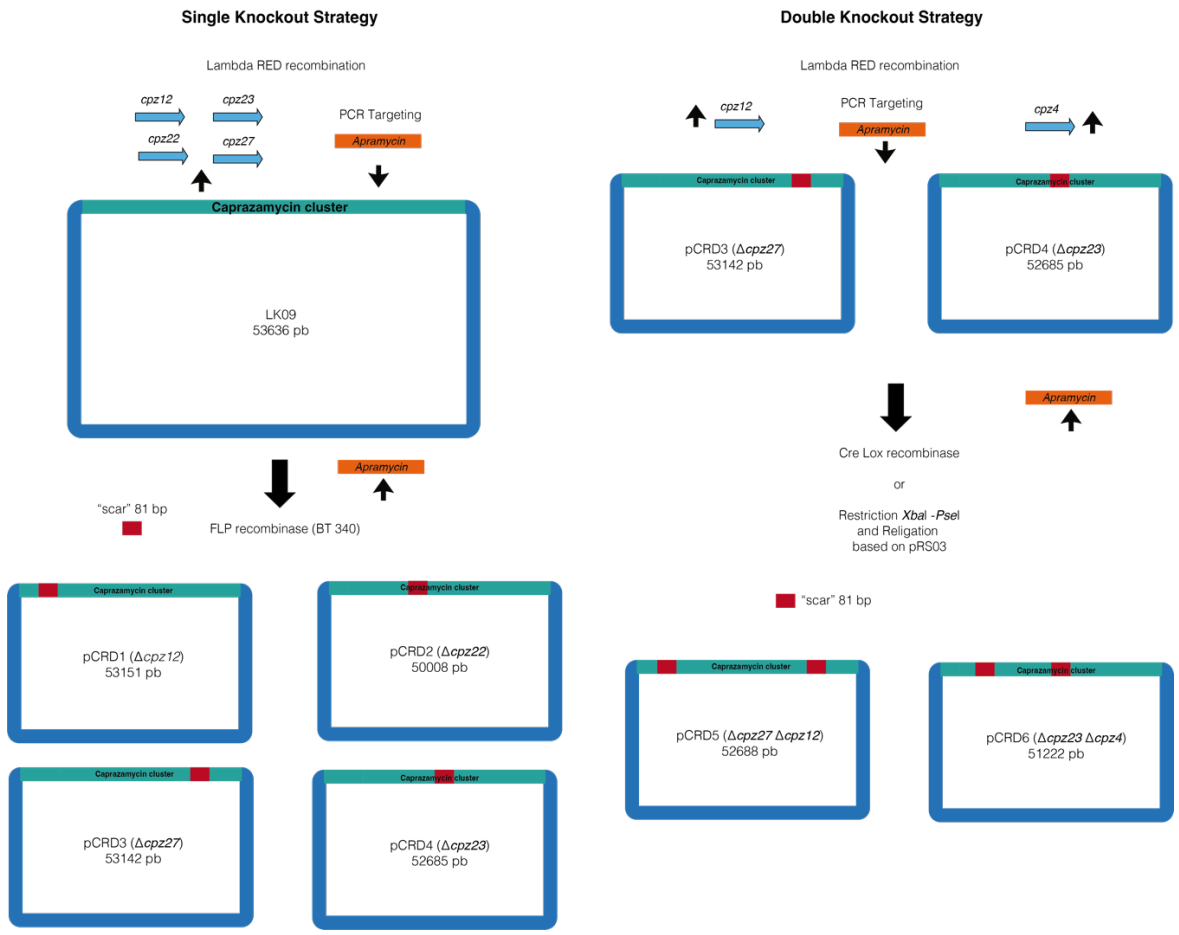

Figure 17. Working steps to construct single and double knock outs.

First column: preparation of cpzLK09 through insertion of apramycin resistance cassette at the position of *cpz12, cpz22, cpz23* and *cpz27*. The Apramycin cassette was excised by FLP recombinase.
Second column: preparation of the single K.O cosmids (pCRD5 and pCRD6) through insertion of an apramycin resistance cassette at the position of *cpz12, and cpz4* respectively. The apramycin cassette was excised with two strategies. Cre-Lox recombinase for the cassette based on pIJ774. For the cassette based on pRS03, restriction with *Xba*I and *Pst*I and religation was used instead.

2.7.19 Total RNA isolation and cDNA synthesis

Total RNA of producer strain *S. olindensis* WT was extracted using RNA protect Bacteria Reagent following the RNeasy Mini Kit according to the manufacturer's instructions (QIAGEN). The frozen samples were ground in dry ice. Residual DNA was removed by treating with RNase-free DNase according to the manufacturer's instructions (QIAGEN). An aliquot of 1 µg DNase-treated RNA was transcribed into cDNA using the iScript™ Reverse Transcription Supermix for RT-qPCR (Bio-Rad Laboratories, Inc).

2.7.20 qPCR analysis

For qPCR, the thermocycler BioRad iQ5, Bio-Rad Laboratories, was used and programmed to an initial denaturation of 5 min at 95°C, followed by 40 cycles of 5 s at 95°C and 15s at 60°C. The specificity of qPCR primer (Table 3) was evaluated by the melting curve using a gradient from 55 - 95°C ranging 1°C each 30 s (Figure S9). For each amplification reaction, 2 µL of cDNA (50 ng), 10 µM of each primer and 10 µL of QuantiNova Probe PCR Kit (QIAGEN) was used.

iQ5 Optical System Software was used to determine a relative quantification of the target genes in comparison to the reference gene. The selection of an endogenous gene, to be used as a normalizer, was made by testing the Ct values for different described endogenous genes (Figure S9). Thereby, the *hdrB* housekeeping gene presented the lowest ΔCt and the higher amplification efficiency, resulting in its selection as the normalizer for gene expression analysis.

2.7.21 Denaturing polyacrylamid gel electrophoresis (SDS-PAGE)

SDS-Page was performed in accordance to the method of Laemmli (1970). Probes were mixed with sample buffer in ratios 1:2 to 1:4, denatured at 95°C for 5 min and subsequently applied to the SDS-Gel. SDS-Gel was prepared with 12.5 % polyacrylamide in the separating gel and 4 % acrylamide in the stacking gel. Gel electrophoresis was carried out with a working voltage of 160 V using a Mini- PROTEAN® II Electrophoresis Cell (Bio-Rad, München, Germany). Protein bands were stained in 50 mL Fixing buffer containing 150 µL Coomassie blue solution over 10 min. Bleaching was performed for 2 h in water. To determine the molecular weight of the proteins, a protein standard was used.

2.7.22 Heterologous production of recombinant protein in E. coli

Heterologous overproduction and purification of 8×His-tagged proteins from *E. coli* were carried out using expression vector pHis8 and *E. coli* Rosetta2 (DE3) pLys (Novagen, Darmstadt, Germany) as the recombinant host strain. The vector provides the sequence encoding an N-terminal His8-tag (Jez et al. 2001).

The respective *E. coli* Rosetta2 (DE3) pLysS strains containing pRCHI01, pRCHI03, pRCHI04 and pCFIS01 were cultivated in 1 L LB broth supplemented with 25 µg/mL

chloramphenicol and 50 µg/mL kanamycin at 37°C and 220 rpm. At OD_{600} 0.6, the temperature was adjusted to 18°C and isopropylgalactoside (IPTG) was added to a final concentration of 0.5 mM.

2.7.23 Heterologous production of recombinant protein in S. lividans TK24

Heterologous overproduction and purification of 8×His-tagged proteins from *S. lividans* were carried out using expression vector pGM1192 received from the Dr. Gunther Muth, University of Tübingen in *S. lividans* TK24 (Eustáquio et al. 2005) as the recombinant host strain. The vector provides the sequence encoding an N-terminal His^8-tag (Jez et al. 2001).

The *S. lividans* strains containing pJH03 or pJH04 were pre-cultivated in 70mL TSB broth supplemented with 50 µg/mL apramycin at 30ºC and 220 rpm during 3 days. Immediately cultures containing 70mL of YEME medium in 300mL flasks were incubated during 3 days at 30ºC and 220 rpm.

2.7.24 Purification of recombinant proteins Cpz12, Cpz27, MPx and Mutant MPx

For *E. coli* protein system: The overnight culture was harvested by centrifugation at 8000 rpm, 4°C for 10 min. The supernatant was discarded and the pellet resuspended in lysis buffer (3 mL/g pellet). The cells were sonicated (Sonifier Generator, Branson) on ice for 10 min (Amplitude: 40%, 5s on/5s off). After centrifugation for 45 min at 18000 rpm, (4°C) the clear lysate was filtered (0.45 µm) for affinity chromatography.

For *Streptomyces* protein system: The overnight culture was harvested by centrifugation at 8000 rpm, 4°C for 30 min. The supernatant was discarded and the pellet resuspended in lysis buffer (25 mL/g pellet, Lysosome concentration was modified to 10mg/mL). The cells were disrupting in a French press, the sample was set in 1000 psi, and maintaining the pressure, adjust the outlet flow rate to a froze falcon. The cell lysate was kept on ice and centrifugated for 45 min at 18000 rpm, (4°C) the clear lysate was filtered (0.45 µm) for affinity chromatography.
Supernatant of each culture was applied to affinity chromatography using an ÄKTA start™ platform (GE Healthcare) equipped with a 5 mL His-Trap™ HP column (GE Healthcare). The His-tagged protein was washed and then eluted from the column using a linear gradient from 0-100 % of elution buffer over 60 min and collected by a Frac-30 system (GE Healthcare). Fractions were tested for the presence of the respective proteins by SDS-PAGE and were

concentrated and buffer exchanged into (25 mM KH_2PO_4,100 mM NaCl, pH8,3) using an Amicon Ultra centrifugal filter (*M*r cutoff of 10,000; Millipore). Concentrations of the purified proteins were measured spectrophotometrically at 280 nm using the calculated extinction coefficients (calculated with http://web.expasy.org/protparam/).The purified proteins were stored in aliquots at −80°C.

2.8 Methods of biochemistry

2.8.1 In vitro studies on Cpz12 and Cpz27

Assays were performed with soluble proteins. All assays were prepared on ice and performed in 50 µL total volume reaction mixture. The phosphorylation assays were performed in a reaction mixture containing 50mM Tris (pH7.5), 10 mM $MgCl_2$,1mM ATP and 1mM caprazamycin or intermediates. The assays were started by addition of Cpz12 or Cpz27 in final concentrations of 5 µM. After overnight incubation the assays were stopped by addition of one volume ice-cold MeOH, put on ice for 10 min and centrifuged at 13000 rpm for 10 min. The supernatant was monitored and analyzed with HPLC and LC-ESI/MS. Product formation was observed at 26- 290 nm.

2.8.2 Enzymatic fatty acid activation with CoA

The enzymatic activation and Cpz23 reaction were carried in cooperation with Cedric Funck. The acyl-CoA synthetase was used to catalyze the formation of the thioester β-hydroxy-myristoyl-CoA. 50 µL of 2 x fatty acylation reaction buffer (to a final reaction concentration of 10 mM Tris-HCL, 5 mM $MgCl_2$, 1 mM DTT and pH 7.4). Then, 10 µL ATP solution (5 mM), 5 µL LiCoA solution (2 mM) and 5 µL Fatty acid (1mM) were added and the solution was thoroughly mixed. To start the reaction, 30 µL of acyl-CoA synthetase solution (300 mU/mL) were added to the solution, and thoroughly mixed in.
Afterwards, the reaction was incubated at 30°C for 3h. Subsequently, the reaction was frozen in -80°C and freeze dried. The freeze-dried products were resuspended in 50 µL Milli Q water and analyzed in LC-MS.

2.8.3 Enzyme assay of Cpz23

The enzyme conditions reaction (100 mM $KHPO_4$, pH 8.0, 5 mM β-hydroxy-myristoyl-CoA and 5 mM (+)-caprazol/phosphorylated (+)-caprazol and (0.4 µg) Cpz23 were added to the

reaction and thoroughly mixed. The reaction was incubated at 30°C for 4 hours. Afterwards, the reaction was frozen at -80°C and subsequently freeze-dried. The freeze-dried pellet was resuspended in 50 µL of a 1:1 ratio (MilliQ) water/100% methanol solution and analyzed with LC-MS and HR-MS.

2.8.4 In vitro studies with micothiol peroxidase enzyme (MPx)

2.8.4.1 Peroxide and protein quantification

The concentration of H_2O_2 stock solutions (Sigma-Aldrich) was measured at 240 nm (ε240nm = 43.6 M−1 cm−1) (Hildebraunt & Roots, 1975). Protein concentrations were determined spectrophotometrically at 280 nm: the molar absorption coefficients were calculated from the amino acidic compositions (http://web.expasy.org/protparam/) (Wilkins et al. 1999). The calculated protein concentrations refer to those of monomers.

2.8.4.2 Ferrous oxidation of xylenol orange (FOX) assay

WT MPx and the Cys38Ser mutant enzyme were reduced with 10x excess DTT in 250 mM Tris buffer, 500 mM NaCl pH 8.0 buffer solution and incubated for 30 min at room temperature. FOX assay (Pedre et al. 2018) was used to determine the H_2O_2 consumption over time by the purified MPx or the mutant and total proteins from *S. olindensis* and *S. peucetius* strains isolated during antibiotic production. All measurements were performed in three replicates for each treatment. The H_2O_2 concentration was calculated based on a H_2O_2 standard curve. In the case of purified MPx and mutant MPx, 100 µM were mixed with 100 µM H_2O_2 in 100 mM assay buffer, pH 8, at 30°C .10 µL of the reaction were taken after 15, 30, 45, 90, and 180 seconds and mixed with 490 µL of the FOX reaction mix (100 µM xylenol orange, 250 µM ammonium ferrous sulfate, 100 mM sorbitol and 25 mM H_2SO_4), and incubated for 30 min at room temperature in darkness. At the end of the reaction, A560 nm was measured on a 96-well plate reader (FLUOstar® Omega) as described elsewhere (Pedre et al., 2018). For the isolation of total proteins from *S. olindensis* and *S. lividans*, cells were initially grown in TSB at 30°C for 24 h. 1% pre-culture was used to inoculate the main R5M culture. This culture was grown at 30ºC for protein extraction at 24, 48 and 72 hours during the production of cosmomycin D for *S. olindensis*. Then, 100 mM H_2O_2 was added to equal concentrations of total proteins. 10 µL aliquots were taken after 100, 200, 300, 400, 500, and 600 seconds as described elsewhere (Pedre et al. 2018).

2.9 Determination of Minimal Inhibitory Concentrations (MICs)

R2YE or Bennett's agar was prepared and contained between 0-256 µg/mL of antibiotics or intermediates from caprazamycin biosynthesis. These mixtures were applied to sterile 96-well plates; each well contained 100 µL of agar media. Each well was inoculated with 5 µL of ~10^8 *Streptomyces* spores. Plates were incubated up to 5 days at 30ºC and growth compared with control wells. For determination of MIC values, each well contained 100µL of Benett`s agar, antibiotics or biosynthetic intermediates with concentrations ranging from 0 to 512 µg/mL. Each well was inoculated with ~10^3 *Streptomyces* spores and plates were incubated overnight at 30ºC. Growth was compared with controls strains.

2.10 Analytical methods

2.10.1 High performance liquid chromatography (HPLC)

HPLC analysis was carried out at an Agilent instrument 1200 series (Waldbronn, Germany) and Waters liquid chromatography system (Waters 2545 Quaternary Gradient Module, 2489 UVV/ Visible Detector, Prep Injector).

The detection was carried out at 261 and 290 nm and a UV spectrum from 200 to 400 nm was logged additionally. A straight calibration line for quantification was set up using different concentrations of caprazamycins, hydroxyacylcaprazol or doxorubicin (Sigma Aldrich) as standard.

The following solvents are used:
A: 0.1% formic acid in water
B: 0.06% formic acid in acetonitrile

The analysis was carried out using following four methods:

Method 1

For caprazamycins and hydroxyacylcaprazols, the column Nucleodur ® PolarTec (MACHEREY-NAGEL, 5µm, 250 mm x 4.6 mm) at a flow rate of 0.5 mL/min was used, with a linear gradient starting at 5% B to 40 % B in 9 min following by a linear gradient from 40% B to 100% B for additional 28 min.

Method 2

A second method for detection of biosynthetic intermediates was carried out using a Luna ® Omega Polar C18 (Phenomenex, 5µm, 250 mm x 4,6 mm) column with a flow rate of 0.5 mL/min. For compound separation, an isocratic gradient was used from 0% B for 15 min following 100% B for 5 min and finally 15 min 0% B to equilibrate.

Method 3

For further purification, the extract was separated through reverse-phase preparative HPLC, column: NUCLEODUR ® PolarTec, (MACHEREY-NAGEL, 5 µm, 250 mm x10 mm) using a linear gradient starting at 5% B to 40 % B in 9 min following 40% B to 100% B for additional 28 min at a flow rate of 5 mL/min. Final flask containing the desired compounds were concentrated in vacuo to dryness and submitted to another purification step.

Method 4

The fraction containing the COS D (*m/z* 1189.54) was further purified using a HPLC Waters liquid chromatography system (Waters 1525 Binary Pump with a 7725i Rheodyne injection port, a Kromega Solvent Degasser and a Waters 996 Photodiode Array Detector) using a linear gradient from 40% B to 60% B in 15 min, followed by a linear gradient from 60% B to 95% B in 20 min and additional 10 min at 95% B (solvent A: 0.06% formic acid in water; solvent B: 0.1% formic acid in acetonitrile) at a flow rate of 2 mL/min, column: (Luna ® Omega Polar C18 (Phenomenex, 5µm, 250 mm x 4.6 mm) to obtain ~5 mg pure COSD.

2.10.2 Purification of caprazamycin and intermediates

Caprazamycins were purified from *S. coelicolor* M512/cpzLK09 *and S. coelicolor* M512/Δ*cpz22*. Caprazamycin intermediates or aglycones were purified from *S. coelicolor* M512/Δ*cpz12;* Δ*cpz21 or* Δ*cpz23*.

A preculture of 70 mL TSB medium containing the appropriate antibiotics and 20 µL of spores (10^8 per mL) was grown for 3 days at 30°C at 220 rpm. For the main culture, 1L was divided to 60 mL aliquots of production medium (PM) in 300 mL flasks, inoculated with 1 mL of the preculture and grown for 7 days at 30°C at 220 rpm.
The cultures were centrifugated at 8000 rpm for 15min to divide supernatant and cell mass. The cell mass was resuspended in ice-cold methanol (3 mL/g), vortexed and sonified. After

centrifugation at 4°C for 5 min and 6000 rpm, the supernatants were combined and the cell lysate removed. The supernatant was extracted 3x using an equal volume of *n*-Butanol. The solvent was evaporated and the crude extract was washed with ethyl acetate until the supernatant was clear. The dry crude extract was resuspended in 50:50 methanol: water or water for polar intermediates. The extract was submitted for HPLC, LC-MS and HR-MS analysis.

2.10.3 Purification of cosmomycin

Cosmomycin D were purified from *S. olindensis* WT. A preculture of 70 mL TSB medium containing the appropriate antibiotics and 20 µL of spores (10^8 per mL) was grown for 3 days at 30°C at 220 rpm. For the main culture, 1L was divided to 30 mL aliquots of R5M medium in 300 mL flasks, inoculated with 1 mL of the preculture and grown for 5 days at 30°C at 220 rpm.

The samples were centrifuged at 4500 rpm for 10 minutes in order to obtain the cell-free supernatant. Soon after centrifugation, the supernatant was transferred to a separatory funnel where it was subjected to the liquid/liquid partition with ethyl acetate. After the chemical partition with the solvent, the organic phases were evaporated from the solvents and concentrated in a vacuum evaporator at 40ºC. The obtained crude extract was redissolved in methanol for HPLC and HR-MS analysis.

For further purification of cosmomycin D, the crude extract was dissolved in methanol (LC-MS grade, Merck) and applied to a solid-phase extraction cartridge (Strata^{TM}-XL 100 µm Polymeric Reversed Phase, 2 g, Phenomenex). The adsorbed compounds were eluted in fractions using a stepwise gradient from 10% to 100% methanol and concentrated under reduced pressure.

2.10.4 Liquid chromatography-electrospray ionization mass spectrometry (LC-ESI/MS) and MS^2

Low-resolution (LR) -ESI/MS and HPLC-ESI/MS^2 analysis were performed at a LC/MSD Ultra Trap System XCT 6330 (Agilent Technology). The samples were analyzed using the same columns and methods as described in the HPLC section. The injection volume was 5 µL. For MS analysis, electrospray ionization (alternating positive and negative ionization) in Ultra Scan mode with a capillary voltage of 3.5 kV and heated capillary temperature of 350°C was used. MS^2 analysis was performed in positive ionization.

2.10.5 High resolution LC-ESI/MS and MS^2 analysis

For structure determination high-resolution LC-ESI/MS and MS^2 measurements were performed which were carried out on a Bruker Daltonics MaXis 4G (Bruker Daltonics, Bremen, Germany) connected to a Thermo Scientific Ultimate 3000 (Thermo Fisher Scientific) system using a reversed-phase Luna Omega polar C18 column (3 µm, 150 x 3 mm) using the same methods of HPLC section, an injection volume of 5 µL and UV monitoring occurred at 210, 254, 280 and 360 nm. The range of MS acquisition was *m/z* 50-1800. The acquisition parameters for the positive ion polarity were a capillary voltage of 4.5, nebulizer gas pressure (nitrogen) was set to 2.0 bar, the dry gas flow of 9.0 L/min at an ion source temperature of 200°C. The measurements were internally calibrated using sodium formate as a reference. The data were compared to published data of various related compounds.

2.10.6 NMR methods and structural characterization

Methods for NMR analysis were developed in cooperation with the group of Prof. H. Groß. (Pharmaceutical Institute, Dept. of Pharmaceutical Biology, University of Tübingen). The analysis was routinely carried out by H. Saad, T. Mayer or K. Bhattarai. NMR spectra were recorded either on a 400 MHz Bruker AVANCE III HD (400 and 100 MHz for ^{1}H and ^{13}C isotopes, respectively) or a 700 MHz Avance III HDX (700 and 283 MHz for ^{1}H and ^{31}P isotopes) NMR spectrometer, equipped with a 5 mm broadband SMART or Prodigy TCI cryo probe head, respectively. All spectra were recorded in D_2O (δH 4.79) and referenced to the residual solvent signals or the internal offset for ^{31}P, assigned by the instrument manufacturer.

2.11 Bioinformatic methods

Analysis of the biosynthetic gene clusters was performed with help of the following tools:

DELTA-BLAST of NCBI (https://blast.ncbi.nlm.nih.gov/Blast.cgi)

HMMER profile (http://hmmer.janelia.org/)

Phyre 2.0 (http://www.sbg.bio.ic.ac.uk/phyre2/html/page.cgi?id=index)

antiSMASH (https://antismash.secondarymetabolites.org)

MultiGeneBlast (http://multigeneblast.sourceforge.net)

MEGA software (Tamura, Stecher, and Kumar 2021)

Geneious Prime® 2021 Biomatters Ltd.

2.11.1 Construction of Sequence similarity Networks (SSN) and Genome Neighborhood Network (GNN) for MPx enzyme

Webtools available at https://efi.igb.illinois.edu/, of EFI - Enzyme function initiative (Zallot, Oberg, and Gerlt 2019) were used to generated SSNs from KDN80073.1 and Glutathione peroxidase PFAM family (PF 00255). For seed SSN obtained with KDN80073.1 FASTA sequence were selected with the option Maximum Number of Retrieve Sequences = 100 in Blast Retrieval Options tab, then the Score threshold was adjusted to 65 using the "Percent Identity vs. Alignment Score Box Plot" in order to set up the presence between nodes only with identity equal to 70% or above.

For initial submission of PF00255 all settings were kept at default, then a first SSN was generated using a Score threshold of 50, which means each edge joining nodes with at least 55% of similarity. The second SSN used a Score threshold slightly higher of 60 (nodes are joined if they share about 61% or more of identity). Using the EFI - Genome Neighborhood Tool (EFI-GNT tab) of the same website a GNN and GNDs (Genome Neighborhood Diagrams) of the second SSN were obtained using as parameters: Neighborhood Size=20 and Co-occurrence Percentage Lower Limit=20.

3. Results

3.1 Identification of plausible caprazamycin resistance determinants

The bioinformatical analysis of the caprazamycin biosynthetic gene cluster (CPZ-BGC) revealed three genes likely to be involved in CPZ resistance: *cpz*22 with 82% similarity to an ABC/ATP binding protein from *Streptomyces* sp. SANK 60405 and *cpz12* and *cpz*27 with a similarity of 81% and 87% with phosphotransferases, respectively. Cpz22 is part of the superfamily of transporter proteins (ATP-dependent ABC type) containing domains for ATPase activity and nucleotide-binding (NBD) (Table 22).

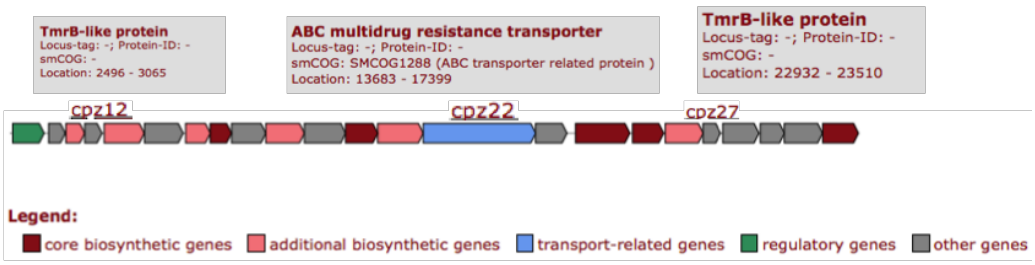

Figure 18. Predicted functions of CPZ cluster obtained from antiSMASH

In this study, a reannotation of the genes was carried out in order to analyze the possible differences of resistance systems with other genes reported in the databases. For this purpose, the tools DELTA BLAST from NCBI, HMMER (http://hmmer.org) and Phyre2 for amino acid analysis were used (http://www.sbg.bio.ic.ac.uk/phyre2/html/page.cgi?id=index) SWISS- MODEL database tool (https://swissmodel.expasy.org) (Figure 20, 22, 26) and the TMHMM server (http://www.cbs.dtu.dk/services/TMHMM) were used for transmembrane protein predictions. Three genes, *cpz*12, *cpz*22 and *cpz*27 were identified encoding plausible resistance determinants:

Table 22. Prediction of the function of resistance genes

Gene	Hypothetical function	# a.a	% Identity (DELTA BLAST)	Valor E- (HMMER)
***cpz*12**	putative TmrB-like protein	189	81% [*Streptomyces* sp. SANK 60405 -ACQ63620.1]	2.4e-87 *Streptomyces atratus*
***cpz*22**	ABC transporter	1238	98% *Streptomyces* sp. SANK 60405 [BAJ05895.1]	2.4e-87 *Streptomyces atratus* SAMN02787144_1010135

cpz27	putative TmrB-like protein	192	87% *Streptomyces* sp. SANK 60405 [BAJ05895.1]	8.1e-77 *Streptomyces atratus* A0A1K2C9S9-1

The two genes (*cpz12* and *cpz27*) encoding for phosphotransferases are likely to be involved in caprazamycin resistance. Both genes showed homology to tunicamycin resistance genes from different *Bacillus* strains (*tmrB*). *tmrB*-like sequences were used to build a phylogenetic analysis, showing a clear division between *cpz12* and cpz27 (Figure 19). Interestingly, a set of two phosphotransferases can only be found in other BGCs responsible for the formation of liponucleosides with similar core-structure such as the liposidomycin and muraminomycin (Figure 21, 23). However, ABC transporter are found in many other BGCs (Figure 27).

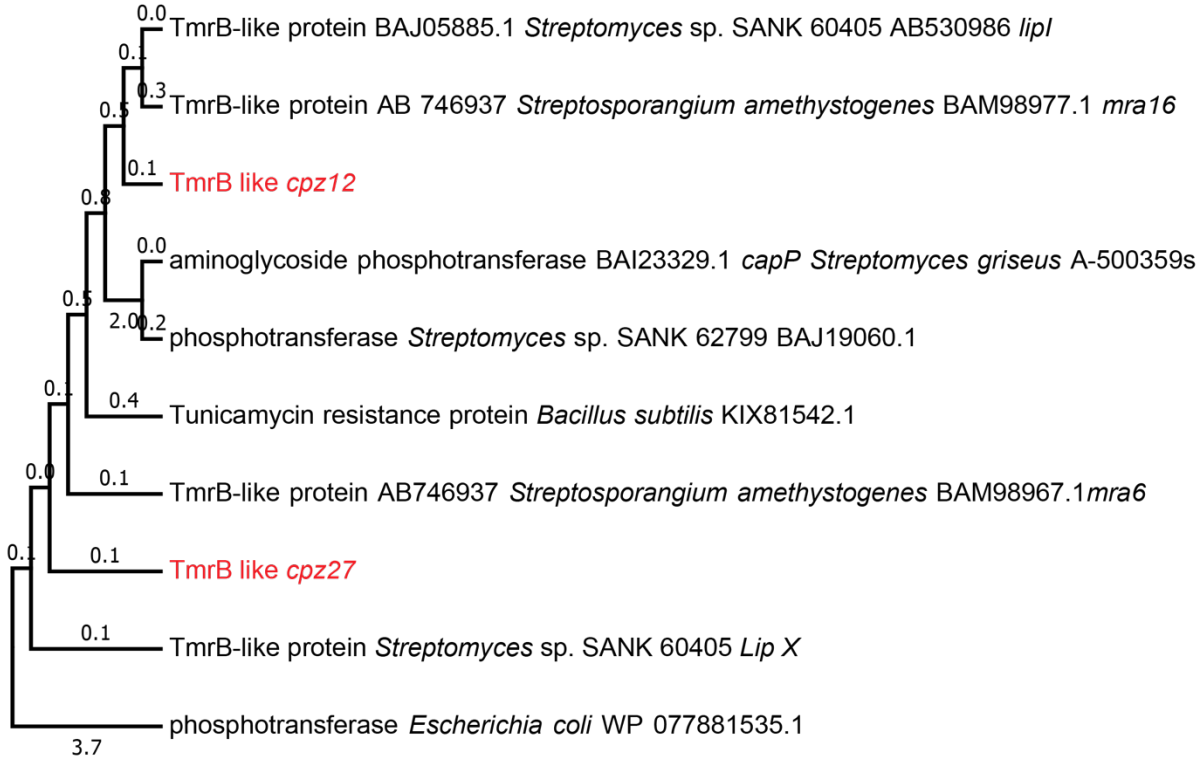

Figure 19. ***Phylogenetic analysis of the tmrB-like genes***.

Maximum likelihood tree. Bootstrap analysis (performed 1,000 times) *E. coli* (WP 077881535.1) was used as the outgroup. Scale bar represents amino acid substitutions per site.

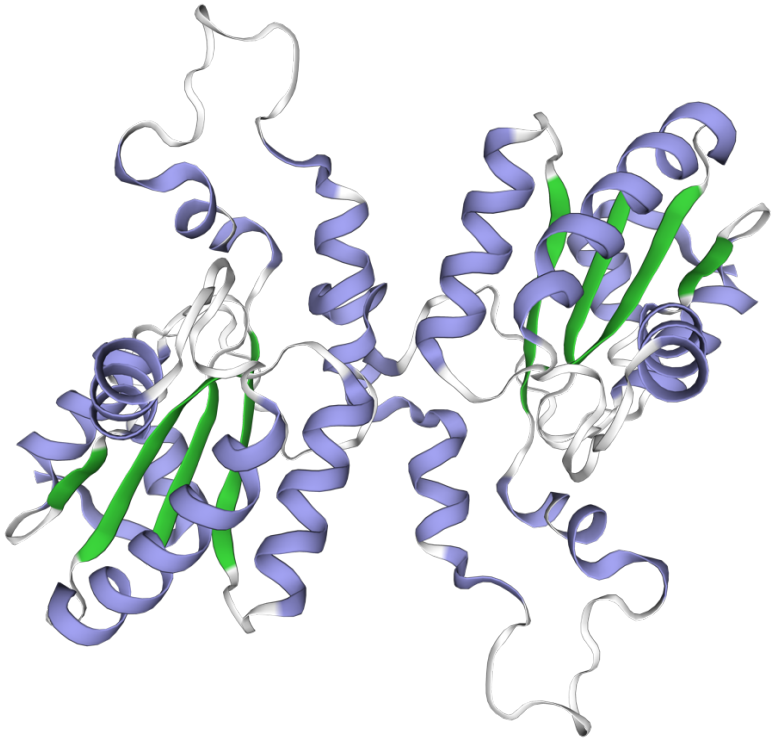

Figure 20. Structure protein model of Cpz12.

Model based on X-ray structure of the tunicamycin resistance protein from *Deinococcus radiodurans* using the SWISS- MODEL database tool (https://swissmodel.expasy.org).

A)

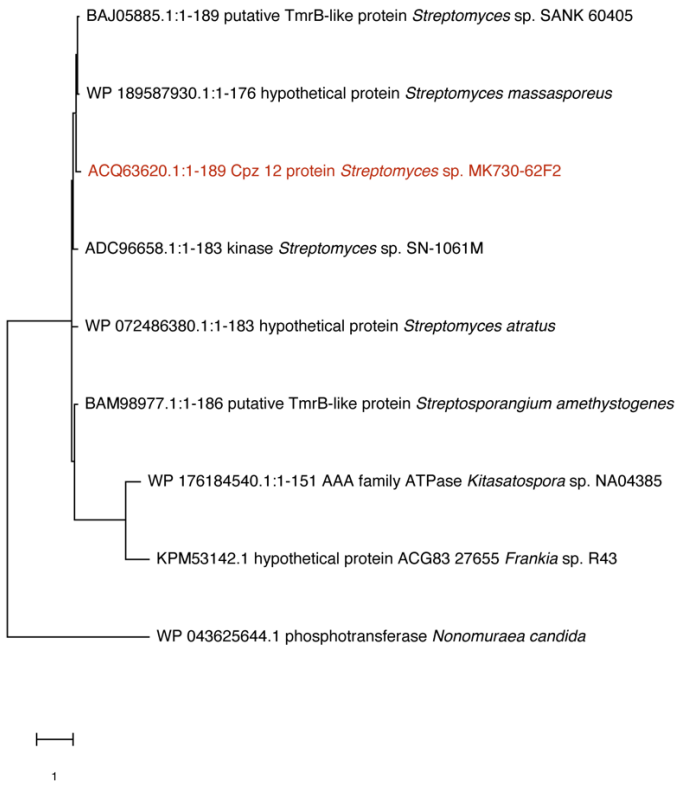

B)

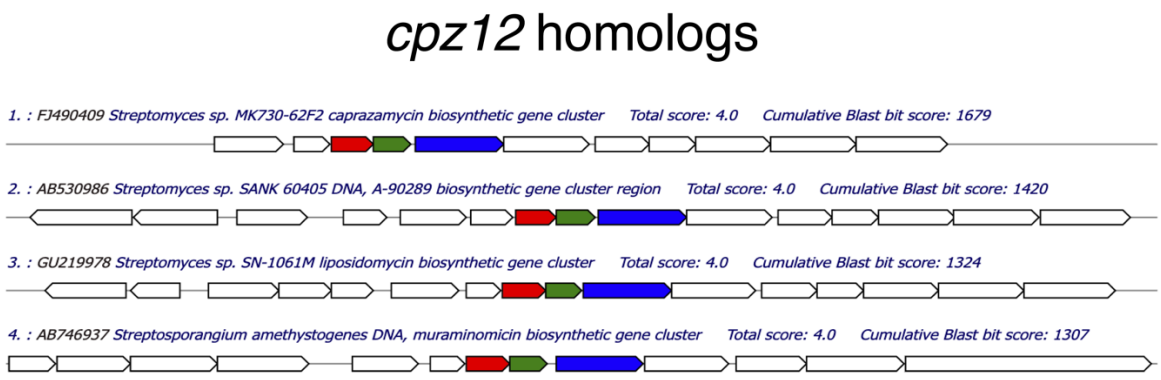

Figure 21. A. Phylogenetic analysis of *cpz12*.

The maximum likelihood tree is based on NCBI database, MultiGeneBlast tool and performed with MEGA X. *Nonomuraea candida* (WP 04362564.1) was used as the outgroup. Bootstrap analysis (performed 1,000 times). Scale bar represents 1 amino acid substitutions per site. **B.** MultiGeneBlast results using *cpz11, cpz12*, and *cpz13* as a template. Phosphotransferase gene *cpz12* homologs are shown in green.

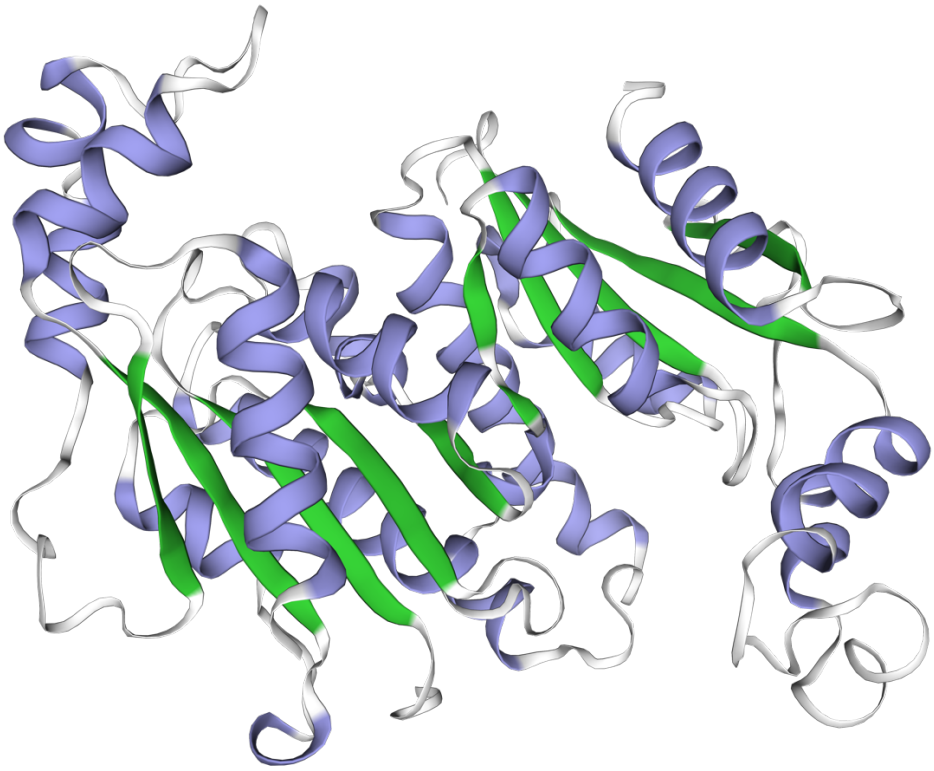

Figure 22. Structure protein model of the Cpz27.

Model based on X-ray structure of *Gluconate kinase* protein from SWISS- MODEL database tool (https://swissmodel.expasy.org).

A.

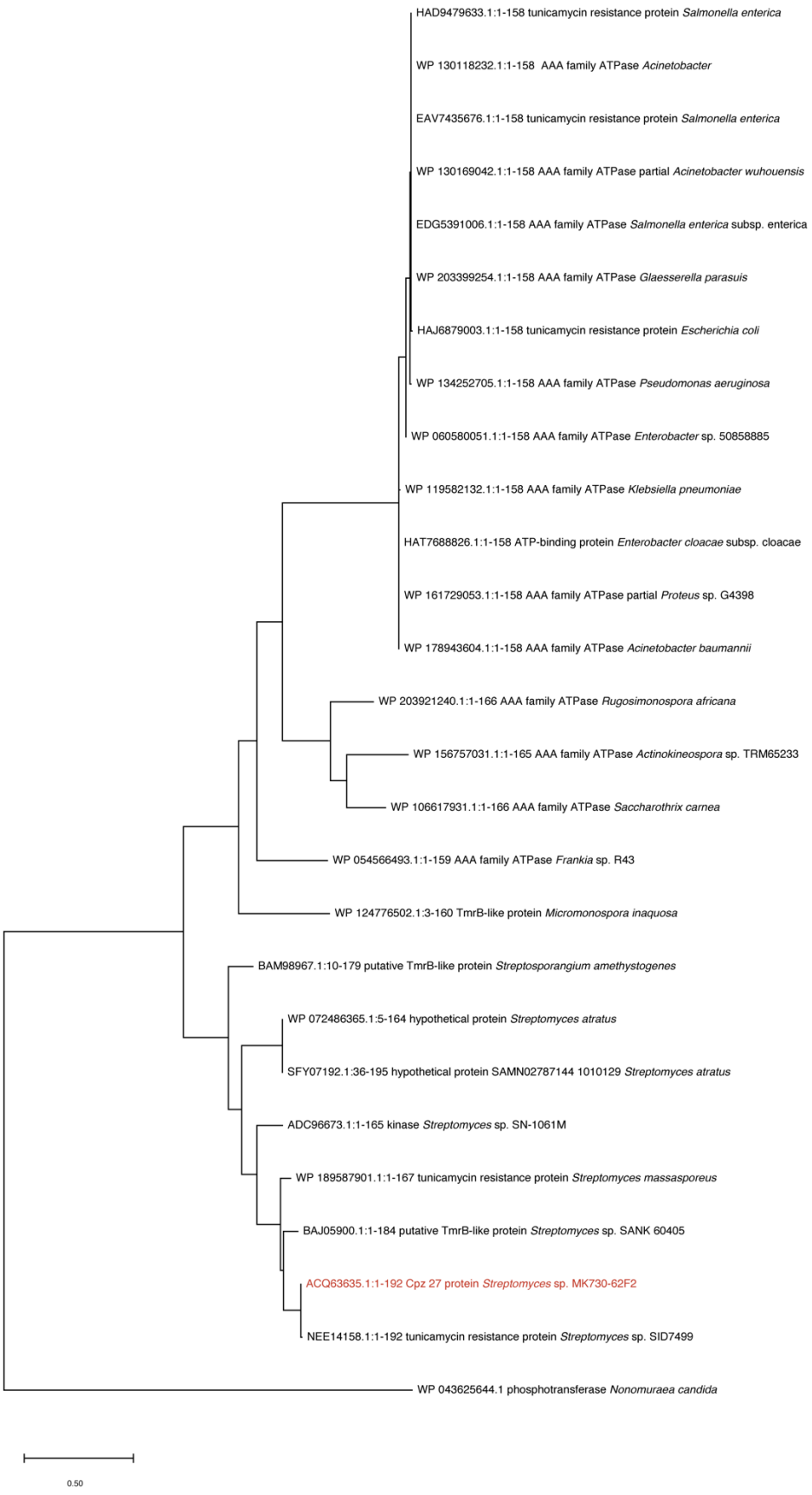
HAD9479633.1:1-158 tunicamycin resistance protein *Salmonella enterica*
WP 130118232.1:1-158 AAA family ATPase *Acinetobacter*
EAV7435676.1:1-158 tunicamycin resistance protein *Salmonella enterica*
WP 130169042.1:1-158 AAA family ATPase partial *Acinetobacter wuhouensis*
EDG5391006.1:1-158 AAA family ATPase *Salmonella enterica* subsp. enterica
WP 203399254.1:1-158 AAA family ATPase *Glaesserella parasuis*
HAJ6879003.1:1-158 tunicamycin resistance protein *Escherichia coli*
WP 134252705.1:1-158 AAA family ATPase *Pseudomonas aeruginosa*
WP 060580051.1:1-158 AAA family ATPase *Enterobacter* sp. 50858885
WP 119582132.1:1-158 AAA family ATPase *Klebsiella pneumoniae*
HAT7688826.1:1-158 ATP-binding protein *Enterobacter cloacae* subsp. cloacae
WP 161729053.1:1-158 AAA family ATPase partial *Proteus* sp. G4398
WP 178943604.1:1-158 AAA family ATPase *Acinetobacter baumannii*
WP 203921240.1:1-166 AAA family ATPase *Rugosimonospora africana*
WP 156757031.1:1-165 AAA family ATPase *Actinokineospora* sp. TRM65233
WP 106617931.1:1-166 AAA family ATPase *Saccharothrix carnea*
WP 054566493.1:1-159 AAA family ATPase *Frankia* sp. R43
WP 124776502.1:3-160 TmrB-like protein *Micromonospora inaquosa*
BAM98967.1:10-179 putative TmrB-like protein *Streptosporangium amethystogenes*
WP 072486365.1:5-164 hypothetical protein *Streptomyces atratus*
SFY07192.1:36-195 hypothetical protein SAMN02787144 1010129 *Streptomyces atratus*
ADC96673.1:1-165 kinase *Streptomyces* sp. SN-1061M
WP 189587901.1:1-167 tunicamycin resistance protein *Streptomyces massasporeus*
BAJ05900.1:1-184 putative TmrB-like protein *Streptomyces* sp. SANK 60405
ACQ63635.1:1-192 Cpz 27 protein *Streptomyces* sp. MK730-62F2
NEE14158.1:1-192 tunicamycin resistance protein *Streptomyces* sp. SID7499
WP 043625644.1 phosphotransferase *Nonomuraea candida*
0.50

B.

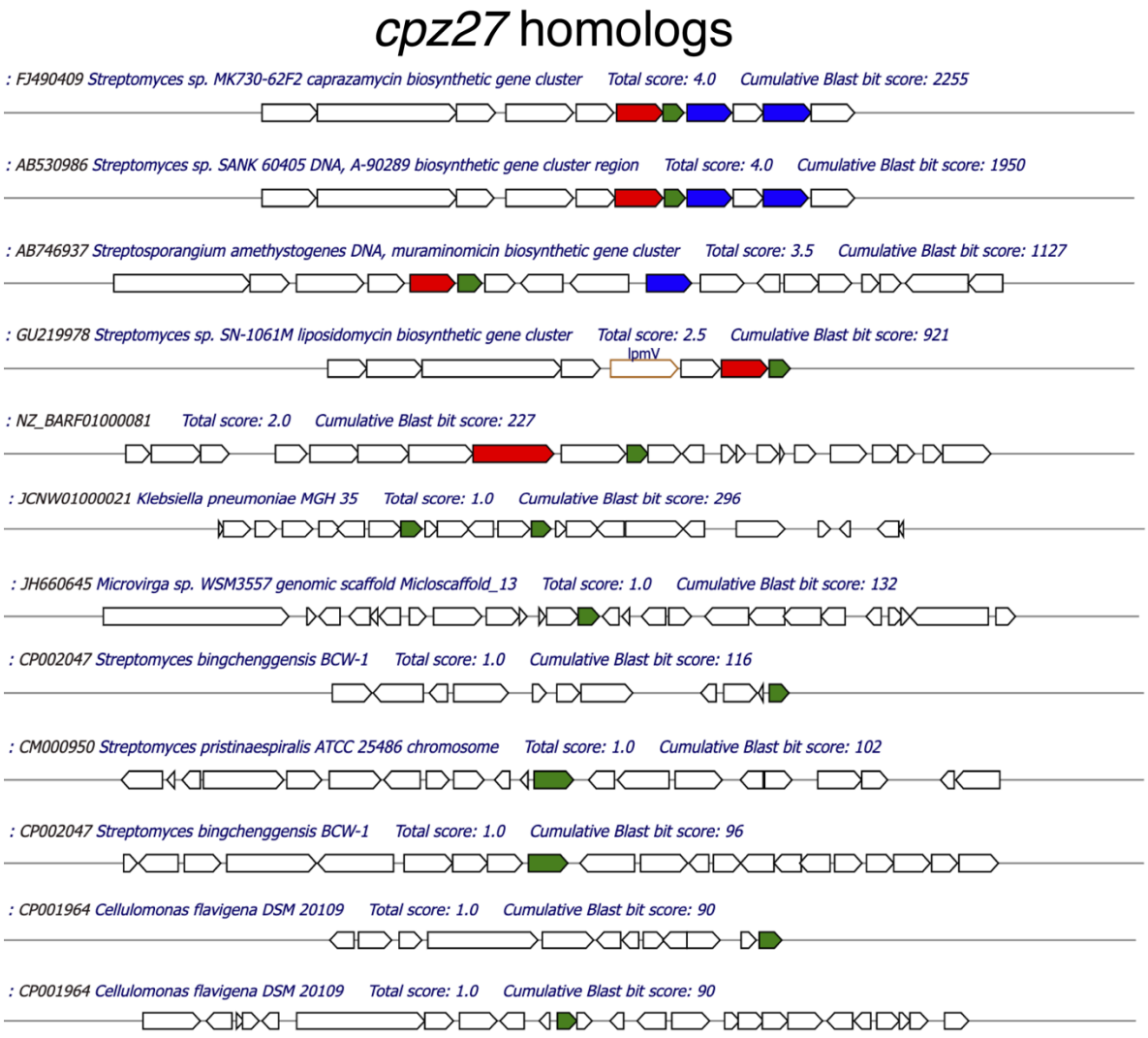

Figure 23. A. Phylogenetic analysis of *cpz*27.

The maximum likelihood tree is based on NCBI database, MultiGeneBlast and performed with MEGA X. *Nonomuraea candida* (WP 04362564.1) was used as the outgroup. Bootstrap analysis (performed 1,000 times). Scale bar represents 0.50 amino acid substitutions per site. **B.** MultiGeneBlast results using *cpz26, cpz27*, and *cpz28* as a template. Phosphotransferase gene *cpz27* homologs are shown in green

Cpz22 is part of the superfamily of transporter proteins (ATP-dependent ABC type) containing domains for ATPase activity and nucleotide-binding (NBD). The protein includes the Walker A and Walker B motifs required for ATP binding. Cpz22 also contains two signature motifs located upstream of the Walker B motif. The amino acid distance between lysine (K) of the Walker A domain and the aspartic acid of the Walker B domain is an important reference point in the classification of ABC transporters. The distance in Cpz22 is 130 aa for the first NBD and 120 aa for the second NBD. Analysis of the transmembrane domains (TMD) by Phyre2

and TMHMM revealed twelve transmembrane regions. This region of Cpz22 is presumably located within the membrane and is responsible for the formation of the channel through which the antibiotic is transported

A

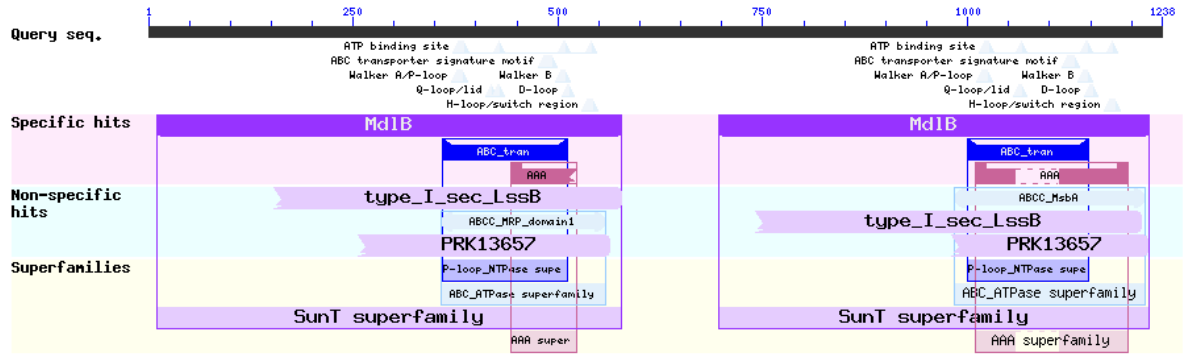

B

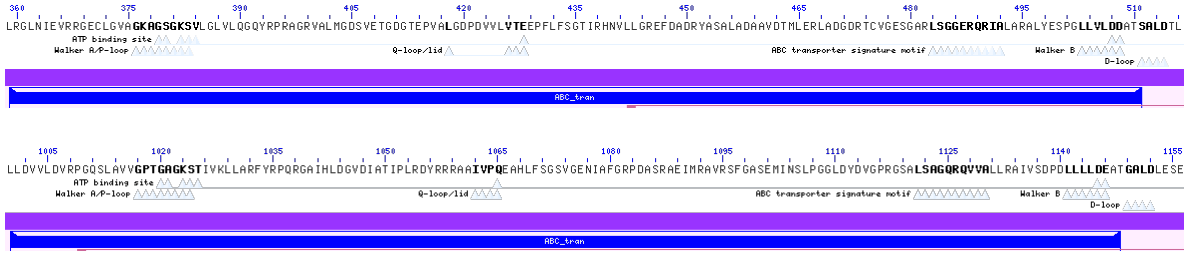

Figure 24. a) Amino acid sequence map analysis of the cpz22 gene B) reference distance between the Walker A and B.

Motif generated using NCBI's Delta Enhanced Lookup Time Accelerated BLAST tool.

Analysis of the transmembrane domains (TMD) has shown that it forms part of the ABC fused complex. This component is associated with the membrane and is responsible for the formation of the channel through which the substance is transported by this type of protein. It is concluded from the analysis by HMMER that the protein belongs to the superfamily of the ABC proteins associated to the membrane, but an amino acid sequence analysis was performed to establish how the structure is distributed in the cell membrane; the Phyre database shows coverage of 98% of residues modelled at >90% confidence by the single highest scoring template (Figure 25) a model with 0,54 value GMQE (Global Model Quality Estimation) from Swiss-model (https://swissmodel.expasy.org) database is also provided (Figure 26).

The sequence of the N-terminal region to the C-terminus has twelve transmembrane helices (Figure 25a). The probability and prediction of the helices was checked with the TMHMM database confirming twelve transmembrane regions of the sequence with value close to 1 (Figure 25b).

A)

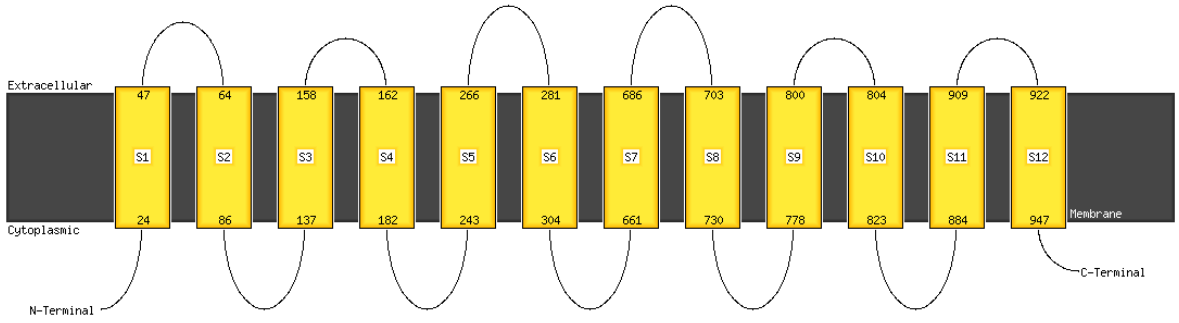

B)

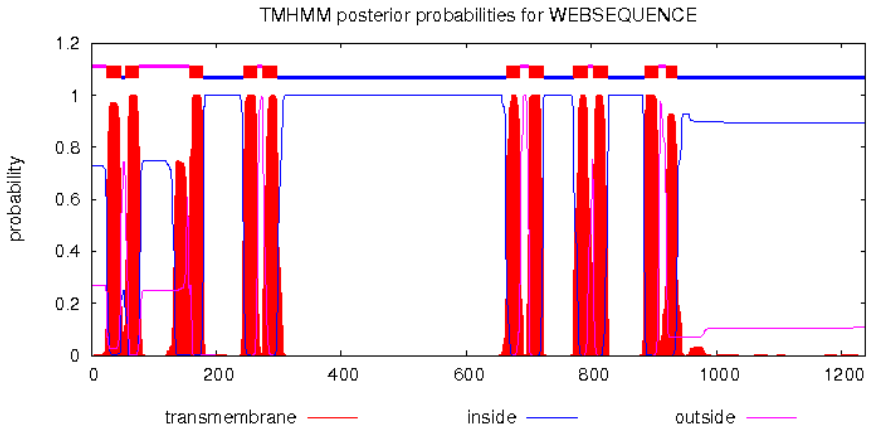

Figure 25. Prediction (b) and topology (a) of the transmembrane helices and amino acids that cross the membrane.

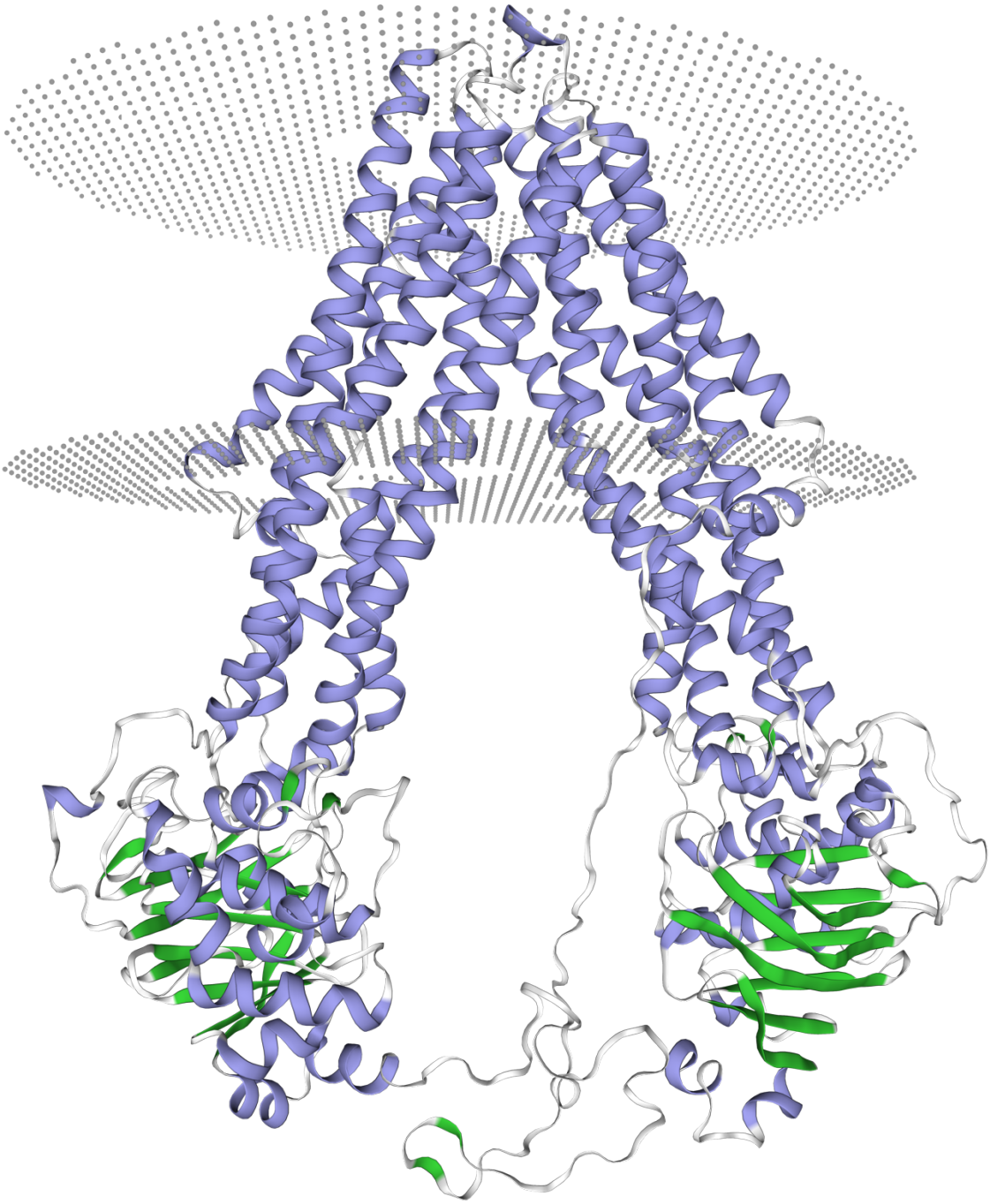

Figure 26. Structure protein model of the Cpz 22.

Model based on X-ray structure of *ATP-dependent translocase ABCB1 P-glycoprotein mutant-F979A and C952A-with BDE100* resistance protein from SWISS- MODEL database tool (https://swissmodel.expasy.org).

A.

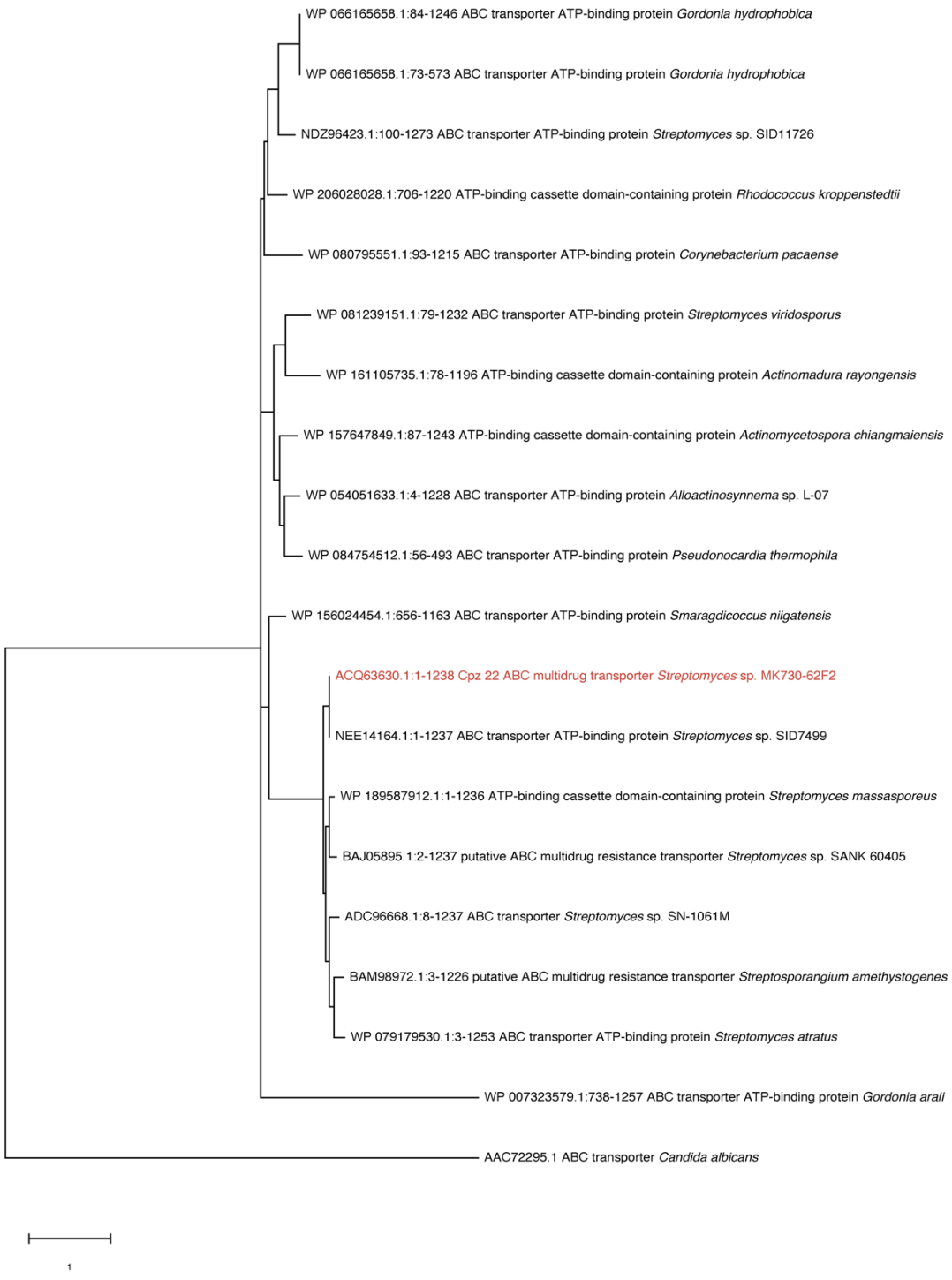
WP 066165658.1:84-1246 ABC transporter ATP-binding protein *Gordonia hydrophobica*
WP 066165658.1:73-573 ABC transporter ATP-binding protein *Gordonia hydrophobica*
NDZ96423.1:100-1273 ABC transporter ATP-binding protein *Streptomyces* sp. SID11726
WP 206028028.1:706-1220 ATP-binding cassette domain-containing protein *Rhodococcus kroppenstedtii*
WP 080795551.1:93-1215 ABC transporter ATP-binding protein *Corynebacterium pacaense*
WP 081239151.1:79-1232 ABC transporter ATP-binding protein *Streptomyces viridosporus*
WP 161105735.1:78-1196 ATP-binding cassette domain-containing protein *Actinomadura rayongensis*
WP 157647849.1:87-1243 ATP-binding cassette domain-containing protein *Actinomycetospora chiangmaiensis*
WP 054051633.1:4-1228 ABC transporter ATP-binding protein *Alloactinosynnema* sp. L-07
WP 084754512.1:56-493 ABC transporter ATP-binding protein *Pseudonocardia thermophila*
WP 156024454.1:656-1163 ABC transporter ATP-binding protein *Smaragdicoccus niigatensis*
ACQ63630.1:1-1238 Cpz 22 ABC multidrug transporter *Streptomyces* sp. MK730-62F2
NEE14164.1:1-1237 ABC transporter ATP-binding protein *Streptomyces* sp. SID7499
WP 189587912.1:1-1236 ATP-binding cassette domain-containing protein *Streptomyces massasporeus*
BAJ05895.1:2-1237 putative ABC multidrug resistance transporter *Streptomyces* sp. SANK 60405
ADC96668.1:8-1237 ABC transporter *Streptomyces* sp. SN-1061M
BAM98972.1:3-1226 putative ABC multidrug resistance transporter *Streptosporangium amethystogenes*
WP 079179530.1:3-1253 ABC transporter ATP-binding protein *Streptomyces atratus*
WP 007323579.1:738-1257 ABC transporter ATP-binding protein *Gordonia araii*
AAC72295.1 ABC transporter *Candida albicans*
1

B.

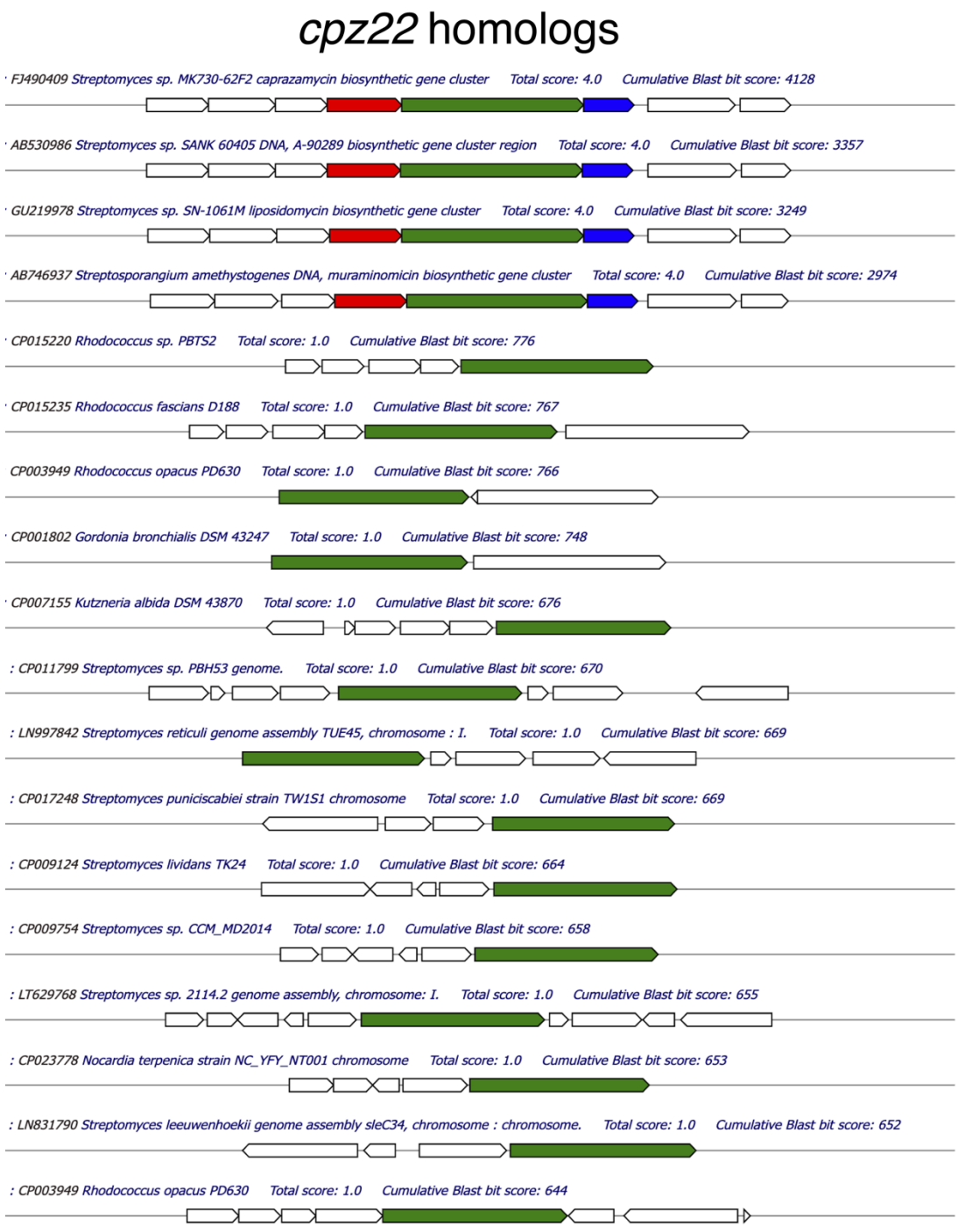

Figure 27. A. Phylogenetic analysis of *cpz*22.

The maximum likelihood tree is based on NCBI database, MultiGeneBlast tool and performed with MEGA X. *Candida albicans* (AAC72295.1) was used as the outgroup. Bootstrap analysis (performed 1,000 times). Scale bar represents 1 amino acid substitutions per site. **B.** MultiGeneBlast results using *cpz21, cpz22*, and *cpz23* as a template. ABC transporter gene *cpz22* homologs are shown in green.

3.2 Generation of knock-out mutants

In order to generate and analyze knock-out mutants, we used the successful heterologous expression system of *Streptomyces coelicolor* M512 leading to the formation of caprazamycin-aglycones, since genes for the formation of dTDP-L-rhamnose are missing in the heterologous host. The caprazamycin-aglycones can be produced in *S. coelicolor* M512 in quantities comparable to that of the wild type producer *Streptomyces* sp. MK730-62F2 (Kaysser et al. 2009) by expressing cosmid cpzLK09. Since the wild type is difficult to manipulate genetically, gene deletions were created on cosmid cpzLK09 by the use of Red/ET recombination and the modified cosmid integrated into the phiC31 attachment site of the heterologous producer *S. coelicolor* M512. Single in-frame gene-deletions were generated for *cpz12*, *cpz22, cpz23, cpz4* and *cpz27,* and a double knock-out mutant of *Δcpz27*/*Δcpz12* constructed to observe the combined effect of both phosphotransferase deletions. The mutant containing *Δcpz23*/*Δcpz4* was generated to confirm previous results of a *Δcpz23* mutant (Shiraishi et al. 2016), however eliminating the additional possibility to detect any sulfation reaction by Cpz4 which would lead to a mass shift of *m/z* = 80 $[M+H]^+$ comparable to that of a phosphorylation event. The resulting cosmids were named cpzCRD1 (Δ*cpz12*), cpzCRD2 (Δ*cpz22*), cpzCRD3 (Δ*cpz27*), cpzCRD4 (Δ*cpz23*), cpzCRD5 (*Δcpz12/Δcpz27*) and cpzCRD6 (*Δcpz23/Δcpz4*). All four generated constructs were introduced into the heterologous producer *Streptomyces coelicolor* M512 by conjugal transfer (Figure 28).

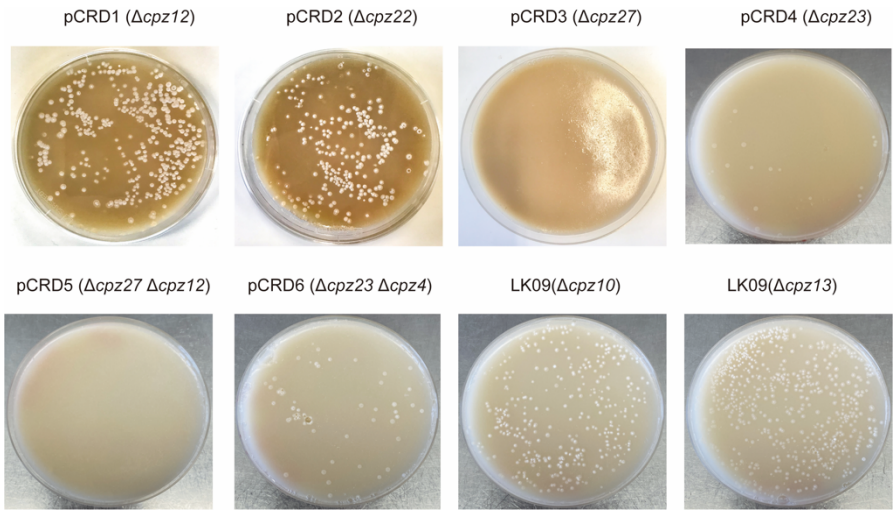

Figure 28. ***Exconjugants of S. coelicolor M512 harboring the cosmid with knock-out of the genes cpz12, cpz22, cpz23,*** **cpz23/cpz4 and** ***cpz27, cpz12/cpz27*** **(no exconjugants).**

3.2.1 Effect of cpz12 and cpz27 deletions

S. coelicolor M512/cpzCRD1 (Δ*cpz12*) was cultivated for seven days in 70 mL P-medium followed by an *n*-butanol/methanol-extraction of the supernatant and the cell pellet, which were afterwards reunited and analyzed by high-resolution mass spectrometry (HR-MS). Extracts of the mutant *S. coelicolor M512/*cpzCRD1 revealed a new peak corresponding to the biosynthetic intermediate (+)-caprazol, with an observed mass-to-charge ratio of 576.17 $[M+H]^+$ to which the chemical formula $C_{22}H_{34}N_5O_{13}$ was assigned (Figure 29a). In addition, the HR-MS data unveiled the formation of a phosphorylated (+)-caprazol with a calculated *m*/*z* of 656.1714 $[M+H]^+$ indicating the chemical formula $C_{22}H_{34}N_5O_{16}P$. A complementary MS/MS analysis of (+)-caprazol and the phosphorylated derivative led to the formation of fragment ions that were in full agreement with the expected structure (Figure 29b,c). Caprazamycin aglycones were also detected by HR-LC-MS in low quantities, indicating that phosphorylation by Cpz12 is not mandatory for the subsequent biosynthetic steps including transfer of a fatty-acyl side chain by the lipase Cpz23 and transfer of the 3-methylglutaryl moiety to the (+)-caprazol core structure by the acyl-transferase Cpz21. The decreased production of caprazamycin aglycones (Figure 31) could partially be restored by complementation with a plasmid (pUWL*cpz12*) containing an intact copy of *cpz12* (Figure 30). Surprisingly, conjugation of *S. coelicolor* M512 with cosmids containing either the single deletion of *cpz27* (cpzCRD3) or the double deletion of *cpz12* and *cpz27* (cpzCRD5) did not result in the growth of any exconjugants. This experiment was repeated three times with cosmid cpzCRD1 as positive control. In none of the conjugations, a single exconjugant was observed for cpzCDR3 or cpzCDR5 in contrast to hundreds of exconjugants observed with cpzCDR1. This is a clear indication that deletion of the phosphotransferase *cpz27* is lethal to the heterologous host *S. coelicolor* M512 (Figure 28).

A)

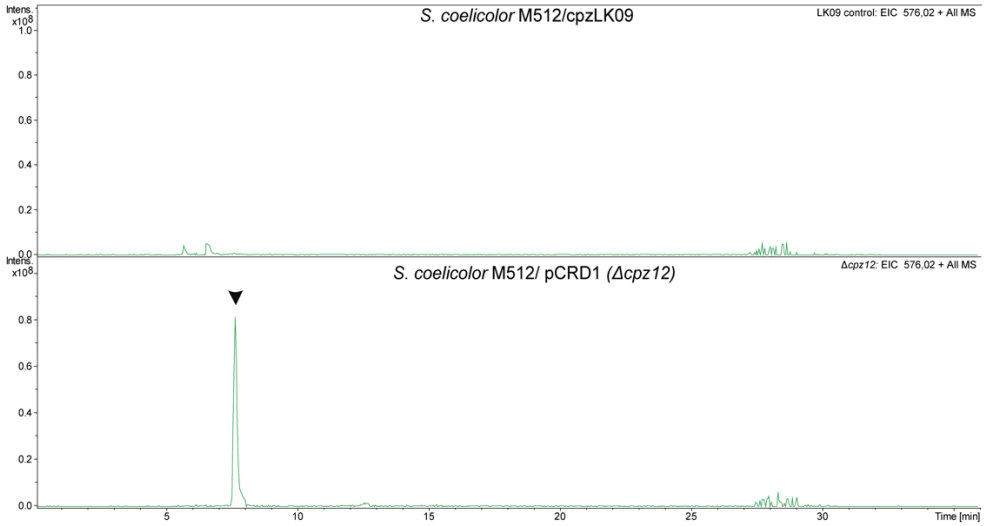

B)

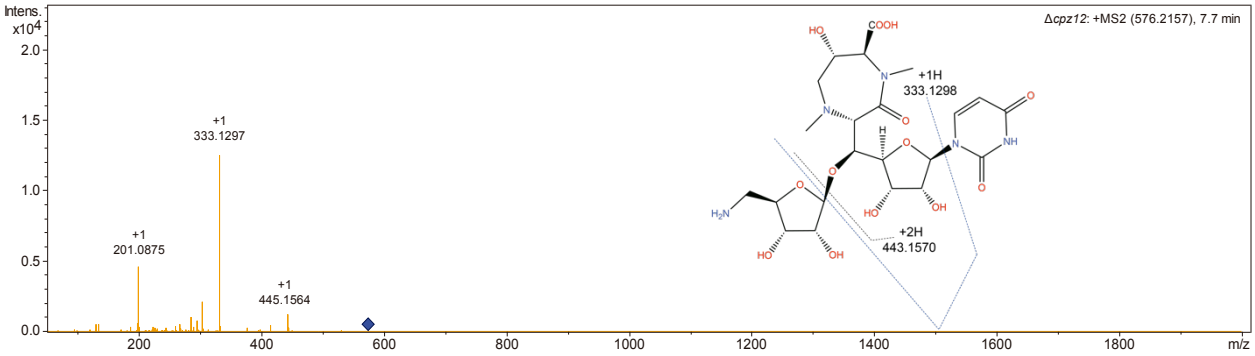

Fragment	Theoretical Mass (Da)	Experimental Mass *(m/z)*	Error [ppm]
$C_{22}H_{33}N_5O_{13}$ $[M+H]^+$	576.2153	576.2157	0.6941
$C_{17}H_{23}N_4O_{10}$ $[M+2H]^+$	445.1570	445.1564	1.3478
$C_{13}H_{20}N_2O_8$ $[M+H]^+$	333.1298	333.1297	-0.3001

C)

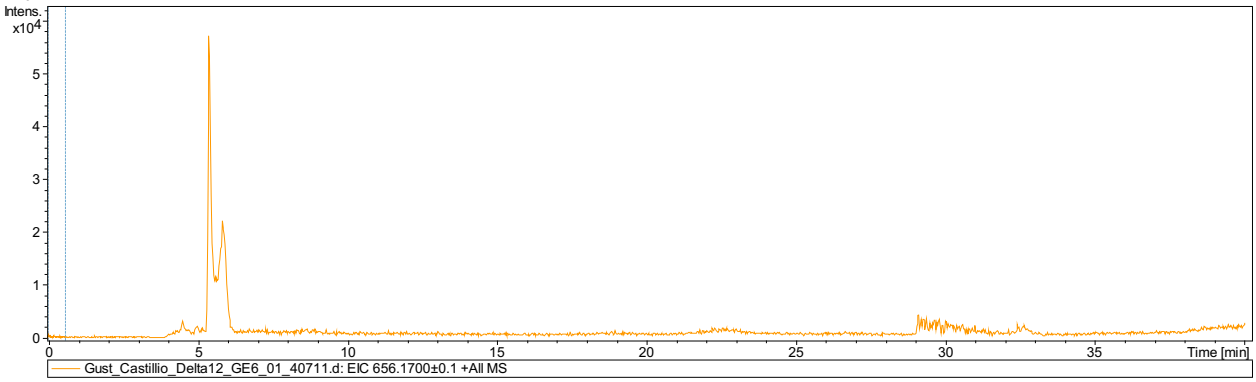

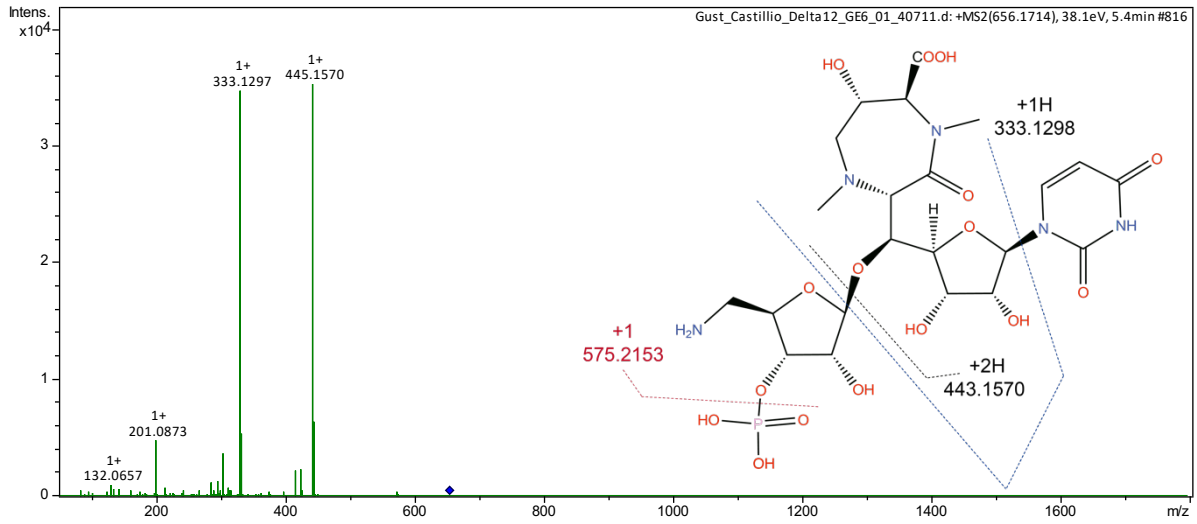

Fragment	Theoretical Mass (Da)	Experimental Mass *(m/z)*	Error [ppm]
$C_{22}H_{35}N_5O_{16}P$ $[M+H]^+$	656.1816	656.1795	-3.2003
$C_{22}H_{33}N_5O_{13}$ $[M+H]^+$	576.2153	576.2156	0.5206
$C_{17}H_{23}N_4O_{10}$ $[M+2H]^+$	445.1570	445.1570	0
$C_{13}H_{20}N_2O_8$ $[M+H]^+$	333.1298	333.1297	-0.3001

Figure 29. LC-MS analysis *Δcpz12*
a) Low Resolution-EIC analysis of *S. coelicolor* M512/cpzLK09 vs. *S. coelicolor* M512/*Δcpz12*
b) High Resolution ESI-MS/MS (MS^2) of caprazol and C) its 3' phosphorylated version. The dotted lines were drawn to explain the intensities of the observed peaks. Bottom scheme shows the key fragments corresponding to the structure and were assigned on the structure.

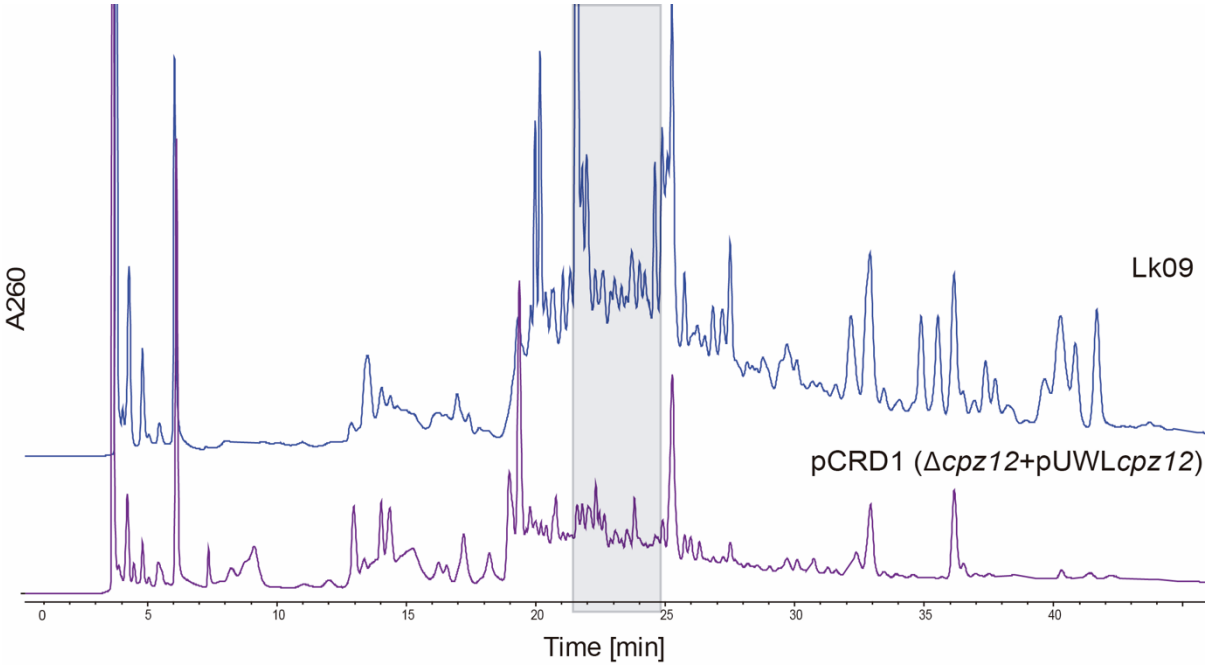

Figure 30. HPLC profile of strain cpzLK09 vs. pCRD1 + pUWL*cpz12* strain.

Caprazamycin aglycon peaks are highlighted, the production was partially restored in the complemented strain.

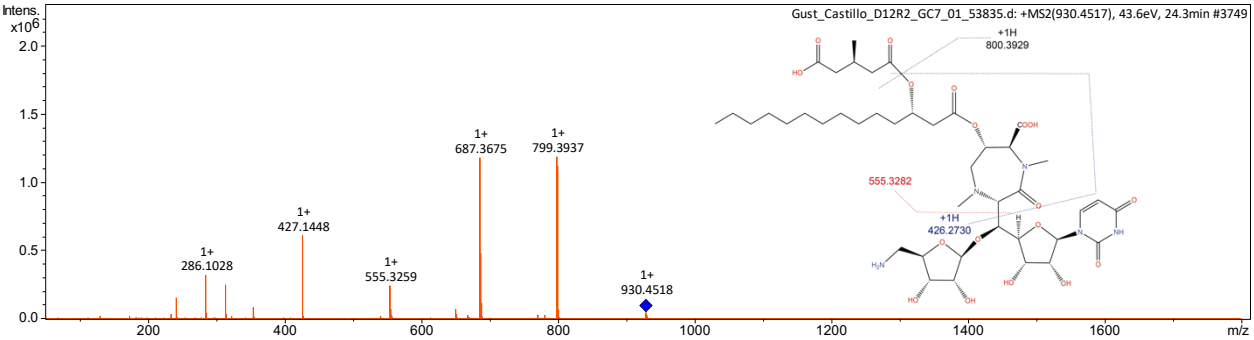

Fragment	Theoretical Mass (Da)	Experimental Mass *(m/z)*	Error [ppm]
$C_{42}H_{67}N_5O_{18}$ $[M+H]^+$	930.4554	930.4518	-3.8690
$C_{36}H_{58}N_5O_{15}$ $[M+H]^+$	799.3971	799.3937	-4.2532
$C_{33}H_{55}N_2O_{13}$ $[M+H]^+$	687.3699	687.3675	-3.4915
$C_{28}H_{47}N_2O_9$	555.3276	555.3259	-3.0612
$C_{22}H_{38}N_2O_6$ $[M+H]^+$	427.1460	427.1448	-2.8093

Figure 31. ESI-MS/MS (MS^2) of CPZAE found in the strain pCRD1 strain.
The dotted lines were drawn to explain the intensities of the observed peaks. Bottom scheme shows the key fragments corresponding to the structure and were assigned on the structure.

3.2.2 Effect of cpz23 deletion

Formation of phosphorylated (+)-caprazols were previously observed by Shiraishi and colleagues from a *cpz23* deletion-mutant of the wildtype *Streptomyces* sp. SANK 60405 (Shiraishi et al. 2016). However, approximately 20% of caprazamycins are sulfated by a two-step sulfation mechanism involving the PAPS-dependent sulfotransferase Cpz8 and the PAPS-independent arylsulfate sulfotransferase Cpz4 (Tang et al. 2013). Since both modifications will result in a mass-shift of *m/z* = 80 $[M+H]^+$, it cannot be excluded, that this mass shift is the consequence of a sulfation rather than a phosphorylation event. Therefore, two different mutants were generated and analyzed by HR-LC-MS. First, *cpz23* was deleted on cpzLK09 as in-frame deletion generating cosmid cpzCRD4 (*Δcpz23*). Second, *cpz4* was deleted, again as in-frame deletion, on cpzCRD4 to generate cpzCRD6 (*Δcpz23*/*Δcpz4*). Both cosmids were introduced into *S. coelicolor* M512 and resulting exconjugants confirmed by PCR and sequencing of the resulting PCR-products. The chemotype of both mutants was analyzed by HR-MS (Figure 32). As expected, both mutants accumulated the same biosynthetic intermediates as the *cpz12* deletion mutant *S. coelicolor* M512/cpzCRD1, namely (+)-caprazol and phosphorylated (+)-caprazol with *m/z* of 576.2159 and *m/z* of 656.1820 $[M+H]^+$, respectively. Again, the same chemical formulas of $C_{22}H_{34}N_5O_{13}$ and $C_{22}H_{34}N_5O_{16}P$ could be assigned for the identified compounds (Δppm= 1.0 and 3.2) (Figure 32).

A)

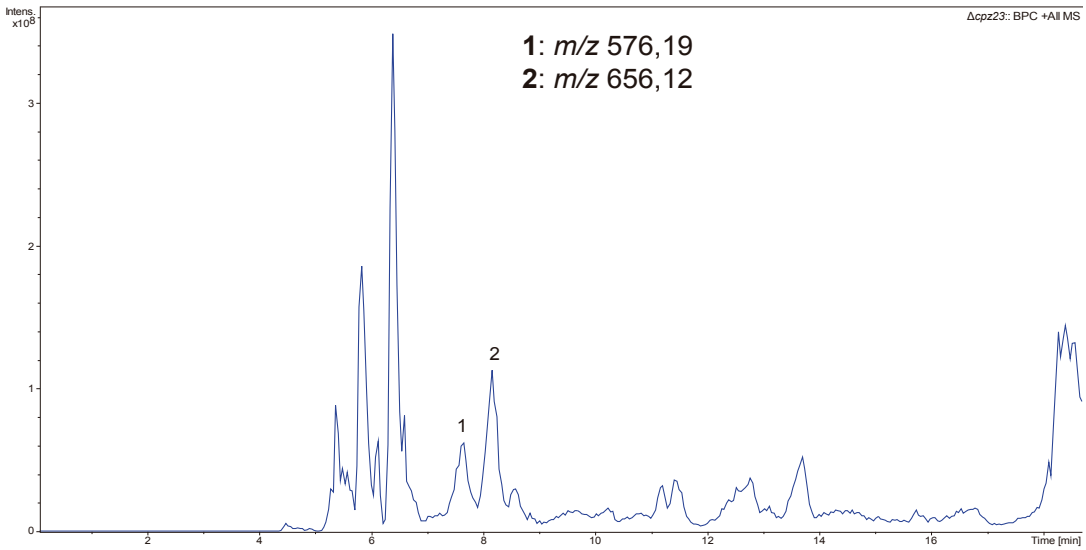

B)

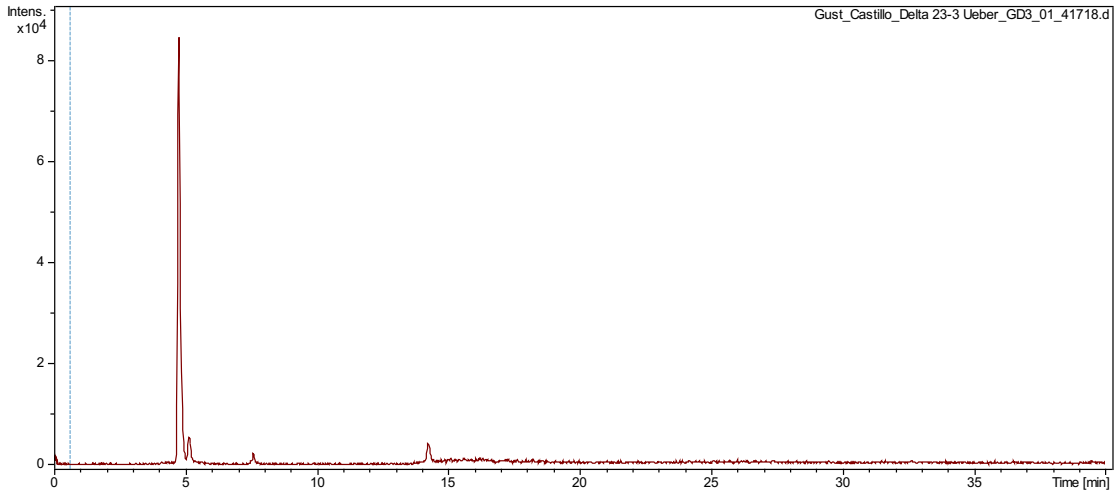

Fragment	Theoretical Mass (Da)	Experimental Mass *(m/z)*	Error [ppm]
$C_{22}H_{33}N_5O_{13}$ $[M+H]^+$	576.2153	576.2159	1.0412
$C_{17}H_{23}N_4O_{10}$ $[M+2H]^+$	445.1570	445.1582	2.6956
$C_{13}H_{20}N_2O_8$ $[M+H]^+$	333.1298	333.1302	1.2007

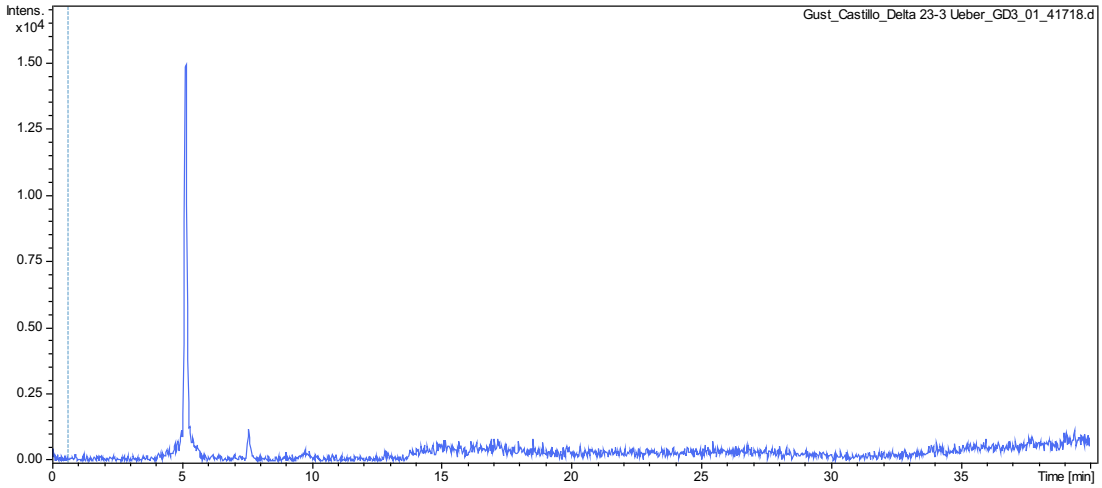

Fragment	Theoretical Mass (Da)	Experimental Mass *(m/z)*	Error [ppm]
$C_{22}H_{35}N_5O_{16}P$ $[M+H]^+$	656.1816	656.1795	3.2003
$C_{22}H_{33}N_5O_{13}$ $[M+H]^+$	576.2153	576.2148	-0.8677
$C_{17}H_{23}N_4O_{10}$ $[M+2H]^+$	445.1570	445.1581	2.4710
$C_{13}H_{20}N_2O_8$ $[M+H]^+$	333.1298	333.1292	-1.8011

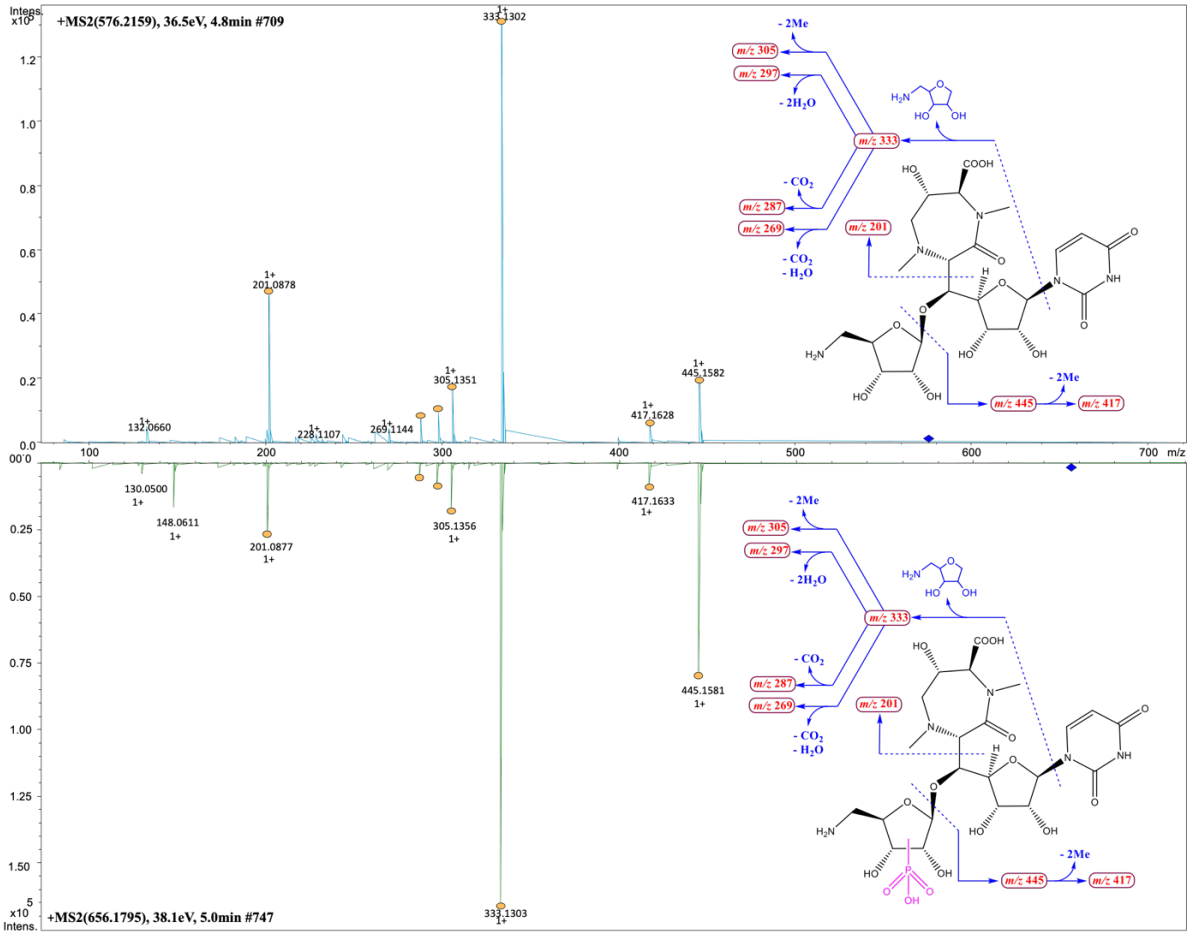

Figure 32. ESI-MS/MS (MS^2) of (+)-caprazol and its 3' phosphorylated derivative found in *S. celicolor* M512/pCRD4.

a) Low Resolution-BPC analysis of *S. coelicolor* M512/pCRD4 (*Δcpz23*)
b) High Resolution ESI-MS/MS (MS^2) of (+)-caprazol and c) its 3' phosphorylated derivative. The dotted lines were drawn to explain the intensities of the observed peaks. Bottom scheme shows the key fragments corresponding to the structure and were assigned on the structure.

Structural analysis of the phosphorylated (+)-caprazol was achieved by HR-MS in combination with HR-MS/MS and ^{31}P NMR spectroscopy (Figure 34). The position of the phosphate was analyzed in a former study and could be allocated to the 3''-position of the aminoribose. Since the mutant containing the deletion of *cpz23* and *cpz4* also produced both biosynthetic intermediates, it can be ruled-out that the observed mass shift of the phosphorylated (+)-caprazol in comparison to (+)-caprazol is an effect of sulfation rather than phosphorylation (Figure 33).

A)

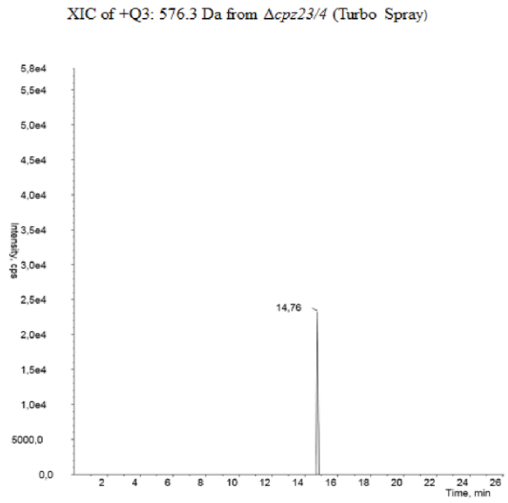

B)

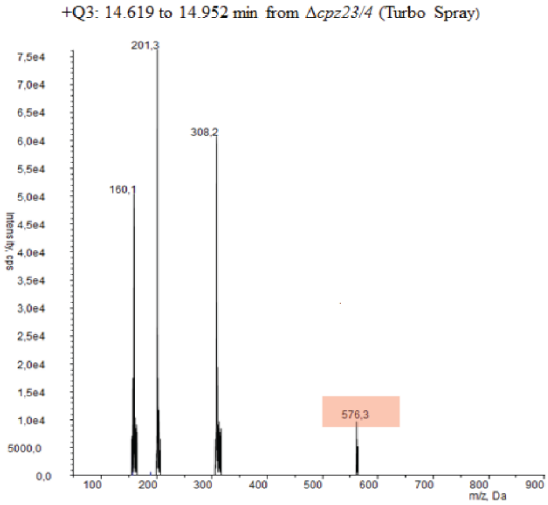

C)

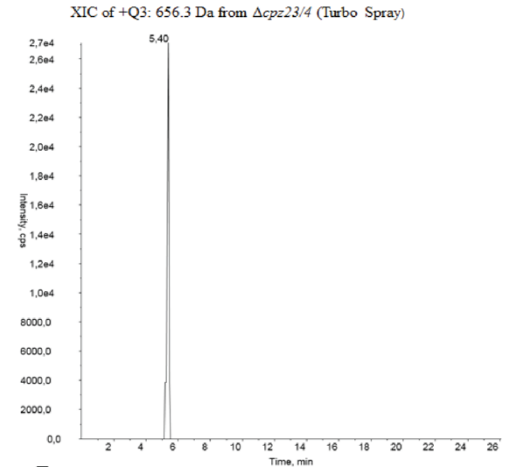

D)

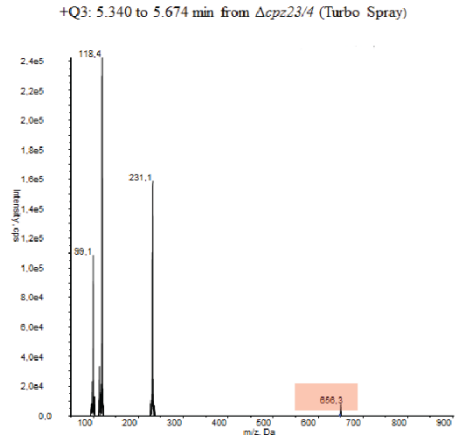

Figure 33. (A-B): low resolution- LC-MS analysis of *S. coelicolor* M512 cpzLK09 Δ*cpz23/4*

XIC of caprazol (A) and its corresponding MS-spectrum (B) (*m/z* 575,21)
XIC of phosphocaprazol (C) and its corresponding MS-spectrum (D) (*m/z* 655,17)

3.2.3 NMR elucidation of phosphorylated caprazol

Complementary to the MS/MS analyses of phosphorylated (+)-caprazol, a ^{31}P NMR spectrum was recorded. The obtained spectrum (Figure 34) exhibited with δ_P = 0.13 a characteristic shift value, indicative for a phosphorus atom of a phosphate group, which corroborated the mass spectrometry-based findings.

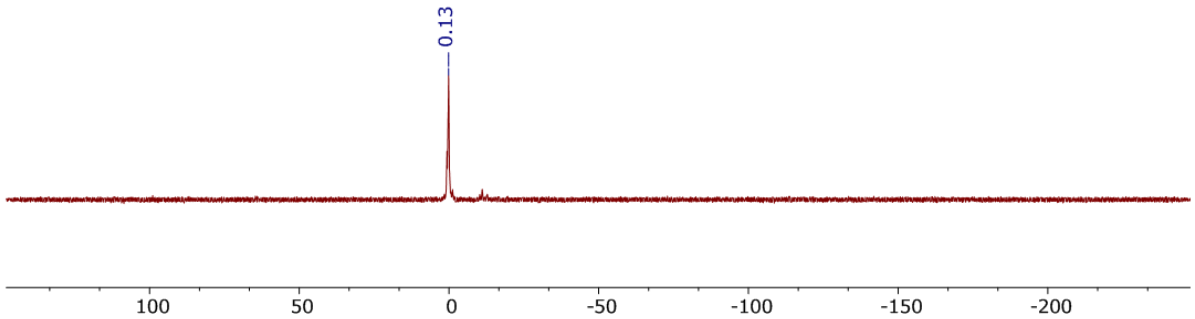

Figure 34. ^{31}P NMR spectrum of phosphorylated (+)-caprazol in D_2O (283 MHz)

3.2.4 In-vitro assays with Cpz23

Sequence analysis of Cpz23 revealed strong homologies with GDSL-like lipases, indicating a role as an acyltransferase. Deletion of *cpz23* resulted in the exclusive production of (+)-caprazol and phosphorylated (+)-caprazols. The same compounds were observed by Shiraishi and colleagues in a *cpz23* deletion mutant of the wildtype producer (Shiraishi et al., 2016). It is therefore most likely that Cpz23 catalyzes the transfer of β-hydroxy-fatty acids onto the caprazamycin core structure to generate hydroxyacylcaprazols differing only in the length (C12 – C16) and configuration (saturated, unsaturated, branched, unbranched) of the β-hydroxy-acyl moiety. Since hydroxyacylcaprazols are the first biosynthetic intermediates that showed anti-mycobacterial activity, Cpz23 is regarded as a crucial enzyme in caprazamycin biosynthesis. To prove the function of Cpz23, the corresponding gene was cloned into the vector pHis8 and expressed in *E. coli* for further purification (Figure 35). An in-vitro assay with Cpz23 was conducted using purified (+)-caprazol or phosphorylated (+)-caprazol and β-hydroxy-myristoyl-CoA as substrates. Considering the readings of HPLC and MS profiles, the respective HACE, which would have been catalyzed by Cpz23, was detected at UV 260 nm possessing a mass of *m/z* 802.4080 (Figure 36, 37). Interestingly, the corresponding mass of the phosphorylated hydroxyacylcaprazol E was not detected, suggesting that Cpz23 might have a substrate specificity towards (+)-caprazol and not phosphorylated (+)-caprazol.

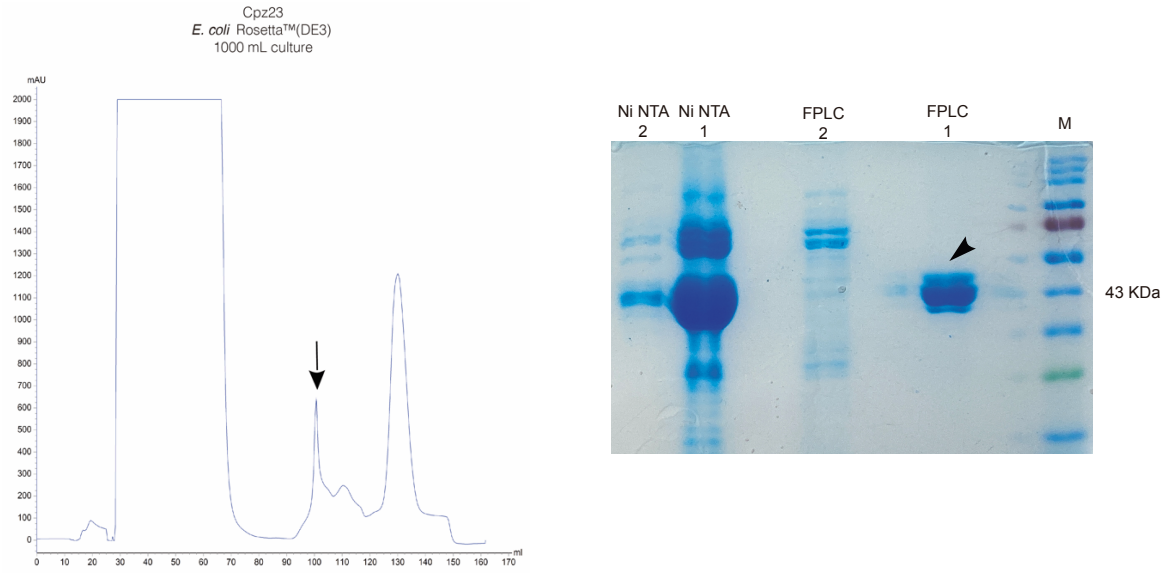

Figure 35. FPLC Chromatogram of the lipase Cpz23 and SDS-PAGE 12% polyacrylamide of the purified protein

FPLC peak 1 showed to be the right protein peak as His8-taged Cpz23 has a size of 38245,48 Da and the Thrombin cleavage site adding another 2589.25 Da resulting in a total of 40834.73 Da.

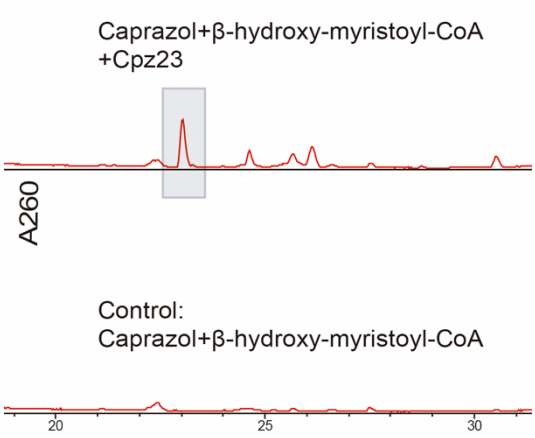

Figure 36. Cpz23 enzyme reaction using (+)-caprazol and β-hydroxy-myristoyl-CoA as substrates to produce hydroxyacylcaprazol E

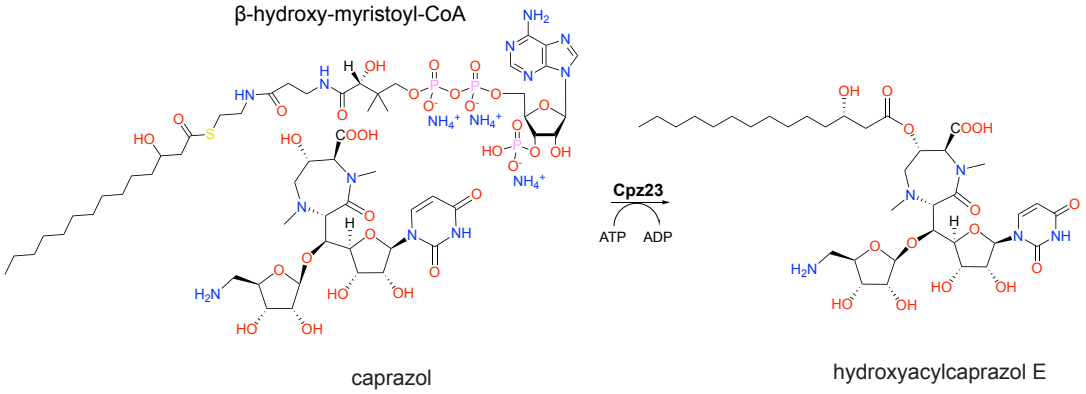

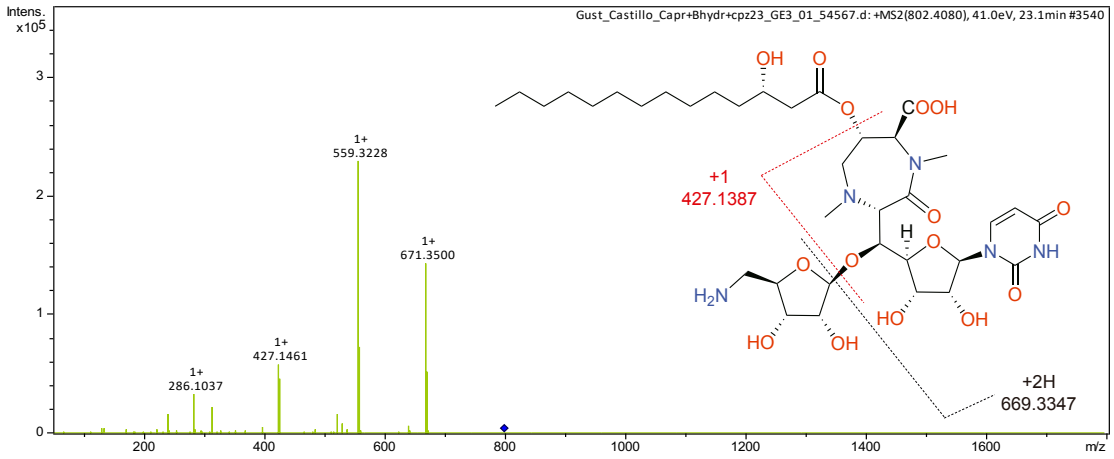

Fragment	Theoretical Mass (Da)	Experimental Mass *(m/z)*	Error [ppm]
$C_{36}H_{59}N_5O_{15}$ $[M+H]^+$	802.4080	802.4080	0
$C_{31}H_{47}N_4O_{12}$ $[M+2H]^+$	671.3498	671.3500	0.2979
$C_{17}H_{23}N_4O_9$ $[M+H]^+$	427.1460	427.1461	0.2341

Figure 37. Figure HR-MS analysis of the Cpz23 reaction product

3.2.5 In-vitro studies of Cpz12 and Cpz27

The phosphotransferases Cpz12 and Cpz27 from *Streptomyces sp. MK730-62F2* consists of 189 and 192 amino acids, respectively. To elucidate their functions in-vitro, both corresponding genes were cloned into the *Streptomyces-E. coli* shuttle vectors pGM1190 and pGM1192 followed by expression of the resulting plasmids pJH01 (pGM1190+*cpz12*), pJH02 (pGM1190+*cpz27*), pJH03 (pGM1192+*cpz12*) and pJH04 (pGM11902+*cpz27*) in *S. lividans* TK24 and *S. albus* J1074. Purified enzymes (Figure 38) were used for in-vitro assays in order to identify possible substrates for phosphotransfer reactions. As substrates, biosynthetic intermediates from early, intermediate and late caprazamycin biosynthetic steps were chosen, precisely compound **7** consisting of a 5''-amino-5''-deoxyribose (ADR) coupled with a short-chain amino acid to form an ADR-GlyU (5′-C-glycyluridine) disaccharide core as the drug warhead, attached with a 3-amino-3-carboxypropyl side chain; compound **11** representing (+)-caprazol and compound **13** representing hydroxyacylcaprazol E (Figure 46). The enzymatic activity was monitored by recruiting the HPLC profiling recorded at a UV absorbance of 260 nm and supported with HR-MS measurement (Figure 39). For all tested compounds, Cpz12 showed no activity towards generation of a phosphorylated derivative. However, compound **7** was readily accepted by the phosphotransferase Cpz27 to generate the phosphorylated

derivative at the expense of one molecule ATP. HR-LC-MS confirmed formation of a new compound with a molecular ion $[M+H]^+$ at *m/z* = 585,17 in comparison to *m/z* = 505,20 of compound **7**. The indicated molecular formula of the new compound also suggested the presence of a phosphate ($C_{19}H_{32}N_5O_{14}P^+$) (Figure 40).

A)

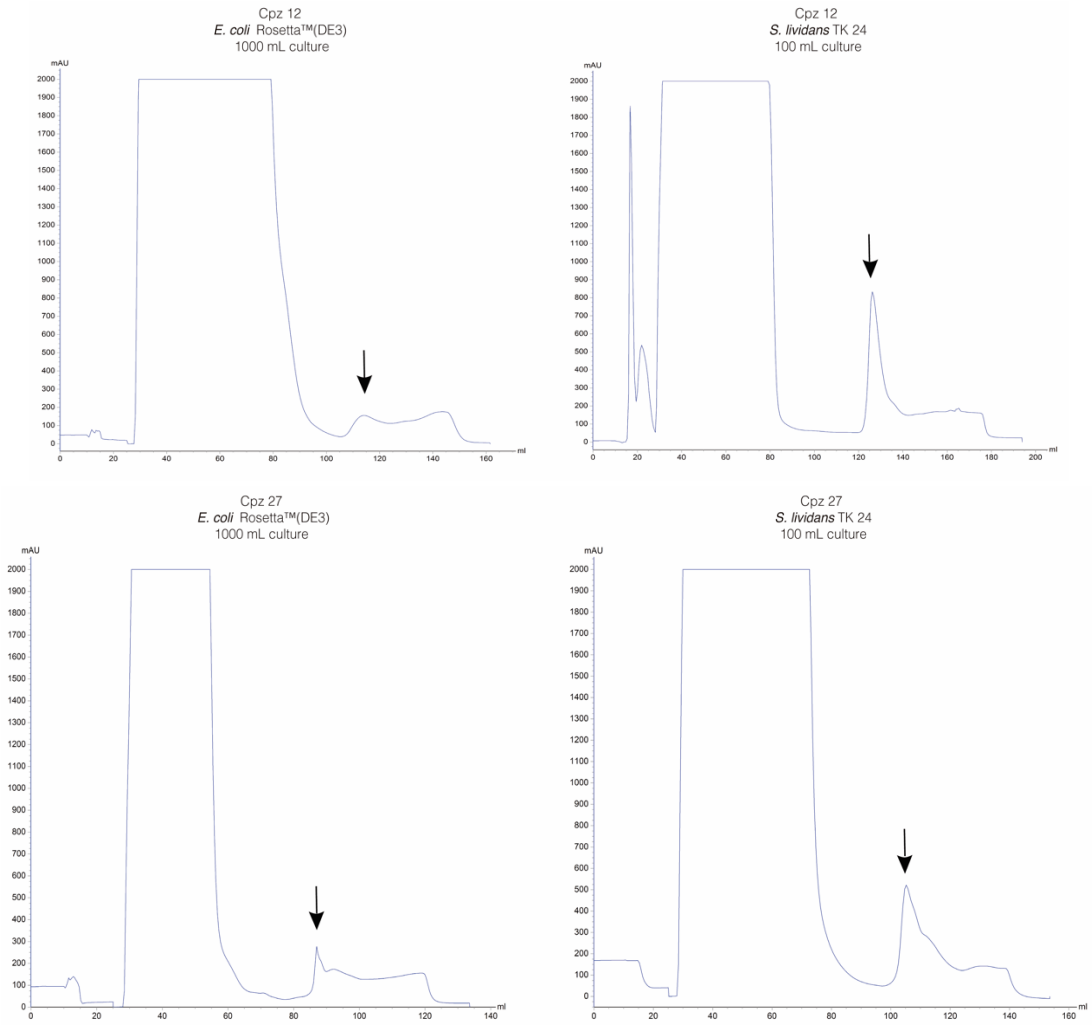

B)

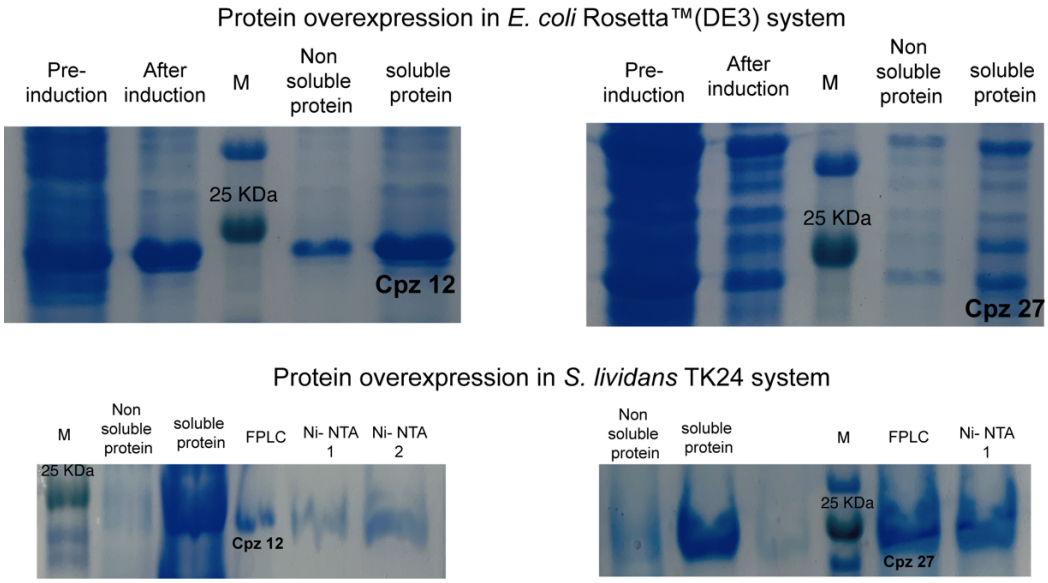

Figure 38. Protein overexpression of Cpz12 and Cpz27

a) FPLC Chromatogram of the two phosphotransferases Cpz12, and Cpz27.

b) SDS-PAGE 12% polyacrylamide of the two phosphotransferases Cpz12 (20,79 kDa), and Cpz27 (21,62 KDa). HisTag-Trombin add 1.83 KDa. PI: pre-induction, AI: after induction, NSP: Non-soluble protein, SP: soluble protein.

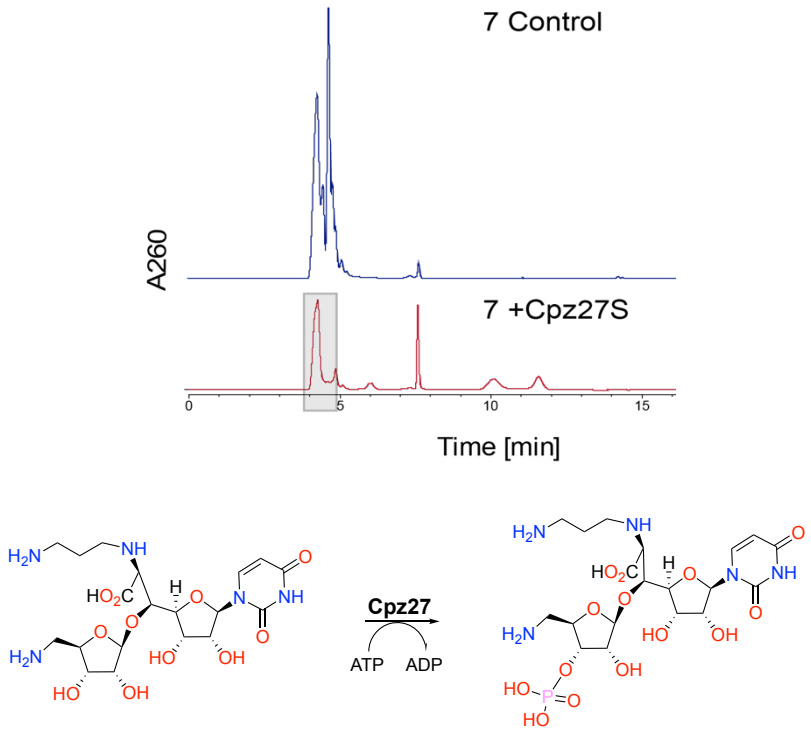

Figure 39. Cpz27 enzyme reaction using compound 7 $C_{19}H_{31}N_5O_{11}$ producing $C_{19}H_{31}N_5O_{11}P$

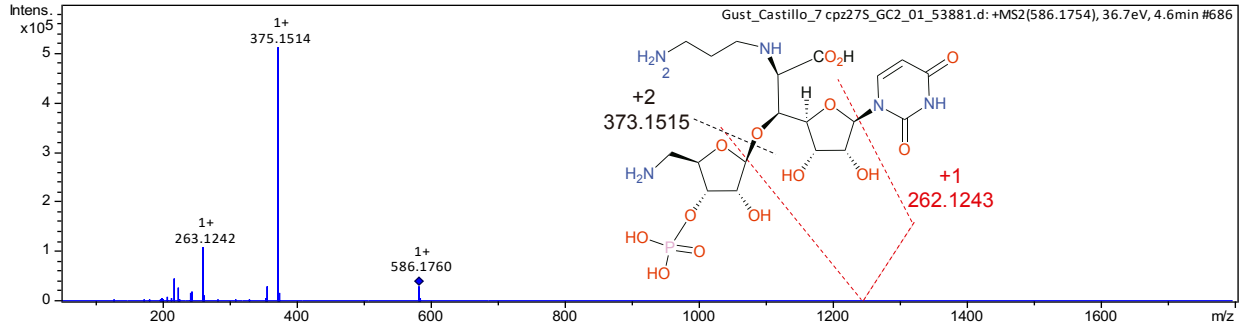

Fragment	Theoretical Mass (Da)	Experimental Mass *(m/z)*	Error [ppm]
Phospho-Compound 7 $C_{19}H_{32}N_5O_{14}P$ $[M+H]^+$	586.1761	586.1760	-0.1705
$C_{14}H_{23}N_4O_8$ $[M+2H]^+$	375.1515	375.1514	-0.2665
$C_{10}H_{19}N_2O_6$ $[M+H]^+$	263.1243	263.1242	-0.3800

Figure 40. HR-MS/MS of $C_{19}H_{31}N_5O_{11}P$

Tandem MS/MS detected daughter ions. Theoretical and observed mass differences are assigned.

3.2.6 Effect of cpz22 deletion

Cpz22 is part of the superfamily of transporter proteins containing domains for ATPase activity and a nucleotide-binding domain (ATP-dependent ABC type). The protein includes the Walker A and Walker B motifs required for ATP binding. In order to study the influence of the ABC-transporter towards caprazamycin resistance, we compared production of caprazamycin-aglycons between the heterologous host containing the entire gene cluster cpzLK09 and the cluster containing the in-frame deletion of *cpz22,* cosmid cpzCRD2. In addition, production of compounds in the supernatant were distinguished from compounds accumulating in the cell. Surprisingly, the production of caprazamycin-aglycons was affected intracellularly as well as extracellularly showing a decreased production of around ~80 % in the *cpz22* deletion mutant *S. coelicolor* M512/cpzCRD2 (Figure 41,42). Although this effect was clearly visible in *S. coelicolor* M512/cpzCRD2, it cannot be ruled out, that other ABC transporters in the heterologous host can complement the *cpz22* deletion or that other indirect effect can

negatively impact caprazamycin production.

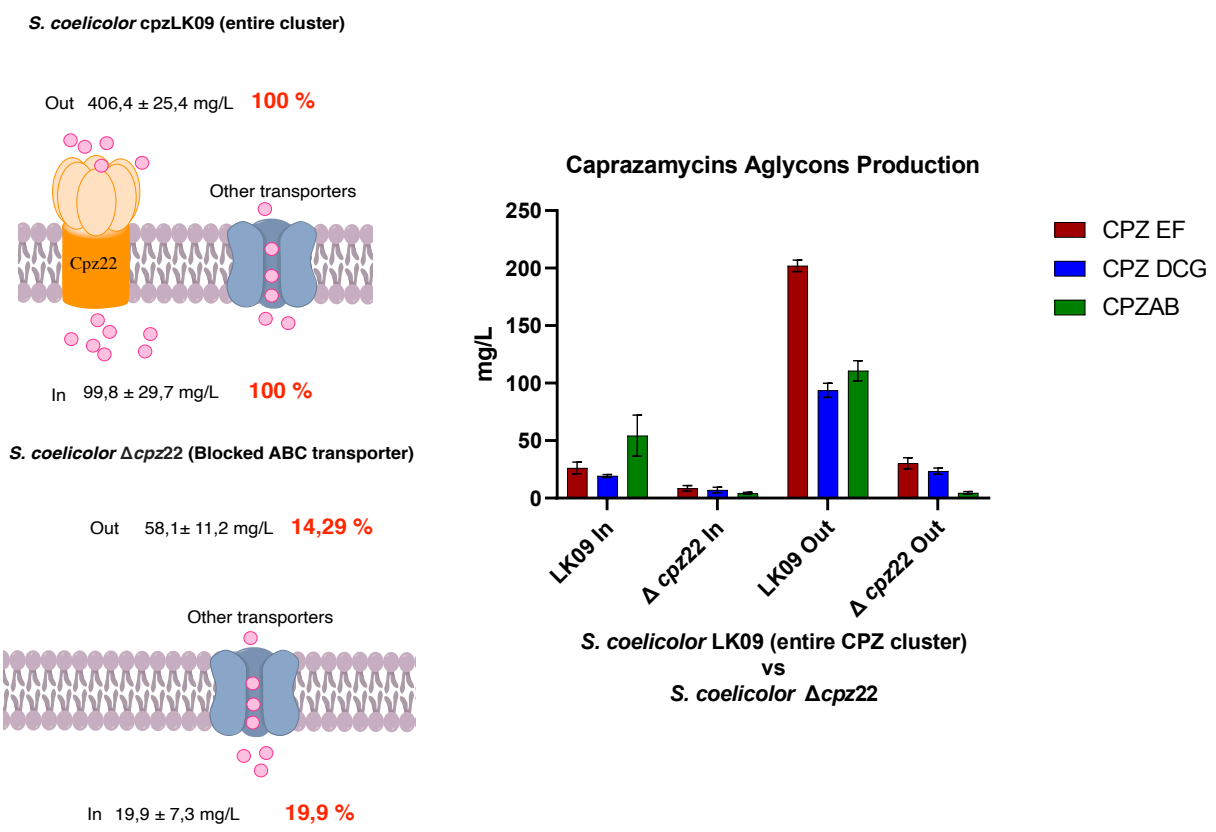

Figure 41. Quantification of caprazamycin-aglycons in *S. coelicolor*/cpzLK09 (containing the entire BGC) vs. *S. coelicolor*/pRCWL02 (containing *Δcpz22*)

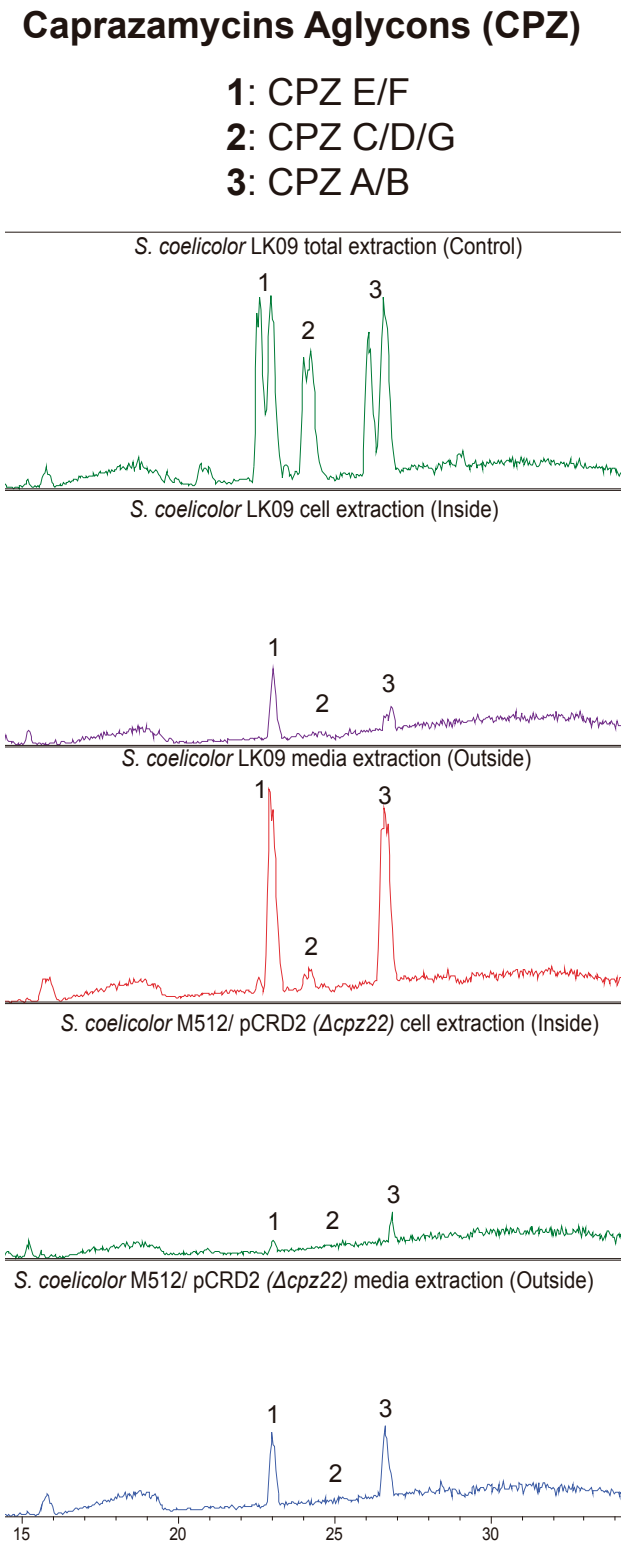

Figure 42. LC-MS Extracted ion chromatogram of *S. coelicolor* M512/cpzLK09 vs. *S. coelicolor* M512/pCRD2 (Δ*cpz*22)

Intracellular and extracellular differences are assigned for caprazamycin production.

3.3 Effects of overexpression of Cpz12, Cpz22 and Cpz27 on caprazamycin resistance

Self-resistance of the caprazamycin producer, *Streptomyces* sp. MK730-62F2, against its own metabolite may be the results from the action of two different mechanisms: an efflux by the action of the ABC-transporter Cpz22 and/or the action of one or two phosphotransferases Cpz12 and Cpz27. To evaluate the contribution of each mechanism for caprazamycin resistance, mutants of the heterologous host, *S. coelicolor* M512, were generated to host a copy of either *cpz12*, *cpz22* or *cpz27* under the control of the strong constitutive promotor PermE*. Introduction of the corresponding replicative plasmids resulted in an over-expression of the different resistance determinants. For each mutant, minimal inhibitory concentrations (MICs) were identified with purified hydroxyacylcaprazols and caprazamycin-aglycons.
Fermentation of *S. coelicolor* M512/cpzLL06 (Δ*cpz21*) and *S. coelicolor* M512/cpzLK09 and the following LC-MS guided fractionation, detected HAC and CPZ aglycons to be produced, HACE at *m/z* 802.4094 $[M+2H]^{2+}$ (calc.for $C_{36}H_{59}N_5O_{15}$, Δ=-1.7 ppm) and CPZE corresponding to the molecular ion at *m/z* 930.4522 $[M+H]^+$ (calc for $C_{42}H_{67}N_5O_{18}$, Δ=-1.0 ppm). Cpz21 encodes for an acyl-transferase responsible for the attachment of the 3-methylglutaryl moiety to the hydroxyacylcaprazols (Kaysser et al. 2009). A complementary MS/MS analysis of both compounds produced fragment ions that were in full agreement with the expected structure (Figure 44, 45).

As a negative control for MIC determinations, an *S. coelicolor* M512 mutant containing the empty vector pUWL-Apra-oriT was used. The positive control, *S. coelicolor* M512/cpzLK09 containing the entire caprazamycin gene cluster showed high resistance to caprazamycin-aglycon E (CPZAE) and hydroxyacylcaprazol E (HACE) (Table 23). *S. coelicolor* M512 harboring *cpz27* showed higher resistance to HACE compared to those recombinant strains containing *cpz*12 or *cpz22*. This result underlined our previous finding of the impossibility to delete *cpz27* in *S. coelicolor*/cpzLK09 and therefore may represent the major resistance mechanism against caprazamycins or bioactive biosynthetic intermediates thereof. Surprisingly, *S. coelicolor* M512 containing a copy of *cpz22*, encoding for the ABC-transporter, showed a decreased resistance towards HACE but not towards CPZAE (Figure 43).

Table 23. Minimum inhibitory concentration (MIC) in [µg/mL] of *S. coelicolor M512* containing putative caprazamycin resistance determinants against hydroxyacylcaprazol E (HACE), caprazamycin- aglycon E (CPZAE), FR-900493, (+)-caprazol, and phosphorylated (+)-caprazol.

Strain	(HACE)	(CPZAE)	FR-900493	(+)-caprazol	phosphorylated (+)-caprazol
S. coelicolor M512/cpzLK09	64	32			
S. coelicolor M512/pRCWL01 (*cpz12*)	32	32			
S. coelicolor M512/pRCWL02 (*cpz22*)	4	<32			
S. coelicolor M512/pRCWL03 (*cpz27*)	64	32			
S. coelicolor M512/pUWL-Apra-oriT	16	16	64	64	256
Mycobacterium phlei DSM750	<2	2			

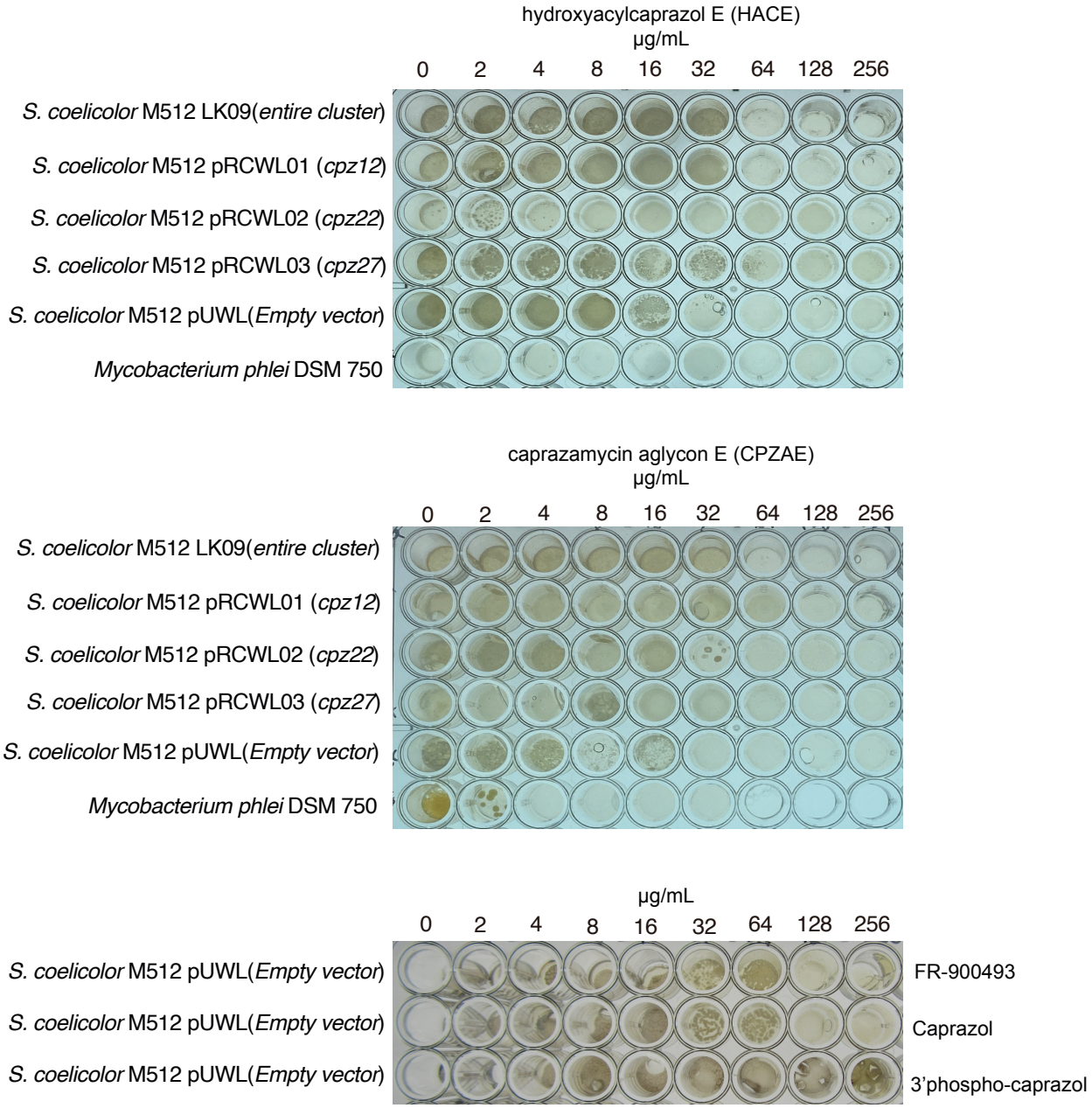

Figure 43. Minimum inhibitory concentration (MIC) of *Streptomyces* strains expressed in (µg/mL) against hydroxyacylcaprazol E, caprazamycin aglycon E, FR-900493, (+)-caprazol, and 3'phosphoylated-(+)-caprazol

A)

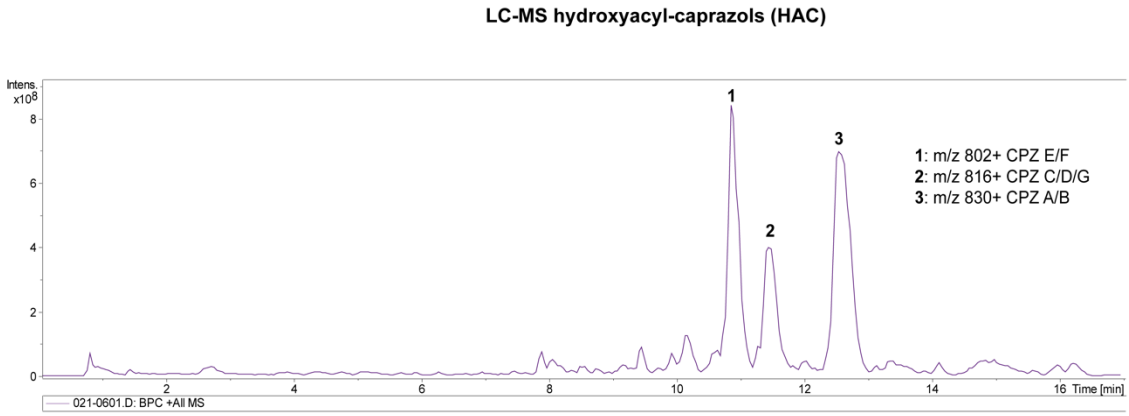
LC-MS hydroxyacyl-caprazols (HAC)
Intens.
x10^8
1
2
3
1: m/z 802+ CPZ E/F
2: m/z 816+ CPZ C/D/G
3: m/z 830+ CPZ A/B
Time [min]
021-0601.D: BPC +All MS

B)

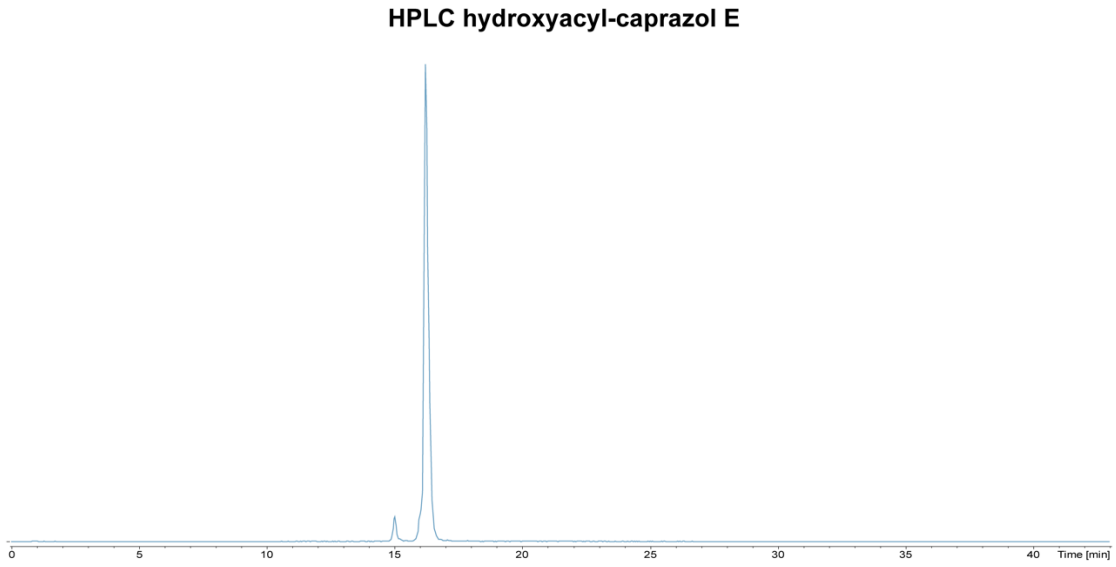
HPLC hydroxyacyl-caprazol E
Time [min]

C)

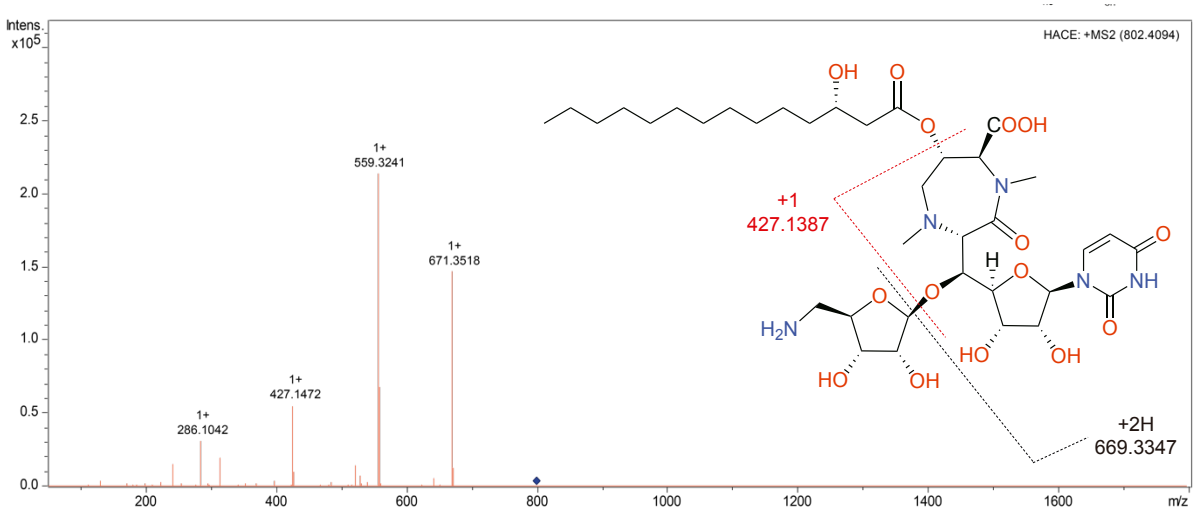
Intens.
x10^5
HACE: +MS2 (802.4094)
1+
559.3241
1+
671.3518
1+
427.1472
1+
286.1042
+1
427.1387
+2H
669.3347
m/z

Fragment	Theoretical Mass (Da)	Experimental Mass *(m/z)*	Error [ppm]
$C_{36}H_{59}N_5O_{15}$ $[M+H]^+$	802.4080	802.4094	1.7447
$C_{31}H_{47}N_4O_{12}$ $[M+2H]^+$	671.3498	671.3518	2.9790
$C_{17}H_{23}N_4O_9$ $[M+H]^+$	427.1460	427.1472	2.8093

Figure 44. HACs produced by *S. coelicolor* M512/cpzLL06

A) Low-resolution LC-MS of HAC A/B (*m/z* 830), HAC E/F (*m/z* 802) and HAC C/D/G (*m/z* 816)

B) HPLC profile of *S. coelicolor* M512/cpzLK09/Δ*cpz*21 HACE

C) Tandem MS/MS, pure HACE was fragmented yielding several daughter ions in the mass spectrum. Theoretical and observed mass differences are assigned

A)

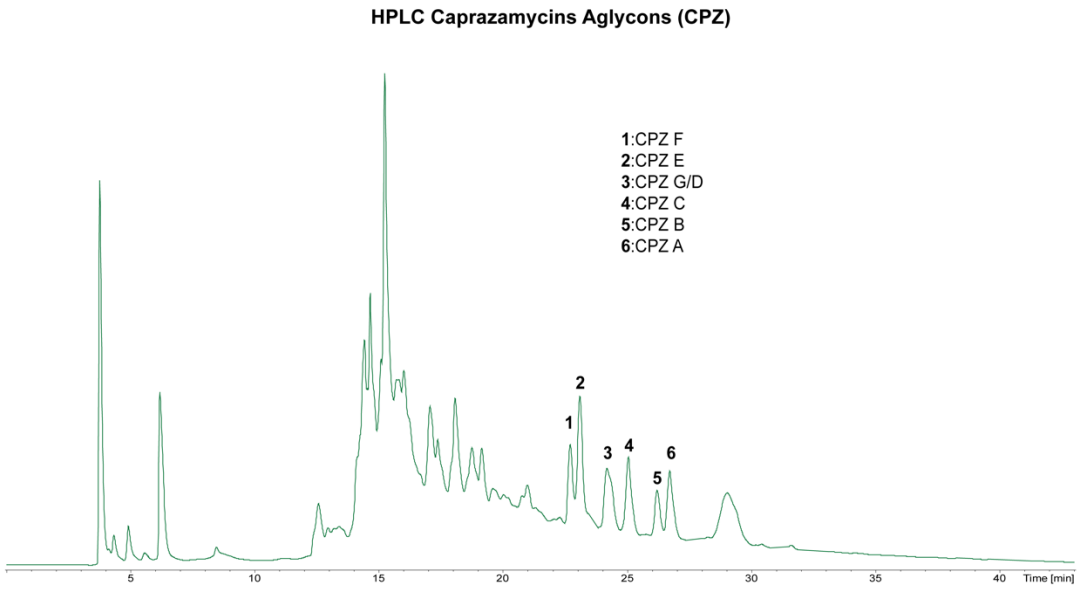

B)

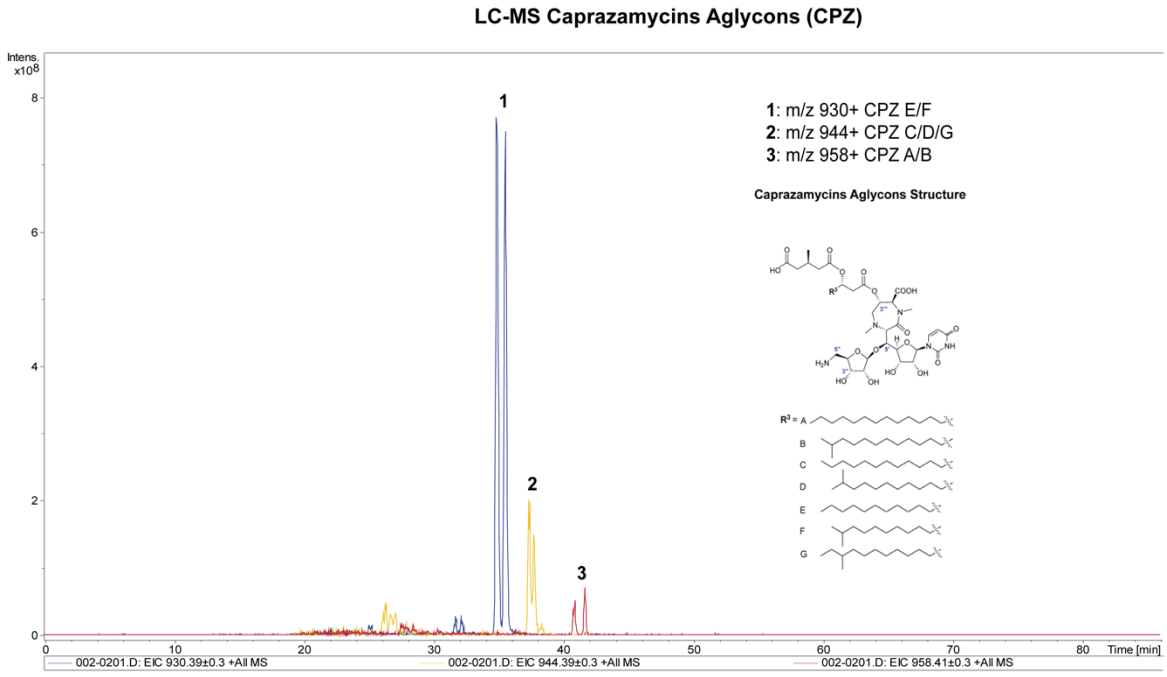
LC-MS Caprazamycins Aglycons (CPZ)
Intens.
x10^8
1
2
3
1: m/z 930+ CPZ E/F
2: m/z 944+ CPZ C/D/G
3: m/z 958+ CPZ A/B
Caprazamycins Aglycons Structure
Time [min]
002-0201.D: EIC 930.39±0.3 +All MS
002-0201.D: EIC 944.39±0.3 +All MS
002-0201.D: EIC 958.41±0.3 +All MS

C)

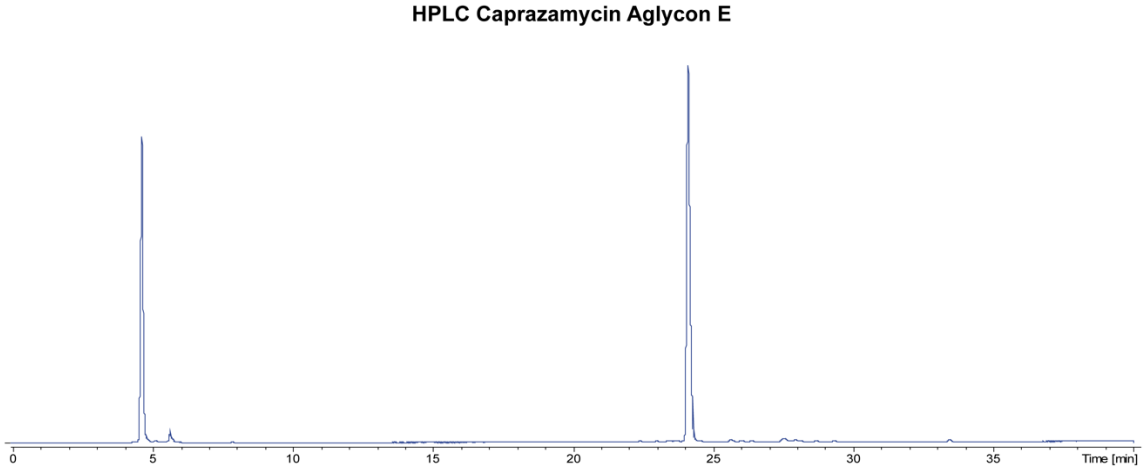
HPLC Caprazamycin Aglycon E
Time [min]

D)

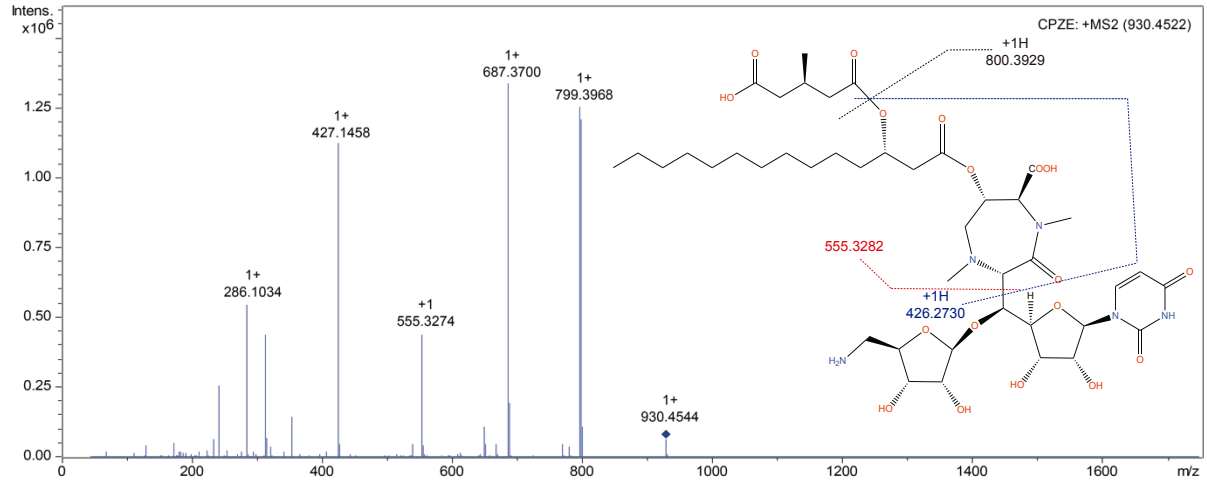

Fragment	Theoretical Mass (Da)	Experimental Mass *(m/z)*	Error [ppm]
$C_{42}H_{67}N_5O_{18}$ $[M+H]^+$	930.4554	930.4544	-1.0747
$C_{36}H_{58}N_5O_{15}$ $[M+H]^+$	799.3971	799.3968	-0.3752
$C_{33}H_{55}N_2O_{13}$ $[M+H]^+$	687.3699	687.3700	0.1454
$C_{28}H_{47}N_2O_9$	555.3276	555.3274	-0.3601
$C_{22}H_{38}N_2O_6$ $[M+H]^+$	427.1460	427.1458	0.4682

Figure 45. CPZs analytic profiles of the producer *S. coelicolor* M512/cpzLK09

A) HPLC chromatogram profile of CPZ aglycones.
B) LC-MS profile and chemical structure and corresponding mass of caprazamycin aglycones.
C) HPLC chromatogram profile of pure CPZ aglycon E.
D) HR-MS of pure CPZ aglycon E, fragmentation yield several daughter ions in the mass spectrum. Theoretical and observed mass differences between were assigned

4. Discussion

The biosynthesis of the MraY inhibitor caprazamycin can be divided into two stages (Cui, Liu, et al. 2018). The initial steps include formation of the disaccharide core structure, a 5-amino-5-deoxyribofuranose (ADR) attached to the 6´-N-alkyl-5´-C-glycyluridine (GlyU) through a ß-O-glycosidic bond. This core structure is shared by the MraY inhibitors caprazamycin, liposidomycin, muraymycin, muraminomicin and sphaerimicin (Cheng et al. 2011; Chi et al. 2013; Funabashi et al. 2010, 2013; Kaysser et al. 2009; Kaysser, Wemakor, et al. 2010; Wiker, Hauck, et al. 2019; Wiker, Konnerth, et al. 2019). Formation of ADR and GlyU has been investigated in great detail by biochemical studies (Barnard-Britson et al. 2012; Chi et al. 2011, 2013; Funabashi et al. 2010; Yang et al. 2011) and also occurs during muraymycin biosynthesis (Cui, Liu, et al. 2018; McErlean et al. 2021). The second stage of caprazamycin biosynthesis includes cyclization of the diazepanone towards (+)-caprazol, a step which is still under investigations, the transfer of ß-hydroxy fatty-acyl side chains by Cpz22, the transfer of 3-methylglutarate by Cpz21, the attachment and methylation of L-rhamnose by Cpz28-Cpz31 and finally sulfation by Cpz4 (Gust et al. 2013; Tang et al. 2013; Wiker, Hauck, et al. 2019; Wiker, Konnerth, et al. 2019) or phosphorylation as described for muraymycins and capuramycin (Cui et al. 2020; Cui, Wang, et al. 2018; Yang et al. 2010).

In this study, we focused on the phosphorylation of caprazamycins as a plausible resistance determinant and on the role of the ABC-transporter encoded by *cpz22*. The heterologous host *S. coelicolor* M512, harboring the caprazamycin gene cluster containing a deletion of *cpz12*, produced almost only non-phosphorylated (+)-caprazol and trace amounts of intact caprazamycin-aglycons. Although biosynthesis seemed to be blocked at the stage of (+)-caprazol formation, the later steps do not seem to be very dependent on phosphorylation. Since the phosphotransferase Cpz27 can phosphorylate compound **7** in-vitro, one can assume that this event occurs during the first stage of caprazamycin biosynthesis, more precisely before ring closure of the diazepanone to generate the (+)-caprazol intermediate. It is worthwhile noticing that phosphorylation by the two phophotransferases Cpz12 and Cpz27 are likely to occur at the same 3''-position of the aminoribose, because no double phosphorylated compounds could be detected by intensive HR-LC-MS analysis. If compound 7 is the genuine substrate for Cpz27, than phosphorylation might be partially removed during the next steps of caprazamycin biosynthesis. Since deletion of the lipase encoded by *cpz23* resulted in the accumulation of both, phosphorylated and non-phosphorylated (+)-caprazol, phosphorylation by Cpz27 may be incomplete or is later been removed. Since formation of the diazepanon ring has not been elucidated yet, one can speculate that phosphorylation is required for the ring closure mechanism and is lost once (+)-caprazol is originated. However,

these speculations do not explain, why a single deletion of *cpz27* or the double knock-out of *cpz12/cpz27* proved to be lethal for the heterologous host. A plausible explanation might be, that compound **7** is toxic for the heterologous host and needs to be de-toxified by phosphorylation involving Cpz27. Compound **7** shows high structural similarities to the known MraY inhibitor FR-900493. FR-900493 was isolated from *Bacillus cereus* No. 2045 and consists of the same ADR-GlyU warhead as compound **7** (Ochi, K. Ezaki, M. Iwami, M. Komori, T. Kohsaka 1989). In only differs in the attached 3-amino-3-carboxypropyl side chain of compound **7** in terms of lacking the 3-carboxyl group. FR-900493 showed antimicrobial activity against *Staphylococcus aureus* (MIC 3,13 – 6,25 µg/mL) and *Bacillus subtilis* ATCC-6633 (MIC 3,13 µg/mL). Recent studies showed that synthetic FR-900493 derivatives were also active against *Clostridium difficile* (Mitachi et al. 2018). FR-900493 has been approved to be an MraY inhibitor, it is therefore likely that compound **7** also shows the same mode of action and therefore is lethal for the heterologous host. It can be questioned, if the ABC-transporter Cpz22 allows efficient efflux of a biosynthetic intermediate like compound **7**.

Following the biosynthesis of caprazamycins, a *cpz23* knock-out mutant generated (+)-caprazol and of phosphorylated (+)-caprazol. This observation has already been described by Shiraishi and colleagues. The authors could also elucidate the structure of phosphorylated (+)-caprazol by mass-spectrometry and NMR to confirm phosphorylation at the 3''-position of the ADR-moiety (Figure 34). No other position of phosphorylation has been observed by intensive HR-LCMS analysis pointing towards only one phosphorylation site in caprazamycins. This opens the question to the function of the second phosphotransferase Cpz12. All compounds available from first and second stage of caprazamycin biosynthesis were tested in-vitro with purified Cpz12 for phosphotransfer activity. However, none of the substrates were accepted by Cpz12. On the other hand, the deletion of *cpz12* showed a clear chemotype, namely accumulation of non-phosphorylated (+)-caprazol. To verify this chemotype, the knock-out of *cpz12* was repeated, generating another three independent mutants. All individual mutants, three from the first knock-out experiment and three from the second round of deletions were verified by sequencing the remaining scar-sequence, to ensure the accurate formation of in-frame deletions, thereby avoiding any downstream effects on *cpz13*. The analysis of all six deletion mutants resulted in the same chemotype, mainly accumulation of non-phosphorylated (+)-caprazol. If the phosphate, introduced by Cpz27 during first stage biosynthesis (e.g., cyclisation towards diazepanon ring formation) was removed, maybe a second phosphorylation takes place by Cpz12. However, Cpz12 did not accepted (+)-caprazol as substrate under the conditions used in the in-vitro assays. It can be speculated, that the isolated and purified Cpz12 is either inactive or that Cpz12 requires another substrate. Interestingly, the *cpz23* knock-out showed a similar chemotype, but in this case, non-phosphorylated and phosphorylated (+)-caprazol were accumulated. This finding

led to the question; what substrate is accepted by the lipase Cpz23. The in-vitro assays clearly demonstrated, that phosphorylation of (+)-caprazol is not required for fatty acyl side-chain transfer. Cpz23 only accepted non-phosphorylated (+)-caprazol as substrate. Cpz23 was anticipated to have a broad substrate specificity or at least some promiscuity, as the enzyme exhibits strong homologies with GDSL lipases, which are known for broad substrate specificity. Since caprazamycins only differ in the length and configuration of their fatty-acyl side chains, this promiscuity of Cpz23 may only apply for this substrate, but not for (+)-caprazol. These results are in agreement with the knock-out of *cpz21*, where hydroxyacylcaprazol A-G were generated, but not the representative phosphorylated compounds (Kaysser et al. 2009). It therefore is likely, that biosynthesis of caprazamycins continue from (+)-caprazol and not phosphorylated (+)-caprazol towards hydroxyacylcaprazols, caprazamycin-aglycons and finally, caprazamycins. The presence of phosphorylated (+)-caprazol in the *cpz23* knock-out mutant may lead to the assumption, that remaining (+)-caprazol, which is not further processed in caprazamycin biosynthesis, needs to be de-toxified by Cpz12. This phosphorylation may occur during an earlier step of the first stage of caprazamycin biosynthesis. Structure activity relationship studies suggested that (+)-caprazol does not show any bioactivity against *Mycobacterium smegmatis*, *Staphylococcus aureus* or *Enterococcus faecalis* (Hirano, Ichikawa, and Matsuda 2007). However, it cannot be ruled out that (+)-caprazol like compound **7** represents efficient MraY inhibitors and thereby are both de-toxified by the action of Cpz27 and Cpz12, respectively.

5. Conclusion

From a chemical and biosynthetic perspective, liponucleoside antibiotics are likely produced using convergent assembly from distinct entities. The alkylated ADR-GlyU disaccharide core is found in several nucleoside antibiotics, including FR-900493, muraymycins, liposidomycins, muraminomycins or caprazamycins. It is tempting to speculate that the caprazamycin BGC was acquired gradually by the wildtype strain, to firstly produce a structurally simplified antibiotic like FR-900493. As a consequence, phosphorylation by Cpz27 would provide a first level of self-resistance. The addition of second stage biosynthetic genes for diazepanone-ring closure, attachment of acyl side chains and sugars by horizontal gene transfer would then require an additional resistance mechanism or repetition of the same phosphorylation due to the loss of phosphate during biosynthesis or transport. Finally, the function of Cpz12 remains speculative at this time and remains to be an interesting subject for further investigations.

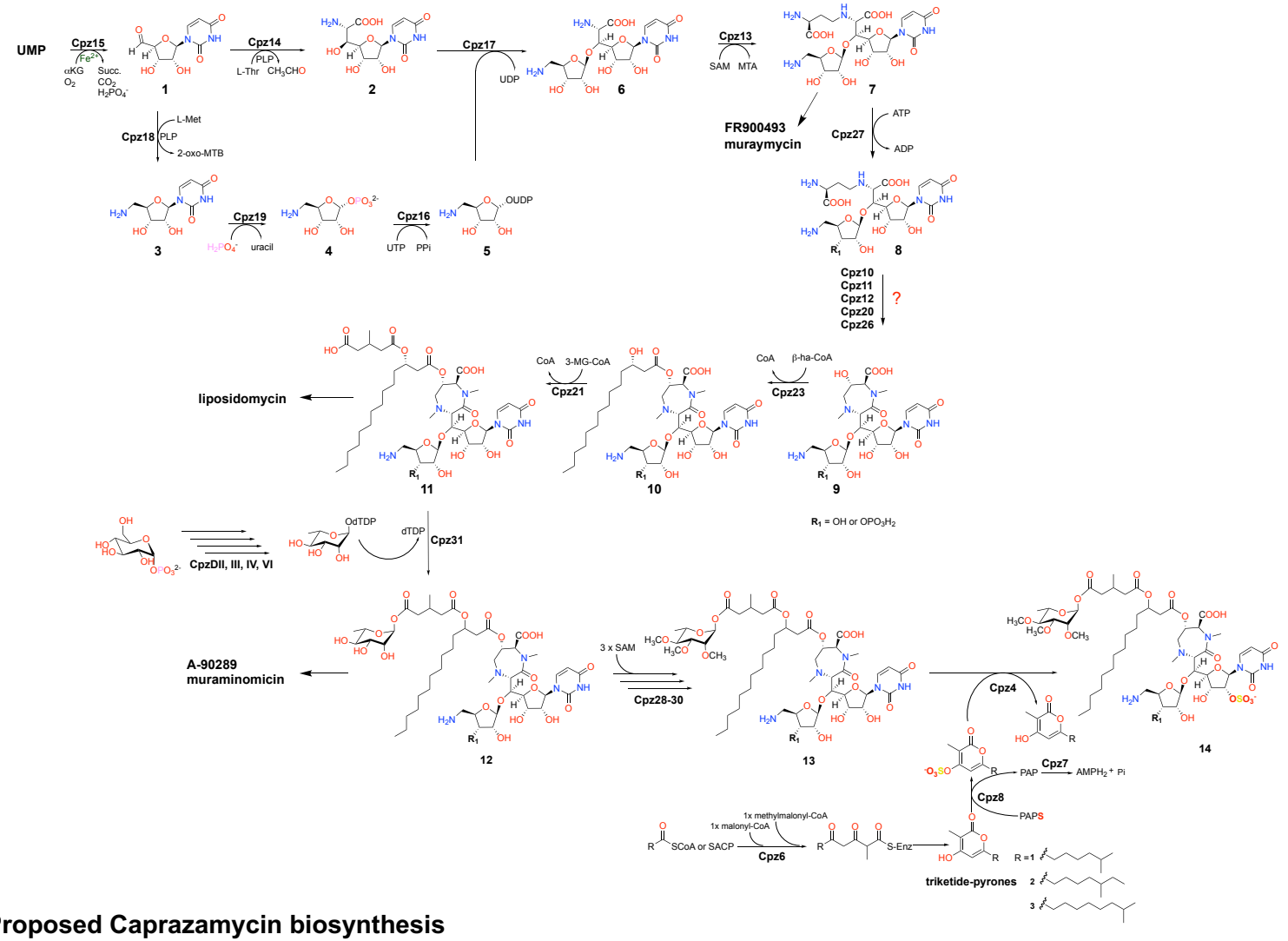

Figure 46. Proposed Caprazamycin biosynthesis

L-Met = L-methionine; Pi = phosphate; PPi = pyrophosphate; UTP = uridine triphosphate; UDP = uridine diphosphate; CoA = coenzyme A; SAM = S-adenosyl-methionine; MTA = methylthioadenosine; dTDP = deoxy-thymidine-5'-diphosphate

Chapter II

Mycothiol peroxidase activity as a part of the self-resistance mechanisms against the antitumoral cosmomycin D

Summary

Streptomyces produce various bioactive natural products and possess resistance systems for these metabolites, which are co-regulated with antibiotic biosynthesis genes. *Streptomyces olindensis* DAUFPE 5622 produces the antitumoral cosmomycin D (COSD), a molecule member of the anthracycline family.

The COSD biosynthetic cluster has been previously studied and the self-resistance mechanisms partially characterized, however the encoding gene micothiol peroxidase (MPx) it's not completely understood.

We observed for the first time that, MPx could also reduce a cysteine–MSH mixed disulfide, using a dithiol disulfide exchange mechanism during the biosynthesis of COSD. Purification and identification of MPx protein became worthy evidence that ROS-detoxifying genes would be enrolled by anthracycline producers. We describe in this study, three self-resistance mechanisms against COSD for in *Streprtomyces olindensis*. Genes *cosI* and *cosJ* encode the first mechanism, an ABC transporter efflux system, the second mechanism encoded by *cosU* gene, similar to *drr*C of *S. peucetius* and UvrA class IIa homologues proteins, and a newly third mechanism encoded by *cos*P, a mycothiol peroxidase (MPx) involved in detoxification of H_2O_2.

Within this project, we want to elucidate the following questions:

Why do we have a micothiol peroxidase gene in the cosmomycin like gene clusters?

How is the toxicity of COSD been affect comparing to other well-known anthracyclines such as DOX?

Is the function of micothiol peroxidase in COSD like gene clusters the major self-resistance mechanism?

Zusammenfassung

Streptomyces produzieren verschiedene bioaktive Naturstoffe und besitzen Resistenzsysteme für diese Metaboliten, die zusammen mit Antibiotika-Biosynthesegenen reguliert werden. *Streptomyces olindensis* DAUFPE 5622 produziert das antitumorale Cosmomycin D (COSD), ein Molekül der Anthracyclin-Familie.

Das COSD-Biosynthese Gencluster wurde bereits untersucht und die Selbstresistenzmechanismen teilweise charakterisiert, die Funktion der vom Gencluster codierten Micothiolperoxidase MPx ist jedoch bis heute nicht vollständig verstanden.

Wir konnten zum ersten Mal zeigen, dass MPx auch ein gemischtes Cystein-MSH-Disulfid mithilfe eines Dithioldisulfid-Austauschmechanismus während der Biosynthese von COSD reduzieren kann. Die durchgeführten Untersuchungen Untersuchungen zu MPx zeigen, dass ROS-entgiftende Gene von Anthrazyklin-Produzenten aufgenommen werden. In dieser Studie beschreiben wir drei Selbstresistenzmechanismen von *Streptomyces olindensis* gegen COSD. Die Gene *cosI* und *cosJ* kodieren für den den ersten Resistenzmechanismus, , ein ABC-Transporter-Efflux-System. Der zweite Mechanismus wird vom *cosU*-Gen kodiert und ist ähnlich wie *drrC* von *Streptomyces peucetius* an der Entgiftung von H_2O_2 beteiligt.

In diesem Projekt wollten wir die folgenden Fragen klären:

Warum besitzt das Cosmomycin-ähnlichen gencluster ein Gen, das für eine Micothiolperoxidase codiert?

Wie wirkt sich die Toxizität von COSD im Vergleich zu anderen bekannten Anthracyclinen wie DOX aus?

Stellt die Micothiolperoxidase MPx bei COSD-ähnlichen Genclustern den Hauptresistenz-Mechanismus dar?

6. Introduction

6.1 Anthracyclines

The anthracyclines are fermentation products of *Streptomyces peucetius* var. *caesius* and were originally described as antitumor antibiotics (Figure 47). Daunomycin and doxorubicin were first shown to have antitumoral effect in 1960. Subsequently, a search for less-toxic derivatives identified additional drugs that have added to the repertoire available to the modern oncologist. Today, the anthracyclines constitute several of our most effective anticancer regimens (Hong and Hait 2010).

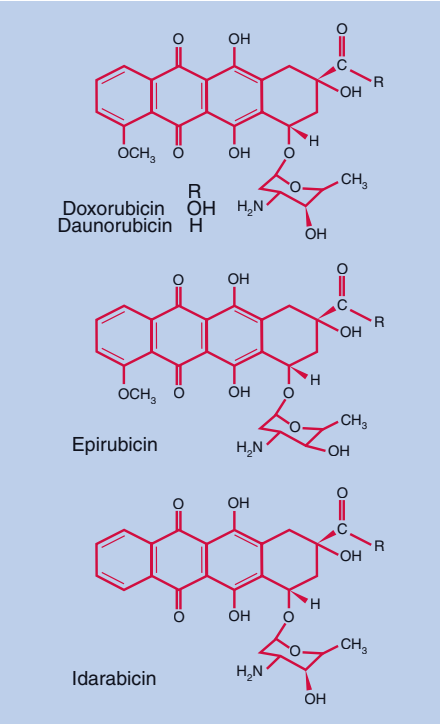

Figure 47. Structures of the clinically used anthracyclines

The compounds consist of a planar, hydrophobic tetracycline ring linked to a daunosamine sugar through a glycosidic linkage. All drugs are positively charged at physiologic pH, favoring intercalation into DNA. In addition, the anthracyclines possess quinone moieties on adjacent rings that allow them to participate in electron transfer reactions and to generate oxygen free radicals (Hong and Hait 2010)

Daunomycin and doxorubicin differ by only a single hydroxyl at position C14, yet have distinct spectra of antitumor activity. Idarubicin is a semisynthetic derivative of daunomycin (4-demethoxy- daunorubicin) lacking the 4-methoxy group present on the parent compound. Epirubicin is an epimer of doxorubicin, having the C4' hydroxyl group on the amino sugar in the equatorial rather than the axial position, which increases lipophilicity as compared with doxorubicin. A liposome-encapsulated formulation of doxorubicin (Doxil) was approved for use in acquired immunodeficiency syndrome (AIDS)–related Kaposi sarcoma, multiple

myeloma, ovarian cancer, and outside of the United States, breast cancer (Hong and Hait 2010).

6.1.1 Activity

The anthracyclines are indicated for use against both solid and hematologic malignancies. Doxorubicin has the broadest spectrum of activity. Its introduction in the 1960s is one of the most active agents in the treatment of breast cancer. Doxorubicin has limited but demonstrable activity against thyroid cancer, ovarian cancer, and small cell lung cancer. Finally, it has also demonstrated activity against endometrial carcinoma; cancer of the testis, prostate, cervix, and head and neck; and multiple myeloma. Daunomycin is used mostly for the treatment of acute lymphocytic and myelocytic leukemias. Although it has some activity against pediatric solid tumors, it has little activity against adult solid malignancies. Idarubicin is used predominantly in the treatment of adult acute myelogenous leukemia (Hong and Hait 2010).

6.1.2 Toxicity

All anthracyclines produce cardiac damage that can result in serious and even life-threatening complications. Cardiac toxicity is more common with doxorubicin and daunorubicin than with epirubicin or idarubicin. The anthracyclines produce myocardial damage by several mechanisms. Perhaps the most important is generation of reactive oxygen species during electron-transfer from the semiquinone to quinone moieties of the molecule (Hong and Hait 2010). The generation of hydrogen peroxide and the peroxidation of myocardial lipids contribute to myocardial damage. The heart may be uniquely susceptible to cardiac damage from oxidation reactions. For example, the low activity of catalase in cardiac tissue renders the myocardium dependent on glutathione peroxidase for detoxification of hydrogen peroxide. Anthracyclines deplete glutathione, thereby leaving the heart vulnerable to oxidative attack (Hong and Hait 2010).

6.1.3 Cosmomycins

Streptomyces olindensis DAUFPE 5622 produces a purple pigment, originally described as an anthracycline with antimicrobial and antitumoral activity (Lima et al. 1969). Structural studies determined that the molecule is an aromatic complex with two trisaccharide chains attached at 7- and 10-positions called comomyin D COSD (Furlan et al. 2004; Garrido et al. 2006) (Figure 48). Cosmomycins are an interesting group of compounds because they show one of the most complex glycosylation patterns found in anthracyclines; i.e, position 10 of the aglycone is not as frequently glycosylated as the 7-position (Miyamoto et al. 2002). COSD synthesized by *S. olindensis*, has a high toxicity comparing with other anthracyclines such as doxorubicin (Carvalho et al. 2010), leading to the hypothesis that these bacteria possess efficient self-resistance strategies (Arteaga 2016).

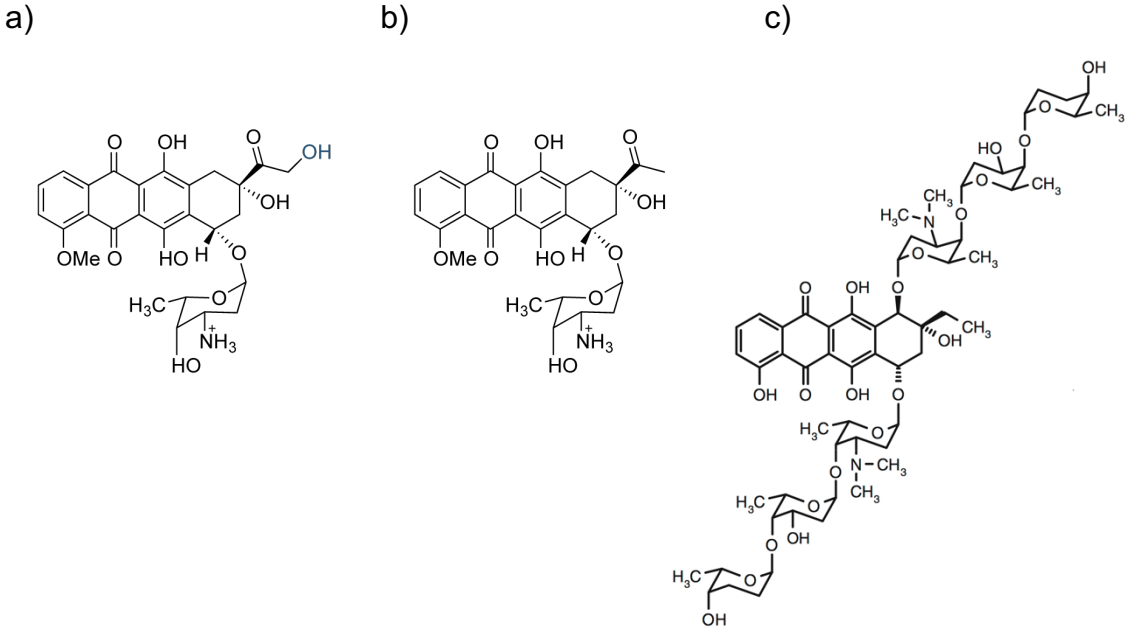

Figure 48. Chemical structures of a) (DOX) and b) (DNR) produced by *S. peucetius and* c) (COSD) by *S. olindensis*

6.2 Self-resistance of anthracyclines

Actinobacteria to survive self-made DNA-damaging metabolites such as angucyclines, anthracyclines, bleomycins, enediynes, mitomycins, and quinoxalines. These molecules are either covalent or non-covalent DNA-binders and their cytotoxicity is a consequence of either DNA distortion, alkylation, crosslinking, and/or oxidative damage thereby impairing replication

and/or transcription. The selected examples illustrate the diversity of strategies developed by Actinobacteria for self-resistance, that is, antibiotic sequestration, antibiotic efflux, antibiotic modification, self-sacrifice, target repair or protection, and stochastic activity (Tenconi and Rigali 2018) (Figure 49).

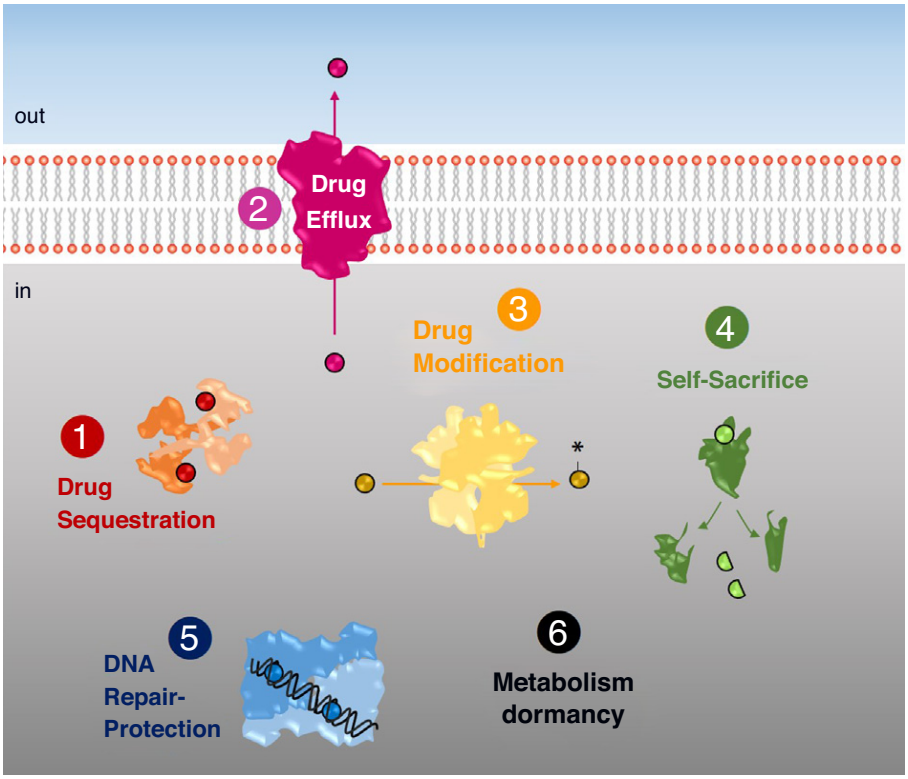

Figure 49. Diversity self-resistance mechanisms developed by DNA-damaging antibiotics producing Actinobacteria

(Tenconi and Rigali 2018).

6.2.1 Drug Efflux

One of the most widespread mechanisms of resistance is to eject a toxic compound out of the cytoplasm and therefore impose a physical barrier between the toxin and its molecular target. The efflux systems described here are multi-drug resistance systems, being able to export different but structurally related molecules. In *Streptomyces peucetius* the efflux system that exports daunorubicin and doxorubicin involves an ABC-type transporter system with DrrA and DrrB as ATP-binding and transmembrane components, respectively (Gandlur et al. 2004; Guilfoile and Hutchinson 1991; Li, Sharma, and Kaur 2014; Malla et al. 2010; Tenconi and Rigali 2018) (Figure 50). Homologues of DrrA and DrrB have also been shown essential for resistance to mithramycin in *Streptomyces argileus* (MtrA and MtrB) (Ernestina

Fernández et al. 1996), and to chromomycin A3 in *Streptomyces griseus* (CmrA and CmrB) (Menéndez et al. 2007).

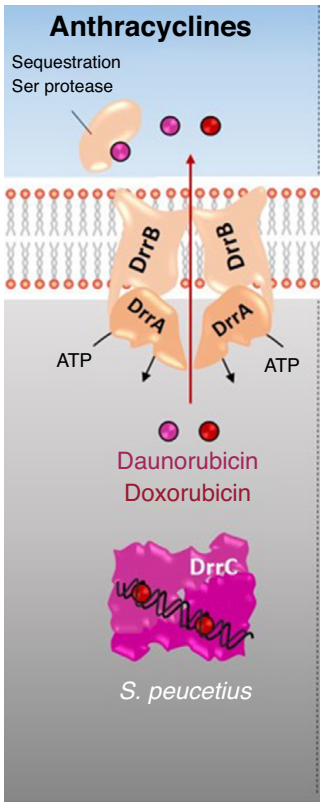

Figure 50. Mechanisms of resistance in *S. peucetius*
Modified from (Tenconi and Rigali 2018)

6.2.2 DNA repair

Producers of compounds that are cytotoxic by inducing DNA damages have unsurprisingly also developed resistance mechanisms aimed to protect/repair the drug target. The gene product of *drrC* from the biosynthetic cluster of anthracyclines daunorubicin (DNR) and doxorubicin of *S. peucetius* is homologous to UvrA-like proteins of ABC excision nuclease systems, which perform the first step in nucleotide excision repair. Like UvrA, DrrC is involved in the recognition of DNA damages and its DNA-binding activity requires ATP and has been shown to be enhanced by DNR. (Furuya and Hutchinson 1998; Tenconi and Rigali 2018). Preliminary data suggest that DrrC would ensure the viability of *S. peucetius* by ejecting DNR intercalated into DNA (Prija and Prasad 2017). Inactivation of *drrC* is only possible in a *S. peucetius* daunorubicin non-producing strain which underlines the importance of this gene in

self-protection as the other mechanism of resistance involving the DrrAB exporter is not able to compensate *drrC* deletion (Lomovskaya et al. 1996). In contrast, prevalence of drug efflux systems (MtrAB and CmrAB) over the DNA repair resistance mechanism (MtrX and CmrX) is observed for self-protection against the aurealic acids family mithramycin and chromomycin A3 (Figure 51) (E Fernández et al. 1996; Garcia-Bernardo et al. 2000; Lomovskaya et al. 1996; Malla et al. 2010; Tenconi and Rigali 2018).

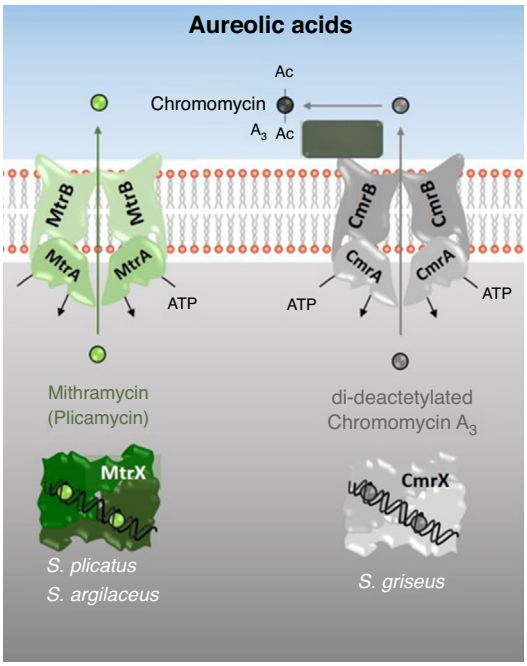

Figure 51. Proteins involved in the resistance mechanisms associated with aureolic acids.
Modified from (Tenconi and Rigali 2018)

6.2.3 Self-resistance mechanism of Streptomyces olindensis against cosmomycin D

In 2016, during the master thesis of Castillo-Arteaga, at that time member of the Prof. G. Padilla group of the University of São Paulo, first preliminary results of three self-resistance mechanisms in *S. olindensis* were obtained: for the ABC transporter (encoded by *cosI* and *cosJ*), for an UvrA like protein (*cosU*) and for a putative detoxification gene *cosP* encoding for a glutathione peroxidase. However, the complete function of *cos*P was elucidated during the existing PhD thesis.

6.2.3.1 ***Cosmomycin efflux***

CosI and CosJ are part of a superfamily of transport proteins (ABC transporters), one of the largest groups of proteins in nature. *cosI* encodes for a nucleotide binding domain (NBD), this component is associated with transmembrane proteins, responsible for the formation of channels through which the substrate is transported, known as transmembrane domain (TMD). The analysis of the second gene *cosJ* shows the typical conformation of TMD likely to be composed of four until eight structures in alpha helices, which are organized as homodimers. Analysis of CosJ by Phyre and TMHMM showed the presence six6 transmembrane helices ranging from N- to C-terminus (Arteaga 2016) (Figure 52).

A

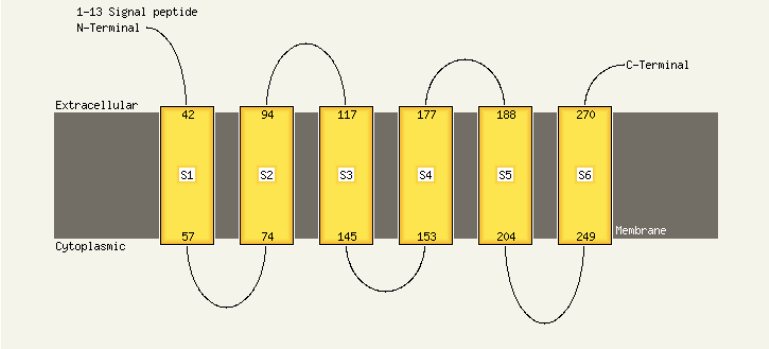

B

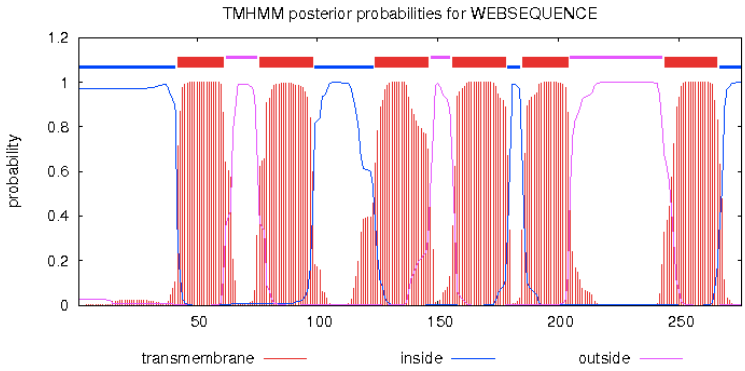

Figure 52. Distribution and probability of transmembrane helices encoded by *cosJ*

A) Prediction and topology of transmembrane helices using Phyre server v 2.0. B) Probability graph of transmembrane amino acids using TMHMM server v 2.0. (Arteaga 2016).

6.2.3.2 ***UvrA like protein***

The protein encoded by *cosU* shows high similarity with UvrA proteins, however it lacks the UvrB-binding domain and the first zinc finger motif. For this reason, the protein function is not involved in NER and is therefore classified within class IIa UvrA like proteins. UvrA class IIa proteins have been shown to behave in-vitro like an ATP-dependent DNA-binding protein of *S. peucetius* encoded by the daunorubicin gene cluster (Furuya and Hutchinson 1998; Lomovskaya et al. 1996) or in *S. nogalater,* the producer organism of nogalamycin (Torkkell et al. 2001), or CmrX which confers resistance to chromomycin in *S. griseus* subsp. *griseus* (Menéndez et al. 2007) or *mtr*X, which encodes for a UvrA-like protein involved in mithramycin resistance in *S. argillaceus* (Garcia-Bernardo et al. 2000).

Interestingly, the common characteristic of these antibiotics is that they intercalate into DNA. DNA-binding protein may therefore play a role in self-resistance, inhibiting or destabilizing the interaction of these drugs and genomic DNA, thus preventing intercalating antibiotics from interfering with transcription and/or replication. It is suggested that the fuction of UvrA class IIa proteins is associated with the removal of non-covalent DNA binding agents (Arteaga 2016).

6.2.3.3 cosP helps to scavenging ROS caused by cosmomycin D

Next to *cosI* and *cosJ* is *cosP, a gene* with 99% identity to gluthatione peroxidases of *Streptomyces* sp. NRRL WC-3641 and *Streptomyces zinciresistens* K42 (Arteaga 2016). Suggesting that anthracyclines such as COSD are determinant in the production of ROS, then an impairment of the activity of antioxidant enzymes such gluthatione peroxidase in *S. olindensis* encoded in the biosynthetic gene cluster may play an important role in the self-resistance against antibiotics with potential cell toxicity (Arteaga 2016). Preliminary results with cosmomycin D were in agreement with previous studies that reported that the reactive oxygen species generated during the oxidation-reduction cycle of anthracyclines might oxidize intracellular glutathione and provide further self-stimulation (Henderson et al. 1978).

In eukaryotes and gram-negative bacteria, glutathione peroxidase (GPx) reduces H_2O_2 or organic hydroperoxides to water, using the reduced glutathione (Herbette, Roeckel-Drevet, and Drevet 2007). However, in gram-positive bacteria such as actinobacteria, it has been reported that MPx exist instead of GPx (Pedre et al. 2015, 2018; Si et al. 2015) and for that reason the correct annotation and function should be corrected.

We observed for the first time that MPx is able to reduce a cysteine–MSH mixed disulfide, using a dithiol disulfide exchange mechanism during the biosynthesis of COSD. Purification and identification of the MPx protein provided evidence that ROS-detoxifying proteins are employed by anthracycline producers. We describe three self-resistance mechanisms against COSD in *Streptomyces olindensis*. Genes *cosI* and *cosJ* encode the first mechanism, an ABC transporter efflux system, while the second mechanism is encoded by *cosU*, similar to *drr*C of *S. peucetius* and UvrA class IIa homologues proteins. Finally, a newly third mechanism encoded by *cosP*, a mycothiol peroxidase (MPx) is involved in the detoxification of H_2O_2.

This work was conducted in cooperation with Prof. Dr. Gabriel Padilla from the University of São Paulo, Brazil, who kindly provided us with the strain *Streptomyces olindensis* DAUFPE 5622 with the objective to provide new and conclusive evidence for the function of MPx.

Aims of this study

The general objective of this study was to confirming the putative function of self-resistant mechanisms in *S. olindensis* against the antitumoral cosmomycin D, focusing on the enzyme mycothiol peroxidase MPx:

First, the bioinformatic analysis was conducted using *cosIJ*, *cosP* and *cosU* as templates and AntiSMASH and MultiGeneBlast as tools. A protein modeling of the ABC-transporter including TMD and NBD prediction was conducted. Then, a phylogenetic analysis of CosP was performed. To evaluate the biological function of the resistance determinants, the genes *cosIJ*, *cosP* and *cosU* were cloned into the expression vector pUWL-apra-oriT and heterologously expressed in *Streptomyces lividans* TK24. Gene expression was monitored by qPCR during production or non-production of COSD. The over-expression mutants were used to determine MICs using different concentrations of cosmomycin and doxorubicin. For this purpose, cosmomycin D was purified from extracts and analyzed by HPLC and HR-LC-MS. Finally, *cosP* encoding for MPx was cloned into the expression vector pHIS8, expressed in *E. coli* Rosetta™(DE3) and purified for enzyme assays. A non-functional mutant MPx was generated by a mutagenesis approach and used as negative control in ROS response assays.

7. Materials and methods

*See section II of the first chapter

8. Results

8.1 Self-resistance genes allocated within the cosmomycin D cluster

Analysis of the COSD biosynthetic gene cluster, located at contig 2 of the genome assembly of *S. olindensis* (JJOH00000002.1), enabled the assignment of each gene based on their homology to proteins of known functions. The genes, *cosI* (DF19_23560), *cosJ* (DF19_23565), *cosP* (DF19_23570) and *cosU* (DF19_23575) were identified as four candidate genes, which might play a role concerning self-resistance. The products of *cosI* and *cosJ* are part of a superfamily of transport proteins (ABC transporters), one of the largest groups of proteins in nature (Bouige et al. 2002). In detail, *cosI* encodes for a nucleotide binding domain (NBD). The sequence of *cosI* shows the same features found in anthracycline resistance prototypal DdrA from *Streptomyces peucetius*, such as the Walker A motif, Q-loop, Signature motif, Walker B motif, switch region, GATE domain, and DEF motif (Zhang et al. 2015) This component is associated with transmembrane proteins, responsible for the formation of chanels through which substances are transported, known as transmembrane domain (TMD) (Higgins 2001). The analysis of the gene product of *cosJ* shows a typical conformation of (TMD) composed of alpha helices, which are organized as homodimers (Holland 2011). Both proteins form part of the ABC transporter complex as it has a 95,14% identity to the ABC transporter of *Streptomyces purpurascens* (accession number: WP_189725841.1 and WP_189725842.1, respectively) (Figure 53). For CosJ, six transmembrane helices, forming a transmembrane domain, can be predicted using Phyre and TMHMM (Figure 52).

In close proximity to *cosI* and *cosJ*, *cosP* could be identified as another plausible resistance determinant. It encodes an enzyme (KDN80073.1) that shows 88,34% identity on amino acid level with the glutathione peroxidase (Gpx) from *Streptomyces purpurascens* (accession number: GHA30648.1). Since this kind of proteins are annotated commonly as glutathione peroxidase (Gpx), in fact in actinobacteria they represent mycothiol peroxidases as enzymatically demonstrated in ASW14906.1 from *Corynebacterium glutamicum* (Pedre et al. 2015).

A.

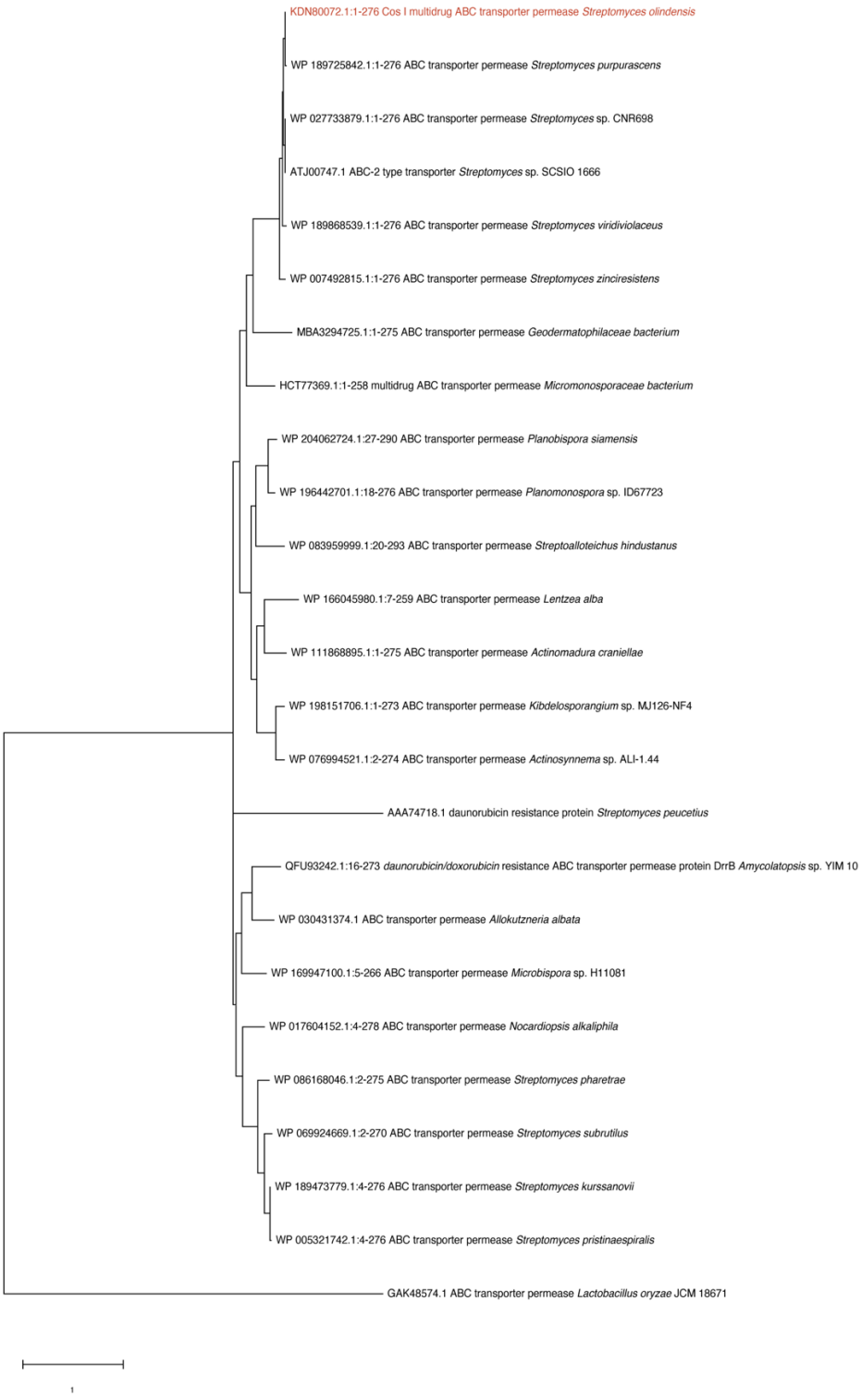
KDN80072.1:1-276 Cos I multidrug ABC transporter permease *Streptomyces olindensis*
WP 189725842.1:1-276 ABC transporter permease *Streptomyces purpurascens*
WP 027733879.1:1-276 ABC transporter permease *Streptomyces* sp. CNR698
ATJ00747.1 ABC-2 type transporter *Streptomyces* sp. SCSIO 1666
WP 189868539.1:1-276 ABC transporter permease *Streptomyces viridiviolaceus*
WP 007492815.1:1-276 ABC transporter permease *Streptomyces zinciresistens*
MBA3294725.1:1-275 ABC transporter permease *Geodermatophilaceae bacterium*
HCT77369.1:1-258 multidrug ABC transporter permease *Micromonosporaceae bacterium*
WP 204062724.1:27-290 ABC transporter permease *Planobispora siamensis*
WP 196442701.1:18-276 ABC transporter permease *Planomonospora* sp. ID67723
WP 083959999.1:20-293 ABC transporter permease *Streptoalloteichus hindustanus*
WP 166045980.1:7-259 ABC transporter permease *Lentzea alba*
WP 111868895.1:1-275 ABC transporter permease *Actinomadura craniellae*
WP 198151706.1:1-273 ABC transporter permease *Kibdelosporangium* sp. MJ126-NF4
WP 076994521.1:2-274 ABC transporter permease *Actinosynnema* sp. ALI-1.44
AAA74718.1 daunorubicin resistance protein *Streptomyces peucetius*
QFU93242.1:16-273 *daunorubicin/doxorubicin* resistance ABC transporter permease protein DrrB *Amycolatopsis* sp. YIM 10
WP 030431374.1 ABC transporter permease *Allokutzneria albata*
WP 169947100.1:5-266 ABC transporter permease *Microbispora* sp. H11081
WP 017604152.1:4-278 ABC transporter permease *Nocardiopsis alkaliphila*
WP 086168046.1:2-275 ABC transporter permease *Streptomyces pharetrae*
WP 069924669.1:2-270 ABC transporter permease *Streptomyces subrutilus*
WP 189473779.1:4-276 ABC transporter permease *Streptomyces kurssanovii*
WP 005321742.1:4-276 ABC transporter permease *Streptomyces pristinaespiralis*
GAK48574.1 ABC transporter permease *Lactobacillus oryzae* JCM 18671
1

B.

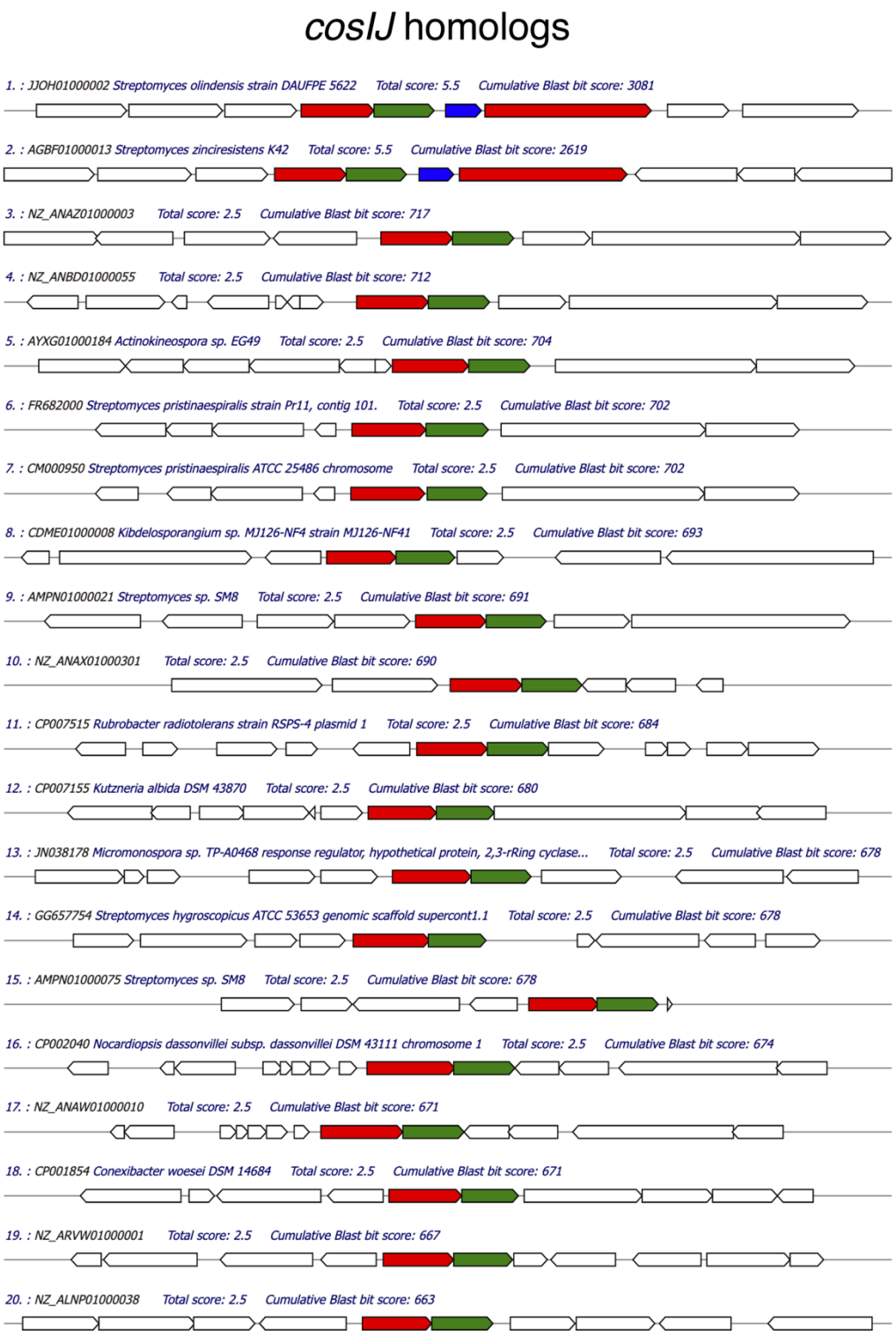

Figure 53. Phylogenetic analysis of the *cosI* gene

The maximum likelihood tree is based on NCBI database, MultiGeneBlast and performed with MEGA X. *Lactobacillus oryzae JCM 18671* (GAK48574.1) was used as the outgroup. Bootstrap analysis (performed 1,000 times). Scale bar represents 1 amino acid substitutions per site. **B.** MultiGeneBlast results using *cosI, cosJ, cosP,* and *cosU* as a template. *cosI, cosJ* (ABC transporter) are shown in red and green

Besides KDN80073.1, there is a second gene annotated with this function in the genome, called DF19_33265, which is found in contig 4 (JJOH00000004.1) and encodes the protein KDN79115.1. When we compared both proteins with MPx of *C. glutamicum* (ASW14906.1), KDN79115.1 shows a higher identity level (53,21%) than CosP-KDN80073.1 (43,4%), which results in higher values of Blast Score and E-value, respectively 175, 2e-57 for KDN79115.1 and 139, 3e-43 for KDN80073.1. When compared, both KDN80073.1 and KDN79115.1 share 55.1% of identity.

Searching selected *Streptomyces* reference genomes for annotated GPx or MPx genes, we found in general only one ortholog per genome, such as those that encode the proteins CAB88451.1 in *S. coelicolor* A3(2), WP_010985209.1 in *S. avermitilis*, WP_100106014.1 in S. *peucetius* subsp. *caesius* ATCC 27952, and EFL32854.1 in *Streptomyces viridochromogenes* DSM 40736 (Figure 54).

A.

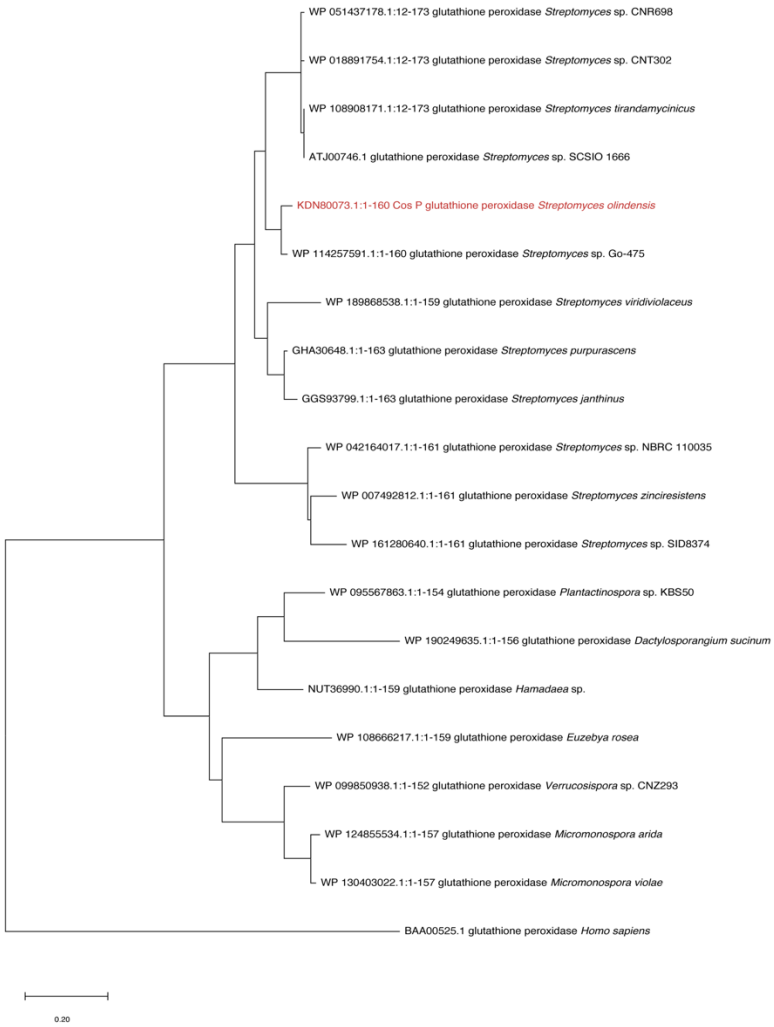

B.

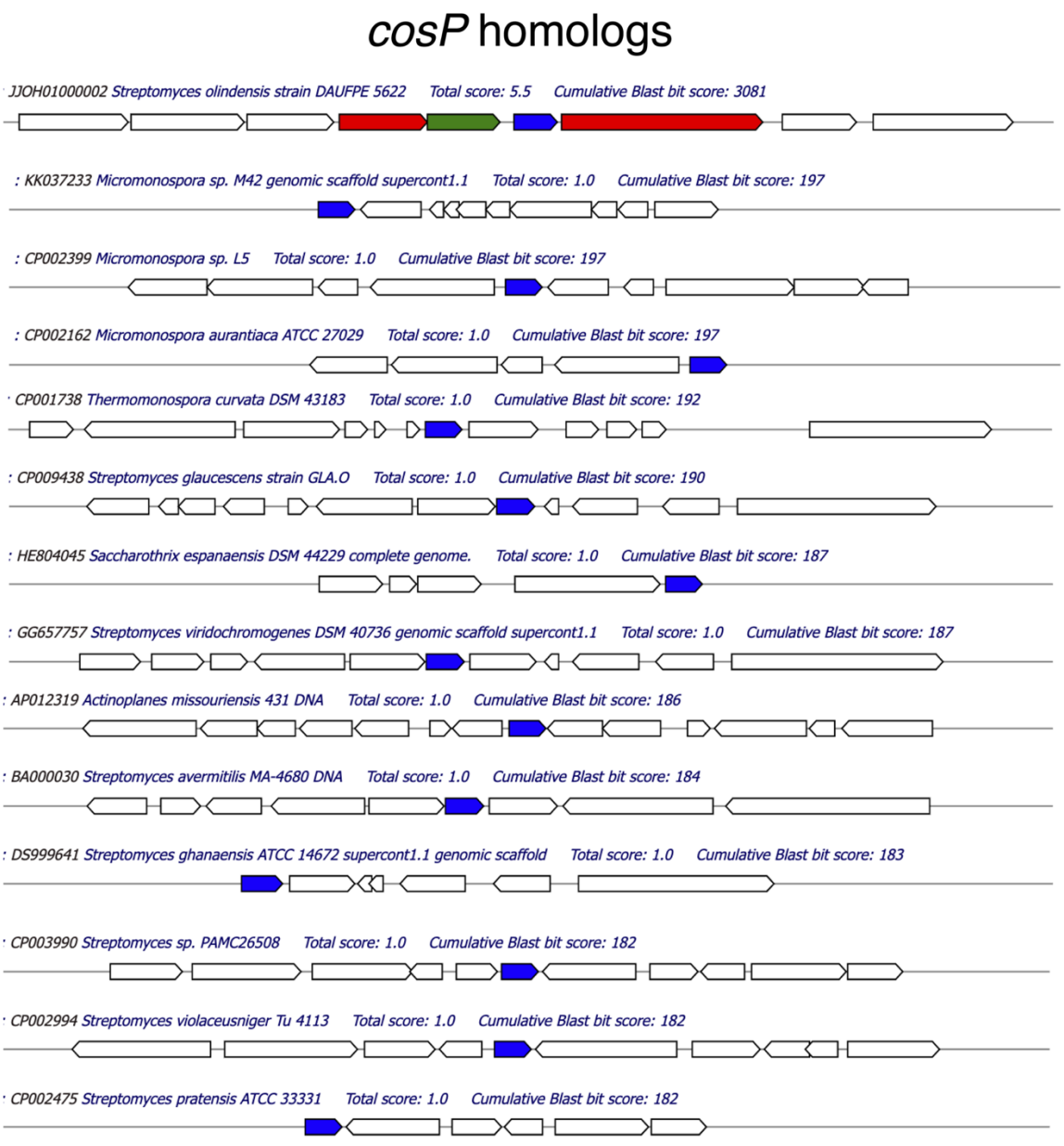
cosP homologs
JJOH01000002 Streptomyces olindensis strain DAUFPE 5622 Total score: 5.5 Cumulative Blast bit score: 3081
: KK037233 Micromonospora sp. M42 genomic scaffold supercont1.1 Total score: 1.0 Cumulative Blast bit score: 197
: CP002399 Micromonospora sp. L5 Total score: 1.0 Cumulative Blast bit score: 197
: CP002162 Micromonospora aurantiaca ATCC 27029 Total score: 1.0 Cumulative Blast bit score: 197
CP001738 Thermomonospora curvata DSM 43183 Total score: 1.0 Cumulative Blast bit score: 192
: CP009438 Streptomyces glaucescens strain GLA.O Total score: 1.0 Cumulative Blast bit score: 190
: HE804045 Saccharothrix espanaensis DSM 44229 complete genome. Total score: 1.0 Cumulative Blast bit score: 187
: GG657757 Streptomyces viridochromogenes DSM 40736 genomic scaffold supercont1.1 Total score: 1.0 Cumulative Blast bit score: 187
: AP012319 Actinoplanes missouriensis 431 DNA Total score: 1.0 Cumulative Blast bit score: 186
: BA000030 Streptomyces avermitilis MA-4680 DNA Total score: 1.0 Cumulative Blast bit score: 184
: DS999641 Streptomyces ghanaensis ATCC 14672 supercont1.1 genomic scaffold Total score: 1.0 Cumulative Blast bit score: 183
CP003990 Streptomyces sp. PAMC26508 Total score: 1.0 Cumulative Blast bit score: 182
CP002994 Streptomyces violaceusniger Tu 4113 Total score: 1.0 Cumulative Blast bit score: 182
CP002475 Streptomyces pratensis ATCC 33331 Total score: 1.0 Cumulative Blast bit score: 182

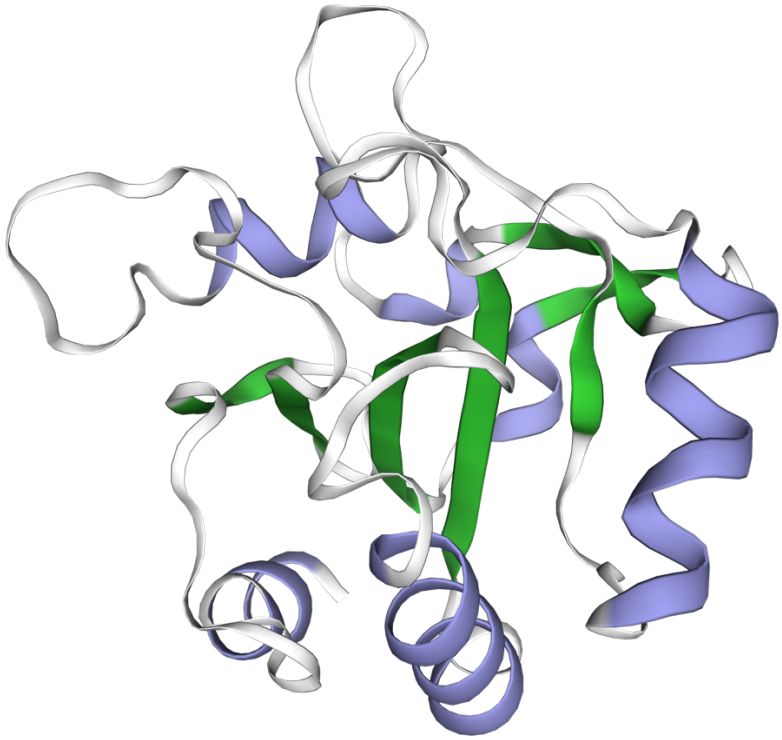

Figure 54. Phylogenetic analysis of the *cosP* gene.

The maximum likelihood tree is based on NCBI database, MultiGeneBlast and performed with MEGA X. *Homo sapiens* (BAA00525.1) was used as the outgroup. Bootstrap analysis (performed 1,000 times). Scale bar represents 0.20 amino acid substitutions per site. **B.** MultiGeneBlast results using *cosI, cosJ, cosP,* and *cosU* as a template. *cosP* (Mpx) homologs are shown in blue **C.** Structure protein model of the Cos P. Model based on crystal structure of *Schistosoma mansoni* glutathione peroxidase from SWISS- MODEL database tool (https://swissmodel.expasy.org).

To understand how both annotated peroxidases of *S. olindensis* correlate with these proteins and the remaining family of Gpx PFAM family (PF00255), “Similarity Sequence Networks” (SSN) were constructed.

Since KDN80073.1 was not in the Uniprot database, first a small SSN denominated “seed” with 100 proteins was generated with the Enzyme Similarity Tool (Zallot et al. 2019) and the FASTA sequence of this protein (Figure 55), with the aim of identify close relatives of KDN80073.1 within GPx Family PFAM. Since an identity level from 60% onwards was assumed to be sufficient to identify isofunctional protein clusters (Zallot et al. 2019), we chose a level of 70% of identity as threshold in the seed SSN, where cluster 2 contained KDN80073.1 and further 12 members listed in Table 24.

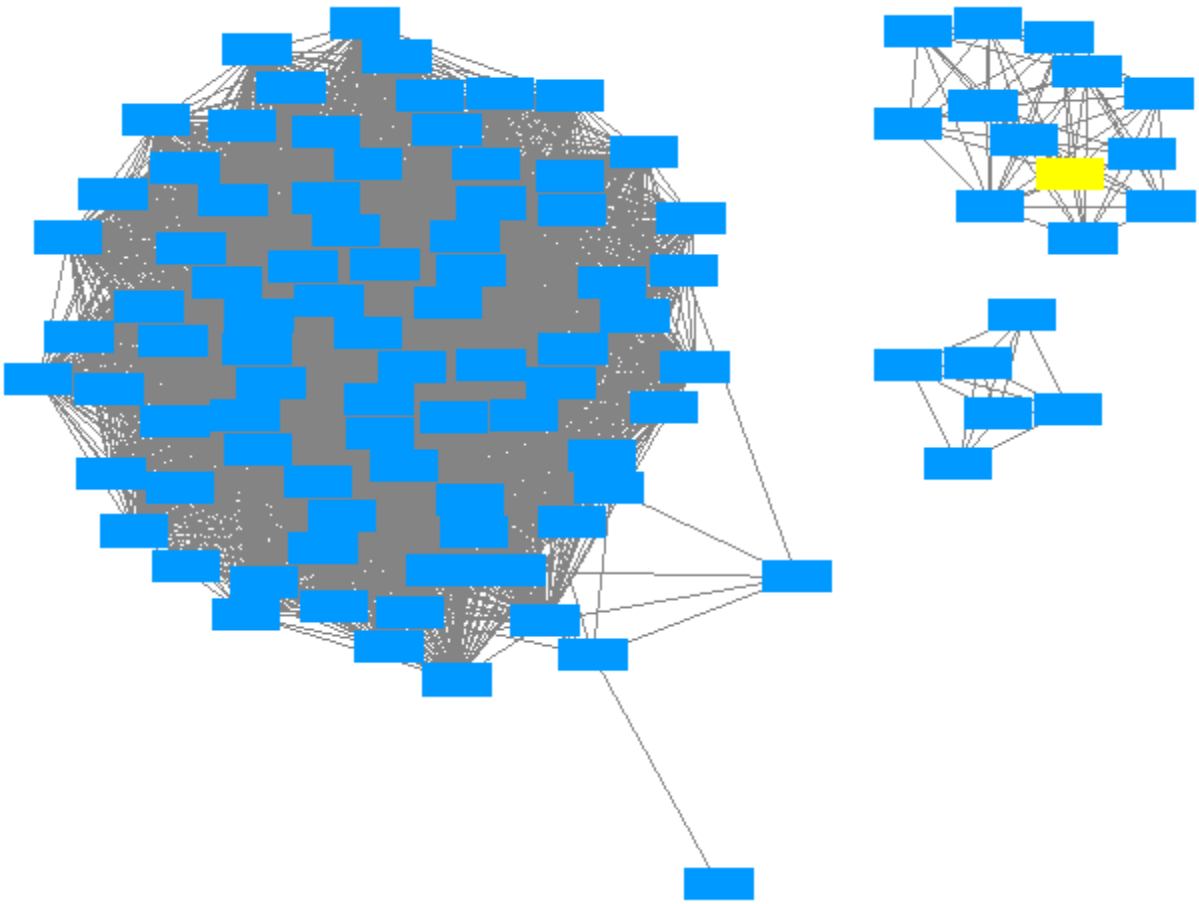

Figure 55. Seed SSN of KDN80073.3

SSN created to found close relatives of CosP (Highlighted in Yellow), to further compare the distribution of them in SSNs of PF00255.

Table 24. Cluster 2 of KDN80073,1 seed SSN

Uniprot Acess number	NCBI protein ID	genome locus_tag	Description	Species
N/A	KDN80073.1	DF19_23570	Glutathione peroxidase (inputed sequence)	*Streptomyces olindensis*
A0A150VSE8	KYG53407.1	AWI43_02085	Glutathione peroxidase	*Streptomyces sp.* WAC04657
A0A291NMV4	ATJ00746	MF773975.1	Glutathione peroxidase	*Streptomyces sp.* SCSIO 1666
A0A2L2PRZ6	AVH94681.1	C5L38_06145	Glutathione peroxidase	*Streptomyces sp.* WAC00288
A0A2S1T0Z9	AWI32167.1	DDW44_27735	Glutathione peroxidase	*Streptomyces tirandamycinicus*
A0A2T7K728	PVC77314.1	DBP18_02655	Glutathione peroxidase	*Streptomyces sp.* CS081A
A0A2Z5K6P4	AXE88381.1	C1703_25560	Glutathione peroxidase	*Streptomyces sp.* Go-475
A0A4Y8MFH8	TFE36212.1	E3E14_30925	Glutathione peroxidase	*Streptomyces sp.* ICN441
A0A5J6ITU2	QEV35549.1	CP977_28010	Glutathione peroxidase	*Streptomyces cinereoruber*
A0A6I5FTD8	WP_161280640.1	GTY67_27700	Glutathione peroxidase	Streptomyces sp. SID8374
A0A7W4ZTC3	MBB3078325 *	FHS41_004832	Glutathione peroxidase	*Streptomyces violarus*
A0A7Y2SC25	NNJ05130.1	HHX38_13425	Glutathione peroxidase	*Streptomyces sp.* PKU-MA01144
G2G7H6	EGX60546.1	SZN_07193	Glutathione peroxidase	*Streptomyces zinciresistens* K42

* Identical to MBB3078325 from another strain of *S. violarus*

After a first SSN of PFAM, PF00255 was obtained using a threshold of about 55% similarity (Figure 56), a large main cluster of 39799 peroxidases includes almost all actinobacterial proteins together with those from other phyla including known prokaryotic (i.e. *E. coli* BtuE P06610) and eukaryotic (i.e. *S. cerevisae* Gpx1 - P36014) GPx. When the threshold was increased to a similarity level of about 61%, the actinobacterial proteins grouped in different clusters. Cluster 2 comprises 3261 proteins and includes, CAB88451.1, WP_010985209.1, WP_100106014.1 and EFL32854.1, however cluster 99 has almost the same composition of seed SSN cluster 2, excluding only KDN80073.1 (Figure 58 and Table 24) that are not in the PF00255 database.

Subsequently, a Genome Neighborhood Network (GNN) was generated from that SSN (Figure 57). The analysis of cluster 99, revealed that all members are in non-previously described cosmomycin clusters of different *Streptomyces* species. These findings could suggest that KDN80073.1 has an increased specificity by some peroxides generated by cosmomycin action.

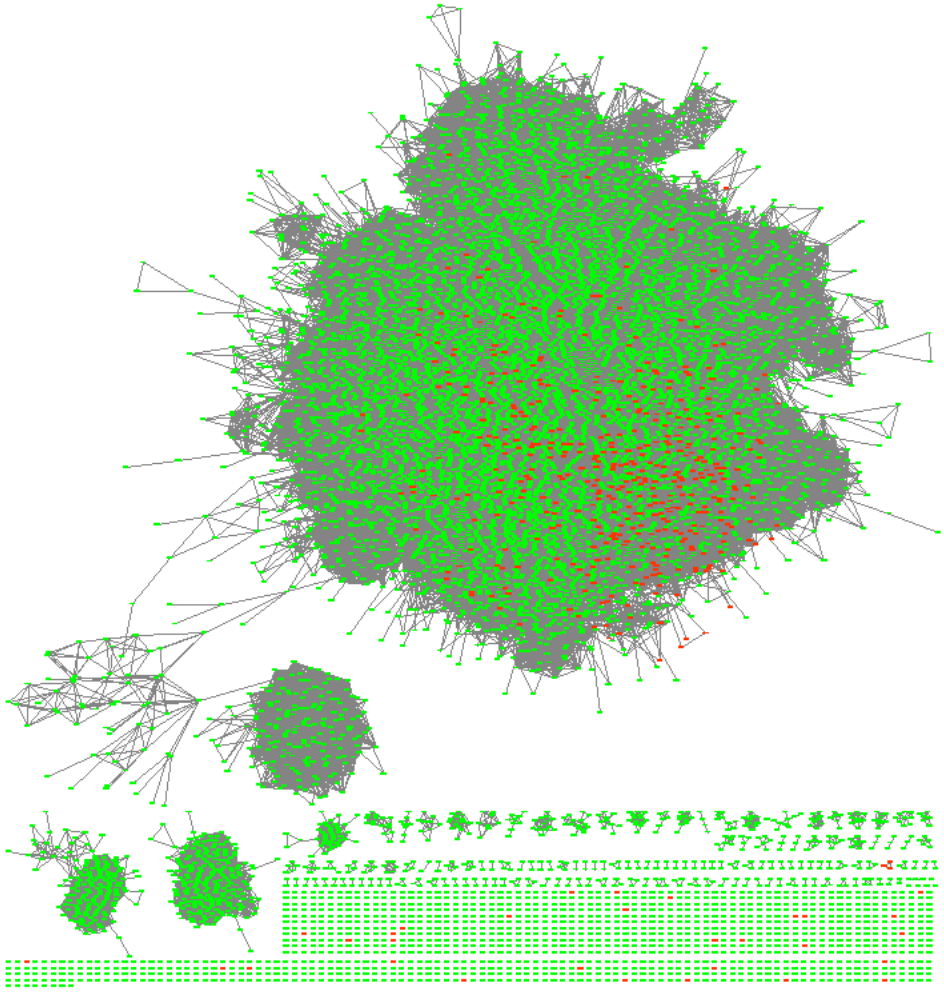

Figure 56. First GPx PFAM Family PF00255 SSN

Identity threshold around 55%. Red nodes denote actinobacteria peroxidases, green nodes represent all the other prokaryotic and eukaryotic members of the family. The biggest cluster (cluster 1) comprises 39799 proteins including prokaryotic and eukaryotic known GPx like *E. coli* BtuE (P06610) and *S. cerevisae* Gpx1 (P36014), as well as most actinobacteria proteins.

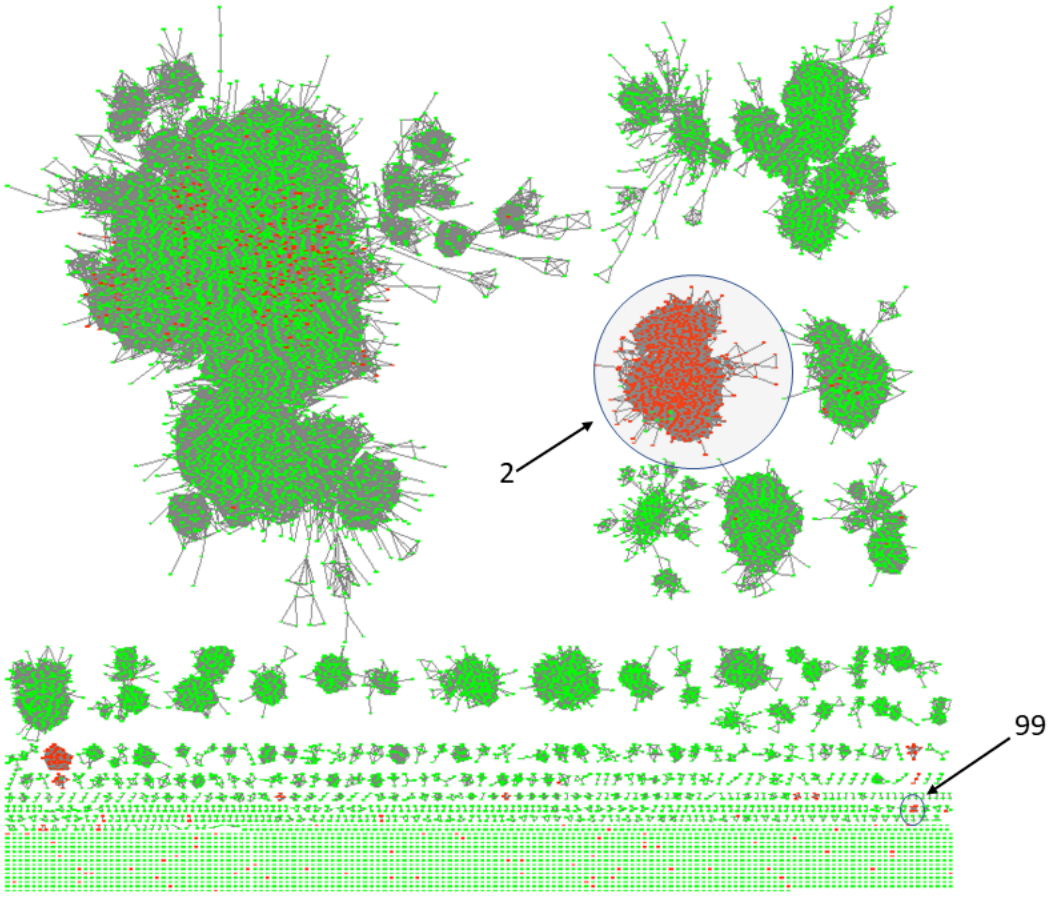

Figure 57. Second GPx PFAM Family PF00255 SSN

Identity threshold around 61%. Red nodes denote actinobacteria members of family, green nodes represents all the other prokaryotic and eukaryotic members of the family. Cluster 2 (where CAB88451.1, WP_010985209.1, WP_100106014.1 and EFL32854.1 group with most actinobacteria peroxidases) and 99 (where lies relatives of KDN800793.1 are highlighted.

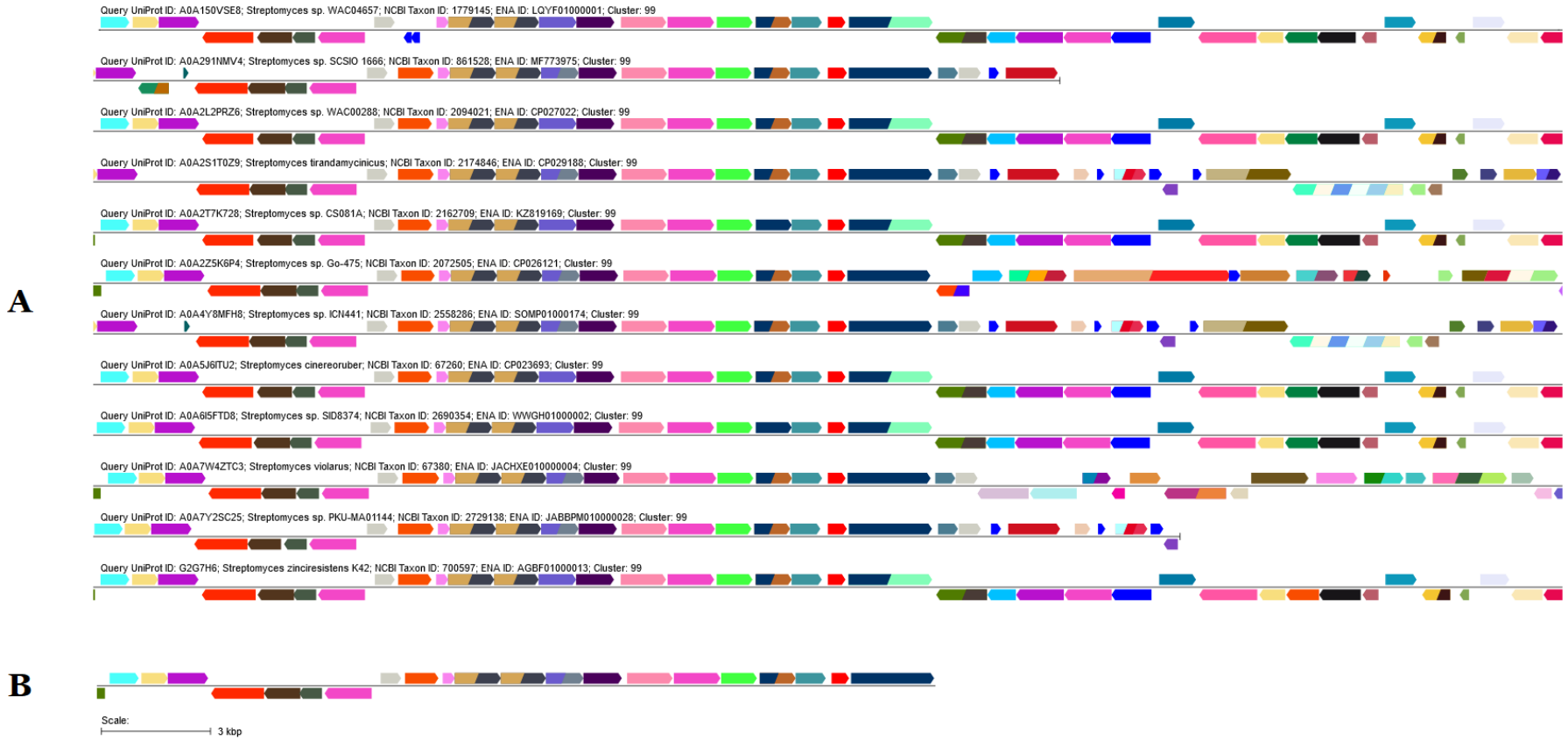

Figure 58. Genome Neighborhood Diagram of cluster 99 (2nd PF00255 SSN)

A-Alignment of genome context alongside of *cosP* orthologs of all cluster 99 members; B: Cosmomycin BGC cluster region of *S. olindensis* corresponding to GND of part A. Orthologs of *cosP* orthologs (painted in red) are at the center of the GND.

The third putative resistance mechanism is encoded by *cosU*, which gene product shows 96,71% similarity to the excinuclease ABC subunit UvrA of *Streptomyces janthinus* (accession number: WP_193483046) (Figure 59), which is a member of a group of proteins associated with DNA repair (Lomovskaya et al. 1996; Prija and Prasad 2017). The prototype of this group is DrrC from *S. peucetius*, which could bind to daunorubicin intercalated to DNA and displaces anthracycline, thereby preventing nucleic acid damage and allowing the drug to be expelled by the DrrA/B system (Prija and Prasad 2017).

A.

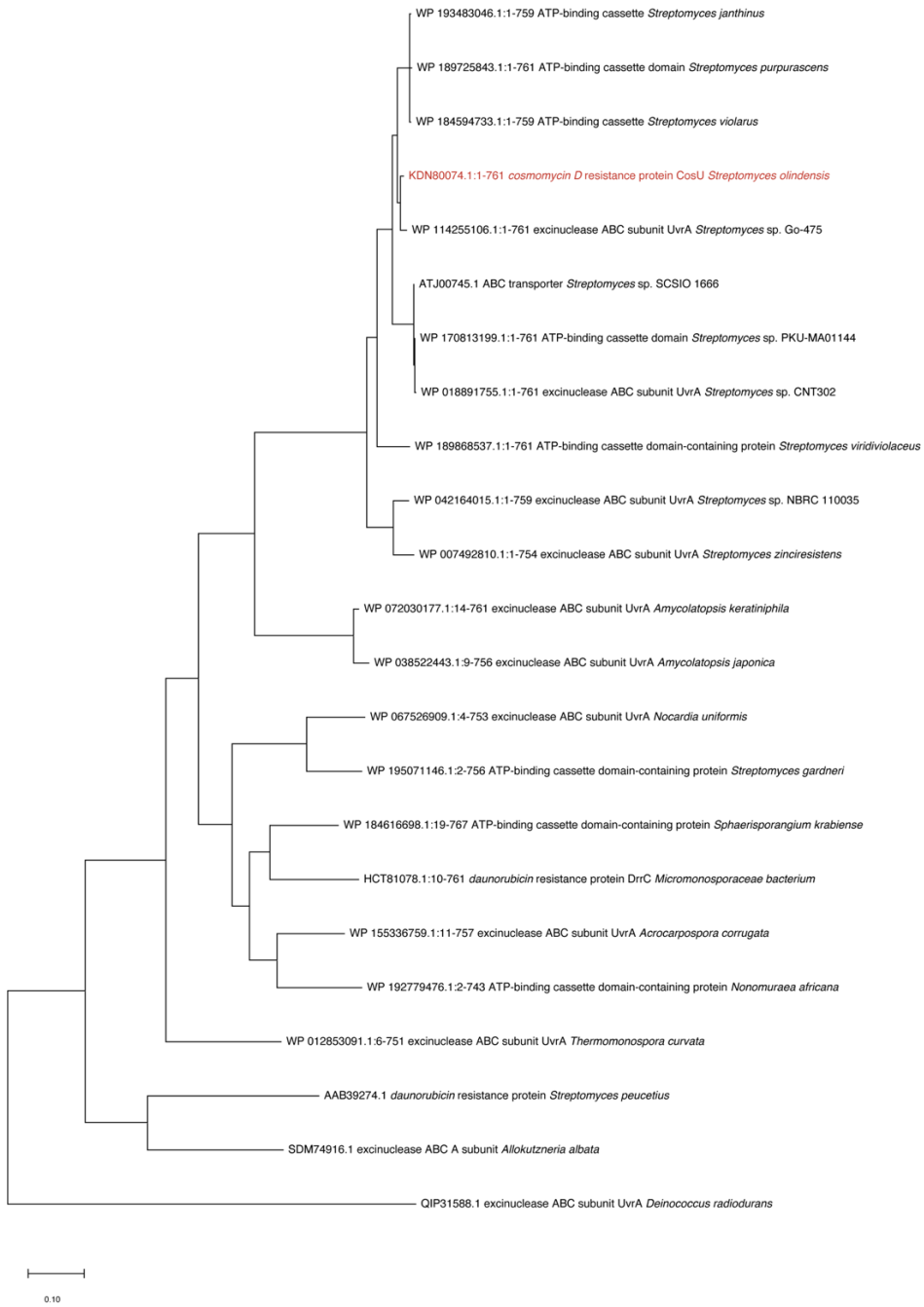

B.

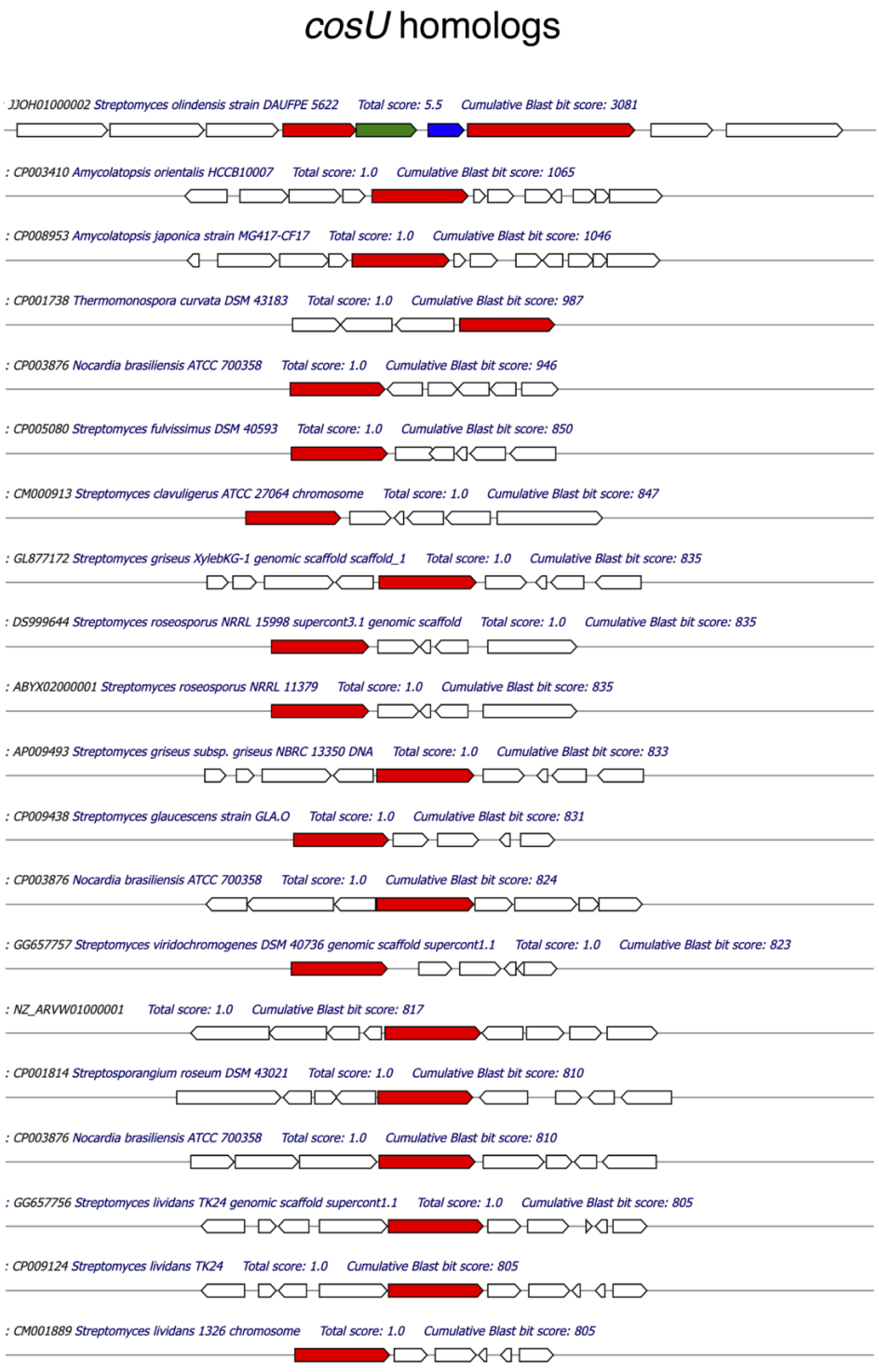

Figure 59. Phylogenetic analysis of the *cosU* gene

A. The maximum likelihood tree is based on NCBI database, MultiGeneBlast and performed with MEGA X. *Deniococcus radiodurans* (QIP31588.1) was used as the outgroup. Bootstrap analysis (performed 1,000 times). Scale bar represents 0.10 amino acid substitutions per site. **B.** MultiGeneBlast results using *cosI, cosJ, cosP,* and *cosU* as a template. *cosU* (UvrA like protein) homologs are shown in red

8.2 Self-resistance mechanisms are essential for *S. olindensis*, when challenged with DOX and COSD

To understand the toxicity of COSD compared with pure DOX, COSD was isolated from *S. olindensis* using analytical fractionation. The fraction of interest showed a red-purple color. HR-MS measurements revealed a candidate compound with protonated molecule masses of *m/z* 1189.5901 ($[M+H]^+$, calculated 1189.590149, Δ=-0.04 ppm) and *m/z* 595.2991 ($[M+2H]^{2+}$, calculated 595.298713, Δ=+0.65 ppm), which were consistent with the molecular formula of COSD ($C_{60}H_{88}N_2O_{22}$) (Figure 60). A complementary MS/MS analysis of COSD, executed on its $[M+2H]^{2+}$ ion, produced fragment ions that were in full agreement with the expected structure (Figure 60-61 and Table 25).

A)

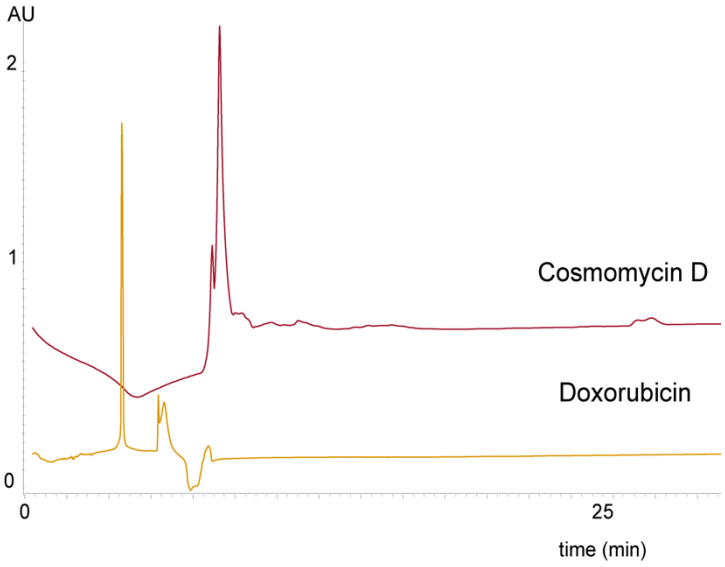

B)

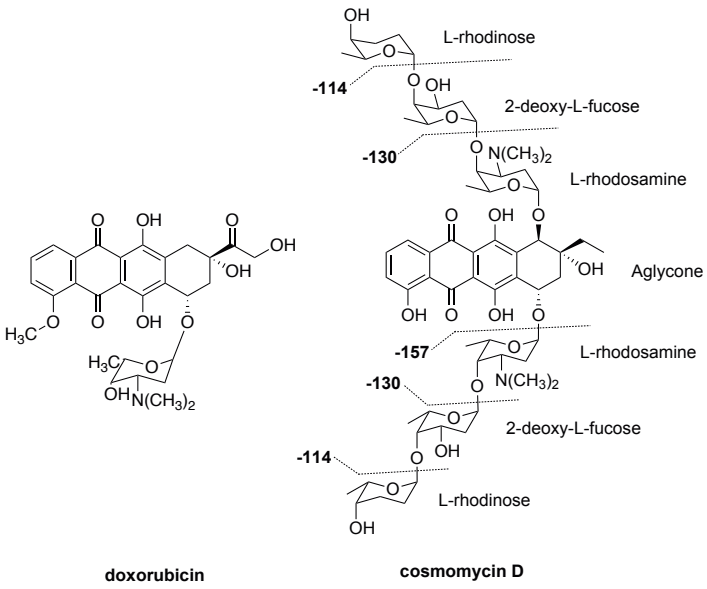

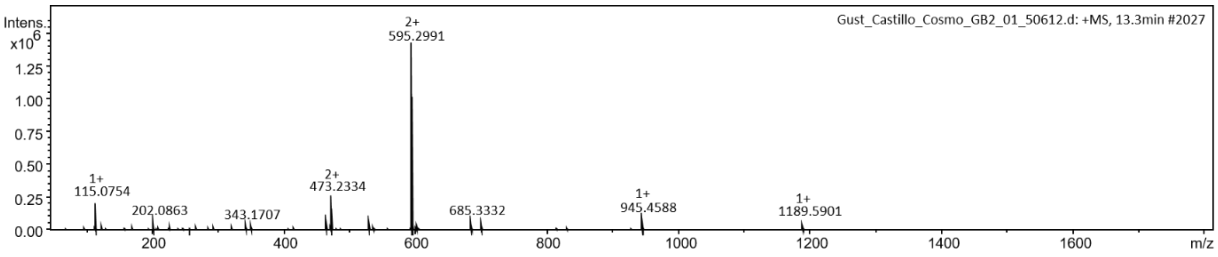

Figure 60. A) HPLC profile of COS D and DOX vs. structure DOX and COSD. B) ESI-MS/MS (MS^2) of COS D

scheme shows the key fragments corresponding to the structure of COSD and were assigned on the structure.

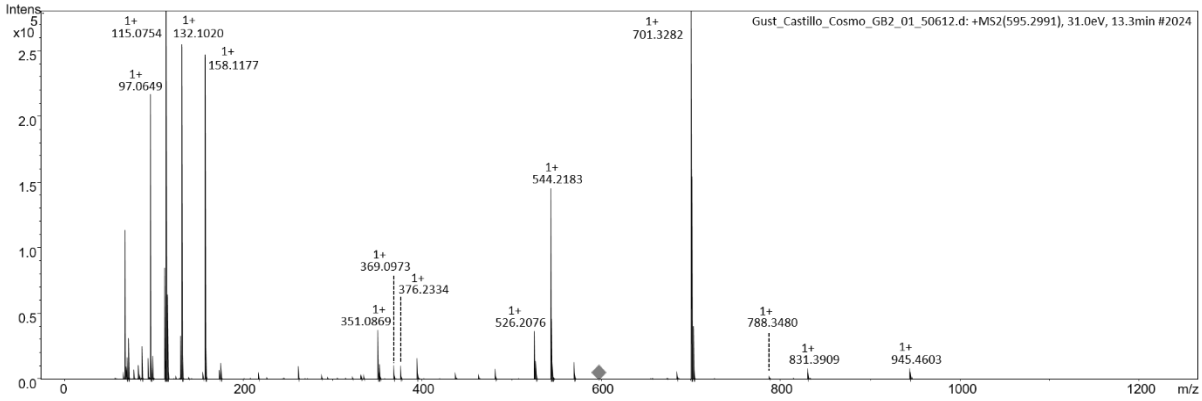

Figure 61. ESI-MS/MS (MS^2) of cosmomycin D (top)

The dotted lines were drawn to explain the intensities of the observed peaks

Table 25. With tandem MS/MS, pure cosmomycin D
Fragmented yielding several daughter ions in the mass spectrum. Theoretical and observed mass differences between these assignments were negligible

Fragments	Elemental composition	Relative Double Bond (Rdb)	Theoretical Mass	Experimental Mass *(m/z)*	Error [ppm]
$[M+H]^{2+}$	$C_{60}H_{90}N_2O_{22}$	18	595.2987	595.2991	0.67
$[M-114-130+H]^+$	$C_{48}H_{69}N_2O_{17}$	16	945.4596	945.4588	-0.85
$[M-2x114-130+H]^+$	$C_{42}H_{59}N_2O_{15}$	15	831.3915	831.3909	-0.72
$[M-114-130-157+H]^+$	$C_{40}H_{54}NO_{15}$	15	788.3493	788.3480	-1.65
$[M-2x114-2x130+H]^+$	$C_{36}H_{49}N_2O_{12}$	14	701.3286	701.3282	-0.57
$[M-2x114-2x130-157+H]^+$	$C_{28}H_{34}NO_{10}$	13	544.2183	544.2183	0.00
$[M-2x114-2x130-157-H_2O+H]^+$	$C_{28}H_{32}NO_9$	14	526.2077	526.2076	-0.19
Aglycone – H_2O	$C_{20}H_{17}O_7$	13	369.0974	369.0973	-0.27
Agylcone – $2xH_2O$	$C_{20}H_{15}O_6$	14	351.0869	351.0869	0.00
Sugar 1, 2 and 3 – $2xCH_3$	$C_{18}H_{34}NO_7$	3	376.2335	376.2334	-0.26
Sugar 3/3‘	$C_8H_{15}NO_2$	2	158.1181	158.1177	-2-53
Sugar 3/3‘ – $2xCH_3$	$C_6H_{14}NO_2$	1	132.1025	132.1020	-3.78
Sugar 2/2‘	$C_6H_{11}O_3$	2	131.0708	131.0704	-3.05
Sugar 1/1‘	$C_6H_{11}O_2$	2	115.0759	115.0754	-4.34
Sugar 1/1‘ – H_2O	C_6H_9O	3	97.0653	97.0649	-4.12

The hypothetical self-resistance genes *cosI, cosJ*, *cosP*, and *cosU* were cloned into the expression plasmid pUWL_Apra_oriT, consequently generating the recombinant constructs

pRCWL04 (*cosI/cosJ*), pRCWL05 (*cosP*) and pRCWL06 (*cosU*) respectively. Exconjugants of *S. lividans* TK24 carrying the correspondent constructs, as well as the empty vector were used to determine the minimum inhibitory concentrations (MICs; Table 26) in a 96 well plate assay format against COSD and doxorubicin (DOX) (Figure 62). As control, *S. olindensis and S. peucetius* were used. *S. lividans* TK24 harboring *cosI* and *cosJ* showed high levels of resistance to COSD and DOX when compared with recombinant strains harboring only *cosP and cosU*.

Table 26. Minimum inhibitory concentration (MIC) of *Streptomyces* strains expressed in (µg/mL) against doxorubicin and cosmomycin D

Strain	doxorubicin	cosmomycin D
S. peucetius DSM 40754	4	4
S. olindensis DAUFPE 5622	4	8
S. lividans TK 24 pRCWL04 (*cosIJ*)	16	8
S. lividans TK 24 pRCWL05 (*cosP*)	8	4
S. lividans TK 24 pRCWL06 (*cosU*)	16	8
S. lividans TK 24 pUWL (empty vector)	2	2

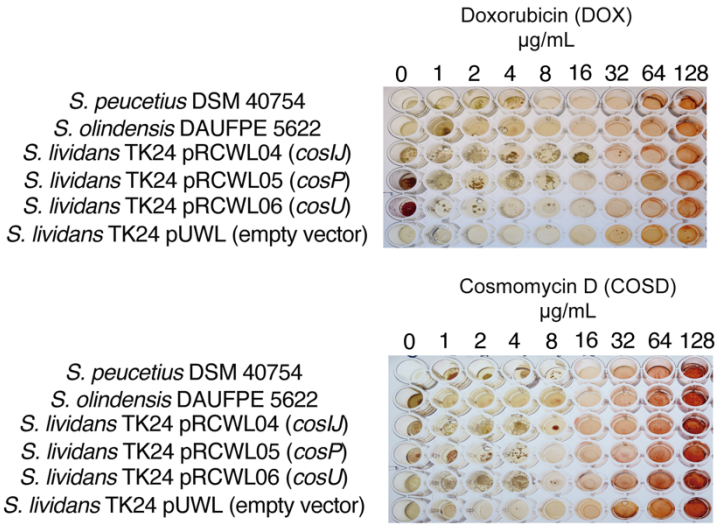

Figure 62. Minimum inhibitory concentrations (MIC) to COSD and DOX for selected *Streptomyces* species by 96-well plate assay

S. peucetius DSM 40754, *S. olindensis* DAUFPE 5622, *S. lividans* TK 24 pRCWL04 (*cosI cosJ*), *S. lividans* TK 24 pRCWL05 (*cosP*), *S. lividans* TK 24 pRCWL06 (*cosU*) and *S. lividans* TK 24 pUWL (empty vector) challenged with DOX (panel A) or COSD (panel B). Final concentrations of DOX and COSD were 0, 1, 2, 4, 8, 16, 32, 64, and 128 µg/mL respectively for both antibiotics (apramycin was added at 50 µg/mL when needed).

The MIC test shows that the overexpression of the ABC transporter generates the highest resistance for DOX and COSD in *S. lividans* TK24, while mutants containing the mycothiol peroxidase (*cosP*) showed similar resistance to the *drrC*-like gene (*cosU*) with 16 and 8 µg/mL for DOX and COSD, respectively. *S. olindensis* had a similar resistance as *S. peucetius* to DOX, however, for COSD, *S. olindensis* is more resistant (8 µg/mL vs. 4µg/mL). On the other hand, *S. lividans* TK24 containing the empty pUWL vector did not show survival to COSD and DOX concentrations higher than 1µg/mL.

8.3 Self-resistance genes are mostly expressed during the production of COSD

We hypothesized that the wild type strain *S. olindensis* overexpresses its self-resistance genes only during production of the antibiotic. Thus, RNA was extracted during COSD production at 72h vs. non-production at 24h (Figure 64) (Garrido et al. 2006), and cDNA was synthesized immediately. The gene expression was determined by qPCR. The endogenous gene *hrdb* (Šmídová et al. 2019) served as the reference (Figure 63).

Melt Curve Peak Chart (-dF/dt vs T) **PCR Amp/Cycle Chart**

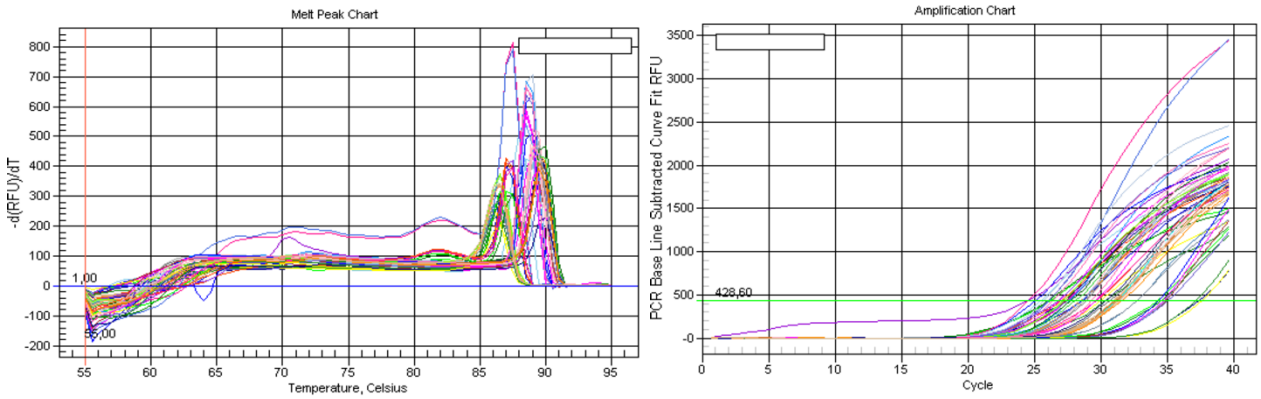

Figure 63. RT- qPCR (Melt Curve and PCR Amp/Cycle) of *cos*I, *cos*J, *cos*P, *cos*U and *Hrdb* during the production and non-production of COSD in *S. olindensis* strain

The analysis includes 3 biological replicates and 2 technical replicates for each treatment. In the same way, positive and negative controls were carried out to evaluate gDNA contamination and primer dimers with the melting curve.

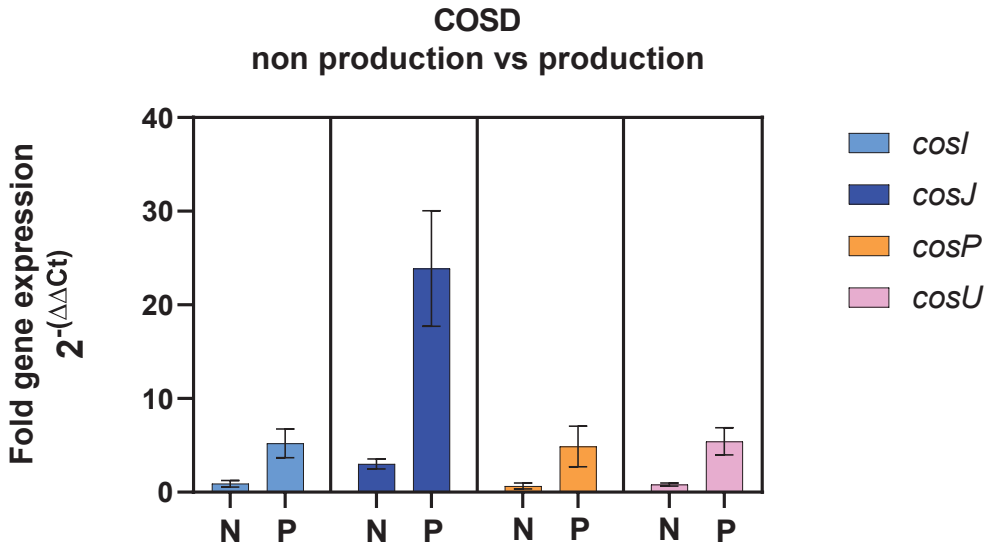

Figure 64. qPCR of *cosI*, *cosJ*, *cosP* and *cosU*, *hrdb* as reference during the production (72 h) and non-production (24 h) of COSD by *S. olindensis*.

8.4 Mycothiol peroxidase (MPx) response against ROS stress

The mycothiol peroxidase from *Streptomyces olindensis* consists of 163 amino acids, from which three are Cys residues (C38, C66, C84). Additionally, we purified a C38S mutant enzyme of MPx, obtained by site directed mutagenesis (Figure 65). We evaluated the peroxidase activity of both enzymes by ferrous oxidation of xylenol orange (FOX assay) to quantify H_2O_2 and *t*-butyl hydroperoxide (tBOOH) reduction with a time frame of 180 s. The WT MPx consumes the majority of H_2O_2 within 15 s whereas the C38S mutant enzyme remained catalytically inactive demonstrated in a constant amount of H_2O_2 remaining in the assay over the time used. The FOX assay performed with tBOOH showed a significant decrease in the concentration of tBOOH which represents the half than the H_2O_2 assay for 200 s (Figure 66).

A

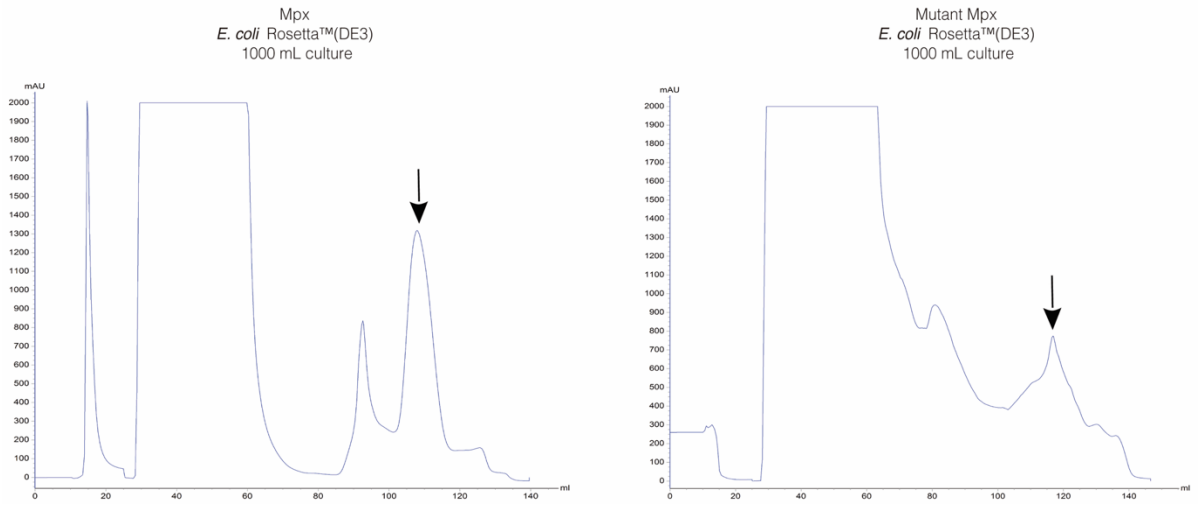

B

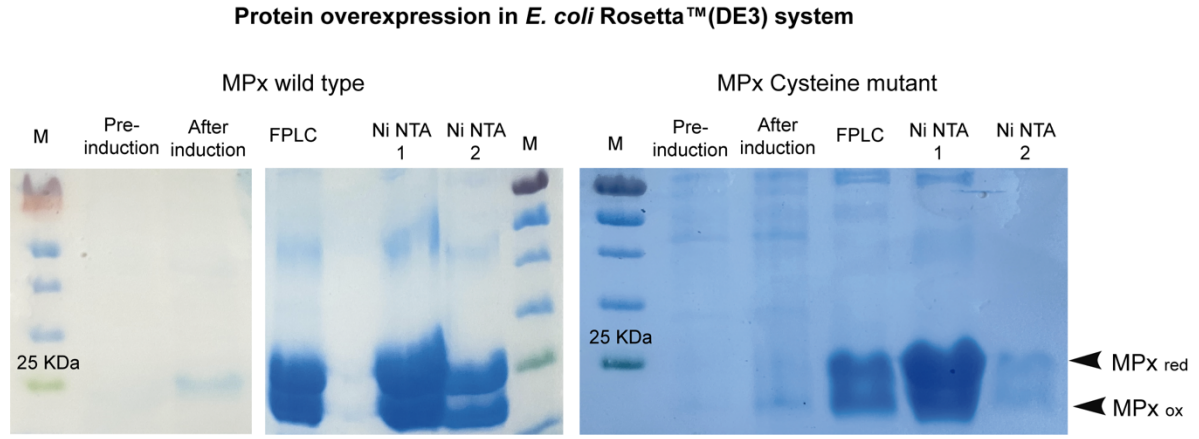

Figure 65. A. FPLC Chromatogram of the Mpx and its mutant Mpx C38S in *E. coli* Rossetta (DE3) as a host B. SDS-PAGE of purified MPx and MPx C38S mutant obtained by FPLC and Ni-NTA

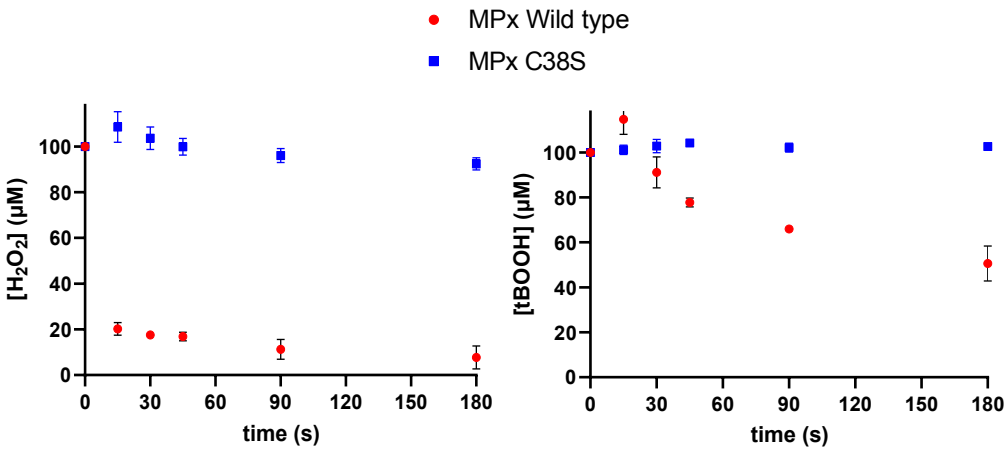

Figure 66. H_2O_2 and tBOOH quantification (FOX assay) of MPx WT and MPx (C38S) during 180 s activity

Values are mean of triplicate determination ± SD

We also evaluated the MIC of *S. olindensis*, *S. peucetius* and *S. lividans* against H_2O_2 (1-512 mM). For tested concentrations, both anthracycline producers *S. olindensis* and *S. peucetius* survive upon 128 mM thereby confirming a good response against H_2O_2. *S. lividans* was very sensitive to H_2O_2 (MIC 8mM, table 2) but its resistance to H_2O_2 notably improved when this strain containg a vector expressing *cosP* (MIC 32mM, table 27). In contrast, *S. lividans* with an MIC of 16 mM showed a considerable difference when harboring *cosP* (table 2, Figure 67). This result indicates that MPx improved *S. olindensis* to survive persistent oxidative conditions.

Table 27. Minimum inhibitory concentration (MIC) of *Streptomyces* strains expressed (in mM) against H_2O_2.

Strain	H_2O_2 [mM]
S. peuceitus DSM 40754	128
S. olindensis DAUFPE 5622	128
S. lividans TK 24 pUWL (empty vector)	8
S. lividans TK 24 pRCWL05 (*cosP*)	32

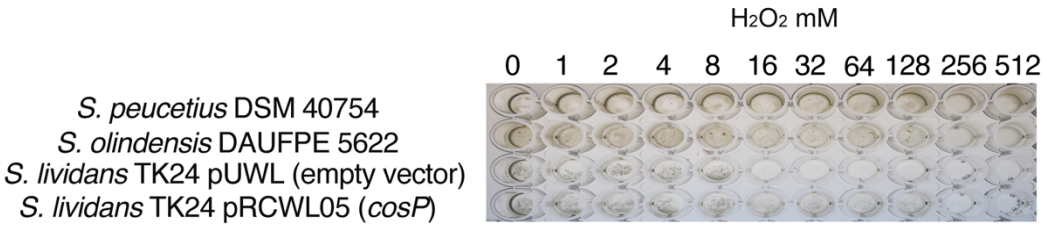

Figure 67. Minimum inhibitory concentrations (MIC) of selected *Streptomyces* species against H_2O_2 in an 96-well plate assay.

S. peucetius DSM 40754, *S. olindensis* DAUFPE 5622, *S. lividans* TK 24 pRCWL05 (*cosP*), and *S. lividans* TK 24 pUWL (empty vector) challenged with H_2O_2.

8.5 *S. olindensis* peroxidase detoxification is important for survival under cosmomycin D production

To understand the role of CosP in *S. olindensis* H_2O_2 consumption, we evaluated the capacity of COSD-producer *S. olindensis* and non-producer *S. lividans* to reduce H_2O_2 over time, in conditions that favor COSD production. For this, we measured the H_2O_2 consumption rate of total protein extracts at 24, 48 and 72h growth (Figure 68). While both *S. olidensis* and *S. lividans* improved their H_2O_2 consumption rate at later growth stages, it was obvious that the cosP-producer *S. olidensis* reduced H_2O_2 faster (Figure 68).

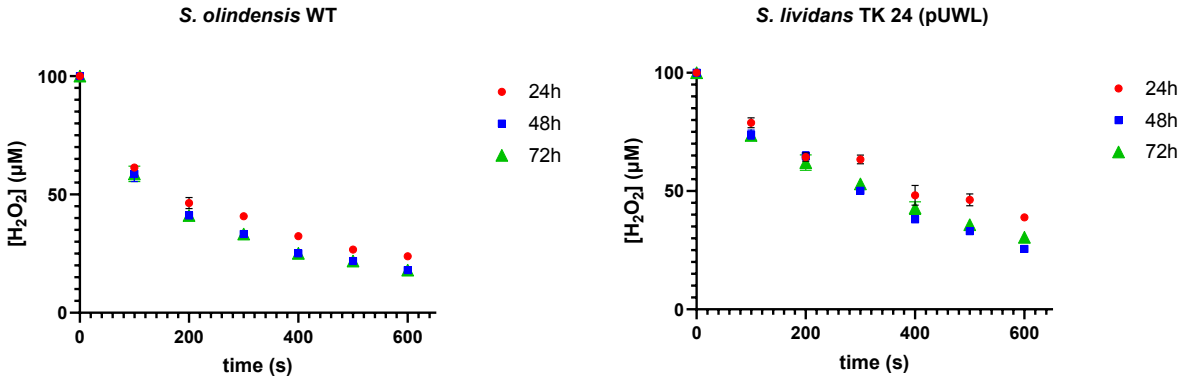

Figure 68. H_2O_2 quantification (FOX assay) of *S. olindensis* WT vs. *S. lividans* Tk24 during 600 s activity

Values are mean of triplicate determination ± SD

9. Discussion

In this work, we highlighted that *S. olindensis* has an extra MPx copy encoded by the cosmomycin BGC to act complementary with anthracycline resistance proteins previously studied: ABC transporter and UvrA class IIa as a possible self-resistance factor during the production of COSD. Since other anthracycline BGC containing the same genes are described in literature, for example cytorhodin BGC (MF773975.1) and other BGCs listed in (Figure 59), our findings can most likely be extended to some anthracycline-producing bacteria.

The protein encoded by *cosI* belongs to the superfamily of ATP-dependent ABC transporters. The organization of this protein include two motifs, Walker A and Walker B, providing an ATP binding site and containing the unique signature motif in ABC transporters located upstream of the Walker B motif. For *S. olindensis* it was classified as Type I; the transporter system consists of two proteins encoded by independent genes: CosI (NBD) contains the nucleotide binding domains (Walker A and Walker B) and CosJ (TMD) the hydrophobic membrane protein (TM) containing six transmembrane helices (Figure 52).

ABC transporters belonging to this class have been so far reported solely in the producer organisms of several antitumor agents (Méndez and Salas 2001). Daunorubicin and doxorubicin are anthracycline drugs produced by *Streptomyces peucetius*. Two genes (*drrA* and *drrB*) forming a type I transporter system have been cloned and found to confer resistance to daunorubicin/doxorubicin and mithramycin (*mtrA* and *mtrB* genes) (Ernestina Fernández et al. 1996; Gandlur et al. 2004; Kaur 1997; Kaur and Russell 1998; Malla et al. 2010; Srinivasan, Palani, and Prasad 2010).

In Gram-positive bacteria, such as actinobacteria, it has been reported that MPx is a novel CysGPx peroxidase family that degrades hydrogen peroxide and alkyl hydroperoxides in the presence of either the thioredoxin/thioredoxin reductase (Trx/TrxR) or mycoredoxin 1/mycothiol/mycothione reductase (Mrx1MSH/Mtr) reducing systems. MPx protects against the damaging effects of ROS induced by multiple stressors using thioredoxin or related redoxins as reductants (Flohe 2011; Pedre et al. 2015; Si et al. 2015). The *S. olindensis* genome has two putative genes which code for a peroxidase-type protein (KDN80073.1 and KDN79115.1) and were involved in the general detoxification of H_2O_2. The protection is not related with anthracycline production and completely agrees with the results shown in (Fig 68) on the challenge with H_2O_2, in which *S. olindensis* and *S. peucetius* showed a good detoxification response that is not related to any type of response against anthracycline

production. Despite *S. olindensis* possesses two proteins that could cooperate in ROS depuration, the activity against H_2O_2 almost disappear in the KDN80073.1 mutant, indicating that this is the main scavenger of this peroxide in the cell, while *S. peucetius* has just one MPx annotated in the genome, however, it is more closely related to KDN79115.1 (67,82% of identity) than KDN80073.1 (56,33% of identity).

It is known that anthracyclines produce free radicals that may, in association with ferric compounds, causing oxidative stress (Ruggiero et al. 2008). Oxidative stress depends on the reactive oxygen species (ROS), which are generated by the action of xenobiotics and as a result of metabolic processes (Findlay, Tapiero, and Townsend 2005). The oxidizing power of O_2^- and H_2O_2 is harmful to cells. These species can inactivate important metabolic enzymes or altering their catalytic activity. H_2O_2 can cross the cell membrane and initiate lipid oxidation by deprotonation of fatty acids (Gechev et al. 2006).

Biochemical and physiological data lead to the hypothesis that anthracyclines such as DOX or in our case COSD can cause the formation of free radicals that stimulate lipid peroxidation and alter cellular integrity (Arteaga 2016; Doroshow et al. 1990; Powis 1989) and a direct relation to their association to DNA. This hypothesis supports the premise that the oxidative metabolism of the anticancer quinones represent a significant contribution to the cytotoxic effects of these compounds (Doroshow et al. 1990). These species can inactivate important metabolic enzymes, altering their catalytic activity. In the case of H_2O_2 it can cross the cell membrane and initiate lipid oxidation by deprotonation of fatty acids, (Gechev et al. 2006) similar as reported for DOX during the redox cycle of anthracyclines (Henderson et al. 1978).

Interestingly, the study of Westman and collaborators (2012) correlated the biological activity of 7-deoxydoxorubicinolone in prokaryotes and eukaryotes. The authors could show that levels of expression of catalase, superoxide dismutase, and glutathione peroxidase in bacterial cells are higher than in human cells from cardiac tissue. They concluded that bacterial cells are much more competent at dealing with the outcomes of anthracycline semiquinone oxidation-reduction cycling, and the resulting reactive oxygen species (ROS) evolved, and that *Streptomyces* are generally well equipped to deal with reactive oxygen stress (Westman et al. 2012). The aglycone molecules may accumulate in membranes due to their hydrophobicity; the rapid growth and division of bacterial cells relative to eukaryotic cardiac tissue may also explain the differential effect of anthracycline aglycones towards prokaryotes and eukaryotes (Westman et al. 2012).

Based on our present findings, we hypothesize that anthracyclines, such as COSD, are determinant in the production of ROS, then a recruitment of additional antioxidant enzymes coded in BGCs like KDN80073.1 can increase the self-resistance of antitumor antibiotics with

potential cell toxicity. Another evidence are KDN80073.1 groups with an independent protein cluster in PFAM PF00255 family SSN, wherein all members belong to cosmomycin-like clusters (Figure 58), which could also indicate that these proteins boost the protection to anthracycline-generated intracellular ROS.

COSD reportedly binds DNA more tightly than DOX (Kelso et al. 2009), but it causes less DNA damage in comparison to DOX, even so the induced apoptosis level for both drugs in nucleotide excision repair-deficient fibroblast are similar (Carvalho et al. 2010), CosU is responsible to minimize the interaction between COSD and DNA, thereby avoiding damage.

Normally, DNA damage recognition is performed by the protein UvrA, which belongs to the ABC-ATPase superfamily. Bacterial UvrA is a dimeric protein and unique among DNA repair enzymes. This feature enables UvrA to detect various DNA lesions by using an indirect readout mechanism. Other proteins namely UvrB, UvrC, and UvrD, are components of nucleotide excision repair NER, and are essential for the survival of almost every living bacterium (Jaciuk et al. 2011; Truglio et al. 2006).

The protein encoded by the *cosU* gene has a high similarity with UvrA proteins, however, contains the deletion of the UvrB-binding domain and the first zinc finger motif. For this reason, the protein function is not involved in NER and is classified as a UvrA-like protein class IIa (Marszałkowska et al. 2013). The latter have been shown to behave *in vitro* like an ATP-dependent DNA-binding protein for *S. peucetius* from the daunorubicin cluster (Furuya, Hutchinson, and Richard Hutchinson 1998; Lomovskaya et al. 1996), in *S. nogalater* producer of nogalamycin (Torkkell et al. 2001), *cmr*X to confer resistance to chromomycin in *S. griseus* subsp. *griseus* (Menéndez et al. 2007) and *mtr*X, which is a UvrA-like protein involved in mithramycin resistance in *S. argillaceus* (Garcia-Bernardo et al. 2000).

Interestingly, the most common characteristic of these antitumor antibiotics is that they intercalate to DNA and could represent a DNA-binding protein that plays a role in self-resistance, inhibiting or destabilizing the interaction of these drugs with genomic DNA, thus preventing intercalating antibiotics from interfering with cell transcription and/or replication, suggesting in turn that the function of UvrA class IIa proteins is associated with the removal of non-covalent DNA binding agents.

10. Conclusion

We propose a model (Figure 69) for the self-resistance in *S. olindensis* DAUFPE 5622 during cosmomycin D biosynthesis. This compound is recognized by the ABC transporter CosI/CosJ, and then mycothiol peroxidase (CosP) participates in the protection against H_2O_2 and lipid peroxidation caused by anthracyclines. The UvrA like protein is important for reducing the interaction between DNA and the antibiotic. This mode of resistance represents an advantage for the producer strain to survive during antibiotic biosynthesis; the organism avoids the interaction of the harmful compound COSD with its intracellular target. *Streptomyces* evolution developed different strategies of self-resistance and these depend on the form of action of the active compound. It is important to understand those mechanisms in producer microorganisms to evaluate plausible horizontal transfer in pathogenic strains, and to develop therapeutic alternatives.

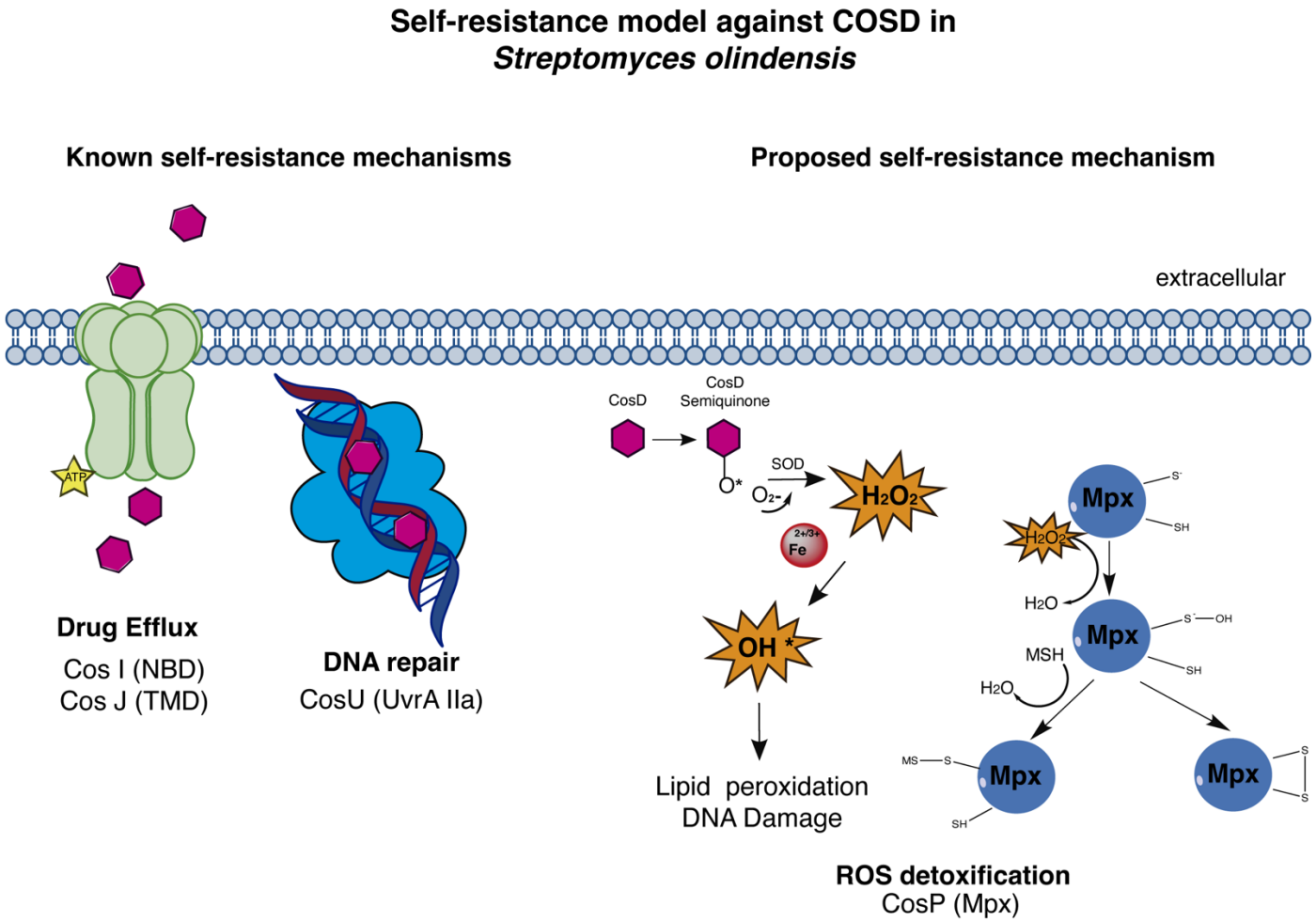

Figure 69. Proposed model for self-resistance to COSD in *Streptomyces olindensis*

Mechanisms of self-resistance for cosmomycin D. Drug efflux function by CosI and CosJ. CosU protein involved in DNA repair scanning COSD-DNA binding complex. CosP (MPx) enzyme proposed as a new self-resistance mechanism for H_2O_2 detoxification

11. References

Adler, Julia, and Eitan Bibi. 2004. "Determinants of Substrate Recognition by the Escherichia Coli Multidrug Transporter MdfA Identified on Both Sides of the Membrane." Journal of Biological Chemistry.

Ahmed, M., L. Lyass, P. N. Markham, S. S. Taylor, N. Vazquez-Laslop, and A. A. Neyfakh. 1995. "Two Highly Similar Multidrug Transporters of Bacillus Subtilis Whose Expression Is Differentially Regulated." Journal of Bacteriology.

Arteaga, Roger David Castillo. 2016. "Characterization of Self-Resistance Mechanisms to the Antitumoral Cosmomycin D." University of São Paulo.

Barnard-Britson, Sandra, Xiuling Chi, Koichi Nonaka, Anatol P. Spork, Nidhi Tibrewal, Anwesha Goswami, Pallab Pahari, Christian Ducho, Jurgen Rohr, and Steven G. Van Lanen. 2012. "Amalgamation of Nucleosides and Amino Acids in Antibiotic Biosynthesis: Discovery of an l-Threonine:Uridine-5'-Aldehyde Transaldolase." Journal of the American Chemical Society 134(45):18514–17.

Benveniste, R., and J. Davies. 1973. "Aminoglycoside Antibiotic-Inactivating Enzymes in Actinomycetes Similar to Those Present in Clinical Isolates of Antibiotic-Resistant Bacteria." Proceedings of the National Academy of Sciences of the United States of America 70:2276–80.

Bouige, Philippe, David Laurent, Linda Piloyan, and Elie Dassa. 2002. "Phylogenetic and Functional Classification of ATP-Binding Cassette (ABC) Systems." Current Protein & Peptide Science 3:541–59.

Carvalho, Helotonio, Leandro M. Garrido, Renata L. A. Furlan, Gabriel Padilla, Mateus Agnoletto, Temenouga Guecheva, João A. P. Henriques, Jenifer Saffi, and Carlos Frederico Martins Menck. 2010. "DNA Damage Induced by the Anthracycline Cosmomycin D in DNA Repair-Deficient Cells." Cancer Chemotherapy and Pharmacology 65:989–94.

Chater, K. F., and L. C. Wilde. 1980. "Streptomyces Albus G Mutants Defective in the SalGI Restriction-Modification System." Journal of General Microbiology.

Cheng, Lin, Wenqing Chen, Lipeng Zhai, Dongmei Xu, Tingting Huang, Shuangjun Lin, Xiufen Zhou, and Zixin Deng. 2011. "Identification of the Gene Cluster Involved in Muraymycin Biosynthesis from Streptomyces Sp. NRRL 30471." Mol. BioSyst. 7(3):920–27.

Cherepanov, Peter P., and Wilfried Wackernagel. 1995. "Gene Disruption in Escherichia Coli: TcR and KmR Cassettes with the Option of Flp-Catalyzed Excision of the Antibiotic-Resistance Determinant." Gene.

Chi, Xiuling, Satoshi Baba, Nidhi Tibrewal, Masanori Funabashi, Koichi Nonaka, and Steven G. Van Lanen. 2013. "The Muraminomicin Biosynthetic Gene Cluster and Enzymatic Formation of the 2-Deoxyaminoribosyl Appendage." Med. Chem. Commun. 4(1):239–43.

Chi, Xiuling, Pallab Pahari, Koichi Nonaka, and Steven G. Van Lanen. 2011. "Biosynthetic Origin and Mechanism of Formation of the Aminoribosyl Moiety of Peptidyl Nucleoside Antibiotics." Journal of the American Chemical Society 133(36):14452–59.

Cui, Zheng, Xiaodong Liu, Jonathan Overbay, Wenlong Cai, Xiachang Wang, Anke Lemke, Daniel Wiegmann, Giuliana Niro, Jon S. Thorson, Christian Ducho, and Steven G. Van

Lanen. 2018. "Enzymatic Synthesis of the Ribosylated Glycyl-Uridine Disaccharide Core of Peptidyl Nucleoside Antibiotics." The Journal of Organic Chemistry 83(13):7239–49.

Cui, Zheng, Jonathan Overbay, Xiachang Wang, Xiaodong Liu, Yinan Zhang, Minakshi Bhardwaj, Anke Lemke, Daniel Wiegmann, Giuliana Niro, Jon S. Thorson, Christian Ducho, and Steven G. Van Lanen. 2020. "Pyridoxal-5'-Phosphate-Dependent Alkyl Transfer in Nucleoside Antibiotic Biosynthesis." Nature Chemical Biology.

Cui, Zheng, Xia Chang Wang, Xiaodong Liu, Anke Lemke, Stefan Koppermann, Christian Ducho, Jürgen Rohr, Jon S. Thorson, and Steven G. Van Lanen. 2018. "Self-Resistance during Muraymycin Biosynthesis: A Complementary Nucleotidyltransferase and Phosphotransferase with Identical Modification Sites and Distinct Temporal Order." Antimicrobial Agents and Chemotherapy.

Cundliffe, Eric, and Arnold L. Demain. 2010. "Avoidance of Suicide in Antibiotic-Producing Microbes." Journal of Industrial Microbiology & Biotechnology 37:643–72.

Datsenko, Kirill A., and Barry L. Wanner. 2000. "One-Step Inactivation of Chromosomal Genes in Escherichia Coli K-12 Using PCR Products." Proceedings of the National Academy of Sciences of the United States of America.

Doroshow, J. H., S. Akman, F. F. Chu, and S. Esworthy. 1990. "Role of the Glutathione-Glutathione Peroxidase Cycle in the Cytotoxicity of the Anticancer Quinones." Pharmacology & Therapeutics 47(3):359–70.

Edgar, Rotem, and Eitan Bibi. 1997. "MdfA, an Escherichia Coli Multidrug Resistance Protein with an Extraordinarily Broad Spectrum of Drug Recognition." Journal of Bacteriology.

Eustáquio, Alessandra S., Bertolt Gust, Ute Galm, Shu Ming Li, Keith F. Chater, and Lutz Heide. 2005. "Heterologous Expression of Novobiocin and Clorobiocin Biosynthetic Gene Clusters." Applied and Environmental Microbiology.

Fernández, E, F. Lombó, C. Méndez, and J. A. Salas. 1996. "An ABC Transporter Is Essential for Resistance to the Antitumor Agent Mithramycin in the Producer Streptomyces Argillaceus." Molecular & General Genetics : MGG 251:692–98.

Fernández, Ernestina, Felipe Lombó, Carmen Méndez, and José A. Salas. 1996. "An ABC Transporter Is Essential for Resistance to the Antitumor Agent Mithramycin in the Producer Streptomyces Argillaceus." Molecular & General Genetics : MGG 251(6):692–98.

Findlay, Victoria J., Haim Tapiero, and Danyelle M. Townsend. 2005. "Sulfiredoxin: A Potential Therapeutic Agent?" Biomedicine & Pharmacotherapy = Biomédecine & Pharmacothérapie 59:374–79.

Flett, Fiona, Vassilios Mersinias, and Colin P. Smith. 1997. "High Efficiency Intergeneric Conjugal Transfer of Plasmid DNA from Escherichia Coli to Methyl DNA-Restricting Streptomycetes." FEMS Microbiology Letters.

Flohe, Leopold. 2011. "F ORUM R EVIEW A RTICLE A Comparison of Thiol Peroxidase Mechanisms." Antioxidants & Redox Signaling 15(3).

Floriano, Belén, and Mervyn Bibb. 1996. "AfsR Is a Pleiotropic but Conditionally Required Regulatory Gene for Antibiotic Production in Streptomyces Coelicolor A3(2)." Molecular Microbiology.

Frelet, Annie, and Markus Klein. 2006. "Insight in Eukaryotic ABC Transporter Function by

Mutation Analysis." FEBS Letters 580:1064–84.

Fronko, R. M., J. C. Lee, J. G. Galazzo, S. Chamberland, F. Malouin, and M. D. Lee. 2000. "New Pacidamycins Produced by Streptomyces Coeruleorubidus, NRRL 18370." The Journal of Antibiotics 53(12):1405–10.

Funabashi, Masanori, Satoshi Baba, Koichi Nonaka, Masahiko Hosobuchi, Yoko Fujita, Tomoyuki Shibata, and Steven G. Van Lanen. 2010. "The Biosynthesis of Liposidomycin-like A-90289 Antibiotics Featuring a New Type of Sulfotransferase." Chembiochem : A European Journal of Chemical Biology 11(2):184–90.

Funabashi, Masanori, Satoshi Baba, Toshio Takatsu, Masaaki Kizuka, Yasuo Ohata, Masahiro Tanaka, Koichi Nonaka, Anatol P. Spork, Christian Ducho, Wei-Chen Leyla Chen, and Steven G. Van Lanen. 2013. "Structure-Based Gene Targeting Discovery of Sphaerimicin, a Bacterial Translocase I Inhibitor." Angewandte Chemie (International Ed. in English) 52(44):11607–11.

Furlan, Renata L. A., Stephen J. Watt, Leandro M. Garrido, Gustavo P. Amarante-Mendes, Mohammad Nur-e-alam, Jurgen Rohr, Alfredo Braña, Carmen Mendez, Jose A. Salas, Margaret M. Sheil, Jennifer L. Beck, and Gabriel Padilla. 2004. "DNA-Binding Properties of Cosmomycin D, an Anthracycline with Two Trisaccharide Chains." The Journal of Antibiotics 57:647–54.

Furuya, K., and C. R. Hutchinson. 1998. "The DrrC Protein of Streptomyces Peucetius, a UvrA-like Protein, Is a DNA-Binding Protein Whose Gene Is Induced by Daunorubicin." FEMS Microbiology Letters 168:243–49.

Furuya, Kaoru, C. R. Hutchinson, and C. Richard Hutchinson. 1998. "The DrrC Protein of Streptomyces Peucetius, a UvrA-like Protein, Is a DNA-Binding Protein Whose Gene Is Induced by Daunorubicin." FEMS Microbiology Letters 168:243–49.

Gandlur, Suvarna M., Ling Wei, Jeoffery Levine, Jack Russell, and Parjit Kaur. 2004. "Membrane Topology of the DrrB Protein of the Doxorubicin Transporter of Streptomyces Peucetius." Journal of Biological Chemistry 279(26):27799–806.

Garcia-Bernardo, Jose, Alfredo F. Braña, Carmen Méndez, and José A. Salas. 2000. "Insertional Inactivation of MtrX and MtrY Genes from the Mithramycin Gene Cluster Affects Production and Growth of the Producer Organism Streptomyces Argillaceus." FEMS Microbiology Letters 186(1):61–65.

Garrido, Leandro M., Felipe Lombó, Irfan Baig, Mohammad Nur-E-Alam, Renata L. A. Furlan, Charlotte C. Borda, Alfredo Braña, Carmen Méndez, José A. Salas, Jürgen Rohr, and Gabriel Padilla. 2006. "Insights in the Glycosylation Steps during Biosynthesis of the Antitumor Anthracycline Cosmomycin: Characterization of Two Glycosyltransferase Genes." Applied Microbiology and Biotechnology 73:122–31.

Gechev, Tsanko S., Frank Van Breusegem, Julie M. Stone, Iliya Denev, and Christophe Laloi. 2006. "Reactive Oxygen Species as Signals That Modulate Plant Stress Responses and Programmed Cell Death." BioEssays : News and Reviews in Molecular, Cellular and Developmental Biology 28:1091–1101.

Guilfoile, P. G., and C. R. Hutchinson. 1991. "A Bacterial Analog of the Mdr Gene of Mammalian Tumor Cells Is Present in Streptomyces Peucetius, the Producer of Daunorubicin and Doxorubicin." Proceedings of the National Academy of Sciences of the United States of America 88(19):8553–57.

Gust, Bertolt, Greg L. Challis, Kay Fowler, Tobias Kieser, and Keith F. Chater. 2003. "PCR-Targeted Streptomyces Gene Replacement Identifies a Protein Domain Needed for Biosynthesis of the Sesquiterpene Soil Odor Geosmin." Proceedings of the National Academy of Sciences of the United States of America 100(4):1541–46.

Gust, Bertolt, Kornelia Eitel, and Xiaoyu Tang. 2013. "The Biosynthesis of Caprazamycins and Related Liponucleoside Antibiotics: New Insights." Biological Chemistry 394(2):251–59.

Hanekop, N., J. Zaitseva, S. Jenewein, I. B. Holland, and L. Schmitt. 2006. "Molecular Insights into the Mechanism of ATP-Hydrolysis by the NBD of the ABC-Transporter HlyB." FEBS Letters 580:1036–41.

Henderson, C. A., E. N. Metz, S. P. Balcerzak, and A. L. Sagone. 1978. "Adriamycin and Daunomycin Generate Reactive Oxygen Compounds in Erythrocytes." Blood 52(5):878–85.

Herbette, Stéphane, Patricia Roeckel-Drevet, and Joël R. Drevet. 2007. "Seleno-Independent Glutathione Peroxidases: More than Simple Antioxidant Scavengers." FEBS Journal 274:2163–80.

Higgins, C. F. 2001. "ABC Transporters: Physiology, Structure and Mechanism--an Overview." Research in Microbiology 152(3–4):205–10.

Hirano, Shinpei, Satoshi Ichikawa, and Akira Matsuda. 2007. "Total Synthesis of (+)-FR-900493 and Establishment of Its Absolute Stereochemistry." Tetrahedron 63(13):2798–2804.

Holland, I. Barry. 2011. "ABC Transporters, Mechanisms and Biology: An Overview." Essays in Biochemistry 50:1–17.

Hong, Waun Ki., and William N. Hait. 2010. "Holland Frei Cancer Medicine Eight, Volume 8." Books.Google.Com.

Hopwood, David A. 2004. "Cracking the Polyketide Code." PLoS Biology 2(2):E35.

Hopwood, David A. 2007. "How Do Antibiotic-Producing Bacteria Ensure Their Self-Resistance before Antibiotic Biosynthesis Incapacitates Them?" Molecular Microbiology 63:937–40.

Jaciuk, Marcin, Elżbieta Nowak, Krzysztof Skowronek, Anna Tańska, and Marcin Nowotny. 2011. "Structure of UvrA Nucleotide Excision Repair Protein in Complex with Modified DNA." Nature Structural & Molecular Biology 18(2):191–97.

Jez, J. M., M. E. Bowman, and J. P. Noel. 2001. "Structure-Guided Programming of Polyketide Chain-Length Determination in Chalcone Synthase." Biochemistry.

Jiang, Xinglin, Mostafa M. Hashi. Ellabaan, Pep Charusanti, Christian Munck, Kai Blin, Yaojun Tong, Tilmann Weber, Morten O. A. Sommer, and Sang Yup Lee. 2017. "Dissemination of Antibiotic Resistance Genes from Antibiotic Producers to Pathogens." Nature Communications.

Kapp, Ulrike, Sofia Macedo, David Richard Hall, Ingar Leiros, Sean M. McSweeney, and Edward Mitchell. 2008. "Structure of Deinococcus Radiodurans Tunicamycin-Resistance Protein (TmrD), a Phosphotransferase." Acta Crystallographica. Section F, Structural Biology and Crystallization Communications 64(Pt 6):479–86.

Kaur, P. 1997. "Expression and Characterization of DrrA and DrrB Proteins of Streptomyces

Peucetius in Escherichia Coli : DrrA Is an ATP Binding Expression and Characterization of DrrA and DrrB Proteins of Streptomyces Peucetius in Escherichia Coli : DrrA Is an ATP Bindi."

Kaur, P., and J. Russell. 1998. "Biochemical Coupling between the DrrA and DrrB Proteins of the Doxorubicin Efflux Pump of Streptomyces Peucetius." Journal of Biological Chemistry 273(28):17933–39.

Kaysser, Leonard, Liane Lutsch, Stefanie Siebenberg, Emmanuel Wemakor, Bernd Kammerer, and Bertolt Gust. 2009. "Identification and Manipulation of the Caprazamycin Gene Cluster Lead to New Simplified Liponucleoside Antibiotics and Give Insights into the Biosynthetic Pathway." Journal of Biological Chemistry 284(22):14987–96.

Kaysser, Leonard, Stefanie Siebenberg, Bernd Kammerer, and Bertolt Gust. 2010. "Analysis of the Liposidomycin Gene Cluster Leads to the Identification of New Caprazamycin Derivatives." Chembiochem : A European Journal of Chemical Biology 11(2):191–96.

Kaysser, Leonard, Xiaoyu Tang, Emmanuel Wemakor, Katharina Sedding, Susanne Hennig, Stefanie Siebenberg, and Bertolt Gust. 2011. "Identification of a Napsamycin Biosynthesis Gene Cluster by Genome Mining." ChemBioChem 12(3):477–87.

Kaysser, Leonard, Emmanuel Wemakor, Stefanie Siebenberg, Jose A. Salas, Jae Kyung Sohng, Bernd Kammerer, and Bertolt Gust. 2010. "Formation and Attachment of the Deoxysugar Moiety and Assembly of the Gene Cluster for Caprazamycin Biosynthesis." Applied and Environmental Microbiology 76(12):4008–18.

Kelso, Celine, Juan Diego Rojas, Renata L. A. Furlan, Gabriel Padilla, and Jennifer L. Beck. 2009. "Characterisation of Anthracyclines from a Cosmomycin D-Producing Species of Streptomyces by Collisionally-Activated Dissociation and Ion Mobility Mass Spectrometry." European Journal of Mass Spectrometry (Chichester, England) 15(2):73—81.

Kleinkauf, H., and H. Von Döhren. 1996. "A Nonribosomal System of Peptide Biosynthesis." European Journal of Biochemistry / FEBS 236:335–51.

Kümmerer, K. 2004. "Resistance in the Environment." The Journal of Antimicrobial Chemotherapy 54:311–20.

Lewis, K. 2008. "Multidrug Tolerance of Biofilms and Persister Cells." Current Topics in Microbiology and Immunology 322:107–31.

Li, Qinglian, Lifei Wang, Yunying Xie, Songmei Wang, Ruxian Chen, and Bin Hong. 2013. "SsaA, a Member of a Novel Class of Transcriptional Regulators, Controls Sansanmycin Production in Streptomyces Sp. Strain SS through a Feedback Mechanism." Journal of Bacteriology.

Li, Wen, Madhu Sharma, and Parjit Kaur. 2014. "The DrrAB Efflux System of Streptomyces Peucetius Is a Multidrug Transporter of Broad Substrate Specificity." Journal of Biological Chemistry.

Lima, O. G., F. D. A. Lyra, M. M. F. Albuquerque, G. M. Maciel, and J. S. B. Coelho. 1969. "Primeiras Observações Sobre o Complexo Antibiótico e Antitumoral Retamicina Produzido Pelo Streptomyces Olindensis Nov. Sp. IAUFPe." Revista Do Instituto de Antibióticos 9(1–2):27–37.

Locher, Kaspar P. 2016. "Mechanistic Diversity in ATP-Binding Cassette (ABC) Transporters."

Nature Structural and Molecular Biology.

Lomovskaya, N., S. K. Hong, S. U. Kim, L. Fonstein, K. Furuya, and R. C. Hutchinson. 1996. "The Streptomyces Peucetius DrrC Gene Encodes a UvrA-like Protein Involved in Daunorubicin Resistance and Production." Journal of Bacteriology 178:3238–45.

MacNeil, D. J., K. M. Gewain, C. L. Ruby, G. Dezeny, P. H. Gibbons, and T. MacNeil. 1992. "Analysis of Streptomyces Avermitilis Genes Required for Avermectin Biosynthesis Utilizing a Novel Integration Vector." Gene 111(1):61–68.

Malla, Sailesh, Narayan Prasad Niraula, Kwangkyoung Liou, and Jae Kyung Sohng. 2010. "Self-Resistance Mechanism in Streptomyces Peucetius: Overexpression of DrrA, DrrB and DrrC for Doxorubicin Enhancement." Microbiological Research 165(4):259–67.

Marszałkowska, Marta, Magdalena Bil, Łukasz Kreft, and Marcin Olszewski. 2013. "A New Division of Bacterial UvrA Homologues." Biotechnologia 94(1):54–56.

McErlean, M., X. Liu, Z. Cui, B. Gust, and S. G. Van Lanen. 2021. "Identification and Characterization of Enzymes Involved in the Biosynthesis of Pyrimidine Nucleoside Antibiotics." Natural Product Reports 38(7):1362–1407.

Méndez, C., and J. A. Salas. 1998. "ABC Transporters in Antibiotic-Producing Actinomycetes." FEMS Microbiology Letters 158:1–8.

Méndez, C., and J. a Salas. 2001. "The Role of ABC Transporters in Antibiotic-Producing Organisms: Drug Secretion and Resistance Mechanisms." Research in Microbiology 152(3–4):341–50.

Menéndez, Nuria, Alfredo F. Braña, José A. Salas, and Carmen Méndez. 2007. "Involvement of a Chromomycin ABC Transporter System in Secretion of a Deacetylated Precursor during Chromomycin Biosynthesis." Microbiology 153(9):3061–70.

Mitachi, Katsuhiko, Hyun Gi Yun, Sara M. Kurosu, Shakiba Eslamimehr, Maddie R. Lemieux, Lada Klaić, William M. Jr Clemons, and Michio Kurosu. 2018. "Novel FR-900493 Analogues That Inhibit the Outgrowth of Clostridium Difficile Spores." ACS Omega 3(2):1726–39.

Miyamoto, Yuji, Osamu Johdo, Yasunori Nagamatsu, and Akihiro Yoshimoto. 2002. "Cloning and Characterization of a Glycosyltransferase Gene Involved in the Biosynthesis of Anthracycline Antibiotic β-Rhodomycin from Streptomyces Violaceus." FEMS Microbiology Letters 206(2):163–68.

Mousa, Jarrod J., and Steven D. Bruner. 2016. "Structural and Mechanistic Diversity of Multidrug Transporters." Natural Product Reports 33(11):1255–67.

Noda, Y., A. Takatsuki, K. Yoda, and M. Yamasaki. 1995. "TmrB Protein, Which Confers Resistance to Tunicamycin on Bacillus Subtilis, Binds Tunicamycin." Bioscience, Biotechnology, and Biochemistry 59(2):321–22.

Noda, Y., K. Yoda, A. Takatsuki, and M. Yamasaki. 1992. "TmrB Protein, Responsible for Tunicamycin Resistance of Bacillus Subtilis, Is a Novel ATP-Binding Membrane Protein." Journal of Bacteriology 174(13):4302–7.

Nomura, S., K. Yamane, T. Sasaki, M. Yamasaki, G. Tamura, and B. Maruo. 1978. "Tunicamycin-Resistant Mutants and Chromosomal Locations of Mutational Sites in Bacillus Subtilis." Journal of Bacteriology 136(2):818–21.

Ochi, K. Ezaki, M. Iwami, M. Komori, T. Kohsaka, M. 1989. "4950605 Fr-900493 Substance, a Process for Its Production and a Pharmaceutical Composition Containing the Same." General Pharmacology: The Vascular System 22(2):iii.

Paget, Mark S. B., Leony Chamberlin, Abdelmadjid Atrih, Simon J. Foster, and Mark J. Buttner. 1999. "Evidence That the Extracytoplasmic Function Sigma Factor σ(E) Is Required for Normal Cell Wall Structure in Streptomyces Coelicolor A3(2)." Journal of Bacteriology.

Pedre, Brand??n, Inge Van Molle, Almudena F. Villadangos, Khadija Wahni, Didier Vertommen, Luc??a Turell, Huriye Erdogan, Luis M. Mateos, and Joris Messens. 2015. "The Corynebacterium Glutamicum Mycothiol Peroxidase Is a Reactive Oxygen Species-Scavenging Enzyme That Shows Promiscuity in Thiol Redox Control." Molecular Microbiology 96(6):1176–91.

Pedre, Brandán, David Young, Daniel Charlier, Álvaro Mourenza, Leonardo Astolfi Rosado, Laura Marcos-Pascual, Khadija Wahni, Edo Martens, Alfonso G de la Rubia, Vsevolod V Belousov, Luis M. Mateos, and Joris Messens. 2018. "Structural Snapshots of OxyR Reveal the Peroxidatic Mechanism of H(2)O(2) Sensing." Proceedings of the National Academy of Sciences of the United States of America 115(50):E11623–32.

Poelarends, Gerrit J., Piotr Mazurkiewicz, and Wil N. Konings. 2002. "Multidrug Transporters and Antibiotic Resistance in Lactococcus Lactis." Biochimica et Biophysica Acta - Bioenergetics.

Pope, Cassie F., Denise M. O'Sullivan, Timothy D. McHugh, and Stephen H. Gillespie. 2008. "A Practical Guide to Measuring Mutation Rates in Antibiotic Resistance." Antimicrobial Agents and Chemotherapy 52:1209–14.

Powis, G. 1989. "Free Radical Formation by Antitumor Quinones." Free Radical Biology & Medicine 6(1):63–101.

Prija, Francis, and Ranjan Prasad. 2017. "DrrC Protein of Streptomyces Peucetius Removes Daunorubicin from Intercalated DnrI Promoter." Microbiological Research.

Putman, M., H. W. van Veen, and W. N. Konings. 2000. "Molecular Properties of Bacterial Multidrug Transporters." Microbiology and Molecular Biology Reviews.

Rackham, Emma J., Sabine Grüschow, Amany E. Ragab, Shilo Dickens, and Rebecca J. M. Goss. 2010. "Pacidamycin Biosynthesis: Identification and Heterologous Expression of the First Uridyl Peptide Antibiotic Gene Cluster." ChemBioChem.

Ruggiero, A., V. Ridola, N. Puma, F. Molinari, P. Coccia, G. De Rosa, and R. Riccardi. 2008. "Anthracycline Cardiotoxicity in Childhood." Pediatric Hematology and Oncology 25:261–81.

Ruiz, Beatriz, Adán Chávez, Angela Forero, Yolanda García-Huante, Alba Romero, Mauricio Snchez, Diana Rocha, Brenda Snchez, Romina Rodríguez-Sanoja, Sergio Sánchez, and Elizabeth Langley. 2010. "Production of Microbial Secondary Metabolites: Regulation by the Carbon Source." Critical Reviews in Microbiology 36(2):146–67.

Sambrook, J., E. F. Fritsch, and T. Maniatis. 1989. Molecular Cloning: A Laboratory Manual. Cold Spring Harbor Laboratory Press. Cold Spring Harbor.

Serpi, Michaela, Valentina Ferrari, and Fabrizio Pertusati. 2016. "Nucleoside Derived Antibiotics to Fight Microbial Drug Resistance: New Utilities for an Established Class of

Drugs?" Journal of Medicinal Chemistry.

Sharom, Frances J. 2008. "ABC Multidrug Transporters: Structure, Function and Role in Chemoresistance." Pharmacogenomics 9(1):105–27.

Shi, Yuanyuan, Zhibo Jiang, Xuan Lei, Ningning Zhang, Qiang Cai, Qinglian Li, Lifei Wang, Shuyi Si, Yunying Xie, and Bin Hong. 2016. "Improving the N-Terminal Diversity of Sansanmycin through Mutasynthesis." Microbial Cell Factories.

Shiraishi, Taro, Noboru Hiro, Masayuki Igarashi, Makoto Nishiyama, and Tomohisa Kuzuyama. 2016. "Biosynthesis of the Antituberculous Agent Caprazamycin: Identification of Caprazol-3"-Phosphate, an Unprecedented Caprazamycin-Related Metabolite." The Journal of General and Applied Microbiology 62(3):164–66.

Si, Meiru, Yixiang Xu, Tietao Wang, Mingxiu Long, Wei Ding, Can Chen, Xinmeng Guan, Yingbao Liu, Yao Wang, Xihui Shen, and Shuang-Jiang Jiang Liu. 2015. "Functional Characterization of a Mycothiol Peroxidase in Corynebacterium Glutamicum That Uses Both Mycoredoxin and Thioredoxin Reducing Systems in the Response to Oxidative Stress." The Biochemical Journal 45–57.

Šmídová, Klára, Alice Ziková, Jirí Pospíšil, Marek Schwarz, Jan Bobek, and Jiri Vohradsky. 2019. "DNA Mapping and Kinetic Modeling of the HrdB Regulon in Streptomyces Coelicolor." Nucleic Acids Research 47(2):621–33.

Solecka, Jolanta, Joanna Zajko, Magdalena Postek, and Aleksandra Rajnisz. 2012. "Biologically Active Secondary Metabolites from Actinomycetes." Central European Journal of Biology.

Srinivasan, Padmanabhan, Sankara Naynar Palani, and Ranjan Prasad. 2010. "Daunorubicin Efflux in Streptomyces Peucetius Modulates Biosynthesis by Feedback Regulation." FEMS Microbiology Letters 305(1):18–27.

Takatsuki, Akira, Kei Arima, and Gazuko Tamura. 1971. "Tunicamycin, a New Antibiotic: 1. Isolation and Characterization of Tunicamycin." The Journal of Antibiotics 24(4):215–23.

Tamura, Koichiro, Glen Stecher, and Sudhir Kumar. 2021. "MEGA11: Molecular Evolutionary Genetics Analysis Version 11." Molecular Biology and Evolution 38(7):3022–27.

Tang, Xiaoyu, Kornelia Eitel, Leonard Kaysser, Andreas Kulik, Stephanie Grond, and Bertolt Gust. 2013. "A Two-Step Sulfation in Antibiotic Biosynthesis Requires a Type III Polyketide Synthase." Nature Chemical Biology 9(10):610–15.

Tenconi, Elodie, and Sébastien Rigali. 2018. "Self-Resistance Mechanisms to DNA-Damaging Antitumor Antibiotics in Actinobacteria." Current Opinion in Microbiology.

Tennent, J. M., B. R. Lyon, M. Midgley, I. G. Jones, A. S. Purewal, and R. A. Skurray. 1989. "Physical and Biochemical Characterization of the QacA Gene Encoding Antiseptic and Disinfectant Resistance in Staphylococcus Aureus." Journal of General Microbiology.

Torkkell, S., T. Kunnari, K. Palmu, P. Mäntsälä, J. Hakala, and K. Ylihonko. 2001. "The Entire Nogalamycin Biosynthetic Gene Cluster of Streptomyces Nogalater: Characterization of a 20-Kb DNA Region and Generation of Hybrid Structures." Molecular Genetics and Genomics 266:276–88.

Truglio, James J., Deborah L. Croteau, Bennett van Houten, and Caroline Kisker. 2006. "Prokaryotic Nucleotide Excision Repair: The UvrABC System." Chemical Reviews 106(2):233–52.

Wang, Jun, Stephen M. Soisson, Katherine Young, Wesley Shoop, Srinivas Kodali, Andrew Galgoci, Ronald Painter, Gopalakrishnan Parthasarathy, Yui S. Tang, Richard Cummings, Sookhee Ha, Karen Dorso, Mary Motyl, Hiranthi Jayasuriya, John Ondeyka, Kithsiri Herath, Chaowei Zhang, Lorraine Hernandez, John Allocco, Angela Basilio, José R. Tormo, Olga Genilloud, Francisca Vicente, Fernando Pelaez, Lawrence Colwell, Sang Ho Lee, Bruce Michael, Thomas Felcetto, Charles Gill, Lynn L. Silver, Jeffery D. Hermes, Ken Bartizal, John Barrett, Dennis Schmatz, Joseph W. Becker, Doris Cully, and Sheo B. Singh. 2006. "Platensimycin Is a Selective FabF Inhibitor with Potent Antibiotic Properties." Nature 441(7091):358–61.

Westman, Erin L., Marc J. Canova, Inas J. Radhi, Kalinka Koteva, Inga Kireeva, Nicholas Waglechner, and Gerard D. Wright. 2012. "Bacterial Inactivation of the Anticancer Drug Doxorubicin." Chemistry and Biology 19(10):1255–64.

Wiker, Franziska, Nils Hauck, Stephanie Grond, and Bertolt Gust. 2019. "International Journal of Medical Microbiology Caprazamycins : Biosynthesis and Structure Activity Relationship Studies." International Journal of Medical Microbiology 309(5):319–24.

Wiker, Franziska, Martin Konnerth, Irina Helmle, Andreas Kulik, Leonard Kaysser, Harald Gross, and Bertolt Gust. 2019. "Identification of Novel α-Pyrones from Conexibacter Woesei Serving as Sulfate Shuttles." ACS Chemical Biology 14(9):1972–80.

Wilkens, Stephan. 2015. "Structure and Mechanism of ABC Transporters." F1000Prime Reports.

Wilkins, M. R., E. Gasteiger, A. Bairoch, J. C. Sanchez, K. L. Williams, R. D. Appel, and D. F. Hochstrasser. 1999. "Protein Identification and Analysis Tools in the ExPASy Server." Methods in Molecular Biology (Clifton, N.J.) 112:531–52.

Yamamoto, Kazuki, and Satoshi Ichikawa. 2019. "Tunicamycin: Chemical Synthesis and Biosynthesis." The Journal of Antibiotics 72(12):924–33.

Yang, Zhaoyong, Xiuling Chi, Masanori Funabashi, Satoshi Baba, Koichi Nonaka, Pallab Pahari, Jason Unrine, Jesse M. Jacobsen, Gregory I. Elliott, Jürgen Rohr, and Steven G. Van Lanen. 2011. "Characterization of LipL as a Non-Heme, Fe(II)-Dependent α-Ketoglutarate:UMP Dioxygenase That Generates Uridine-5'-Aldehyde during A-90289 Biosynthesis." The Journal of Biological Chemistry 286(10):7885–92.

Yang, Zhaoyong, Masanori Funabashi, Koichi Nonaka, Masahiko Hosobuchi, Tomoyuki Shibata, Pallab Pahari, and Steven G. Van Lanen. 2010. "Functional and Kinetic Analysis of the Phosphotransferase Capp Conferring Selective Self-Resistance to Capuramycin Antibiotics." Journal of Biological Chemistry 285(17):12899–905.

Zaburannyi, Nestor, Mariia Rabyk, Bohdan Ostash, Victor Fedorenko, and Andriy Luzhetskyy. 2014. "Insights into Naturally Minimised Streptomyces Albus J1074 Genome." BMC Genomics.

Zallot, Rémi, Nils Oberg, and John A. Gerlt. 2019. "The EFI Web Resource for Genomic Enzymology Tools: Leveraging Protein, Genome, and Metagenome Databases to Discover Novel Enzymes and Metabolic Pathways." Biochemistry 58(41):4169–82.

Zhang, Han, Sadia Rahman, Wen Li, Guoxing Fu, and Parjit Kaur. 2015. "Characterization of a Novel Domain 'GATE' in the ABC Protein DrrA and Its Role in Drug Efflux by the DrrAB Complex." Biochemical and Biophysical Research Communications 459(1):148–53.

Zhang, Wenjun, Ioanna Ntai, Megan L. Bolla, Steven J. Malcolmson, Daniel Kahne, Neil L.

Kelleher, and Christopher T. Walsh. 2011. “Nine Enzymes Are Required for Assembly of the Pacidamycin Group of Peptidyl Nucleoside Antibiotics.” Journal of the American Chemical Society.

Zhang, Wenjun, Bohdan Ostash, and Christopher T. Walsh. 2010. “Identification of the Biosynthetic Gene Cluster for the Pacidamycin Group of Peptidyl Nucleoside Antibiotics.” Proceedings of the National Academy of Sciences of the United States of America.

List of figures

Figure 1. Schematic of the structural organization of the components forming an ABC-type transport in bacteria. 15
Figure 2. Structure of TMD pore. 16
Figure 3. Architecture of ABC transporters 17
Figure 4. Distinct mechanisms of B-family ABC exporters 18
Figure 5. Structure and organization of the different types of ABC transporters in antibiotic-producing actinomycetes: 19
Figure 6. Structures of known uridylpeptide antibiotics 21
Figure 7. a) Structures of streptovirudins 2a−j. b) Structures of corynetoxins 3a−n 22
Figure 8. Structures of liponucleoside antibiotics 22
Figure 9. Structured of capuramycin analogues 36a−h, 37a−g, and 39. Muraymycins 42a-43b. 23
Figure 10. Organization of the liposidomycin and the caprazamycin gene cluster 24
Figure 11. Biosynthetic gene clusters and proposed biosynthesis of liponucleoside antibiotics 25
Figure 12. Structures of tunicamycins 26
Figure 13. (A) Structure of 3-phospho-muraymycin D2 catalyzed by *mur*28. (B) Structure of 3-monoadenylated muramycin D1 catalyzed by *mur*29. 27
Figure 14. Working steps to prepare the constructs on pUWL expression vector. 57
Figure 15. Working steps to prepare the constructs on pHIS8 protein expression vector. 58
Figure 16. Overview of the site-directed mutagenesis method 59
Figure 17. Working steps to construct single and double knock outs. 61
Figure 18. Predicted functions of CPZ cluster obtained from antiSMASH 71
Figure 19. *Phylogenetic analysis of the tmrB-like genes*. 72
Figure 20. Structure protein model of Cpz12. 73
Figure 21. A. Phylogenetic analysis of *cpz12*. 74
Figure 22. Structure protein model of the Cpz27. 74
Figure 23. A. Phylogenetic analysis of *cpz*27. 76
Figure 24. a) Amino acid sequence map analysis of the cpz22 gene B) reference distance between the Walker A and B. 77
Figure 25. Prediction (b) and topology (a) of the transmembrane helices and amino acids that cross the membrane. 78
Figure 26. Structure protein model of the Cpz 22. 79
Figure 27. A. Phylogenetic analysis of *cpz*22. 81
Figure 28. *Exconjugants of S. coelicolor M512 harboring the cosmid with knock-out of the genes cpz12, cpz22, cpz23,* cpz23/cpz4 and *cpz27, cpz12/cpz27* (no exconjugants). 82
Figure 29. LC-MS analysis *Δcpz12* 85
Figure 30. HPLC profile of strain cpzLK09 vs. pCRD1 + pUWL*cpz12* strain. 86
Figure 31. ESI-MS/MS (MS^2) of CPZAE found in the strain pCRD1 strain. 86
Figure 32. ESI-MS/MS (MS^2) of (+)-caprazol and its 3' phosphorylated derivative found in *S. celicolor* M512/pCRD4. 89
Figure 33. (A-B): low resolution- LC-MS analysis of *S. coelicolor* M512 cpzLK09 Δ*cpz23/4* 90
Figure 34. ^{31}P NMR spectrum of phosphorylated (+)-caprazol in D_2O (283 MHz) 91
Figure 35. FPLC Chromatogram of the lipase Cpz23 and SDS-PAGE 12% polyacrylamide of the purified protein 92
Figure 36. Cpz23 enzyme reaction using (+)-caprazol and β-hydroxy-myristoyl-CoA as substrates to produce hydroxyacylcaprazol E 92
Figure 37. Figure HR-MS analysis of the Cpz23 reaction product 93

Figure 38. Protein overexpression of Cpz12 and Cpz27 95
Figure 39. Cpz27 enzyme reaction using compound 7 $C_{19}H_{31}N_5O_{11}$ producing $C_{19}H_{31}N_5O_{11}P$ 96
Figure 40. HR-MS/MS of $C_{19}H_{31}N_5O_{11}P$ 96
Figure 41. Quantification of caprazamycin-aglycons in *S. coelicolor*/cpzLK09 (containing the entire BGC) vs. *S. coelicolor*/pRCWL02 (containing *Δcpz22*) 97
Figure 42. LC-MS Extracted ion chromatogram of *S. coelicolor* M512/cpzLK09 vs. *S. coelicolor* M512/pCRD2 (Δ*cpz*22) 98
Figure 43. Minimum inhibitory concentration (MIC) of *Streptomyces* strains expressed in (μg/mL) against hydroxyacylcaprazol E, caprazamycin aglycon E, FR-900493, (+)-caprazol, and 3'phosphoylated-(+)-caprazol 101
Figure 44. HACs produced by *S. coelicolor* M512/cpzLL06 103
Figure 45. CPZs analytic profiles of the producer *S. coelicolor* M512/cpzLK09 105
Figure 46. Proposed Caprazamycin biosynthesis 109
Figure 47. Structures of the clinically used anthracyclines 113
Figure 48. Chemical structures of a) (DOX) and b) (DNR) produced by *S. peucetius and* c) (COSD) by *S. olindensis* 115
Figure 49. Diversity self-resistance mechanisms developed by DNA-damaging antibiotics producing Actinobacteria 116
Figure 50. Mechanisms of resistance in *S. peucetius* 117
Figure 51. Proteins involved in the resistance mechanisms associated with aureolic acids. 118
Figure 52. Distribution and probability of transmembrane helices encoded by *cosJ* 119
Figure 53. Phylogenetic analysis of the *cosI* gene 125
Figure 54. Phylogenetic analysis of the *cosP* gene. 128
Figure 55. Seed SSN of KDN80073.3 129
Figure 56. First GPx PFAM Family PF00255 SSN 131
Figure 57. Second GPx PFAM Family PF00255 SSN 132
Figure 58. Genome Neighborhood Diagram of cluster 99 (2nd PF00255 SSN) 133
Figure 59. Phylogenetic analysis of the *cosU* gene 135
Figure 60. A) HPLC profile of COS D and DOX vs. structure DOX and COSD. B) ESI-MS/MS (MS^2) of COS D 137
Figure 61. ESI-MS/MS (MS^2) of cosmomycin D (top) 137
Figure 62. Minimum inhibitory concentrations (MIC) to COSD and DOX for selected *Streptomyces* species by 96-well plate assay 139
Figure 63. RT- qPCR (Melt Curve and PCR Amp/Cycle) of *cos*I, *cos*J, *cos*P, *cos*U and *Hrdb* during the production and non-production of COSD in *S. olindensis* strain 140
Figure 64. qPCR of *cosI*, *cosJ*, *cosP* and *cosU*, *hrdb* as reference during the production (72 h) and non-production (24 h) of COSD by *S. olindensis*. 141
Figure 65. A. FPLC Chromatogram of the Mpx and its mutant Mpx C38S in *E. coli* Rossetta (DE3) as a host B. SDS-PAGE of purified MPx and MPx C38S mutant obtained by FPLC and Ni-NTA 142
Figure 66. H_2O_2 and tBOOH quantification (FOX assay) of MPx WT and MPx (C38S) during 180 s activity 143
Figure 67. Minimum inhibitory concentrations (MIC) of selected *Streptomyces* species against H_2O_2 in an 96-well plate assay. 144
Figure 68. H_2O_2 quantification (FOX assay) of *S. olindensis* WT vs. *S. lividans* Tk24 during 600 s activity 144
Figure 69. Proposed model for self-resistance to COSD in *Streptomyces olindensis* 149

List of tables

Table 1. Features of antibiotic ABC transporters from producing actinomycetes 19
Table 2. Columns for analytical chromatography 30
Table 3. Primers designed in this study 30
Table 4. Reagents 33
Table 5. Enzymes and kits 34
Table 6. Plasmids used in this study 35
Table 7. Cosmids used in this study 37
Table 8. *E. coli* strains used in this study 38
Table 9. *Streptomyces* strains used in this study 39
Table 10. Antibiotics stocks solutions 44
Table 11. Buffers and solutions for plasmid isolation 45
Table 12. Buffers and solutions for DNA gel electrophoresis 45
Table 13. Buffers for protein purification by nickel affinity chromatography 46
Table 14. Buffers and solutions for protein gel electrophoresis (SDS-page) 46
Table 15. Solutions for protein gel electrophoresis 47
Table 16. Fatty acid activation solutions 47
Table 17. Cpz23 enzymatic assay buffers 47
Table 18. Standard PCR reaction and amplification conditions using the *Taq* or *Pfu*-polymerase system. 51
Table 19. Standard PCR reaction and amplification conditions using the Phusion® High-Fidelity system. 51
Table 20. Standard colony PCR reaction and amplification conditions using the *Taq* or *Pfu*-polymerase system. 52
Table 21. PCR conditions for amplification of resistance cassettes for targeting recombineering 53
Table 22. Prediction of the function of resistance genes 71
Table 23. Minimum inhibitory concentration (MIC) in [µg/mL] of *S. coelicolor M512* containing putative caprazamycin resistance determinants against hydroxyacylcaprazol E (HACE), caprazamycin- aglycon E (CPZAE), FR-900493, (+)-caprazol, and phosphorylated (+)-caprazol. 100
Table 24. Cluster 2 of KDN80073,1 seed SSN 130
Table 25. With tandem MS/MS, pure cosmomycin D 138
Table 26. Minimum inhibitory concentration (MIC) of *Streptomyces* strains expressed in (µg/mL) against doxorubicin and cosmomycin D 139
Table 27. Minimum inhibitory concentration (MIC) of *Streptomyces* strains expressed (in mM) against H_2O_2. 143

Appendix

Appendix 1. Phyre 2 analysis of Cpz12 protein sequence 166
Appendix 2. Phyre 2 analysis of Cpz 27 protein sequence 166
Appendix 3. Phyre 2 analysis of Cpz 22 protein sequence 168
Appendix 4. Scar verification of Knock outs 168
Appendix 5. Phyre 2 analysis of Cos IJ protein sequence 169
Appendix 6. Phyre 2 analysis of Cos P protein sequence.....170
Appendix 7. Phyre 2 analysis of Cos U protein sequence.....171
Appendix 8. NMR of 3'phospho-(+)-caprazol 172

Acknowledgements

First, I would like to express my sincere gratitude to my advisor PD. Dr. Bertolt Gust to give me the opportunity to become part of his wonderful team, for the kindly advise, patience, and professionalism during my formation. I learned a lot all the time!

I would like to thank Prof. Dr. Harald Groß for acting as my second supervisor, giving me a space in his group, and for his advice during the analytical part of my work. I feel also part of his team!

I would like to thank Prof. Dr. Leonard Kaysser for acting as a referee and always having time to advise me during his time in Tübingen. As well, many thanks to PD. Dr. Evi Stegmann for acting as an examiner and for valuable suggestions for the work.

Specially thanks to my colleagues on the 6th and 9th floor: Patrick, Richard, Hanna, Daniel, Alicia, Cathrin, Felix, Franzi, Kerstin, Marius, Simon, Tobias, Tomke, Patricia, Irina, Nils, Nhomsai, Sarah, Gesa, Keshab, Hamada, Thomas, Tarik, Julia, Johanna, Emmanuel, Cedric and all not mentioned. I would like to highlight the enjoyable work atmosphere, teamwork, kindness, fun activities. Thanks for having a place without borders.

I am especially grateful for the excellent management, organization, and care of our supplies and documents by Emmanuel Wemakor, Lucia Westrich, Corinna Fischer, Manuela Haußmann and Wolfgang Kornberger.

I wish to thank Prof. Dr. Gabriel Padilla (USP), Dr. Leandro Garrido (USP) and Dr. Brandán Pedré (DKFZ) for the nice collaboration during the cosmomycin project.

I would like to thank Dr. Dorothee Wistuba and Mr. Andreas Kulik for the mass spectrometry analysis.

I would like to thank DAAD for the scholarship and support during my studies, and the GIZ, where I had the opportunity to volunteer in science projects in Colombia, especially during the pandemic.

Thanks to my friends in Colombia, Brazil and Germany: Cami, Diego, Eddie, Leo, Andre, Eli, Martin, Hency, Karen, Alejo, Sebas, Aaron, Maria, Lau, Manu, Yiyi, Yuli and all not mentioned for becoming a small family during my time in Tübingen.

Finally, I would like to thank my parents, my sister, and all my family for their support and for being proud that I am pursuing my scientific career.

Dedicated to my parents, Adalberto, Aura and my sister Anabel!

¡Mi gratitud es tan absoluta que las palabras sobran!

„Gewagte Ideen sind wie das Ziehen von Schachfiguren. Sie können geschlagen werden, aber sie können eine Siegespartie eröffnen.“

Johann Wolfgang von Goethe

Appendix

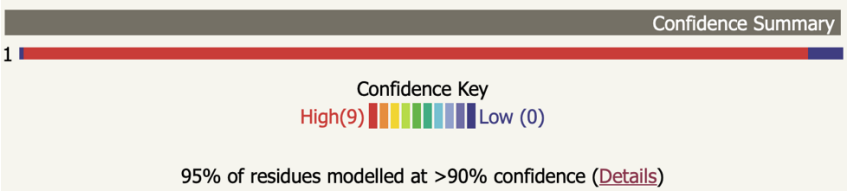

#	Template	Alignment Coverage	3D Model	Confidence	% i.d.	Template Information
1	c2vliB_	Alignment		96.5	23	**PDB header:**transferase **Chain:** B: **PDB Molecule:**antibiotic resistance protein; **PDBTitle:** structure of deinococcus radiodurans tunicamycin resistance protein
2	c4xrpA_	Alignment		81.6	16	**PDB header:**protein binding **Chain:** A: **PDB Molecule:**pnkp1; **PDBTitle:** structure of the pnkp1/rnl/hen1 rna repair complex

Appendix 1. Phyre 2 analysis of Cpz12 protein sequence

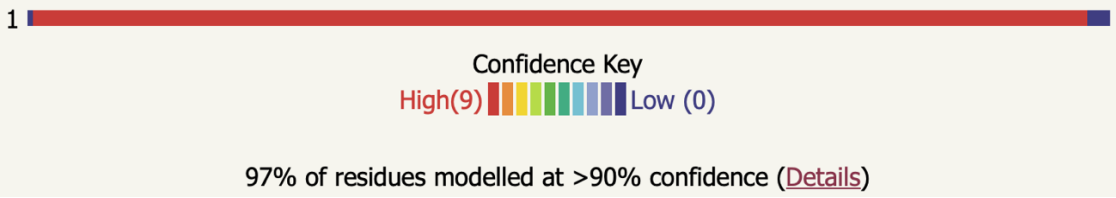

#	Template	Alignment Coverage	3D Model	Confidence	% i.d.	Template Information
1	c2vliB_	Alignment		99.8	20	**PDB header:**transferase **Chain:** B: **PDB Molecule:**antibiotic resistance protein; **PDBTitle:** structure of deinococcus radiodurans tunicamycin resistance protein
2	c2yvuA_	Alignment		99.8	14	**PDB header:**transferase **Chain:** A: **PDB Molecule:**probable adenylyl-sulfate kinase; **PDBTitle:** crystal structure of ape1195
3	c1m8pB_	Alignment		99.8	12	**PDB header:**transferase **Chain:** B: **PDB Molecule:**sulfate adenylyltransferase; **PDBTitle:** crystal structure of p. chrysogenum atp sulfurylase in the t-state
4	c2gksB_	Alignment		99.8	15	**PDB header:**transferase **Chain:** B: **PDB Molecule:**bifunctional sat/aps kinase; **PDBTitle:** crystal structure of the bi-functional atp sulfurylase-aps kinase from2 aquifex aeolicus, a chemolithotrophic thermophile
5	c7l4aA_	Alignment		99.8	17	**PDB header:**transferase **Chain:** A: **PDB Molecule:**cytidylate kinase; **PDBTitle:** crystal structure of cytidylate kinase from encephalitozoon cuniculi2 gb-m1 in complex with two cdp molecules

Appendix 2. Phyre 2 analysis of Cpz 27 protein sequence

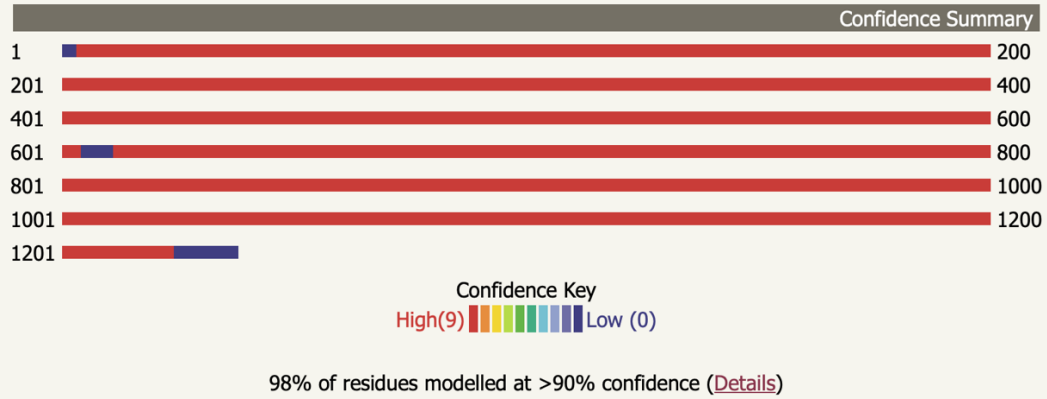

#	Template	Alignment Coverage	3D Model	Confidence	% i.d.	Template Information
1	c6bhuA_	Alignment		100.0	20	**PDB header:**transport protein **Chain:** A: **PDB Molecule:**multidrug resistance-associated protein 1; **PDBTitle:** cryo-em structure of atp-bound, outward-facing bovine multidrug2 resistance protein 1 (mrp1)
2	c5ykfH_	Alignment		100.0	23	**PDB header:**membrane protein **Chain:** H: **PDB Molecule:**atp-binding cassette sub-family c member 8 isoform x2; **PDBTitle:** structure of pancreatic atp-sensitive potassium channel bound with2 glibenclamide and atpgammas (3d class1 at 4.33a)
3	c6c3oE_	Alignment		100.0	23	**PDB header:**transport protein **Chain:** E: **PDB Molecule:**atp-binding cassette sub-family c member 8; **PDBTitle:** cryo-em structure of human katp bound to atp and adp in quatrefoil2 form
4	c4f4cA_	Alignment		100.0	22	**PDB header:**hydrolase,protein transport **Chain:** A: **PDB Molecule:**multidrug resistance protein pgp-1; **PDBTitle:** the crystal structure of the multi-drug transporter
5	c5ujaA_	Alignment		100.0	20	**PDB header:**protein transport **Chain:** A: **PDB Molecule:**bovine multidrug resistance protein 1 (mrp1),multidrug **PDBTitle:** cryo-em structure of bovine multidrug resistance protein 1 (mrp1)2 bound to leukotriene c4
6	c5uj9A_	Alignment		100.0	20	**PDB header:**transport protein **Chain:** A: **PDB Molecule:**bovine multidrug resistance protein 1 (mrp1),multidrug **PDBTitle:** cryo-em structure of bovine multidrug resistance protein 1 (mrp1)
7	c3g5uB_	Alignment		100.0	25	**PDB header:**membrane protein **Chain:** B: **PDB Molecule:**multidrug resistance protein 1a; **PDBTitle:** structure of p-glycoprotein reveals a molecular basis for2 poly-specific drug binding

Appendix 3. Phyre 2 analysis of Cpz 22 protein sequence

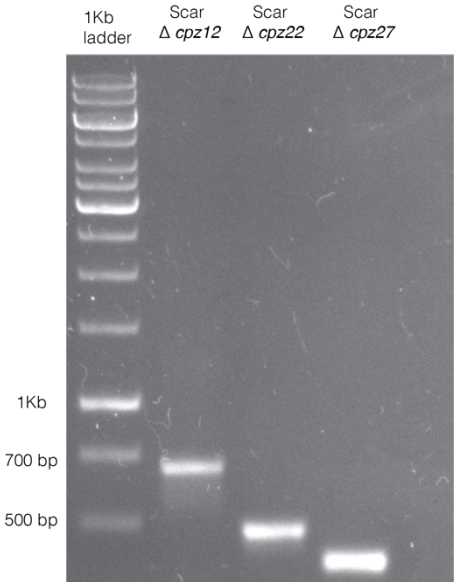

Scar Δ*cpz12*	Scar Δ*cpz22*	Scar Δ*cpz27*
636 bp	405 bp	301 bp

Appendix 4. Scar verification of Knock outs

Chapter II Appendix

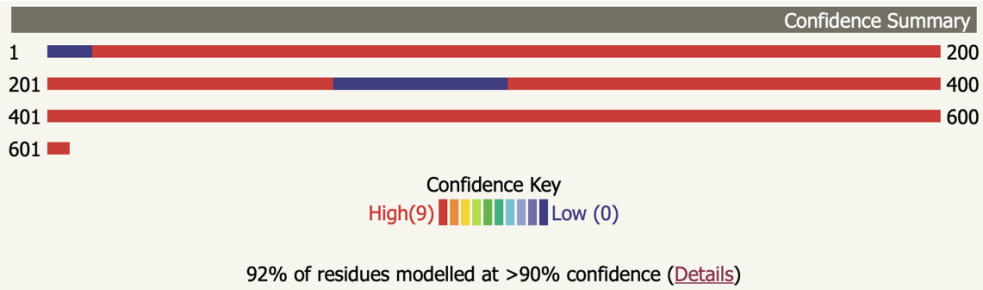

#	Template	Alignment Coverage	3D Model	Confidence	% i.d.	Template Information
1	c5nj3B_	Alignment		100.0	19	**PDB header:**transport protein **Chain:** B: **PDB Molecule:**atp-binding cassette sub-family g member 2; **PDBTitle:** structure of an abc transporter: complete structure
2	c5do7A_	Alignment		100.0	18	**PDB header:**transport protein **Chain:** A: **PDB Molecule:**atp-binding cassette sub-family g member 5; **PDBTitle:** crystal structure of the human sterol transporter abcg5/abcg8
3	c5do7B_	Alignment		100.0	18	**PDB header:**transport protein **Chain:** B: **PDB Molecule:**atp-binding cassette sub-family g member 8; **PDBTitle:** crystal structure of the human sterol transporter abcg5/abcg8
4	c7lkzA_	Alignment		100.0	26	**PDB header:**translocase **Chain:** A: **PDB Molecule:**retinal-specific phospholipid-transporting atpase abca4; **PDBTitle:** structure of atp-bound human abca4
5	c5xjyA_	Alignment		100.0	25	**PDB header:**transport protein **Chain:** A: **PDB Molecule:**atp-binding cassette sub-family a member 1; **PDBTitle:** cryo-em structure of human abca1
6	c4rvcA_	Alignment		100.0	26	**PDB header:**transport protein **Chain:** A: **PDB Molecule:**abc transporter atp-binding protein; **PDBTitle:** structure of atp binding subunit of abc transporter
7	c2olkD_	Alignment		100.0	30	**PDB header:**hydrolase **Chain:** D: **PDB Molecule:**amino acid abc transporter; **PDBTitle:** abc protein artp in complex with adp-beta-s

Appendix 5. Phyre 2 analysis of Cos IJ protein sequence

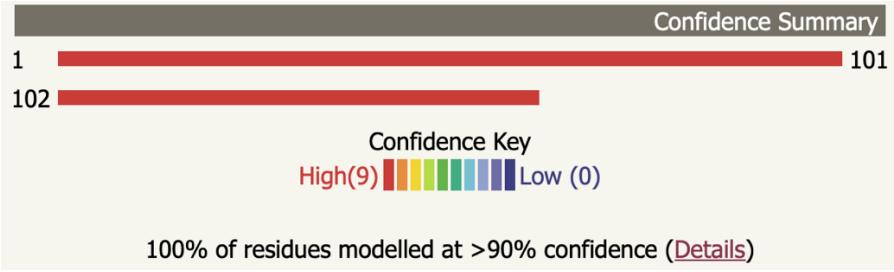

#	Template	Alignment Coverage	3D Model	Confidence	% i.d.	Template Information
1	d1gp1a_	Alignment		100.0	39	**Fold:**Thioredoxin fold **Superfamily:**Thioredoxin-like **Family:**Glutathione peroxidase-like
2	c2r37A_	Alignment		100.0	34	**PDB header:**oxidoreductase **Chain:** A: **PDB Molecule:**glutathione peroxidase 3; **PDBTitle:** crystal structure of human glutathione peroxidase 3 (selenocysteine to2 glycine mutant)
3	c2v1mA_	Alignment		100.0	32	**PDB header:**oxidoreductase **Chain:** A: **PDB Molecule:**glutathione peroxidase; **PDBTitle:** crystal structure of schistosoma mansoni glutathione peroxidase
4	c2he3A_	Alignment		100.0	33	**PDB header:**oxidoreductase **Chain:** A: **PDB Molecule:**glutathione peroxidase 2; **PDBTitle:** crystal structure of the selenocysteine to cysteine mutant of human2 glutathionine peroxidase 2 (gpx2)
5	d2f8aa1	Alignment	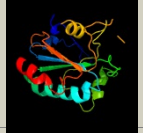	100.0	38	**Fold:**Thioredoxin fold **Superfamily:**Thioredoxin-like **Family:**Glutathione peroxidase-like

Appendix 6. Phyre 2 analysis of Cos P protein sequence

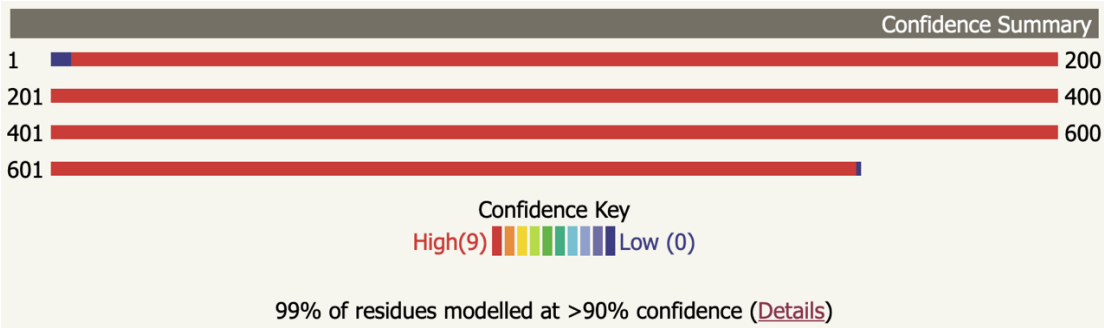

#	Template	Alignment Coverage	3D Model	Confidence	% i.d.	Template Information
1	c2vf7B_	Alignment		100.0	40	**PDB header:**dna binding protein **Chain:** B: **PDB Molecule:**excinuclease abc, subunit a.; **PDBTitle:** crystal structure of uvra2 from deinococcus radiodurans
2	c3zqjC_	Alignment	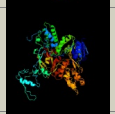	100.0	42	**PDB header:**dna binding protein **Chain:** C: **PDB Molecule:**uvrabc system protein a; **PDBTitle:** mycobacterium tuberculosis uvra
3	c3pihA_	Alignment		100.0	45	**PDB header:**hydrolase/dna **Chain:** A: **PDB Molecule:**uvrabc system protein a; **PDBTitle:** t. maritima uvra in complex with fluorescein-modified dna
4	c2ygrD_	Alignment	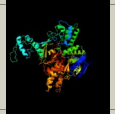	100.0	41	**PDB header:**hydrolase **Chain:** D: **PDB Molecule:**uvrabc system protein a; **PDBTitle:** mycobacterium tuberculosis uvra
5	c3zqjF_	Alignment		100.0	40	**PDB header:**dna binding protein **Chain:** F: **PDB Molecule:**uvrabc system protein a; **PDBTitle:** mycobacterium tuberculosis uvra
6	c2r6fA_	Alignment		100.0	42	**PDB header:**hydrolase **Chain:** A: **PDB Molecule:**excinuclease abc subunit a; **PDBTitle:** crystal structure of bacillus stearothermophilus uvra
7	c6n9lA_	Alignment		100.0	49	**PDB header:**dna binding protein **Chain:** A: **PDB Molecule:**uvrabc system protein a; **PDBTitle:** crystal structure of t. maritima uvra d117-399 with adp
8	c3ux8A_	Alignment		100.0	52	**PDB header:**dna binding protein **Chain:** A: **PDB Molecule:**excinuclease abc, a subunit; **PDBTitle:** crystal structure of uvra

Appendix 7. Phyre 2 analysis of Cos U protein sequence

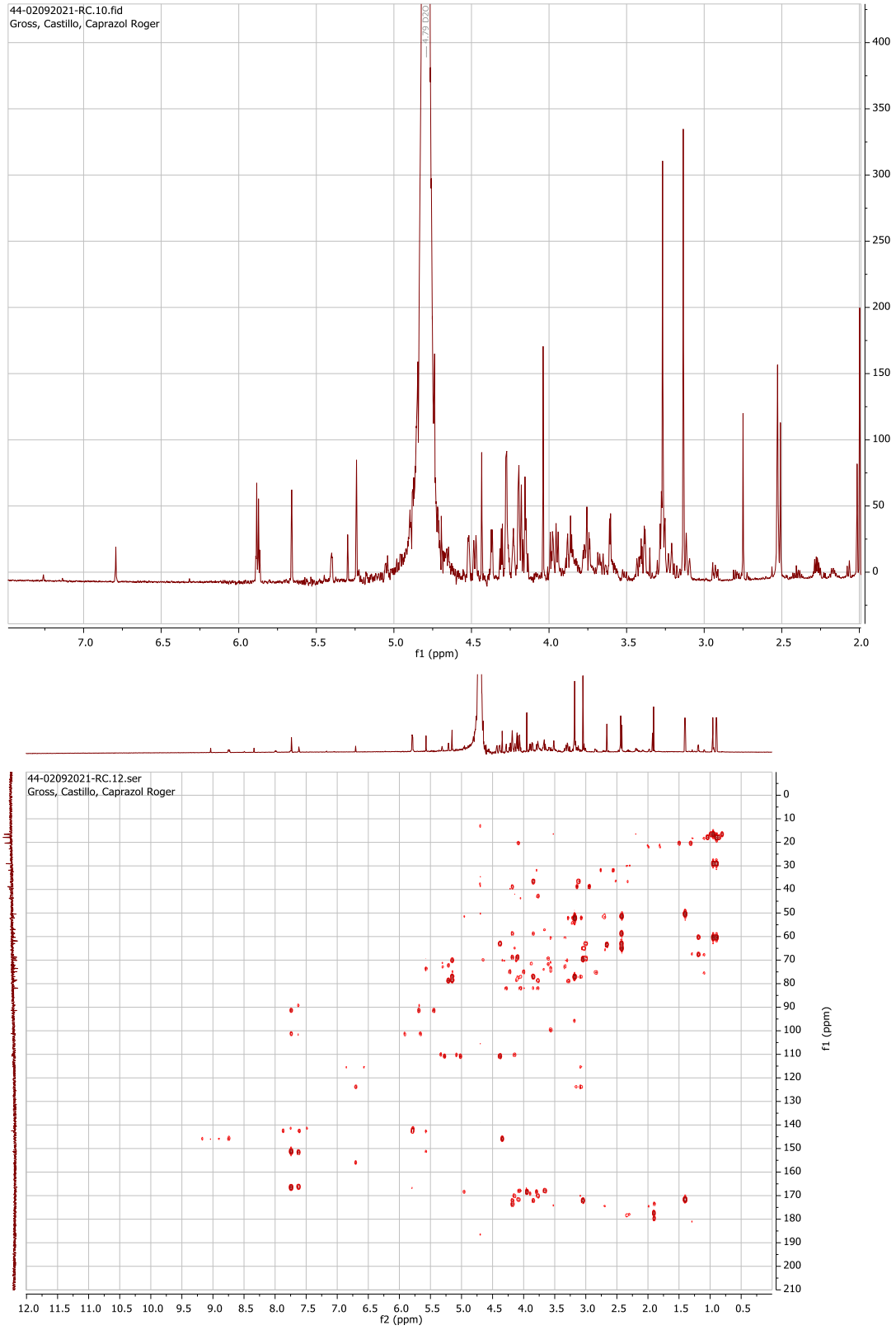

Appendix 8. NMR of 3'phospho-(+)-caprazol

Top: ^{1}H NMR of 3'phospho-caprazol in D2O (700 MHz). Bottom: ^{1}H-^{13}C- HMBC spectrum of 3'phospho-caprazol in D_2O (700 MHz).